ABSTRACT

Testing Theories of Gravity by Gravitational Wave Observations

Chao Zhang, Ph.D.

Advisor: Anzhong Wang, Ph.D.

In this dissertation, Einstein-æther theory is studied. As a candidate of modified theories to general relativity, Einstein-æther theory shows some different features compared to Einstein's theory. The studies of these features can serve for the test and development of gravitational theories. In this dissertation, the study of Einstein-æther theory is closely related to the gravitational wave observations. In fact, those observations can potentially provide a variety of ways to test general relativity and put severe constraints on Einstein-æther theory. This thesis will mainly focus on the gravitational waves emitted by compact celestial bodies in the universe, and calculate the gravitational waveforms, innermost stable circular orbits, universal horizons, quasi-normal modes, etc. in the framework of Einstein-æther theory. With the continuous improvement of the accuracy of detectors around the world, as well as the accumulation of gravitational wave events, these investigations will become more and more important for understanding the nature of gravity and the dynamics of the universe.

Testing Theories of Gravity by Gravitational Wave Observations

by

Chao Zhang, B.S., M.A.

A Dissertation

Approved by the Department of Physics

Dwight P. Russell, Ph.D., Interim Chairperson

Submitted to the Graduate Faculty of
Baylor University in Partial Fulfillment of the
Requirements for the Degree
of
Doctor of Philosophy

Approved by the Dissertation Committee

Anzhong Wang, Ph.D., Chairperson

Gerald B. Cleaver, Ph.D.

Lorin Swint Matthews, Ph.D.

Dwight P. Russell, Ph.D.

Qin (Tim) Sheng, Ph.D.

Accepted by the Graduate School
May 2021

J. Larry Lyon, Ph.D., Dean

Page bearing signatures is kept on file in the Graduate School.

TABLE OF CONTENTS

LIST OF FIGURES

LIST OF TABLES

ACKNOWLEDGMENTS

First of all, I want to say thank you to my supervisor, Dr. Anzhong Wang. It was him who led me into the spectacular realm of gravity physics. Learning and discussing with him in the past four years really benefited me a lot.

On the other hand, I also want to express my appreciations to Dr. Matthews, Dr. Russell, Dr. Cleaver and Dr. Sheng for serving on my committee. I understand that they have their busy schedules as researchers. Thus, I am really glad to have their time.

Besides, I feel quite grateful to Mr. Xiang Zhao, who is also working in my research group. We worked together in the past three years and conquered many difficulties. It is hard to tell if I can reach this far without his support. In addition, he also helped me a lot in my daily life in the past years. I wish him a bright future and wonderful life.

I would like also to thank all my teachers and professors in the Physics Department of Baylor University. I really learnt a lot from them in the past years. Thank you for bringing me to the fascinating knowledge of physics and sharpening my mind. The same to Mrs. Chava Baker and Mrs. Marian Nunn-Graves. They helped me in various ways for administrative problems.

It is also my great pleasure to thank Dr. Kai Lin, Dr. Wen Zhao, Dr. Tao Zhu, Dr. Kent Yagi, Dr. Nicolas Yunes, Dr. Ted Jacobson, Dr. Bin Wang, Dr. Shaojun Zhang, Mr. Tan Liu, Dr. Lijing Shao, Dr. Xing Zhang, Dr. Xiongjun Fang and Rui Niu for their help and kind collaborations. I appreciate their academic support so

much. We had a lot of valuable discussions during the past years. I sincerely hope we can meet again in the future.

Additionally, I would like to thank my friends at Baylor University, including Dr. Xinwen Wang, Mr. Bowen Li, Dr. Baofei Li, Dr. Yang Liu, Ms. Jingyi Yang, Mr. Jingdong Chen, Mr. Abinash Kar, Mr. Bryan Caraway, Sudip, Ms. Qingqing Chen etc. Thank you for all the help in the past years.

Also, I am very proud to have Mr. Tianqi Yu, Mr. Chenxi Yao as well as Mr. Chenhao Wang being the best friends in my life. Although we are separated by the Pacific Ocean all the time, I can frequently hear from them when I feel lonely.

Finally, I would like to express my appreciation to my mom. She will always stand at my side when I need help. Although she is living in my hometown and is more than 10,000 km away from me, her encouragements are always around me.

Dedicated to Beijing, my dear hometown, who has just celebrated her 600th birthday.

CHAPTER ONE

Introduction to Einstein-Æther Theory

1.1 A Succinct History of Gravity

As human beings, we always have some natural feelings about this living cosmos. However, the essence of gravity, universe, space and time remains an enigma for quite a long time. People have been pursuing the answers since more than 4,000 years ago. Actually, those ancient philosophers left some interesting records and comments about the universe and the spacetime. For instance, the Roman philosopher St. Augustine (354 - 430 AD) once mentioned that the time does not exist before the creation of universe [1]. Similarly, the Chinese philosopher An Liu (179 - 122 BC) also said that space and time were born from absolute vacancy [2]. Their statements implicitly revealed the connections between space and time, which is close to some modern ideas.

The systematic study of gravity could probably be dated to more than three hundred years ago, i.e., to Isaac Newton's era [3]. After that, the birth of general relativity (GR) marks a new era for the study of gravity [4]. As we know, Albert Einstein unified time and space in a creative way and brought us a new way of thinking about the cosmos. His serendipity provides a powerful tool to study gravity and understand the dynamics of the universe. It's true that GR is quite successful in many aspects. For instance, during the past decades, GR passed all the experimental tests with flying colors (See, e.g., [5, 6].). One of the blockbusters is the observation of the eclipse by Eddington in 1919 [7].

Some mysterious phenomena are happening in this cosmos according to GR. The most famous one is probably the black hole (BH). By using Einstein's field equations, Karl Schwarzschild was able to obtain an exact solution of the Einstein field equations for static spherically symmetric spacetimes in 1916 [8]. Due to the peculiar properties of such a spacetime, it is referred as "black hole". There are plenty of theoretical works around the BHs. For instance, for spinning BHs we have the Kerr solution [9], for charged BHs we have the Reissner-Nordström solution [10,11], etc. In addition, people are also trying to find experimental proofs of the existence of BHs. Actually, this is quite successful so far, including the recent observation of the M87 center BH (See, e.g., [12].).

In fact, the detection of gravitational waves (GWs) provides one of the strongest evidence to the existence of BHs. The concept of GW was first introduced by Einstein about one century ago [13]. It could be simply described as the ripples of the spacetime. As before, the theoretical studies are generally prior to those experimental works. It was the detection of GW150914 [14, 15], which is emitted from the coalescence of a binary black hole (BBH) system, that initiated the era of GW physics. Soon after that, the 2017 Nobel Prize in Physics was given to K. Thorne, B. Barish and R. Weiss for their contributions to GW physics. Later, several other GWs were identified by the LIGO/Virgo Scientific Collaboration [16] and more are still on the way. Specially, among them there is a binary neutron star (BNS) detection, GW170817 [21].

The physics behind GWs is quite rich. For instance, GWs provide a new way to test the theory of GR as well as those modified theories. There are some clues imply that GR is not the end of the story of gravity. Because of this, different kinds

of modified theories are developed (See, e.g., [22].). While expecting the discrepancy from GR in the GW observations (which implies brand new physics and may ignite a big progress), people are also trying to put more and more stringent constraints on modified theories. By using the data from the GW observations, many modified theories have already been ruled out. Einstein-æther theory (æ-theory) is one of the modified theories that still survive. It has successfully passed all the tests by adjusting several built-in coefficients of this theory (Of course, more constraints were added as time goes on.). That is the main goal of this dissertation to study æ-theory systematically in the framework of GW physics.

1.2 ABC of Æ-theory

This dissertation will focus on the study of GWs in the framework of æ-theory [23]. This theory locally breaks Lorentz symmetry (Lorentz invariance) [24] by the presence of a globally timelike unit vector field - the aether (æ-) field (or simply referred as aether). The Lorentz invariance is considered to be one of the pillars of modern physics in general. However, breaking it may bring us the dawn of quantum gravity [25]. This is one of the reasons for us to study this kind of theories.

In æ-theory, the fundamental variables of the gravitational sector are [23],

$$(g_{\mu\nu}, u^{\mu}, \lambda)\,, \tag{1.1}$$

with the Greek indices $\mu, \nu = 0, 1, 2, 3$. Here, $g_{\mu\nu}$ is the four dimensional metric of the spacetime while u^{μ} represents the aether four-velocity (or æ-field), and λ is a Lagrangian multiplier [26], which guarantees that the æ-field is always timelike and unit.

The general action of the theory is given by [27],

$$S = S_{æ} + S_m, \tag{1.2}$$

where S_m denotes the action [24] of matter, and $S_{æ}$ the gravitational action of the æ-theory, given, respectively, by

$$\begin{aligned} S_{æ} &= \frac{1}{16\pi G_{æ}} \int \sqrt{-g}\, d^4x \Big[\mathcal{L}_{æ}\left(g_{\mu\nu}, u^\alpha, c_i\right) + \mathcal{L}_\lambda\left(g_{\mu\nu}, u^\alpha, \lambda\right) \Big], \\ S_m &= \int \sqrt{-g}\, d^4x \Big[\mathcal{L}_m\left(g_{\mu\nu}, u^\alpha; \psi\right) \Big]. \end{aligned} \tag{1.3}$$

Here ψ collectively denotes the matter fields, R and g are, respectively, the Ricci scalar [28] and determinant [29] of $g_{\mu\nu}$, and

$$\begin{aligned} \mathcal{L}_\lambda &\equiv \lambda\left(g_{\alpha\beta}u^\alpha u^\beta + 1\right), \\ \mathcal{L}_{æ} &\equiv R(g_{\mu\nu}) - M^{\alpha\beta}{}_{\mu\nu}\left(D_\alpha u^\mu\right)\left(D_\beta u^\nu\right), \end{aligned} \tag{1.4}$$

where D_μ denotes the covariant derivative [30] with respect to $g_{\mu\nu}$, and $M^{\alpha\beta}{}_{\mu\nu}$ is defined as

$$M^{\alpha\beta}{}_{\mu\nu} \equiv c_1 g^{\alpha\beta}g_{\mu\nu} + c_2\delta^\alpha_\mu\delta^\beta_\nu + c_3\delta^\alpha_\nu\delta^\beta_\mu - c_4 u^\alpha u^\beta g_{\mu\nu}, \tag{1.5}$$

where δ^β_ν stands for the Kronecker delta [31]. Note that here we need to assume that matter fields couple not only to $g_{\mu\nu}$ but also to the aether field u^μ, in order to model effectively the radiation of a compact object [32, 33], such as a neutron star [34]. However, in order to satisfy the severe observational constraints, such a coupling in general is assumed to be absent [27].

The four coupling constants c_i's are all dimensionless (and here i=1, 2, 3, 4), and $G_{æ}$ is related to the Newtonian constant G_N [35] via the relation [36],

$$G_N = \frac{G_{æ}}{1 - \frac{1}{2}c_{14}}, \tag{1.6}$$

where $c_{ij} \equiv c_i + c_j$.

The variations of the total action with respect to $g_{\mu\nu}$, u^μ and λ, lead to the field equations (Details will be provided in the following sections.). Different from GR, æ-theory allows three different kinds of modes [37], namely, the scalar (spin-0), vector (spin-1) and tensor (spin-2) modes. Their corresponding speeds are given, respectively, by [32]

$$\begin{aligned} c_S^2 &= \frac{c_{123}(2-c_{14})}{c_{14}(1-c_{13})(2+c_{13}+3c_2)}\,, \\ c_V^2 &= \frac{2c_1-c_{13}(2c_1-c_{13})}{2c_{14}(1-c_{13})}\,, \\ c_T^2 &= \frac{1}{1-c_{13}}, \end{aligned} \tag{1.7}$$

where $c_{ijk} \equiv c_i + c_j + c_k$. One should note that we have $c_I \gtrsim 1$, where $I = S, V, T$ to avoid the vacuum gravi-Čerenkov radiation by matter such as cosmic rays [38].

1.3 Some Achievements in Æ-theory

Here I would like to summarize some of the achievements of æ-theory in recent years. The work of this thesis benefits a lot from these pioneers.

Under the parameterized post-Newtonian (PPN) framework [6], Foster and Jacobson calculated the ten post-Newtonian parameters in [39]. In the same treatise, some constraints to the four c_i's are also given. It's worth mentioning here that there are only two PPN parameters that deviate from GR, viz., α_1 and α_2. They are given by

$$\begin{aligned} \alpha_1 &= -\frac{8\,(c_1c_{14}-c_-c_{13})}{2c_1-c_-c_{13}}, \\ \alpha_2 &= \frac{1}{2}\alpha_1 + \frac{(c_{14}-2c_{13})\,(3c_2+c_{13}+c_{14})}{c_{123}(2-c_{14})}, \end{aligned} \tag{1.8}$$

where we have defined $c_- \equiv c_1 - c_3$. They characterize the local Lorentz invariance (LLI) for the gravitational interactions [40].

Then, Foster calculated the energy loss rate [41]. Based on the previous work, Foster and Yagi *et al.* derived the metric and the equations of motion to the first post-Newtonian (PN) [22] order for a N-body system [32, 42].

As a special case of N-body systems, 3-body problems also attracted a lot of attentions in the past three centuries. To the theoretical level, only a limited number of such systems were found [43]. When one of the three bodies being a test mass, it reduces to the restricted 3-body problem, and a collinear solution was found by Euler [44]. In 1772 Lagrange found a second class of periodic orbits for an equilateral triangle configuration [45] (A historic review of this subject can be found in [46].). In GR, neither analytical nor numerical solutions of 3-body problem of the full theory have been found, and most of the studies were restricted to PN approximations, see, for example, [47–53] and references therein. Lately, the existence and uniqueness of the 1PN collinear solution in the scalar-tensor theory were studied in [54, 55]. Will extended the work of æ-theory to study 3-body systems [56]. He obtained the accelerations of a 2-body system in the presence of the third body at the quasi-Newtonian order. Note that in [42] the influence of sensitivities are also taken into account (Nonetheless, those results need to be updated due to the latest constraints on c_i's.).

With all of these in hand, the GW in æ-theory was studied in [57]. Besides, the waveforms and angular momentum losses were also calculated [58,59]. After that, by using the latest constraints on $c_i's$ [60], we calculated the waveforms (also referred as GW forms or polarizations), response functions, energy losses, etc. in detail for some triple configurations [61] and plotted the main results. Additionally, we also discussed the detectability of GWs of triple systems. What's more, based on the

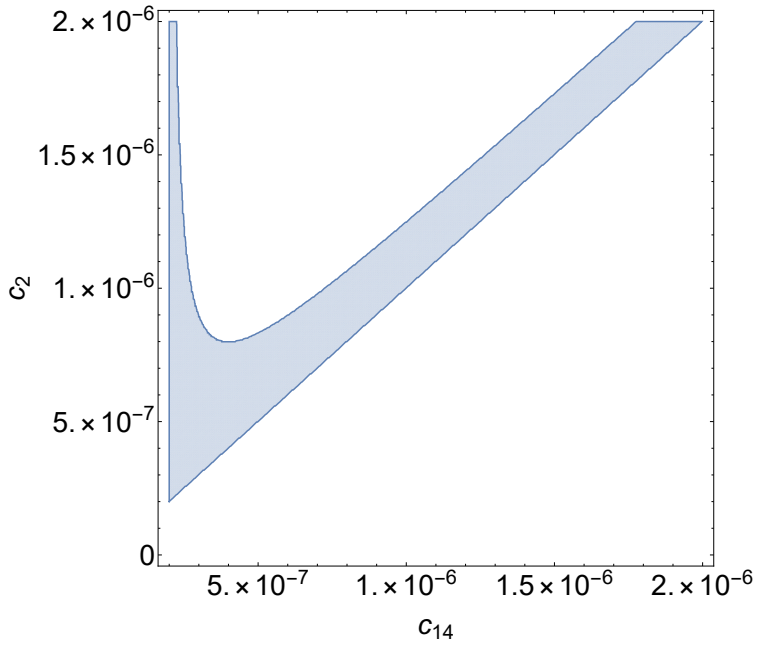

Figure 1.1: The physically viable (c_2, c_{14}) in the intermediate interval (ii) as shown in [60]. Note that here we have assumed $c_{13} = 0$ since it is extremely small.

work of [62], we focused on a specific observed triple system, PSR J0337+1715 [63] [In there we also studied the Brans-Dicke (BD) theory of gravity (See, e.g., [64]).].

For later convenience, I would like to quickly review the constraints on c_i's given in [60]. The constraint of c_{13} is quite simple, which is $|c_{13}| < 10^{-15}$. The constraints on $\{c_2, c_{14}\}$ are a little bit more sophisticated. The $c_2 - c_{14}$ plane is divided into three regions, i.e., (i) $0 \lesssim c_{14} \leq 2 \times 10^{-7}$; (ii) $2 \times 10^{-7} < c_{14} \lesssim 2 \times 10^{-6}$; and (iii) $2 \times 10^{-6} \lesssim c_{14} \lesssim 2.5 \times 10^{-5}$. In the first and last intervals, one finds

$$\text{(i)} \quad 0 \lesssim c_{14} \leq 2 \times 10^{-7}, \quad c_{14} \lesssim c_2 \lesssim 0.095, \tag{1.9}$$

$$\text{(iii)} \quad 2 \times 10^{-6} \lesssim c_{14} \lesssim 2.5 \times 10^{-5}, \quad 0 \lesssim c_2 - c_{14} \lesssim 2 \times 10^{-7}. \tag{1.10}$$

The results in the intermediate interval (ii) were shown explicitly by Fig. 1 in [60]. It is also exhibited here in Fig. 1.1 (Note that a small typo in the original graph is corrected.). Interested readers may check this reference to find out more details.

The study of binary systems in æ-theory was carried out in detail in the past years. There are a lot of works covering the different stages of the coalescence of a binary system (Generally, such a coalescence is characterized by three different stages, viz., inspiral, merger and ringdown [65, 66].). For instance, the motion of two stars and the corresponding gravitational radiation during the process of circularization was calculated in [67]. Additionally, the response function in the time and frequency domain for a compact binary during its quasicircular inspiral was studied in [58]. Nevertheless, many of these results need to be updated due to the new constraints on c_i's [60]. At the same time, one should notice that there are some misconceptions and typos in the literature. For these reasons, we repeated some of the previous work [68] with some amendments and improvements. What's more, in there the parametrized post-Einsteinian (ppE) framework [69] is extended to allow for different propagation speeds among different polarization modes [70].

The investigatons mentioned above mainly focus on the inspiral stage of a binary (or other multi-body) system. For theoretical purposes, we are also interested in the ringdown stage. This interest provokes the topic of the quasi-normal modes. From the classical point of view, quasi-normal modes (QNMs or QNM frequencies) are eigenmodes of dissipative systems. The detection of QNMs of a black hole will provide us a new way to measure its spin and mass as well as test GR. According to the no-hair theorem, the quasi-normal frequencies and damping times will depend only on the mass and angular momentum of the final BH. Therefore, to extract the physics from the ringdown phase, at least two QNMs are needed. This will require the signal-to-noise ratio (SNR) to be of the order 100. It is certain that they will be detected by the space-based detectors, such as LISA, TianQin [71] and Taiji in the

near future. This also spurs one's enthusiasm on QNMs. As a novice, one may find a whole picture of the related concepts of QNMs in [72].

QNMs in GR have been studied extensively in the past decades. In æ-theory, some attempts can also be found in the literature (See, e.g., [73, 74].). Actually, we are also focusing on this topic recently. We have made some progress in this direction, as to be shown. However, a deeper study is still needed.

As a preparation to the study of QNMs, we first focus on the solutions for the background metric of a BH. To be specific, we systematically studied the spherically symmetric static spacetimes in the framework of æ-theory. This area has been exploited in the past couple of years both analytically [62, 75–85] and numerically [86–92]. Besides, it was shown that this kind of BHs can be formed from gravitational collapse [93, 94]. We reviewed some of the previous work and added more calculations to several physically observable quantities like the radius of the spin-0 horizon (denoted by r_{S0H}), the location of the innermost stable circular orbits (denoted by r_{ISCO}), the radii of the universal horizons (denoted by r_{UH}), etc. [95]. More importantly, the latest constraints on c_i's are considered in there and we have improved the techniques of solving the metric numerically.

1.4 Other Modified Theories

Outside the regime of æ-theory, I also participated in the investigations of other modified theories of gravity, although not intensively. Here I'd like to briefly review the related works.

As has been mentioned, in [63] we calculated the waveforms and response functions of PSR J0337+1715 in Brans-Dicke theory.

On the other hand, we calculated in detail the waveforms, gravitational wave polarizations, response functions, and energy losses due to gravitational radiation in screened modified gravity (SMG) [96–98] to the leading PN order, with which we then considered projected constraints from the third generation detectors.

Finally, in [99] we studied the Einstein-complex-scalar-Gauss-Bonnet gravity. To be specific, We found that static regular BH solutions with complex scalar hairs do not exist.

1.5 Structure of the Dissertation

This rest of this dissertation is organized as follows.

Chapter Two will mainly pay attention to the inspiral stage during the coalescence of a binary system. In there, binary systems with quasicircular orbits are studied in æ-theory. Some results of this part are published in [68]. In this chapter, the waveforms (GW forms) and energy loss rate for a binary with a changing orbit are calculated. Besides, the response functions for different kinds of detectors are derived and the ppE parameters are explored. During this procedure, some errors and typos in the literature are corrected.

To study the ringdown stage of the coalescence for, e.g., a BBH system, Chapter Three digs into the study of the spherically symmetric static spacetimes systematically in the framework of æ-theory. A part of the results presented in this chapter are published in [95]. In this chapter, I will clarify several subtle points in the literature. With them being crystal clear, I am able to obtain more useful results compared to those previous works. The quantities obtained, such as the metric, r_{S0H}, r_{UH}, etc. will be exhibited with some comments.

After that, in Chapter Four I will show some attempts to the QNMs in æ-theory. The shooting method will be used and some of the current results will be shown. Specially, I will show how the resutls in æ-theory deviate from GR. Besides, as mentioned above, this is actually a huge topic. A deeper study in this direction is still needed.

Chapter Five consists of some concluding remarks and outlooks to the future work.

1.6 Conventions

In this dissertation, I will adopt the following conventions:

First of all, the units are chosen so that the speed of light equals 1 ($c = 1$). For certain parts of this dissertation, more unit choices may be introduced. They will all be indicated when it is necessary.

All the Greek indices will run from 0 to 3. Generally, Romanian (or Latin) letters i, j, k and l run from 1 to 3. Besides, repeated i, j, k, l and Greek indices represent the Einstein's convention of summations [100], regardless of whether the indices are subscripts or superscripts. It will be indicated clearly for exceptions when it is necessary. The usage of other kinds of indices will be described at suitable places.

As mentioned earlier, some coefficients in æ-theory are defined by

$$c_{ij} \equiv c_i + c_j, \quad c_{ijk} \equiv c_i + c_j + c_k, \quad c_{\pm} \equiv c_1 \pm c_3. \tag{1.11}$$

As a result, we will have $c_+ = c_{13}$. For historical reasons, both of them will be used in this dissertation. Note that in Eq. (1.11) we have $i, j, k = 1, 2, 3, 4$.

Finally, the signature (-, +, +, +) [37, 41, 93] will be used here.

It is worth mentioning here that the demonstration of the following topics requires tons of different notations. As a result, those normal Greek and Latin letters are far from being sufficient. So, in several places, the same symbol may represent different quantities. In this dissertation, the author shall try his best to keep such cases to minimum.

CHAPTER TWO

Gravitational Waves from the Quasicircular Inspiral of Compact Binaries in Einstein-Aether Theory

This chapter is published in [68]: C. Zhang, X. Zhao, A. Wang, B. Wang, K. Yagi, N. Yunes, W. Zhao and T. Zhu, Gravitational waves from the quasicircular inspiral of compact binaries in Einstein-aether theory, Phys. Rev. D**101**, 044002 (2020).

In this chapter, we study gravitational waves emitted by a binary system of non-spinning bodies in a quasi-circular inspiral within the framework of Einstein-aether theory. In particular, I compute explicitly and analytically the expressions for the time- and frequency-domain waveforms, gravitational wave polarizations, and response functions for both ground- and space-based detectors in the post-Newtonian approximation. I find that, when going beyond leading-order in the post-Newtonian approximation, the non-Einsteinian polarization modes contain terms that depend on both the first and the second harmonics of the orbital phase. I also calculate analytically the corresponding parameterized post-Einsteinian parameters, generalizing the existing framework to allow for different propagation speeds among scalar, vector and tensor modes, without assumptions about the magnitude of its coupling parameters, and meanwhile allowing the binary system to have relative motions with respect to the aether field. Such results allow us for the easy construction of Einstein-aether templates that could be used in Bayesian tests of general relativity in the future. Note that several typos in the original work [68] are corrected here.

2.1 Introduction

As has been mentioned in Chapter One, the detection of the first GW event from the coalescence of two massive BHs by advanced LIGO marked the beginning of the GW era [14]. Following this observation, a few tens of GW candidates were identified by the LIGO/Virgo scientific collaboration [16–20][1]. The LIGO and Virgo detectors are sensitive to GWs with frequencies between 20 and 2000Hz [102], since at frequencies lower than 20Hz they are limited by the Newtonian seismic noise on the earth. As a consequence, LIGO and Virgo are only able to observe GWs produced in the late inspiral and merger of low-mass compact binaries, such as binary black holes (BBHs), binary neutron stars (BNSs) and BH-NSs.

One of the remarkable observational results obtained so far is the discovery that the BBHs can be composed of objects with individual masses much larger than what was previously expected, both theoretically and observationally [103–105], leading to the proposal and refinement of various formation scenarios [106, 107]. A consequence of this discovery is that the early inspiral phase may also be detectable by space-based observatories, such as LISA, TianQin, Taiji and DECIGO, for several years prior to their coalescence [108, 109]. The analysis of the BBHs' population observed by LIGO and Virgo has shown that such space-based detectors may be able to see many such systems, with a variety of profound scientific consequences.

In particular, multiple observations with different detectors at different frequencies of signals from the same source can provide excellent opportunities to study

[1] Recently, various GWs have been detected after LIGO/Virgo resumed operations on April 1, 2019, possibly including the coalescence of a neutron-star (NS)/BH binary. As far as I can tell, the details of these detections have not yet been released [101] so far.

the evolution of the binary in detail. Since different detectors observe at disjoint frequency bands, together they cover different evolutionary stages (i.e., inspiral, merger and ringdown) of the same binary system. Each stage of the evolution carries information about different physical aspects of the source. Technically, it also provides early warnings for an upcoming coalescence, so that ground-based detectors could know the sky localization of the source and its time to coalescence well in advance.

Combining high- and low-frequency GW detections of the same source can also help us identify the astrophysical channel responsible to BBH formations. Different scenarios in fact result in different masses, mass ratios, spins and eccentricity distributions of the detected sources [110–115]. Because of the GW circularization, BBHs may have small eccentricity in the LIGO/Virgo band, regardless of their formation channels. However, space-based detectors will be able to observe GW signals from BBHs that did not have enough time to fully circularize, allowing for measurements of eccentricities in excess of 10^{-3} [111]. In addition, stellar-mass BBHs observed in the space-based detector bands provide a very promising class of standard sirens (See, e.g., [116].). In the absence of a distinctive electromagnetic counterpart, it was estimated [117] that LISA might measure the Hubble constant within a few percent error, thus helping in the resolution of the discrepancy between the local measurement of this quantity [118] and that obtained from the cosmic microwave background (CMB) [119, 120] (Note that using ground-based detectors, e.g., aLIGO, the Hubble constant could also be measured with good precisions even if we do not identify electromagnetic counterparts [121, 122].).

In addition, multi-band GW detections will enhance the potential to test gravitational theories in the strong, dynamical field regime of merging compact objects [123–128]. Massive systems will be observed by ground-based detectors with high signal-to-noise ratios, after being tracked for years by space-based detectors in their inspiral phase. The two portions of signals can be combined to make precise tests for different theories of gravity. In particular, joint observations of BBHs with a total mass larger than about 60 solar masses by LIGO/Virgo and space-based detectors can potentially improve current bounds on dipole emission from BBHs by more than six orders of magnitude [123], which will impose severe constraints on various theories of gravity [129].

All the above work, however, depends crucially on the accurate description of GWs in order to track the signal during the early inspiral phase all the way to the merger phase. During the inspiral phase, GWs can be modeled using the post-Newtonian (PN) formalism [130]. Within general relativity (GR), waveforms at low PN orders (i.e., at or below the 2PN order) are sufficiently accurate for an unbiased recovery of the source parameters [131]. As the signal-to-noise ratio increases, however, our ability to test GR will be systematically limited by the accuracy of our waveform models.

In recent work, I and my colleagues generalized the PN formalism to certain modified theories of gravity and applied it to the quasi-circular inspiral of compact binaries. In particular, we calculated in detail the waveforms, gravitational wave polarizations, response functions and energy losses due to gravitational radiation in Brans-Dicke (BD) theory [64] and screened modified gravity (SMG) [96–98] to the leading PN order, with which we then considered projected constraints from

the third-generation detectors. Such studies have been further generalized to triple systems in Einstein-aether theory [62, 63]. When applying such formulas to the first relativistic triple system discovered in 2014 [132,133], we studied the radiation power, and found that quadrupole emission has almost the same amplitude as that in GR, but the dipole emission can be as big as the quadrupole emission. This can provide a promising window to place severe constraints on Einstein-aether theory with multi-band gravitational wave observations [123, 126].

In this chapter, we study the gravitational waves emitted by a compact binary during its quasi-circular inspiral within Einstein-aether theory. This is, of course, not the first time gravitational waves that have been studied in this theory. The first studies were carried out by Foster in the mid 2000s [32, 41], who computed the gravitational waves and the radiative losses of a generic binary through a multipolar decomposition. Using these results, Yagi, *et al.* [42, 67] calculated the effects of such waves on the rate of change of the orbital period of binary pulsars, placing stringent constraints on a sector of the theory. Following this work, Hansen, *et al.* [58] calculated the GW polarizations and response functions in the time- and frequency-domain for a compact binary during its quasi-circular inspiral, but again in a restricted sector of the theory. More recently, more severe constraints were placed on Einstein-aether theory [57, 60], using the recent binary NS observation by LIGO, which constrained the speed of gravity to better than one part in 10^{15} [58].

We here revisit some of these calculations without imposing any restrictions on the parameter space. First, I compute, once more, the gravitational waves emitted by a binary system and its associated radiative energy loss for a generic binary system in the PN approximation without assumptions about the magnitude of its coupling

parameters. I then specialize this calculation to a compact binary in a quasi-circular inspiral and compute the time-domain response function both for ground- and space-based detectors. In doing so, we will discover that previous expressions for the GW polarizations that compose the time-domain response function [70] are not applicable to Einstein-aether theory due to the different speeds of propagation of its scalar and vector modes. This implies that the results of [58] are corrected by terms that depend on these different speeds; in particular, this generates terms in the non-Einsteinian polarizations that depend explicitly on the speed of the center of mass of the binary with respect to the aether field. With these waveforms computed, I then calculate their Fourier transform in the stationary phase approximation (SPA) [69, 70, 134], and map the results to the parameterized post-Einsteinian (ppE) framework [69] that was extended to allow for different propagation speeds among different polarization modes [70]. Our results, therefore, allow for the straightforward construction of waveform templates with which to carry out tests of Einstein-aether theory using Bayesian theory and matched filtering in the future.

The remainder of this chapter presents the results summarized above. In particular, in Sec.2.2 I give a brief introduction to Einstein-aether theory, and in Sec.2.3 I calculate the GW polarizations and energy loss rate, and correct some typos in the literature. In Sec.2.4, I study the GW polarizations and response function for an inspiraling binary. In Sec.2.5, I calculate the response function and its Fourier transform for both ground- and space-based detectors using the SPA [69, 70, 134]. In Sec.2.6, I map the results of the last section to the parametrized post-Einsteinian (ppE) framework [69, 70, 134], while in Sec.2.7, I summarize the main results and present discussions as well as concluding remarks. Besides, in Appendix A, I present

a brief review on the SPA, while in Appendices B, C and D I provide some additional mathematical formulas. We follow here the conventions of Misner, Thorne and Wheeler [24] and use units in which $c = 1$.

2.2 Einstein-æther Theory

A brief introduction to the æ-theory has been given in Sec.1.2. As mentioned in there, the aether field (æ-field) is always timelike and unit,

$$u^\lambda u_\lambda = -1. \tag{2.1}$$

Recall that, all repeated Latin letters represent spatial indices that are to be summed over from 1 to 3, while repeated Greek letters represent spacetime indices to be summed over from 0 to 3, regardless of whether they are superscripts or subscripts.

It has been mentioned in Sec.1.3, the current theoretical and observational constraints on the four dimensionless coupling constants c_i's were given explicitly in [60]. It was found that

$$0 \leq c_{14} \leq 2.5 \times 10^{-5}, \qquad |c_{13}| \leq 10^{-15}. \tag{2.2}$$

More details can be found in Sec.1.3 (See also [135], in which it also shows that æ-theory is a well-posed theory.).

Strong field effects can be important in the vicinity of a compact body, such as a neutron star or a black hole, and need to be taken into account. This is what I am going to do in this chapter. Following Eardley [34], these effects can be included by considering the test-particle action [32],

$$\begin{aligned} S_A &= -\int d\tau_A \tilde{m}_A[\gamma_A] \\ &= -\tilde{m}_A \int d\tau_A \left[1 + \sigma_A(1-\gamma_A) + \frac{1}{2}(\sigma_A + \sigma_A^2 + \bar{\sigma}_A)(1-\gamma_A)^2 + ...\right], \end{aligned} \tag{2.3}$$

where $\gamma_A \equiv -u^\mu v_\mu^A$, and v_μ^A is the four-velocity of the body, defined as $v_A^i \equiv dx_A^i/d\tau_A$. The index A labels the Ath body, and τ_A is its proper time. We also note that $\tilde{m}_A$ in (2.3) has the dimension of mass, σ_A and $\bar{\sigma}_A$ are defined as

$$\sigma_A \equiv -\left.\frac{d\ln\tilde{m}_A[\gamma_A]}{d\ln\gamma_A}\right|_{\gamma_A=1}, \quad \bar{\sigma}_A \equiv \left.\frac{d^2\ln\tilde{m}_A[\gamma_A]}{d(\ln\gamma_A)^2}\right|_{\gamma_A=1}, \tag{2.4}$$

which can be determined by considering asymptotic properties of perturbations of static stellar configurations [42]. Here, ln denotes the natural log [31].

The variations of the total action with respect to $g_{\mu\nu}$ and u^μ yield, respectively, the field equations [62],

$$R^{\mu\nu} - \frac{1}{2}g^{\mu\nu}R - S^{\mu\nu} = 8\pi G_{æ} T^{\mu\nu}, \tag{2.5}$$

$$Æ_\mu = 8\pi G_{æ} T_\mu, \tag{2.6}$$

with the constraint of Eq. (2.1). Note that we can recognize the $R_{\mu\nu} - \frac{1}{2}g_{\mu\nu}R = G_{\mu\nu}$ [28, 35, 136] from Eq. (2.5), where $R_{\mu\nu}$ is the Ricci tensor. Here we have [32],

$$\begin{aligned}
S_{\alpha\beta} &\equiv D_\mu\Big[J^\mu{}_{(\alpha}u_{\beta)} + J_{(\alpha\beta)}u^\mu - u_{(\beta}J_{\alpha)}{}^\mu\Big] \\
&\quad + c_1\Big[\left(D_\alpha u_\mu\right)\left(D_\beta u^\mu\right) - \left(D_\mu u_\alpha\right)\left(D^\mu u_\beta\right)\Big] \\
&\quad + c_4 a_\alpha a_\beta + \lambda u_\alpha u_\beta - \frac{1}{2}g_{\alpha\beta}J^\delta{}_\sigma D_\delta u^\sigma, \\
Æ_\mu &\equiv D_\alpha J^\alpha{}_\mu + c_4 a_\alpha D_\mu u^\alpha + \lambda u_\mu, \\
T^{\mu\nu} &\equiv \frac{2}{\sqrt{-g}}\frac{\delta\left(\sqrt{-g}\mathcal{L}_m\right)}{\delta g_{\mu\nu}} \\
&= \sum_A \tilde{m}_A\tilde{\delta}_A[A_A^1 v_A^\mu v_A^\nu + 2A_A^2 u^{(\mu}v_A^{\nu)}], \\
T_\mu &\equiv -\frac{1}{\sqrt{-g}}\frac{\delta\left(\sqrt{-g}\mathcal{L}_m\right)}{\delta u^\mu} = \sum_A \tilde{m}_A\tilde{\delta}_A A_A^2 v_\mu^A,
\end{aligned} \tag{2.7}$$

with parentheses in index pairs denoting index symmetrization and

$$J^\alpha{}_\mu \equiv M^{\alpha\beta}{}_{\mu\nu}D_\beta u^\nu, \quad a^\mu \equiv u^\alpha D_\alpha u^\mu, \tag{2.8}$$

and

$$\begin{aligned} A^1_A &\equiv 1+\sigma_A+\frac{(\sigma_A+\sigma_A^2+\bar{\sigma}_A)}{2}[(u_\mu v^\mu_A)^2-1], \\ A^2_A &\equiv -\sigma_A-(\sigma_A+\sigma_A^2+\bar{\sigma}_A)(u_\mu v^\mu_A+1), \\ \tilde{\delta}_A &\equiv \frac{\delta^3(\vec{x}-\vec{x}_A)}{v^0_A\sqrt{|g|}}. \end{aligned} \tag{2.9}$$

Here the vector $\vec{x}$ describes the position of the system that we are looking at while $\vec{x}_A$ describes the position of the Ath body (We will come back to this point later.). Note that we don't have $(A^1_A)^2 = A^2_A$. From Eq. (2.6) and the normalization condition, we also find that

$$\lambda = u_\beta D_\alpha J^{\alpha\beta} + c_4 a^2 - 8\pi G_{æ} T_\alpha u^\alpha, \tag{2.10}$$

where $a^2 \equiv a_\lambda a^\lambda$.

2.3 Gravitational Wave Polarizations and Energy Loss of Binary Systems in Einstein-æther Theory

The linear perturbations of Einstein-aether theory over a Minkowski background were studied by several authors [23,41,42,63]. For the sake of convenience, in this section I first give a brief review of the relevant materials, following mostly [62]. For more details on the PN approximations for many bodies in Einstein-aether theory, I refer the reader to [23,41,42,62]. Readers familiar with æ-theory may skip the first two subsections and go directly to the third part of this section if they wish, in which I apply previous results to binary systems.

Let us first note that

$$g_{\mu\nu} = \eta_{\mu\nu}, \qquad u^\mu = \delta^\mu_t, \tag{2.11}$$

satisfies the Einstein-aether field equations in Eqs. (2.5) and (2.6) in the coordinates $x^\mu = (t, x, y, z)$, where $\eta_{\mu\nu} = \text{diag}(-1, 1, 1, 1)$ is the Minkowski metric [35]. Clearly, Eq. (2.11) shows that the aether field u^μ is at rest in this Minkowski background [2], so any motion with respect to this coordinate system also represents motion with respect to the aether field. In addition, as far as the aether field is concerned, the time-like vector u^μ is invariant under the general spatial diffeomorphism $x'^j = x'^j(x^i)$, $(i, j = 1, 2, 3)$. Later, without loss of generality, we will use this gauge freedom to choose the plane of the binary system to coincide with the (x, y)-plane.

Now, we consider the linear perturbations,

$$h_{\mu\nu} = g_{\mu\nu} - \eta_{\mu\nu}, \quad w^0 = u^0 - 1, \quad w^i = u^i, \tag{2.12}$$

where $h_{\mu\nu}$, w^0 and w^i are decomposed into the forms [41],

$$\begin{aligned} h_{0i} &= \gamma_i + \gamma_{,i}, \quad w_i = \nu_i + \nu_{,i}, \\ h_{ij} &= \phi_{,ij} + \frac{1}{2}P_{ij}[f] + 2\phi_{(i,j)} + \phi_{ij}, \end{aligned} \tag{2.13}$$

with $P_{ij} \equiv \delta_{ij}\Delta - \partial_i\partial_j$, where $\Delta \equiv \delta^{ij}\partial_i\partial_j$ and the "," in the subscript stands for the derivative respect to the x^i. Note that the γ_i here has nothing to do with the γ_A in Eq. (2.3). In addition, the vector and tensor fields satisfy the conditions,

$$\partial^i\gamma_i = \partial^i\nu_i = \partial^i\phi_i = 0, \quad \partial^j\phi_{ij} = 0, \quad \phi_i{}^i = 0. \tag{2.14}$$

To the linear order in perturbation theory, it is convenient to define a non-symmetric tensor,

$$\tau^{\mu\nu} \equiv T^{\mu\nu} - T^\mu\delta^\nu_0, \ \ (\tau^{\mu\nu} \neq \tau^{\nu\mu}), \tag{2.15}$$

[2] In cosmology, the aether field is often chosen to be comoving with the CMB [27]. Thus, it is consistent here to choose the aether to be comoving with the Minkowski coordinate system $x^\mu = (t, x, y, z)$.

which satisfies the conservation law

$$\partial^{\nu}\tau_{\mu\nu} = 0. \tag{2.16}$$

Defining the center-of-mass (COM) coordinate and its velocity as

$$X^i \equiv \frac{\sum\limits_A m_A x^i_A}{\sum\limits_A m_A}, \tag{2.17}$$

$$V^i \equiv \frac{dX^i}{dt}, \tag{2.18}$$

we find that conservation of momentum requires

$$\frac{dV^i}{dt} = \ 0, \quad \Rightarrow \quad V^i = \text{Constant}. \tag{2.19}$$

2.3.1 Linearized Einstein-Æther Field Equations

Substituting the above expressions into the linearized Einstein-aether field equations, one finds that the tensor, vector and scalar parts can be written as follows [62]. For the tensor part, we have

$$\frac{1}{c_T^2}\ddot{\phi}_{ij} - \Delta\phi_{ij} \ = \ 16\pi G_{æ}\tau_{ij}^{TT}, \tag{2.20}$$

where "TT" stands for the transverse-traceless operator [137] acting on the tensor. Besides, a dot above represents the time derivative with respect to time t.

For the vector part, we have [3]

$$\frac{1}{c_V^2}(\ddot{\nu}^i + \ddot{\gamma}^i) - \Delta(\nu^i + \gamma^i) \ = \ \frac{16\pi G_{æ}}{2c_1 - c_{13}c_-}\left[c_{13}\tau_{i0} - (1-c_{13})T^i\right]^T, \tag{2.21}$$

$$\Delta\left(c_{13}\nu_i + \gamma_i\right) \ = \ -16\pi G_{æ}\tau_{i0}^T, \tag{2.22}$$

with the T above stands for the transverse operator [137] acting on the vector.

[3] Notice that the last term of Eq. (2.21) corrects a sign error in Eq. (44) of [41].

For the scalar part, we have

$$\frac{1}{c_S^2}\ddot{F} - \Delta F = \frac{16\pi G_{æ} c_{14}}{2 - c_{14}} \left(\tau_{kk} + \frac{2}{c_{14}} \tau_{00} - \frac{2 + 3c_2 + c_{13}}{c_{123}} \tau^L_{kk} \right), \quad (2.23)$$

$$\Delta \left(F - c_{14} h_{00} \right) = -16\pi G_{æ} \tau_{00}, \quad (2.24)$$

$$\left[(1 + c_2)\dot{F} + c_{123} \Delta \dot{\phi} \right]_{,i} = -16\pi G_{æ} \tau^L_{i0}, \quad (2.25)$$

where $F \equiv \Delta f$. Here the L above stands for the longitudinal operator [137] acting on the vector. In addition, the constraint in Eq. (2.1) gives

$$h_{00} = 2w^0. \quad (2.26)$$

Recall that c_T, c_V and c_S have already been provided in Sec.1.2. Also recall that we have $c_I \gtrsim 1$, where $I = S, V, T$ to avoid vacuum gravi-Čerenkov radiation [138] by matter. From these equations, we can easily infer that the tensor, vector and scalar modes propagate with speeds c_T, c_V and c_S, respectively.

2.3.2 Gravitational Wave Polarizations and Energy Loss

To consider the polarizations of gravitational waves in Einstein-aether theory, let us consider the time-like geodesic deviation equation. In the spacetime described by the metric, $g_{\mu\nu} = \eta_{\mu\nu} + h_{\mu\nu}$, the spatial deviation vector, ζ_i satisfies

$$\ddot{\zeta}_i = -R_{0i0j}\zeta^j \equiv \frac{1}{2}\ddot{\mathcal{P}}_{ij}\zeta^j, \quad (2.27)$$

where ζ_μ describes the four-dimensional deviation vector between two nearby trajectories of test particles, and

$$\begin{aligned} R_{0i0j} &\simeq \frac{1}{2}(h_{0j,0i} + h_{0i,0j} - h_{ij,00} - h_{00,ij}) \\ &= -\frac{1}{2}\ddot{\phi}_{ij} + \dot{\Psi}^{\rm II}_{(i,j)} + \Phi^{\rm IV}_{,ij} - \frac{1}{2}\delta_{ij}\ddot{\Phi}^{\rm II}, \end{aligned} \quad (2.28)$$

with $R_{\alpha\beta\mu\nu}$ denotes the Reimann tensor [28]. Here, $\Psi^{\rm II}_i$, $\Phi^{\rm IV}$ and $\Phi^{\rm II}$ are the gauge-invariant quantities defined in [62]. In particular, we have $\Phi^{\rm II} \equiv F/2$.

In the wave zone, $|\vec{x}| \gg d$, where d denotes the size of the source and $\vec{x}$ is the vector pointing to the observer from the COM, we have

$$\Phi^{\rm IV} = \frac{c_{14} - 2c_{13}}{2c_{14}(c_{13}-1)}\Phi^{\rm II}, \quad \Psi_i^{\rm II} = -\frac{c_{13}}{1-c_{13}}\Psi_i^{\rm I}, \tag{2.29}$$

and

$$\Psi^{\rm I}_{i,j} = -\frac{1}{c_V}\dot{\Psi}^{\rm I}_i N_j, \quad \Phi^{\rm II}_{,i} = -\frac{1}{c_S}\dot{\Phi}^{\rm II} N_i, \tag{2.30}$$

where N_k denotes the unit vector along the direction between the source (the COM) and the observer, and $\Psi_i^{\rm I}$ is another gauge-invariant quantity defined in [62] via the relation (More details about the gauge invariants mentioned here can be found in [62, 63].),

$$\Psi_i^{\rm I} \equiv \gamma_i + \nu_i. \tag{2.31}$$

Then, inserting the above expressions into (2.27) and (2.28) we obtain

$$\mathcal{P}_{ij} \;=\; \phi_{ij} - \frac{2c_{13}}{(1-c_{13})c_V}\Psi^{\rm I}_{(i}N_{j)} - \frac{c_{14}-2c_{13}}{c_{14}(c_{13}-1)c_S^2}\Phi^{\rm II}N_iN_j + \delta_{ij}\Phi^{\rm II}. \tag{2.32}$$

Assuming that $(\mathbf{e}_X, \mathbf{e}_Y, \mathbf{e}_Z)$ are three unit vectors that form a set of right-hand orthogonal basis [139] with $\mathbf{e}_Z \equiv \mathbf{N}$ (N_k), so that $(\mathbf{e}_X, \mathbf{e}_Y)$ lay on the plane orthogonal to the propagation direction $\mathbf{N}$ of the gravitational wave, we find that, in the coordinates $x^\mu = (t, x^i)$, these three vectors can be specified by two angles, ϑ and φ, via the relations [22],

$$\begin{aligned}
\mathbf{e}_X &= (\cos\vartheta\cos\varphi, \cos\vartheta\sin\varphi, -\sin\vartheta)\,, \\
\mathbf{e}_Y &= (-\sin\varphi, \cos\varphi, 0)\,, \\
\mathbf{e}_Z &= (\sin\vartheta\cos\varphi, \sin\vartheta\sin\varphi, \cos\vartheta)\,.
\end{aligned} \tag{2.33}$$

Then, we can define the six GW polarizations h_N's by

$$\begin{aligned} h_+ &\equiv \frac{1}{2}\left(\mathcal{P}_{XX}-\mathcal{P}_{YY}\right), \quad h_\times \equiv \frac{1}{2}\left(\mathcal{P}_{XY}+\mathcal{P}_{YX}\right), \\ h_b &\equiv \frac{1}{2}\left(\mathcal{P}_{XX}+\mathcal{P}_{YY}\right), \quad h_L \equiv \mathcal{P}_{ZZ}, \\ h_X &\equiv \frac{1}{2}\left(\mathcal{P}_{XZ}+\mathcal{P}_{ZX}\right), \quad h_Y \equiv \frac{1}{2}\left(\mathcal{P}_{YZ}+\mathcal{P}_{ZY}\right), \end{aligned} \tag{2.34}$$

where $\mathcal{P}_{AB} \equiv \mathcal{P}_{ij}e^i_A e^j_B$, with $A, B = \{X, Y, Z\}$. However, in Einstein-aether theory, only five GW polarizations are independent. With the help of Eq. (2.28) and some related equations, we find that the above expressions can be written explicitly in the form

$$\begin{aligned} h_+ &= \frac{1}{2}\phi_{ij}e^{ij}_+, & h_\times &= \frac{1}{2}\phi_{ij}e^{ij}_\times, \\ h_b &= \frac{1}{2}F, & h_L &= (1+2\beta_2)h_b, \\ h_X &= \frac{1}{2}\beta_1\nu^i e^i_X, & h_Y &= \frac{1}{2}\beta_1\nu^i e^i_Y, \end{aligned} \tag{2.35}$$

where $e^{kl}_+ \equiv e^k_X e^l_X - e^k_Y e^l_Y$ and $e^{kl}_\times \equiv e^k_X e^l_Y + e^k_Y e^l_X$, and

$$\beta_1 \equiv -\frac{2c_+}{c_V}, \quad \beta_2 \equiv +\frac{c_{14}-2c_+}{2c_{14}(1-c_+)c_S^2}. \tag{2.36}$$

Notice that a typo in [68] has been corrected here for β_2.

Observe that these equations for the GW polarizations are quite similar to those found for generic modified gravity theories in Chatziioannou, *et al.* [70] (See, e.g., Eq. 8 in [70].). The main difference here is that Chatziioannou, *et al.*, following Poisson and Will [22], made the implicit assumption that all GW modes travel at the same speed, and this speed is equal to the speed of light. As seen in the previous section, this is not the case in Einstein-aether theory, with some speeds already stringently constrained but others essentially unconstrained: $-3\times10^{-15} < c_T - 1 < 7\times10^{-16}$ due to GW170817 [60], which leads to $|c_{13}| = |c_+| \lesssim 10^{-15}$, but

$c_V \sim (c_1/c_{14})^{1/2} > 1$ and $c_S \sim (c_2/c_{14})^{1/2} > 1$ and are essentially unconstrained. Therefore, the results of Chatziioannou, *et al.* [70] cannot be straightforwardly applied to Einstein-aether theory, but rather they would have to be extended to allow for modes with different and arbitrary speeds.

In order to calculate the waveforms, let us first assume that the observers (or detectors) are located in a region far away from the source, $R \equiv |\vec{x}| \gg d$ (Of course, this R is not the Ricci scalar anymore.), where d is the typical size of the system. In this region, we have a useful mathematical method to solve the wave equations. That is, for equations in the form

$$\frac{1}{v_s^2}\ddot{\psi} - \Delta\psi = \ 16\pi\tau, \tag{2.37}$$

where ψ, v_s and τ are expediently used to denote the field we are going to solve for, the speed for the corresponding field, and a source term, respectively, we have the following asymptotic solution [6],

$$\psi(t,\vec{x}) \ = \ \frac{4}{R}\left[\sum_{n=0}^{\infty}\frac{1}{n!v_s^n}\frac{\partial^n}{\partial t^n}\int \tau(t-R/v_s,|\vec{x}^{\,\prime}|)\left(x^{\prime i}\cdot\frac{x^i}{R}\right)^n d^3x^{\prime}\right] + \mathcal{O}\Big(R^{-2}\Big). \tag{2.38}$$

Then, in the gauge [41],

$$\phi_i = 0, \qquad \nu = \gamma = 0, \tag{2.39}$$

we find that the wave equations given in the last subsection have the solutions

$$\phi_{ij} = \frac{2G_{æ}}{R}(\ddot{Q}_{ij})^{TT}, \tag{2.40}$$

$$\nu_i = -\frac{2G_{æ}}{(2c_1 - c_{13}c_-)R}\left[\frac{1}{c_V}\left(\frac{c_{13}}{1-c_{13}}\ddot{Q}_{ij} - \ddot{\mathcal{Q}}_{ij} - \mathcal{V}_{ij}\right)N^j + 2\Sigma^i\right]^T,$$

$$\gamma_i = -c_{13}\nu_i, \tag{2.41}$$

$$F = \frac{G_{æ}}{R}\frac{c_{14}}{2-c_{14}}\left[6(Z-1)\ddot{Q}_{ij}N^iN^j + 2Z\ddot{I} - \frac{4}{c_{14}c_S^2}\ddot{\mathcal{I}}_{ij}N^iN^j - \frac{8}{c_{14}c_S}\Sigma^iN^i\right],$$

$$h_{00} = 2\omega^0 = \frac{1}{c_{14}}F, \quad \phi = -\frac{1+c_2}{c_{123}}f, \tag{2.42}$$

where

$$\begin{aligned}
I_{ij} &\equiv \sum_A m_A x_A^i x_A^j, \quad I \equiv I_{kk}, \\
Q_{ij} &\equiv I_{ij} - \frac{1}{3}\delta_{ij}I, \\
\mathcal{I}_{ij} &\equiv \sum_A \sigma_A \tilde{m} x_A^i x_A^j, \quad \mathcal{I} \equiv \mathcal{I}_{ii}, \\
\mathcal{Q}_{ij} &\equiv \mathcal{I}_{ij} - \frac{1}{3}\delta_{ij}\mathcal{I}, \\
\Sigma^i &\equiv -\sum_A \sigma_A \tilde{m}_A v_A^i, \\
\mathcal{V}_{ij} &\equiv 2\sum_A \sigma_A \tilde{m}_A \dot{v}_A^{[i} x_A^{j]},
\end{aligned} \tag{2.43}$$

and

$$Z \equiv \frac{(\alpha_1 - 2\alpha_2)(1-c_+)}{3(2c_+ - c_{14})}. \tag{2.44}$$

α_1 and α_2 can be found in Eq. (1.8).

Finally, we note that for any symmetric tensor S_{ij} [I borrowed this notation temporarily from Eq. (2.7)], we will have $S_{ij}^{TT} = \Lambda_{ij,kl}S_{kl}$ and $S_i^T = P_{ij}S_j$, where $\Lambda_{ij,kl}$ and P_{ij} are the projection operators defined, respectively, by Eqs. (1.35) and (1.39) in [137].

Inserting Eqs. (2.40) - (2.42) into (2.35) and using the above equations, we find that

$$
\begin{aligned}
h_+ &= \frac{G_{æ}}{R}\ddot{Q}_{kl}e^{kl}_+, \qquad h_\times = \frac{G_{æ}}{R}\ddot{Q}_{kl}e^{kl}_\times,\\
h_b &= \frac{c_{14}G_{æ}}{R(2-c_{14})}\left[3(Z-1)\ddot{Q}_{ij}e^i_Z e^j_Z + Z\ddot{I} - \frac{4}{c_{14}c_S}\Sigma_i e^i_Z - \frac{2}{c_{14}c_S^2}\ddot{\mathcal{I}}_{ij}N^iN^j\right],\\
h_L &= \left[1 - \frac{c_{14}-2c_{13}}{c_{14}(c_{13}-1)c_S^2}\right]h_b,\\
h_X &= \frac{2c_{13}G_{æ}}{(2c_1-c_{13}c_-)c_V R}\left[\frac{e^i_Z}{c_V}\left(\frac{c_{13}}{1-c_{13}}\ddot{Q}_{ij} - \ddot{\mathcal{Q}}_{ij} - \mathcal{V}_{ij}\right) - 2\Sigma_j\right]e^j_X,\\
h_Y &= \frac{2c_{13}G_{æ}}{(2c_1-c_{13}c_-)c_V R}\left[\frac{e^i_Z}{c_V}\left(\frac{c_{13}}{1-c_{13}}\ddot{Q}_{ij} - \ddot{\mathcal{Q}}_{ij} - \mathcal{V}_{ij}\right) - 2\Sigma_j\right]e^j_Y. \qquad (2.45)
\end{aligned}
$$

The above expressions differ from the work of Hansen, *et al.* [58] because the latter built on the work of Chatziioannou, *et al.* [70], which as already explained, cannot be applied to Einstein-aether theory. Note, however, that although some of the dependence of the modes on the coupling constants c_i are different, the general structure of the solution found by Hansen, *et al.* [58] remains correct. For example, as found in that paper, and shown again by the above equations, the scalar longitudinal mode h_L is proportional to the scalar (breathing) mode h_b, which then means that out of the six possible GW polarizations, only five are independent. Moreover, as shown again in Hansen, *et al.* [58] and also in the equations above, the breathing and longitudinal modes are suppressed by a factor $c_{14} \lesssim \mathcal{O}\left(10^{-5}\right)$ [60] with respect to the transverse-traceless modes h_+ and $h_\times$[4], while the vectorial modes h_X and h_Y are suppressed by a factor $c_{13} \lesssim \mathcal{O}\left(10^{-15}\right)$ [60].

[4] The overall c_{14} cancels with $1/c_{14}$ in the last two terms inside the square brackets of h_b in Eq. (2.45). However, Σ_i and $\ddot{\mathcal{I}}_{ij}$ in these terms are proportional to $\sigma \sim s$. The sensitivity s scales with α_1 and α_2 [see Eq. (2.53)], which scale with c_{14} when $c_{13} \simeq 0$.

With the GW polarizations at hand, we can now move to the calculation of the energy flux. Using the Noether current method described in [32, 140], we find that the energy loss rate is given by

$$\dot{E}_b = -\frac{1}{16\pi G_{\text{æ}}}\left\langle \int d\Omega R^2 \left[\frac{1}{2c_T}\dot{\phi}_{ij}\dot{\phi}_{ij} + \frac{(2c_1 - c_{13}c_-)(1-c_{13})}{c_V}\dot{\nu}^i\dot{\nu}^i + \frac{2-c_{14}}{4c_S c_{14}}\dot{F}\dot{F}\right]\right\rangle + \dot{O}, \tag{2.46}$$

where an overhead dot stands for a time derivative, Ω is the solid angle, and the angular brackets stand for an average over one period, defined by

$$\langle \mathcal{H}(t)\rangle \equiv \frac{1}{P_b}\int_0^{P_b}\mathcal{H}(t)dt, \tag{2.47}$$

with P_b the orbital period [141]. The last term $\dot{O}$ will be omitted from now on, since its purpose is just to cancel secular terms that arise from the other terms in this equation, as discussed in detail in [32, 42]. Using the mathematical tricks presented in [137], we find that Eq. (2.46) becomes

$$\dot{E}_b = -G_{\text{æ}}\left\langle \frac{\mathcal{A}_1}{5}\dddot{Q}_{ij}\dddot{Q}_{ij} + \frac{\mathcal{A}_2}{5}\dddot{Q}_{ij}\ddot{\mathcal{Q}}_{ij} + \frac{\mathcal{A}_3}{5}\ddot{\mathcal{Q}}_{ij}\ddot{\mathcal{Q}}_{ij} + \mathcal{B}_1\ddddot{I}\ddddot{I} + \mathcal{B}_2\ddddot{I}\ddddot{\mathcal{I}} + \mathcal{B}_3\ddddot{\mathcal{I}}\ddddot{\mathcal{I}} + \mathcal{C}\dot{\Sigma}^i\dot{\Sigma}^i + \mathcal{D}\dot{\mathcal{V}}_{ij}\dot{\mathcal{V}}_{ij}\right\rangle, \tag{2.48}$$

where

$$\begin{aligned}
&\mathcal{A}_1 \equiv \frac{1}{c_T} + \frac{2c_{14}c_{13}^2}{(2c_1 - c_{13}c_-)^2 c_V} + \frac{3c_{14}(Z-1)^2}{2(2-c_{14})c_S},\\
&\mathcal{A}_2 \equiv -\frac{2c_{13}}{(2c_1 - c_{13}c_-)c_V^3} - \frac{2(Z-1)}{(2-c_{14})c_S^3}, \quad \mathcal{A}_3 \equiv \frac{1}{2c_{14}c_V^5} + \frac{2}{3c_{14}(2-c_{14})c_S^5},\\
&\mathcal{B}_1 \equiv \frac{c_{14}Z^2}{4(2-c_{14})c_S},\\
&\mathcal{B}_2 \equiv -\frac{Z}{3(2-c_{14})c_S^3}, \quad \mathcal{B}_3 \equiv \frac{1}{9c_{14}(2-c_{14})c_S^5},\\
&\mathcal{C} \equiv \frac{4}{3c_{14}c_V^3} + \frac{4}{3c_{14}(2-c_{14})c_S^3}, \quad \mathcal{D} \equiv \frac{1}{6c_{14}c_V^5}.
\end{aligned} \tag{2.49}$$

Note that in the above expressions, we corrected a simple typo (minus signs in $\mathcal{A}_2$) in previous work [42], which originates from the sign error in [32], and which has been corrected in Eq. (2.21) as already mentioned.

2.3.3 Binary Systems

In this part, we apply the general formula developed in the last two sections to a binary system. Before doing so, let us first note that such a problem has already been considered in Hansen, *et al.* [58], as discussed earlier. The work here differs from that of Hansen, *et al.* in that (i) I include in the calculation of the GW polarization modes by considering the fact that the different fields of Einstein-aether theory travel at different velocities, and (ii) I allow for the COM to not be comoving with the aether, i.e., I allow $V^i \neq 0$. The latter condition is more general than that adopted previously in the literature, thus allowing for the possibility that the aether flow may be in a different direction as compared to the motion of the COM.

With the above in mind, we first assume that the binary components are in a quasi-circular orbit. By "quasi-circular" we mean that the two celestial bodies are rotating in a fixed plane and the orbit for its one-body effective model is almost a circle within one period [142]. In addition, we also assume that $\dot{\omega}_s \ll \omega_s^2$, where $\omega_s = 2\pi/P_b$ denotes the orbital angular frequency of the orbit [137]. Then, to leading (Newtonian) order in the PN theory, we have

$$\dot{v}^i \equiv \ddot{r}^i \simeq -\frac{\mathcal{G}m}{r^2}\hat{r}^i\left[1+\mathcal{O}\left(\frac{\mathcal{G}m}{r}\right)\right], \tag{2.50}$$

$$v^2 \equiv v^i v^i \simeq \frac{\mathcal{G}m}{r}\left[1+\mathcal{O}\left(\frac{\mathcal{G}m}{r}\right)\right], \tag{2.51}$$

where $r = |x_1^i - x_2^i|$ is the distance between the two bodies and $\hat{r}^i \equiv r^i/r \equiv (x_1^i - x_2^i)/r$ and m is the total mass. Here, the relation between $\mathcal{G}$ and G_N is given by

$$\mathcal{G} \equiv G_N(1 - s_1)(1 - s_2), \tag{2.52}$$

where s_A is related to σ_A via the relation, $s_A \equiv \sigma_A/(1 + \sigma_A)$. In [42], the sensitivities for neutron stars were calculated numerically for various choices of the coupling constants c_i's. Unfortunately, all of those choices are out of the current physically viable region defined in Eq. (1.9). In [32], an analytical expression in the weak-field approximations was given,

$$s_A = \left(\alpha_1 - \frac{2}{3}\alpha_2\right)\frac{\Omega_A}{m_A} + \mathcal{O}\left(\frac{G_N m}{d}\right)^2, \tag{2.53}$$

where Ω_A is the binding energy of the A-th body [5] and we recall d represents the characteristic size of the system. This expression is only valid for weakly-gravitating bodies, and thus, strictly speaking, it does not apply to neutron stars or to black holes when considering strong-field effects; for neutron stars, the sensitivities are about an order of magnitude larger and they depend on the equation of state, while for black holes, they may be identically zero, as in the case of khronometric gravity within a parameter space that is of physical interest [131].

Since the choice of coordinates x^μ comoving with the æ-field [cf. Eq. (2.11)] is fixed only up to the spatial diffeomorphism $x'^i = x'^i\left(x^k\right)$, as mentioned earlier, we can use this remaining gauge freedom to choose the spatial coordinates so that the binary system is always on the (x, y)-plane. This then implies that $\hat{\mathbf{r}}$ $(\hat{r}^i)$ can be

[5] Note that there is an extra factor c_{14} appearing in Eq. (70) of [32] in the published version, which has been corrected in the arXiv version.

parameterized via

$$\hat{\mathbf{r}} = \cos\Phi\hat{\mathbf{i}} + \sin\Phi\hat{\mathbf{j}}, \tag{2.54}$$

where $\Phi(t) \equiv \int^t w_s(t')dt'$ is the orbital phase of the binary system, and $\hat{\mathbf{i}}$, $\hat{\mathbf{j}}$, $\hat{\mathbf{k}}$ are unit vectors along the x, y and z directions respectively, with $\hat{\mathbf{k}} = \hat{\mathbf{i}} \times \hat{\mathbf{j}}$.

Substituting the above expressions into Eq. (2.45) and only keeping terms up to relative $\mathcal{O}(v^2)$, where V^i is assumed to be of $\mathcal{O}(v)$, we find,

$$h_+ = -\frac{2G_{æ}}{R}\mathcal{M}\mathcal{U}^2(1+\cos^2\vartheta)\cos(2\Theta) + \underbrace{\frac{2G_{æ}}{R}mV^kV^le_+^{kl}}, \tag{2.55}$$

$$h_\times = \frac{4G_{æ}}{R}\mathcal{M}\mathcal{U}^2\cos\vartheta\sin(2\Theta) + \underbrace{\frac{2G_{æ}}{R}mV^kV^le_\times^{kl}}, \tag{2.56}$$

$$\begin{aligned} h_b = {} & \frac{2G_{æ}}{R}\frac{c_{14}}{2-c_{14}} \\ & \times\Bigg[\frac{2\Delta s}{c_{14}c_S}\eta^{1/5}\mathcal{M}\mathcal{U}\sin\vartheta\sin\Theta + \frac{2\mathcal{S}-3c_{14}(Z-1)c_S^2}{c_{14}c_S^2}\mathcal{M}\mathcal{U}^2\sin^2\vartheta\cos(2\Theta) \\ & \quad - \frac{4\Delta s}{c_{14}c_S^2}\eta^{1/5}\mathcal{M}\mathcal{U}(V^iN^i)\sin\vartheta\sin\Theta \\ & \quad + \underbrace{\frac{3c_{14}c_S^2(Z-1)-2\mathcal{S}'}{c_{14}c_S^2}mV^iV^jN^iN^j} + \underbrace{\frac{2\mathcal{S}'}{c_{14}c_S}mV^iN^i + mV^iV^i}\Bigg], \end{aligned} \tag{2.57}$$

$$h_L = \left[1 + \frac{c_{14}-2c_{13}}{c_{14}(1-c_{13})c_S^2}\right]h_b, \tag{2.58}$$

$$\begin{aligned} h_X = {} & -\frac{\beta_1 G_{æ}}{R}\frac{1}{2c_1 - c_{13}c_-} \\ & \times\Bigg[-2\Delta s\eta^{1/5}\mathcal{M}\mathcal{U}\cos\vartheta\sin\Theta + \frac{1}{c_V}\left(\mathcal{S} - \frac{c_{13}}{1-c_{13}}\right)\mathcal{M}\mathcal{U}^2\sin(2\vartheta)\cos(2\Theta) \\ & \quad - \frac{2\Delta s}{c_V}\eta^{1/5}\mathcal{M}\mathcal{U}\big(\sin\vartheta e_X^i + \cos\vartheta N^i\big)V^i\sin\Theta \\ & \quad - \underbrace{\frac{2m}{c_V}\left(\mathcal{S}' - \frac{c_+}{1-c_+}\right)V^iV^je_X^iN^j} - \underbrace{2\mathcal{S}'me_X^iV^i}\Bigg], \end{aligned} \tag{2.59}$$

$$
\begin{aligned}
h_Y &= -\frac{\beta_1 G_{æ}}{R}\frac{1}{2c_1 - c_{13}c_-} \\
&\quad \times\Bigg[-2\Delta s\eta^{1/5}\mathcal{M}\mathcal{U}\cos\Theta - \frac{2}{c_V}\left(\mathcal{S} - \frac{c_{13}}{1-c_{13}}\right)\mathcal{M}\mathcal{U}^2\sin(\vartheta)\sin(2\Theta) \\
&\qquad - \frac{2\Delta s}{c_V}\eta^{1/5}\mathcal{M}\mathcal{U}\big(\sin\vartheta\sin\Theta e_Y^i + \cos\Theta N^i\big)V^i \\
&\qquad \underbrace{- \frac{2m}{c_V}\left(\mathcal{S}' - \frac{c_+}{1-c_+}\right)V^iV^je_Y^iN^j} \underbrace{- 2\mathcal{S}'me_Y^iV^i}\Bigg],
\end{aligned}
\tag{2.60}
$$

where

$$
\begin{aligned}
&m \equiv m_1 + m_2, \quad \mu_A \equiv \frac{m_A}{m}, \quad \mu \equiv \mu_1\mu_2 m, \\
&\eta \equiv \frac{\mu}{m}, \quad \mathcal{M} \equiv m\eta^{3/5}, \quad \mathcal{U} \equiv (\mathcal{G}\mathcal{M}\omega_s)^{1/3},
\end{aligned}
\tag{2.61}
$$

and

$$
\begin{aligned}
&\Delta s \equiv s_1 - s_2, \quad \mathcal{S} \equiv s_1\mu_2 + s_2\mu_1, \\
&\Theta \equiv \varphi - \Phi, \quad \mathcal{S}' \equiv s_1\mu_1 + s_2\mu_2.
\end{aligned}
\tag{2.62}
$$

Now several comments are in order. First, the above expressions for the plus and cross polarization modes [Eqs. (2.55) and (2.56)] reduce to those of GR [6] [58, 70], when c_i's and s_i's are set to be zero. The quantity φ determines the coalescence phase, the value of which can be chosen arbitrarily. References [58, 70] use the convention $\varphi = 0$, which will be adopted in this chapter. Second, these expressions are also similar to those found in Hansen, *et al.* [58] to leading order in the PN expansion. However, since Hansen, *et al.* [58] used a formalism that implicitly assumed the speed of all modes is the speed of light, which is not the case in Einstein-aether theory, there are factors of (c_T, c_V, c_S) missing in that work, which I correct here. Third, the under-braced terms have not appeared in the literature previously. That's because they will

[6] There is a simple transcription typo in [58], which accidentally dropped factor of $\eta^{1/5}$ in these modes.

be safely neglected for our current studies, since they are time-independent, and lead to no contributions to the geodesic deviation equation [Eq. (2.27)], as can be seen from Eqs. (2.27)-(2.32). Fourth, the above expressions contain terms that are sub-leading in the PN approximation [i.e. they are of $\mathcal{O}(v)$ smaller than the leading-order modifications], and these have also never appeared in the literature. This is not just because they are sub-leading in the PN approximation, but also because they depend on the COM velocity V^i, which is typically assumed to be of order 10^{-3} with respect to the CMB rest frame [32], and thus is much smaller than the relative velocity of binary constituents before coalescences. These terms, however, cannot be neglected as they are time-dependent, and proportional to $\cos\Theta,\ \sin\Theta$. Fifth, strictly speaking, Eqs. (2.55)-(2.60) should be evaluated at the retarded time t_r, where $t_r \equiv t - R/c_N$, with c_N being any of (c_T, c_V, c_S), depending on the mode under consideration.

With the above in mind, substituting (2.50), (2.51), (2.43) and (2.54) into Eq. (2.48), we find that

$$\begin{aligned}
\dot{E}_b &= -\frac{G_{æ}\mathcal{G}^2\mu^2 m^2}{r^4} \\
&\times\Bigg\langle \frac{8}{15}(\mathcal{A}_1+\mathcal{S}\mathcal{A}_2+\mathcal{S}^2\mathcal{A}_3)(12v^2-11\dot{r}^2)+4(\mathcal{B}_1+\mathcal{S}\mathcal{B}_2+\mathcal{S}^2\mathcal{B}_3)\dot{r}^2 \\
&\quad+\frac{1}{5}\Delta s[8(\mathcal{A}_2+2\mathcal{S}\mathcal{A}_3)(3\dot{r}^j-2\dot{r}^i\hat{r}^i\hat{r}^i\hat{r}^j)+60(\mathcal{B}_2+2\mathcal{S}\mathcal{B}_3)\dot{r}^i\hat{r}^i\hat{r}^j]V^j \\
&\quad+\Delta s^2\left[\left(\frac{6}{5}\mathcal{A}_3+36\mathcal{B}_3-2\mathcal{D}\right)(\hat{r}^iV^i)^2+\left(\frac{18}{5}\mathcal{A}_3+2\mathcal{D}\right)V^iV^i+\mathcal{C}\right]\Bigg\rangle.
\end{aligned} \tag{2.63}$$

It is interesting to note that this result reduces identically to that found by Yagi, *et al.* [42], since in that work, no assumption was made on the speed of the propagating modes.

Equation (2.63) includes Einstein-æther corrections both at -1PN ($\dot{E}_b \propto v^8$) and 0PN ($\dot{E}_b \propto v^{10}$) orders. When deriving this equation, I only considered the Newtonian contribution in the conservative sector in Eqs. (2.50) and (2.51). Formerly, the 1PN correction to the conservative dynamics can affect $\dot{E}_b$ at 0PN order. This is because such 1PN effect can couple to the -1PN dipole radiation in Eq. (2.48) to give rise to a 0PN effect in Eq. (2.63). This section does not include such corrections since they can never become a dominant correction (as they are 1PN correction to the -1PN effect). On the other hand, the 0PN effect included in Eq. (2.63) can dominate the -1PN effect when, e.g., $s_1 \sim s_2$ and the dipole radiation is suppressed.

2.4 Evolution of the Orbital Angular Frequency

The emission of gravitational waves causes the separation of the two bodies in a binary system to shrink, which thus leads the orbital frequency to grow, until coalescence occurs. In this section, we find the evolution of the orbital angular frequency ω_s through the use of the energy loss rate. Note that there is a different, yet equivalent, way to get the same result through the Virial theorem (See, e.g., [137, 143].).

The evaluation of the time-domain waveform requires that one solves the equations of motion in Einstein-aether theory. As explained in the previous section, these equations take on a Newtonian-like form, and their solution can be described effectively by Eq. (2.54). All one needs to prescribe now is the evolution of the orbital angular frequency, which we study here to the leading PN order. This equation can be obtained through the Einstein-aether version of Kepler's law [137],

$$\omega_s^2 \simeq \frac{\mathcal{G}m}{r^3}, \tag{2.64}$$

which yields

$$\frac{\dot{\omega}_s}{\omega_s} = \frac{3}{2}\frac{\dot{E}_b}{E_b}, \tag{2.65}$$

where E_b in the denominator is the binding energy [42], namely

$$E_b = -\frac{\mathcal{G}\mu m}{2r}. \tag{2.66}$$

Substitution of Eqs. (2.66), (2.63), (2.64) and (2.54) into Eq. (2.65) leads to

$$(\mathcal{G}m)^2\dot{\omega}_s = (\mathcal{G}m)^2\frac{d\omega_s}{dt} = \kappa_1(\mathcal{G}m\omega_s)^{11/3}\left[1+\epsilon_x\left(\mathcal{G}m\omega_s\right)^{-2/3}\right], \tag{2.67}$$

where

$$\kappa_1 \equiv \frac{48\eta(2-c_{14})}{5(1-s_1)(1-s_2)}\left(\mathcal{A}_1+\mathcal{S}\mathcal{A}_2+\mathcal{S}^2\mathcal{A}_3\right), \tag{2.68}$$

$$\epsilon_x \equiv \frac{\Delta s^2}{32(\mathcal{A}_1+\mathcal{S}\mathcal{A}_2+\mathcal{S}^2\mathcal{A}_3)} \times\left[(21\mathcal{A}_3+90\mathcal{B}_3+5\mathcal{D})V^iV^i-(3\mathcal{A}_3+90\mathcal{B}_3-5\mathcal{D})(V^3)^2+5\mathcal{C}\right]. \tag{2.69}$$

Also note that we have used the quasi-circular condition.

Solving Eq. (2.67) exactly is not possible, but a good approximation to the solution can be obtained when ϵ_x is small enough, i.e., when $\epsilon_x \ll 1$. Since $\mathcal{A}_1$ is $\mathcal{O}(1)$ and $\mathcal{S}$, as well as $\mathcal{S}^2$, are suppressed by the sensitivities according to the definition in Eq. (2.62), the contribution of the denominator of Eq. (2.69) is $\mathcal{O}(1)$. Moreover, by using Eq. (2.49), we see that the coefficients of the V^i-related terms are all of $\mathcal{O}(c_{14}^{-1}c_{V,S}^{-5})$, while $\mathcal{C}$ is of $\mathcal{O}(c_{14}^{-1}c_V^{-3}+c_{14}^{-1}c_S^{-3})$. Now recall that for $|c_{13}| \lesssim 10^{-15}$ we have $c_S \simeq \mathcal{O}(c_2/c_{14})^{1/2}$ and $c_V \simeq \mathcal{O}(c_1/c_{14})^{1/2}$, as one can see from Eq. (1.7). Thus, because V^i is assumed to be of $\mathcal{O}(v)$ or smaller (see [32]), the contribution from the numerator is of $\mathcal{O}(\Delta s^2\mathcal{C})$. Putting everything together and using the expressions for $\mathcal{C}$, we first find that

$$\epsilon_x \leq \frac{5}{24}\Delta s^2 c_{14}^{1/2}\left(c_1^{-3/2}+c_2^{-3/2}\right). \tag{2.70}$$

Observe that if $\Delta s^2 \ll 1$, either because $s_1 = 0 = s_2$ (as may be the case in black hole binaries) or because $s_1 = s_2$ (equal-mass neutron star binaries), then ϵ_x is always small and the approximation is automatically well-justified. Moreover, if we insert the weak-field limit for the sensitivities in Eq. (2.53), the above expression could be further written as

$$\epsilon_x \leq \frac{605}{216} c_{14}^{5/2} \left(\frac{\Omega_1}{m_1} - \frac{\Omega_2}{m_2} \right)^2 \left(c_1^{-3/2} + c_2^{-3/2} \right) \leq 7 \times 10^{-5}, \tag{2.71}$$

where we have used that $c_{14} \lesssim 2.5 \times 10^{-5}$ and $c_{1,2} \gtrsim c_{14}$ from Eq. (1.9), and that $\Omega_A \leq m_A$. Clearly then, the above analysis justifies the search for a perturbative solution to Eq. (2.67) in $\epsilon_x \ll 1$.

Even though the requirement that $\epsilon_x \ll 1$ is satisfied when one saturates current constraints on the theory, a perturbative solution to Eq. (2.67) actually requires

$$\epsilon_x \ll (\mathcal{G} m \omega_s)^{2/3}, \tag{2.72}$$

which may be more severe when the binary's orbital velocity is small enough. Notice, however, that this implies that $v \gtrsim 0.05$, which is true in the regime of interest of the second-generation ground-based gravitational wave detectors. In such a region, we can perturbatively expand the solution to find

$$\omega_s(t) \simeq \kappa_2^{-3/8} (\mathcal{G} m)^{-5/8} (t_c - t)^{-3/8} \left[1 - \frac{3}{10} \epsilon_x \kappa_2^{1/4} \left(\frac{t_c - t}{\mathcal{G} m} \right)^{1/4} \right], \tag{2.73}$$

where

$$\kappa_2 \equiv \frac{128 \eta (2 - c_{14})}{5(1 - s_1)(1 - s_2)} \left(\mathcal{A}_1 + \mathcal{S} \mathcal{A}_2 + \mathcal{S}^2 \mathcal{A}_3 \right), \tag{2.74}$$

and t_c is the moment of coalescence. Clearly, the above results reduce to the well-known expression [137] in GR limit:

$$\omega_s^{GR}(t) = \frac{1}{8} \left(\frac{\eta}{5} \right)^{-3/8} (G_N m)^{-5/8} (t_c^{GR} - t)^{-3/8}. \tag{2.75}$$

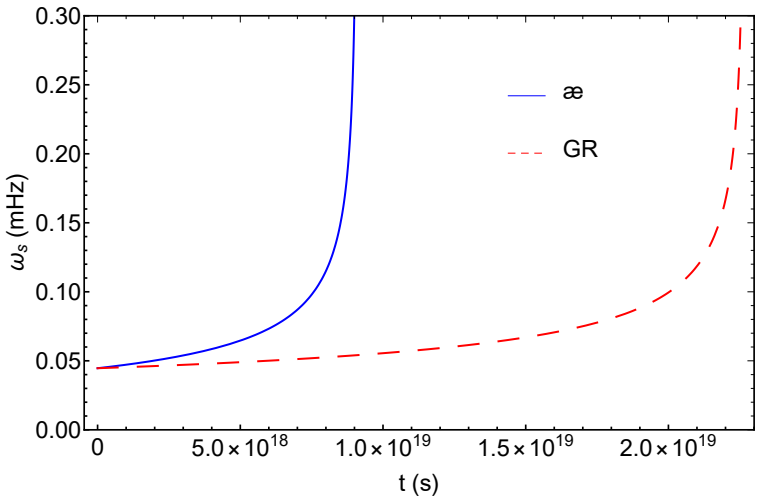

Figure 2.1: Evolution of the orbital angular frequency $\omega_s(t)$ of the inner binary in the hierarchy triple system J0337 starting at January-04-2012 to the binary's final stage [132], as given by Eqs. (2.73) and (2.75) for æ-theory and GR, respectively. It is clear that the orbital angular frequency grows and becomes unbounded at the coalescence time. Note, however, that the coalescence time for the two theories is different ($t_c \sim 9\times10^{18}$ s and $t_c^{GR} \sim 2\times10^{19}$ s), because the additional polarization modes of Einstein-aether theory cause the binary to lose binding energy faster than in GR, thus forcing the binary to merge earlier.

Fig. 2.1 shows the difference between the GR and æ-theory evolution of the orbital angular frequency [7] for the inner binary in the hierarchy triple system PSR J0337+1715 (denoted J0337 henceforth) [132,147]. Specifically, we set $m_1 = 1.4378M_\odot$, $m_2 = 0.19751M_\odot$, and $\omega_s(t=0) \approx 0.0000446$ Hz , where $t = 0$ stands for the time that J0337 was first observed and $M_\odot$ denotes the solar mass. Moreover, we choose the coupling constants to be $c_1 = 4\times10^{-5}$, $c_2 = 9\times10^{-5}$, $c_4 = -2\times10^{-5}$ and $c_3 = -c_1$ as in [62]. These choices won't strictly satisfy all constraints in [60], although they are quite close to the physical viable region (this point is accidentally overlooked in the published version). Nonetheless, they are currently sufficient for an illustrative

[7] In plotting Fig. 2.1 we just used the time coordinate t, instead of the retarded time, $t_r^A \equiv t - R/c_A$ [144–146]. Since ω_s is a function of $(t_c - t)$, there is no difference, as $t_c - t = (t_c - R/c_A) - (t - R/c_A) = t^A_{r,c} - t^A_r$ (the subscript "A" here is to distinguish the different kinds of propagation modes: scalar, vector and tensor).

purpose. Actually, I also investigated the results with the latest physical viable c_i's. It turns out that the quantitative results are just slightly changed while our conclusions addressed from these present results are not influenced at all qualitatively. For the COM velocity, we randomly choose $\vec{V} = (0.002, 0.01, 0.03)$, which satisfies the constraints given in [32]. The sensitivities of neutron stars are not known in this region of parameter space, so for illustrative purposes only, we use there the weak-field expression of Eq. (2.53), with $\Omega_A/m_A = G_N m_A/R_A$ and $(R_1, R_2) = (12.7, 6.33 \times 10^4)$ km. These parameter choices satisfy the perturbative condition $\epsilon_x(\mathcal{G}m\omega_s)^{-2/3} \ll 1$ for about 1/1000 of its life time, viz., the duration from the date J0337 was first observed in 2012 to its future merger. Because the time interval before merger is so long, the parameter choices satisfy the perturbative condition $\epsilon_x(\mathcal{G}m\omega_s)^{-2/3} \ll 1$ during a time much longer than the designed observing window of LISA-like detectors.

Once ω_s is known, one can insert it into Eqs. (2.55) - (2.60) to find the GW polarizations. Given the large number of cycles present in these time-domain waveforms, however, it is impractical to plot them straightly as functions of time. A better alternative is to decompose the signals into an amplitude and a phase, via

$$\begin{aligned} h_+ &\equiv A_+ \cos(2\Theta), \\ h_\times &\equiv A_\times \sin(2\Theta), \\ h_b &\equiv A_{b2} \cos(2\Theta) + A_{b1} \sin(\Theta), \\ h_L &\equiv A_{L2} \cos(2\Theta) + A_{L1} \sin(\Theta). \end{aligned} \tag{2.76}$$

Recall that the phase Θ here is defined from the orbital phase Φ through Eq. (2.62). Figures 2.2 and 2.3 show the time-domain amplitudes and orbital phase for a binary

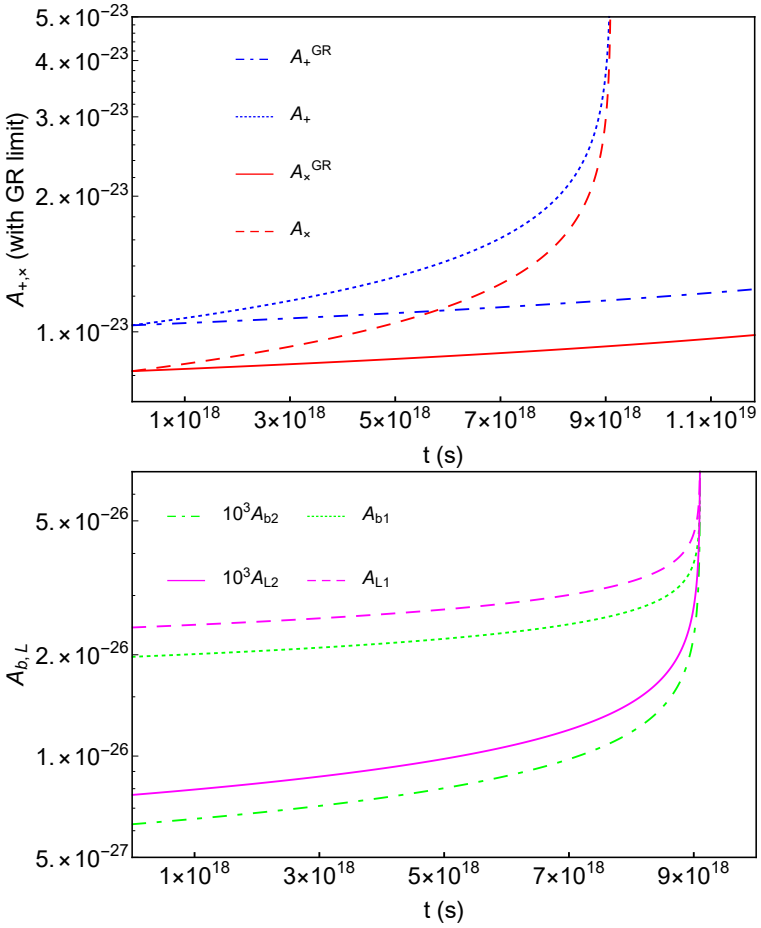

Figure 2.2: Temporal evolution of the amplitudes of the GW polarizations for the inner binary in the hierarchy triple system J0337 [132]. The upper panel shows the + and × modes in GR and in æ-theory. The lower panel shows the breathing and longitudinal modes in æ-theory, where the subscript 1 and 2 correspond to the harmonic sequence number. Observe that the second harmonic is rescaled by a factor of 10^3 relative to the first harmonic, which implies the latter is much larger. Observe also that the amplitudes in æ-theory diverge faster than in GR because the binary inspirals more rapidly.

with the same parameters as those chosen for Fig. 2.1. In addition, we have here chosen $\vartheta = 39.254$ degrees, according to [132], and $\varphi = 70$ degrees as a heuristic example. To more clearly see the difference between the GR and the æ-theory evolution, we also plot the amplitudes in the GR limit (see also Eq. (4.29) of [137]).

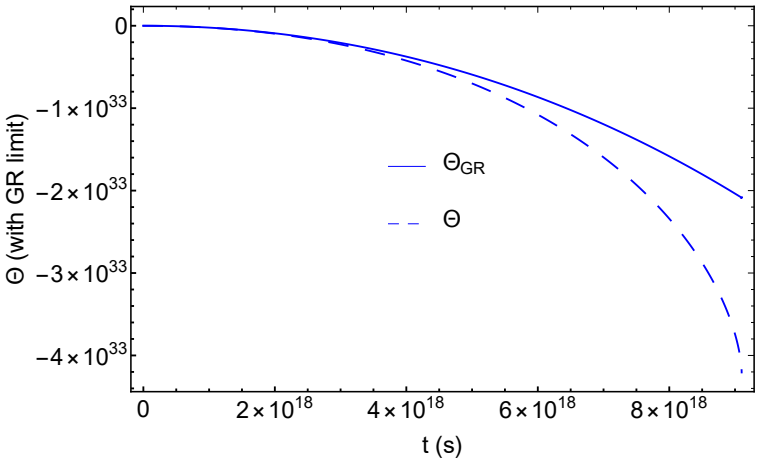

Figure 2.3: Temporal evolution of the phases of the GW polarizations for the inner binary in the hierarchy triple system J0337 [132] in GR and in æ-theory. Note that the phases here are different from the orbital phases in Eq. (2.62), although the differences are trivial.

These figures deserve several comments. First, notice that with the choice of parameters we have made to make these figures (specifically with $c_{13} = 0$), the $h_{X,Y}$ modes vanish identically. Even if we had saturated current constraints by setting $c_{13} = 10^{-15}$, the amplitudes of these vector modes would be suppressed by at least 15 orders of magnitude relative to the plus and cross modes. The implication then is clear: GW interferometers will never be able to detect these modes directly. Second, observe that the scalar modes $h_{b,L}$ are suppressed relative to the tensor modes $h_{+,\times}$ by a factor of 10^3. This then implies that it will be extremely difficult for GW detectors to measure these modes directly (This is one of the crucial motivations for us to move

to the realm of ringdown stage, although we are also caring about the inspiral stage.). However, we observe from the figures that the amplitude and the phase of the tensor mode is clearly modified, and this is a feature that could be constrained with GW instruments. This is true especially for BNSs since the approximation in Eq. (2.53) is better in that case, as discussed previously. Therefore, in the case of Einstein-aether theory, it is clear that constraints on the temporal (or frequency) evolution of the tensor modes are much more stringent than any polarization test that proves that GW signals only contain + and × modes.

2.5 Response Function

Gravitational waves emitted by massive binary systems have attracted a lot of attention recently, as they could be ideal sources for both ground- and space-based detectors, such as LIGO, Virgo, KAGRA [148], LISA, TianQin [71], Taiji and DECIGO [108]. Therefore, in this section we consider the response function for both kinds of detectors.

2.5.1 Ground-Based L-Shape Detectors

With the expressions for the GW polarization modes in the coordinate space in hand, we are ready to calculate the response function $h(t)$ and its Fourier transform $\tilde{h}(f)$ [of course, this f is different from the one in Eq. (2.42)]. In this subsection, we shall focus on L-shape detectors, such as LIGO, Virgo and KAGRA [149]. From [22, 70], we find

$$h(t) = \sum_N F_N(\theta, \phi, \psi)\, h_N(t), \tag{2.77}$$

where

$$
\begin{aligned}
F_+ &\equiv \frac{1}{2}(1+\cos^2\theta)\cos 2\phi\cos 2\psi - \cos\theta\sin 2\phi\sin 2\psi,\\
F_\times &\equiv \frac{1}{2}(1+\cos^2\theta)\cos 2\phi\sin 2\psi + \cos\theta\sin 2\phi\cos 2\psi,\\
F_b &\equiv -\frac{1}{2}\sin^2\theta\cos 2\phi, \quad F_L \equiv \frac{1}{2}\sin^2\theta\cos 2\phi,\\
F_X &\equiv -\sin\theta(\cos\theta\cos 2\phi\cos\psi - \sin 2\phi\sin\psi),\\
F_Y &\equiv -\sin\theta(\cos\theta\cos 2\phi\sin\psi + \sin 2\phi\cos\psi).
\end{aligned}
\tag{2.78}
$$

Here $\{\theta, \phi, \psi\}$ are the three angles that specify the relative orientations of the detector with respect to the source [note that the angle ϕ here is not the same as the metric perturbation ϕ used in Eq. (2.13)]. Their definitions can be found in [22] (see, for example, Fig. 11.5 in that reference). To calculate the Fourier transform (FT) of the response function $h(t)$, we shall adopt the SPA [70,96,134]. In Appendix A, I present a brief summary of this method. For more details, I refer readers to [70, 96, 134] and references therein.

Let us first write Eq. (2.77) in the form,

$$
h(t) \equiv \sum_N H_N(t), \tag{2.79}
$$

where $H_N(t) \equiv F_N h_N(t)$, and the subscript N ranges over all the polarization modes, i.e., $N \in \{+, \times, b, L, X, Y\}$. We can then define the Fourier transform $\tilde{h}(f)$ as

$$
\tilde{h}(f) \equiv \int h(t) e^{i2\pi ft} dt = \sum_N \tilde{H}_N(f), \tag{2.80}
$$

where $\tilde{H}_N(f)$ is the Fourier transform of $H_N(t)$. Note that the above definition is slightly different from the one used in [62,63] (actually, the definitions of FT will vary in different references [29, 150]). For computational convenience, let us also rewrite

$H_N(t)$ as

$$H_N(t) = \left[q_{N(1)}\cos(2\Phi) + q_{N(2)}\sin(2\Phi)\right]\omega_s^{2/3} + \left[q_{N(3)}\cos\Phi + q_{N(4)}\sin\Phi\right]\omega_s^{1/3}, \tag{2.81}$$

where ω_s and Φ are all functions of time, and $q_{N(n)}$ are time-independent [8], and given explicitly in Appendix B.

To apply the SPA to our problem, we need to find t and $\dot{\omega}_s$ as functions of ω_s. Inverting Eq. (2.73) perturbatively in $\epsilon_x \ll 1$, we find

$$t - t_c = -\frac{3}{8}\frac{1}{\kappa_1\omega_s}(\mathcal{G}m\omega_s)^{-5/3}\left\{1 - \frac{4}{5}\epsilon_x(\mathcal{G}m\omega_s)^{-2/3} + \mathcal{O}[(\mathcal{G}m\omega_s)^{2/3}, \epsilon_x]\right\}. \tag{2.82}$$

But note very importantly that the time-domain waveform is to be evaluated at retarded time, thus $t \to t - R/c_N$ when evaluating the orbital phase in the integrand of the Fourier integral. Typically, the factor of R/c_N is re-absorbed in the time of coalescence t_c because it is a constant, but in æ-theory, this constant will be *different* for each of the modes present in the response function, and thus, more care must be taken.

With the results given in Eqs. (2.67) and (2.82), we are now able to apply the SPA to Eq. (2.81) by following the procedure outlined in Appendix A. However, note that there are several tiny differences between the example in Appendix A and the problem here. For instance, the speed term in Appendix A is absorbed into the phase. Of course, this will not bother us since the final result could be easily modified

[8] For detectors, such as LIGO, Virgo and KAGRA, one can treat $q_{N(l)}$ as time-independent, since their observation windows are very short [65]. However, for detectors like LISA, this approximation needs to be relaxed, as we will discuss in the next subsection.

to get the desired form in this section. After simple but tedious calculations, we find

$$\begin{aligned}\tilde{h}(f) &= \sum_N \Bigg\{ \frac{\sqrt{\pi}}{2} (\mathcal{G}m)^{1/3} \kappa_1^{-1/2} (q_{N(1)} + i q_{N(2)}) (\mathcal{G}\pi m f)^{-7/6} \\ &\quad \times \left[1 - \frac{1}{2} (\mathcal{G}\pi m f)^{-2/3} \epsilon_x \right] e^{-i2\pi f R \left(1 - c_N^{-1}\right)} e^{i\Psi_{(2)}} \\ &\quad + \frac{\sqrt{\pi}}{4} (\mathcal{G}m)^{2/3} \kappa_1^{-1/2} (q_{N(3)} + i q_{N(4)}) (\mathcal{G}\pi m f)^{-3/2} \\ &\quad \times \left[1 - \frac{1}{2} (2\mathcal{G}\pi m f)^{-2/3} \epsilon_x \right] e^{-i2\pi f R \left(1 - c_N^{-1}\right)} e^{i\Psi_{(1)}} \Bigg\}, \end{aligned} \tag{2.83}$$

where $N \in \{+, \times, b, L, X, Y\}$ and $c_+ = c_\times = c_T$, $c_b = c_L = c_S$, $c_X = c_Y = c_V$ [9]. Note that a typo of Eq. (2.83) in the published version is corrected here. The $e^{-i2\pi f R\left(1 - c_N^{-1}\right)}$ term exists because of the retarded time argument discussed above (see also Appendix A for a more detailed discussion). The Fourier phases $\Psi_{(1)}$ and $\Psi_{(2)}$, corresponding to the first and second harmonics of the orbital period respectively, are given by

$$\begin{aligned}\Psi_{(2)} &\equiv \frac{9}{20} \kappa_1^{-1} (\mathcal{G}\pi m f)^{-5/3} \left[1 - \frac{4}{7} (\mathcal{G}\pi m f)^{-2/3} \epsilon_x \right] + 2\pi f \bar{t}_c - 2\Phi(t_c) - \frac{\pi}{4}, \\ \Psi_{(1)} &\equiv \frac{9}{40} \kappa_1^{-1} (2\mathcal{G}\pi m f)^{-5/3} \left[1 - \frac{4}{7} (2\mathcal{G}\pi m f)^{-2/3} \epsilon_x \right] + 2\pi f \bar{t}_c - \Phi(t_c) - \frac{\pi}{4}, \end{aligned} \tag{2.84}$$

where we have redefined the coalescence time via $\bar{t}_c \equiv t_c + R$.

Note that the above expressions are different from the ones given in Eqs. (66) - (74) in [58] because here we do not assume the different polarization modes travel all at the speed of light. Moreover, in my calculation of the Fourier amplitudes, I have included Einstein-aether corrections of $\mathcal{O}(v)$ relative to the leading-order correction. Therefore, while in [58] the non-tensor modes are all proportional to the first harmonic, here we also have contributions that are proportional to the second harmonic, i.e. $q_{b,L,X,Y(1)} \neq 0 \neq q_{b,L,X,Y(2)}$. Finally, Eq. (2.83) contains a term proportional to

[9] Note that the c_+ here is the speed of plus mode instead of the constant c_{13} as in (1.11).

$\exp[-2\pi i f R(1-1/c_N)]$, which was absent from previous studies because all modes were assumed to travel at the speed of light.

We would also like to note that in the present case since now the breathing and longitudinal modes are degenerate [cf. Eq. (2.35)], the $q_{b(i)}$ and $q_{L(i)}$ terms in Eq. (2.83) can be combined together to simplify the results,

$$q_{S(i)} \equiv q_{b(i)} + q_{L(i)} = q_{b(i)}(1 - a_{bL}), \tag{2.85}$$

where Eqs. (B.1), (B.3) and (2.78) had been used and a_{bL} is given by (B.5).

2.5.2 Space-Based Equilateral-Shape Detectors

In this subsection we calculate the response function for a space-based equilateral-shape detector, such as LISA, TianQin, Taiji and DECIGO [151–156]. Because all such detectors share many similarities in their construction, we will mainly focus on calculations for LISA; similar work applicable to TianQin can be found in [153, 157] for GR.

Following [158], we can cast the response function of LISA in the following form, which is similar to Eq. (2.79),

$$h'(t) = \frac{\sqrt{3}}{2} \sum_N H'_N(t), \tag{2.86}$$

where $N \in \{+, \times, b, L, X, Y\}$, and where $H'_N(t)$ is given by

$$\begin{aligned} H'_N(t) &= \left[q'_{N(1)} \cos(2\Phi + \Phi_{DN(2)}) + q'_{N(2)} \sin(2\Phi + \Phi_{DN(2)})\right] \omega_s^{2/3} \\ &\quad + \left[q'_{N(3)} \cos(\Phi + \Phi_{DN(1)}) + q'_{N(4)} \sin(\Phi + \Phi_{DN(1)})\right] \omega_s^{1/3}, \end{aligned} \tag{2.87}$$

and the $q'_{N(l)}$ expressions are explicitly given in Appendix C. Note that the latter are now functions of time, unlike for ground-based L-shape detectors, as mentioned

previously. This is due to the fact that the observational windows of LISA is relatively long and sometimes comparable to the orbital period of the detector.

The quantities $\Phi_{DN(2)}$ and $\Phi_{DN(1)}$ are the corresponding Doppler phases due to the motion of the detector around the sun; gravitational waves reach LISA and the Solar System barycenter at different times [158]. Using the geometry of LISA, we can show that to first order of r_{so}/λ_N, where λ_N is the wavelength of the N-th mode [158] and r_{so} is the radius of the center of mass of LISA which is equal to 1AU, we have [10],

$$\begin{aligned} \Phi_{DN(2)} &= \frac{2\omega_s}{c_N} r_{so} \sin\bar{\theta} \cos[\bar{\Phi}(t) - \bar{\phi}], \\ \Phi_{DN(1)} &= \frac{\omega_s}{c_N} r_{so} \sin\bar{\theta} \cos[\bar{\Phi}(t) - \bar{\phi}]. \end{aligned} \tag{2.88}$$

The quantities $\bar{\theta}$ and $\bar{\phi}$ are generated in the same way as in Fig. 11.5 of [22] (See also [158]). The quantity $\bar{\Phi}(t)$ is the orbital phase of the center of mass of LISA in its orbit around the sun, which is given by

$$\bar{\Phi}(t) = \bar{\Phi}_0 + \frac{2\pi t}{T_0}, \tag{2.89}$$

where $\bar{\Phi}_0$ is a constant and T_0 is the period of LISA around the sun, which is equal to the sidereal period of Earth [159].

Since detector-related quantities should be evaluated at the current time t, and source-related quantities should be evaluated at the retarded time, one finds that

[10] For the basic construction of LISA, readers are referred to Figs. 1 and 2 of [158].

Eq. (2.87) needs to be modified to

$$\begin{aligned} H'_N(t) &= Q_{N(1)}|_t \cdot [\omega_s^{2/3}\cos(2\Phi)]|_{t_{rN}} + Q_{N(2)}|_t \cdot [\omega_s^{2/3}\sin(2\Phi)]|_{t_{rN}} \\ &\quad + Q_{N(3)}|_t \cdot [\omega_s^{1/3}\cos\Phi]|_{t_{rN}} + Q_{N(4)}|_t \cdot [\omega_s^{1/3}\sin\Phi]|_{t_{rN}}, \end{aligned} \tag{2.90}$$

where

$$\begin{aligned} Q_{N(1)} &\equiv \left[q'_{N(1)}\cos\Phi_{DN(2)} + q'_{N(2)}\sin\Phi_{DN(2)}\right], \\ Q_{N(2)} &\equiv -\left[q'_{N(1)}\sin\Phi_{DN(2)} - q'_{N(2)}\cos\Phi_{DN(2)}\right], \\ Q_{N(3)} &\equiv \left[q'_{N(3)}\cos\Phi_{DN(1)} + q'_{N(4)}\sin\Phi_{DN(1)}\right], \\ Q_{N(4)} &\equiv -\left[q'_{N(3)}\sin\Phi_{DN(1)} - q'_{N(4)}\cos\Phi_{DN(1)}\right], \end{aligned} \tag{2.91}$$

with $t_{rN} \equiv t - R/c_N$ being the retarded time for each mode.

With the above expressions, we can now calculate the Fourier transform for LISA by using SPA technique. The final result is

$$\begin{aligned} \tilde{h}'(f) = \frac{\sqrt{3}}{2}\sum_N \Bigg\{ & \frac{\sqrt{\pi}}{2}(\mathcal{G}m)^{1/3}\kappa_1^{-1/2}\left[Q_{N(1)}|_{t_{a2}+R/c_N} + iQ_{N(2)}|_{t_{a2}+R/c_N}\right](\mathcal{G}\pi mf)^{-7/6} \\ & \times\left[1 - \frac{1}{2}(\mathcal{G}\pi mf)^{-2/3}\epsilon_x\right] e^{-i2\pi fR\left(1-c_N^{-1}\right)} e^{i\Psi_{(2)}} \\ & + \frac{\sqrt{\pi}}{4}(\mathcal{G}m)^{2/3}\kappa_1^{-1/2}\left[Q_{N(3)}|_{t_{a1}+R/c_N} + iQ_{N(4)}|_{t_{a1}+R/c_N}\right](\mathcal{G}\pi mf)^{-3/2} \\ & \times\left[1 - \frac{1}{2}(2\mathcal{G}\pi mf)^{-2/3}\epsilon_x\right] e^{-i2\pi fR\left(1-c_N^{-1}\right)} e^{i\Psi_{(1)}} \Bigg\}, \end{aligned} \tag{2.92}$$

where $\Psi_{(i)}$ are given by Eq. (2.84), and t_{a1} and t_{a2} are the stationary points [cf. Appendix A]. From Eqs. (2.82) and (2.67) we find

$$t_{a1,2} - t_c = -\frac{3}{8}\frac{1}{\kappa_1\omega_s(t_{a1,2})}\left(\mathcal{G}m\omega_s(t_{a1,2})\right)^{-5/3}\left[1 - \frac{4}{5}\epsilon_x\left(\mathcal{G}m\omega_s(t_{a1,2})\right)^{-2/3}\right], \tag{2.93}$$

where $\omega_s(t_{a2}) = \pi f$ and $\omega_s(t_{a1}) = 2\pi f$.

Just like in Eq. (2.83), the $Q_{b(i)}$ and $Q_{L(i)}$ terms in Eq. (2.92) could be combined together, too, since the breathing and longitudinal modes are degenerate [cf. Eq. (2.35)],

$$Q_{S(i)} \equiv Q_{b(i)} + Q_{L(i)} = Q_{b(i)}(1 - a_{bL}), \tag{2.94}$$

where Eqs. (C.1), (B.3) and (2.78) have been used and a_{bL} is given by (B.5).

2.6 Parameterized Post-Einsteinian Parameters

By using the results given in the previous section, we are ready to calculate the ppE parameters of æ-theory [58,69,70]. Since the calculations for LISA-like detectors are too complicated, we will just focus here on the ground-based response functions. What is more, since the LIGO constraint on the speed of tensor modes c_T is so stringent, in this section we will set $c_T = c$.

Before we move to the following calculations, I want to first share some comments to ppE parameters. Actually, by extracting physical information from the observational data and then compare to that predicted in the calculated waveforms, we are able to check our theory. The reason for us to further calculate these ppE parameters is because they are basically just some numbers. By using them, it will be easier for us to compare them with the observational data to judge our theoretical predictions. Hopefully, they will be useful in the future.

2.6.1 Generalized ppE Scheme

One of the generalization of the simplest ppE waveforms to theories with multiple polarizations can be written in the form [70] [11],

$$\begin{aligned}
\tilde{h}(f) &= \tilde{h}^{GR}(f)\left(1+c_{ppE}\beta_{ppE}\mathcal{U}_2^{b_{ppE}+5}\right)e^{i2\beta_{ppE}\mathcal{U}_2^{b_{ppE}}} \\
&+\frac{\mathcal{M}^2}{R}\mathcal{U}_2^{-7/2}e^{i\Psi^{(2)}_{GR}}e^{i2\beta_{ppE}\mathcal{U}_2^{b_{ppE}}}\left(1-\kappa_3^{1/2}c_{ppE}\beta_{ppE}\mathcal{U}_2^{b_{ppE}+5}\right) \\
&\quad\times\left[\alpha_+F_+(1+\cos^2\vartheta)+\alpha_\times F_\times\cos\vartheta\right] \\
&+\frac{\mathcal{M}^2}{R}\mathcal{U}_2^{-7/2}e^{i\Psi^{(2)}_{GR}}e^{i2\beta_{ppE}\mathcal{U}_2^{b_{ppE}}}\left(1+\kappa_3c_{ppE}\beta_{ppE}\mathcal{U}_2^{b_{ppE}+5}\right) \\
&\quad\times\Big\{e^{i2\pi fR(1-c_S^{-1})}\left[\alpha_bF_b\sin^2\vartheta+\alpha_LF_L\sin^2\vartheta\right] \\
&\qquad+e^{i2\pi fR(1-c_V^{-1})}\left[\alpha_XF_X\sin(2\vartheta)+\alpha_YF_Y\sin\vartheta\right]\Big\} \\
&+\eta^{1/5}\frac{\mathcal{M}^2}{R}\mathcal{U}_1^{-9/2}e^{i\Psi^{(1)}_{GR}}e^{i\beta_{ppE}\mathcal{U}_1^{b_{ppE}}}\left(1+\kappa_3c_{ppE}\beta_{ppE}\mathcal{U}_1^{b_{ppE}+5}\right) \\
&\quad\times\Big\{e^{i2\pi fR(1-c_S^{-1})}\Big[\gamma_bF_b\sin\vartheta+\gamma_LF_L\sin\vartheta\Big] \\
&\qquad+e^{i2\pi fR(1-c_V^{-1})} \\
&\qquad\quad\times\left[\gamma_{X1}F_X\cos\vartheta+\gamma_{X2}F_X\sin\vartheta+\gamma_{Y1}F_Y+\gamma_{Y2}F_Y\sin\vartheta\right]\Big\},
\end{aligned} \tag{2.95}$$

where [70]

$$\tilde{h}^{GR}(f) = -\sqrt{\frac{5\pi}{96}}G_N^2\left[F_+(1+\cos^2\vartheta)+2iF_\times\cos\vartheta\right]\frac{\mathcal{M}^2}{R}\mathcal{U}_2^{-7/2}e^{i\Psi^{(2)}_{GR}}, \tag{2.96}$$

and

$$\begin{aligned}
\Psi^{(2)}_{GR} &= \frac{3}{128}(G_N\pi\mathcal{M}f)^{-5/3}+2\pi f\bar{t}_c-2\Phi(t_c)-\frac{\pi}{4}, \\
\Psi^{(1)}_{GR} &= \frac{3}{256}(2G_N\pi\mathcal{M}f)^{-5/3}+2\pi f\bar{t}_c-\Phi(t_c)-\frac{\pi}{4},
\end{aligned} \tag{2.97}$$

[11] This is different from its original form in [70], in order to accommodate different propagation speeds, as mentioned above.

with $\mathcal{U}_l \equiv (2\pi G_N \mathcal{M} f/l)^{1/3}$ and $l \in \mathbb{Z}^+$. Note that the angle φ in (2.96) has been set to zero to agree with those in [58, 70]. This result could be directly compared with its counterpart in [137] to confirm the correctness. Also note that the (1) and (2) in the superscripts do not stand for derivatives.

Comparing Eq. (2.83) with Eq. (2.95) we see immediately that there is a mismatch. This is because the gravitational constants in æ-theory that control binary motion are $\mathcal{G}$ and $G_{æ}$, and thus, these constants appear in Eq. (2.83), while the ppE formalism is parameterized in terms of the gravitational constant observed on Earth G_N, which is why this constant appears in $\mathcal{U}_\ell$ in Eq. (2.95). The relation between $\mathcal{G}$ and G_N is given explicitly in Eq. (2.52), where we see that $\mathcal{G} = G_N + \mathcal{O}(s_1, s_2)$. Similarly, from Eq. (1.6) we see that $G_{æ} = G_N + \mathcal{O}(c_{14})$. The ppE formalism, however, is *defined* only in the limit of small deformations away from GR, and since $s_{1,2} \to 0$ and $c_{14} \to 0$ in the GR limit, one should really insert Eqs. (2.52) and (1.6) into Eq. (2.83), then re-expand in small deformations, and then compare to Eq. (2.95), keeping only terms of leading-order in the coupling parameters and to leading-order in the PN approximation. To be specific, in the procedure of finding ppE parameters, we are going to apply the following approximations so that we can match Eqs. (2.83) and (2.95):

$$(1 - c_{14})^{n_1} \left[(1 - s_1)(1 - s_2)\right]^{n_2} = \left[1 + \mathcal{O}(s_1, s_2)\right] \left[1 + \mathcal{O}(c_{14})\right] \backsimeq 1, \qquad (2.98)$$

where n_1 and n_2 are arbitrary real numbers and the neglected contribution of $\mathcal{O}(s_1, s_2)$ and $\mathcal{O}(c_{14})$ enters at higher order in terms of the small coupling constants in the waveform.

The resulting Fourier transform of the response function in æ-theory is still different from that in [70] because the former contains the factors of $\exp[-2\pi i f R(1-1/c_N)]$ discussed earlier. Therefore, in theories which contain additional polarization modes with different propagation speeds, we must generalize the results of [70] by replacing every appearance of F_N in Eq. (2.95) with $F_N \exp[-2\pi i f R(1-1/c_N)]$.

If we can re-cast Eq. (2.80) into the form of Eq. (2.95), then we can read off the set of ppE parameters $\{c_{ppE}, b_{ppE}, \beta_{ppE}, \alpha_+, \alpha_\times, \alpha_b, \alpha_L, \alpha_X, \alpha_Y, \gamma_b, \gamma_L, \gamma_{X1}, \gamma_{X2}, \gamma_{Y1}, \gamma_{Y2}\}$. First, we observe that

$$\Psi_{(2)} = \Psi^{(2)}_{GR} + \mathcal{U}_2^{-7}\phi_1, \quad \Psi_{(1)} = \Psi^{(1)}_{GR} + \frac{1}{2}\mathcal{U}_1^{-7}\phi_1, \tag{2.99}$$

where

$$\phi_1 \equiv -\frac{3}{224}\eta^{2/5}\kappa_3^{-1}\epsilon_x, \tag{2.100}$$

with

$$\kappa_3 \equiv \ \mathcal{A}_1 + \mathcal{S}\mathcal{A}_2 + \mathcal{S}^2\mathcal{A}_3. \tag{2.101}$$

Note that Eq. (2.98) has been used above and the f-dependent terms in ϕ_1 are omitted to keep only the leading PN correction. With Eqs. (2.98) and (2.99) at hand, we could write Eq. (2.80) as the desired form, i.e., Eq. (2.95). Here, I will omit the devilishly tedious expression for $\tilde{h}(f)$. Instead, I will first find the full expression of $\tilde{h}(f)$ and then read off the ppE parameters. The results are

$$\begin{aligned}
c_{ppE} &= \frac{224}{3}, \\
b_{ppE} &= -7, \\
\beta_{ppE} &= \frac{1}{2}\phi_1 = -\frac{3}{448}\kappa_3^{-1}\eta^{2/5}\epsilon_x, \\
\alpha_+ &= \frac{\sqrt{5\pi}}{8\sqrt{6}}G_N^2 e^{i2\varphi}\left(\kappa_3^{-1/2} - 1\right) g_+,
\end{aligned}$$

$$
\begin{aligned}
\alpha_\times &= -i\frac{\sqrt{5\pi}}{8\sqrt{6}}G_N^2 e^{i2\varphi}\left(\kappa_3^{-1/2}-1\right)g_\times,\\
\alpha_b &= \frac{\sqrt{5\pi}}{8\sqrt{6}}\kappa_3^{-1/2}G_N^2 e^{i2\varphi}g_{b1},\\
\alpha_L &= \frac{\sqrt{5\pi}}{8\sqrt{6}}\kappa_3^{-1/2}G_N^2 e^{i2\varphi}g_{L1},\\
\alpha_X &= \frac{\sqrt{5\pi}}{8\sqrt{6}}\kappa_3^{-1/2}G_N^2 e^{i2\varphi}g_{X1},\\
\alpha_Y &= -i\frac{\sqrt{5\pi}}{8\sqrt{6}}\kappa_3^{-1/2}G_N^2 e^{i2\varphi}g_{Y1},\\
\gamma_b &= -i\frac{\sqrt{5\pi}}{8\sqrt{3}}\kappa_3^{-1/2}\eta^{-1/5}G_N^2 e^{i\varphi}(g_{b2}+g_{b4}),\\
\gamma_L &= -i\frac{\sqrt{5\pi}}{8\sqrt{3}}\kappa_3^{-1/2}\eta^{-1/5}G_N^2 e^{i\varphi}(g_{L2}+g_{L4}),\\
\gamma_{X1} &= -i\frac{\sqrt{5\pi}}{8\sqrt{3}}\kappa_3^{-1/2}\eta^{-1/5}G_N^2 e^{i\varphi}(g_{X2}+g_{X4}),\\
\gamma_{X2} &= -i\frac{\sqrt{5\pi}}{8\sqrt{3}}\kappa_3^{-1/2}\eta^{-1/5}G_N^2 e^{i\varphi}g_{X3},\\
\gamma_{Y1} &= \frac{\sqrt{5\pi}}{8\sqrt{3}}\kappa_3^{-1/2}\eta^{-1/5}G_N^2 e^{i\varphi}(g_{Y2}+g_{Y4}),\\
\gamma_{Y2} &= -i\frac{\sqrt{5\pi}}{8\sqrt{3}}\kappa_3^{-1/2}\eta^{-1/5}G_N^2 e^{i\varphi}g_{Y3},
\end{aligned}
\tag{2.102}
$$

where $\{g_+,\ g_\times,\ g_{b1,2,4},\ g_{L1,2,4},\ g_{X1,2,3,4},\ g_{Y1,2,3,4}\}$ are functions given in Appendix D. Note that $g_{b2,4}$, $g_{L2,4}$, $g_{X2,3,4}$ and $g_{Y2,3,4} \propto \eta^{1/5}$. In other words, the η terms in α_N and γ_N (or γ_{Nl}) actually have the same power, namely, 0. Also note that g_+ and $g_\times$ are actually simply -2 and 4 respectively. One may notice that g_N's are not defined in the most economic manner. As briefly reviewed in Appendix D, this is a historical problem with our notation system. Another thing is that c_{ppE}, which corresponds to the ratio between the amplitude and phase ppE corrections, agrees with that given in [70, 160].

Additionally, due to the degeneracy of breathing and longitudinal modes, in Eq. (2.95) we can put these terms together by introducing the quantities,

$$\alpha_S \equiv \alpha_b(1 - a_{bL}), \tag{2.103}$$

where Eqs. (D.2), (2.102) and (2.78) had been used and a_{bL} is given by (B.5).

2.6.2 Fully Restricted ppE Approximation

Now, we move to the regime of the fully restricted ppE approximation by mainly following [58]. We generalize [58, 70] to allow for different propagation speeds of scalar, vector and tensor modes. This time, Eq. (2.80) is written in the form of

$$\tilde{h}(f) = \sum_{N=S,V,T} \sum_{l=1}^{\infty} A_{ppE}^{(l,N)}(f) e^{i\Psi_{ppE}^{(l,N)}(f)}, \tag{2.104}$$

where

$$A_{ppE}^{(l,N)}(f) = A_{GR}^{(l)}(f) \left[1 + \mathcal{U}_l^{\bar{a}_{ppE}^{(l)}} \sum_{k=0}^{\infty} \bar{\alpha}_{ppE,k}^{(l,N)} (\mathcal{U}_l)^k \right], \tag{2.105}$$

$$\Psi_{ppE}^{(l,N)}(f) = \Psi_{GR}^{(l)}(f) + \mathcal{U}_l^{\bar{b}_{ppE}^{(l)}} \sum_{k=0}^{\infty} \bar{\beta}_{ppE,k}^{(l)} (\mathcal{U}_l)^k - 2\pi f R \left(1 - c_N^{-1}\right). \tag{2.106}$$

Here l stands for the l-th harmonics and quantities with a GR subscript referring to expressions in the GR limits as in Sec.2.6.1. We also note that $\bar{\alpha}_{ppE,0}^{(l,N)} \neq 0$ and $\bar{\beta}_{ppE,0}^{(l)} \neq 0$, which means that the terms proportional to $\mathcal{U}_l^{\bar{a}_{ppE}^{(l)}}$ and $\mathcal{U}_l^{\bar{b}_{ppE}^{(l)}}$ correspond to the term that enters at leading (lowest) PN order. We can choose $c_T = 1$ since this effect has been absorbed by the redefinition of the coalescence time. Notice that when $c_S = c_V = c_T = 1$, the phase is common to all of the scalar, vector and tensor modes, and the above formulation agrees with that in [70].

The restricted ppE waveform consists of amplitude corrections truncated to the leading PN order (which corresponds to -1 PN in our case) while phase corrections

are kept to higher PN orders. In this subsection, we consider the *fully restricted* ppE waveform, in which we only consider the dominant $l = 2$ harmonic mode. Then, the above expressions can be reduced to

$$\tilde{h}(f) \simeq \sum_{N=S,V,T} A^{(2,N)}_{ppE}(f) e^{i\Psi^{(2,N)}_{ppE}(f)}, \tag{2.107}$$

with

$$A^{(2,N)}_{ppE}(f) = A^{(2)}_{GR}(f)\left[1 + \mathcal{U}_2^{\bar{a}^{(2)}_{ppE}} \bar{\alpha}^{(2,N)}_{ppE,0}\right], \tag{2.108}$$

$$\Psi^{(2,N)}_{ppE}(f) = \Psi^{(2)}_{GR}(f) + \mathcal{U}_2^{\bar{b}^{(2)}_{ppE}} \sum_{k=0}^{\infty} \bar{\beta}^{(2)}_{ppE,k} (\mathcal{U}_2)^k - 2\pi f R(1 - c_N^{-1}). \tag{2.109}$$

Here $\Psi^{(2)}_{GR}$ is given by Eq. (2.97) while $A^{(2)}_{GR}$ is given by

$$A^{(2)}_{GR} = -\sqrt{\frac{5\pi}{96}} \frac{\mathcal{M}^2}{R} (G_N \pi \mathcal{M} f)^{-7/6} G_N^2 \left[F_+\left(1 + \cos^2\vartheta\right) + i2F_\times \cos\vartheta\right]. \tag{2.110}$$

Let us now determine the ppE parameters in æ-theory. Rewriting the waveform in Eq. (2.83) for the l=2 terms in a form given by Eq. (2.107), the ppE phase parameters can be extracted as

$$\begin{aligned}
&\bar{b}^{(2)}_{ppE} = -7, \\
&\bar{\beta}^{(2)}_{ppE,0} = \phi_1 = -\frac{3}{224} \kappa_3^{-1} \eta^{2/5} \epsilon_x, \\
&\bar{\beta}^{(2)}_{ppE,1} = 0, \\
&\bar{\beta}^{(2)}_{ppE,2} = -\frac{3}{128}\left[-\frac{2}{3}(s_1 + s_2) - \frac{1}{2} c_{14} + (\kappa_3 - 1)\right].
\end{aligned} \tag{2.111}$$

Notice that $\bar{\beta}^{(2)}_{ppE,0}$ is different from $\beta^{(2)}_{ppE}$ in Eq. (2.102) by a factor of 2 due to a prefactor 2 in front of $\beta^{(2)}_{ppE}$ in Eq. (2.95). When deriving $\bar{\beta}^{(2)}_{ppE,2}$, we kept $\mathcal{O}(s_1, s_2, c_{14})$ contribution in Eq. (2.98) for consistency. Next, the ppE amplitude parameters are

extracted as

$$
\begin{aligned}
\bar{a}^{(2)}_{ppE} &= -2, \\
\bar{\alpha}^{(2,T)}_{ppE,0} &= -\frac{1}{2}\kappa_3^{-1/2}\eta^{2/5}\epsilon_x, \\
\bar{\alpha}^{(2,S)}_{ppE,0} &= \bar{\alpha}^{(2,T)}_{ppE,0}\frac{g_{b1}F_b\sin^2\vartheta + g_{L1}F_L\sin^2\vartheta}{g_+F_+\big(1+\cos^2\vartheta\big) - ig_\times F_\times\cos\vartheta} \\
&= \bar{\alpha}^{(2,T)}_{ppE,0}\frac{g_{b1}F_b\sin^2\vartheta(1-a_{bL})}{g_+F_+\big(1+\cos^2\vartheta\big) - ig_\times F_\times\cos\vartheta}, \\
\bar{\alpha}^{(2,V)}_{ppE,0} &= \bar{\alpha}^{(2,T)}_{ppE,0}\frac{g_{X1}F_X\sin(2\vartheta) - ig_{Y1}F_Y\sin\vartheta}{g_+F_+\big(1+\cos^2\vartheta\big) - ig_\times F_\times\cos\vartheta}.
\end{aligned}
\tag{2.112}
$$

The above F_N and ϑ dependence in the ppE amplitude parameters for the scalar and vector modes seem to be a generic feature, as predicted in [70]. We note that even if the denominator $g_+F_+\big(1+\cos^2\vartheta\big) - ig_\times F_\times\cos\vartheta$ in $\bar{\alpha}^{(2,S)}_{ppE,0}$ and $\bar{\alpha}^{(2,V)}_{ppE,0}$ becomes 0, the scalar and vector mode corrections to the waveform amplitude do not diverge since the ppE parameters are multiplied by $A^{(2)}_{GR}$, which contains the same factor that cancels the denominator of $\bar{\alpha}^{(2,S)}_{ppE,0}$ and $\bar{\alpha}^{(2,V)}_{ppE,0}$.

Let us now compare the results presented here against those in [58,160]. First, $\bar{b}^{(2)}_{ppE}$ agrees with that in [58, 160], while $\bar{a}^{(2)}_{ppE}$ agrees with that in [160], which corrected [58]. Second, in [58], the aether field is assumed to be aligned with the CMB frame and $V \sim 10^{-3}$, which is much slower than the relative velocity of the binary constituents before coalescence. In this case, the dominant contribution in ϵ_x in Eq. (2.69) arises from the term proportional to $\mathcal{C}$. Moreover, the denominator $\mathcal{A}_1 + \mathcal{S}\mathcal{A}_2 + \mathcal{S}^2\mathcal{A}_3$ originates from factoring out the 0PN contribution in $\dot{\omega}_s$ in Eq. (2.67). If we neglect the Einstein-aether correction at 0PN order, this factor can be simply set to the GR value of 1 (and one can take the similar limit in κ_3). Then, the leading ppE phase $\bar{\beta}^{(2)}_{ppE,0}$ in Eq. (2.111) agrees with that in [58, 160] within the approximation in Eq. (2.98). Similarly, $\bar{\alpha}^{(2)}_{ppE,0}$ reduces to the leading ppE amplitude correction in [160]

under the small coupling approximation. On the other hand, $\bar{\beta}^{(2)}_{ppE,2}$ in Eq. (2.111) corrects that in [58].

2.7 Summary

In this chapter, we studied the waveforms and polarizations of GWs emitted by a binary system in Einstein-æther theory, which contains four dimensionless coupling parameters c_i's. We focused on the inspiral phase, adopted the PN approximations and assumed that the Einstein-aether coupling constants are small. In æ-theory, all the six polarization modes of GWs, referred to as $h_N(N = +, \times, b, L, X, Y)$, are present, although only five of them are independent, as the breathing and longitudinal modes (h_b and h_L) are proportional to each other. In the GR limit of $c_i \to 0$ ($i = 1, 2, 3, 4$), only the "+" and "×" modes remain and they reduce to those of GR as expected.

Gravitational waveforms and GW polarizations emitted by a binary system in the inspiral phase in æ-theory were already studied in [58]. In the current dissertation, I have first re-derived these formulas, and corrected some typos, by keeping all the terms to $\mathcal{O}(v^2)$. In particular, I have shown explicitly that the non-relativistic GW modes $h_{b,L,X,Y}$ contain not only the first harmonic terms of the orbital phase, as shown in [58], but also the second harmonic ones when one includes higher PN order terms.

Note also that in deriving the expressions of the GW polarization modes h_N's [cf. (2.55)-(2.60)], we have not assumed that COM of the binary system is always comoving with the aether field. In fact, in cosmology the aether field is normally assumed to be comoving with CMB [27]. As a result, individual compact objects

in the universe, such as galaxies and massive stars, are in general expected to have peculiar velocities with respect to the CMB. A typical velocity of compact objects in our own galaxy in this frame is about $V^2 \simeq 10^{-6}$, for which Foster had shown that the PN approximations adopted here are valid [32].

Using the SPA method [70,96,134], I have also calculated the response function and its Fourier transform for both ground- and space-based GW detectors. We then generalized the ppE framework to allow for different propagation speeds among scalar, vector and tensor modes. The ppE parameters within this new framework is given by Eqs. (2.102), (2.111) and (2.112), which depend on all six polarization modes. The leading ppE phase correction at -1PN order agrees with that in [58, 160] under the small coupling approximation and within the CMB frame. Similarly, the leading ppE amplitude correction agrees with that in [160] under the same approximation. On the other hand, the next-to-leading ppE correction in the phase at 0PN order corrects the corresponding expression in [58].

Additionally, it should be mentioned here that some typos and minor mistakes were found in reviewing the original treatise [68] (Some of them have already been pointed out explicitly in the previous article.). To a certain degree, it is sound to have them since the derivations and calculations within this chapter are extremely tedious. Fortunately, most of the flaws have quite limited influence on the results and the framework of [68] is concrete. Even though, it is worth suspecting and repeating some parts of [68] in the future to remove all the harmful flaws. Hopefully, this future task could improve the reliability of our results.

CHAPTER THREE

Spherically Symmetric Static Black Holes in Einstein-Aether Theory

This chapter is published in [95]: C. Zhang, X. Zhao, K. Lin, S.-J. Zhang, W. Zhao and A.-Z. Wang, Spherically symmetric static black holes in Einstein-aether theory, Phys. Rev. D**102**, 064043 (2020).

In this chapter, we systematically study spherically symmetric static spacetimes in the framework of Einstein-aether theory, and pay particular attention to the existence of black holes. As has been mentioned, in this theory two additional gravitational modes (one scalar and one vector) appear. To avoid the vacuum gravi-Čerenkov radiation, they must all propagate with speeds greater than or at least equal to the speed of light. However, in the spherical case, only the scalar mode is relevant, so BH horizons are defined by this mode, which are always inside or at most coincide with the metric (Killing) horizons. In the present studies I first clarify several subtle issues. In particular, we will find that, out of the five non-trivial field equations, only three are independent, so the problem is well-posed, as now generically there are only three unknown functions, $F(r), B(r), A(r)$, where F and B are metric coefficients, and A describes the aether field. In addition, the two nonlinear homogeneous second-order ordinary differential equations (ODEs) for A and F are independent of B, and once they are found, B is given simply by an algebraic expression of F, A and their derivatives. To simplify the problem further, we will explore the symmetry of field redefinitions, and work first with the redefined metric and aether field, and then obtain the physical ones by the inverse transformations. These clarifications significantly simplify the computational labor, which is pivotal,

as the problem is highly involved mathematically. In fact, it is exactly because of these, we can find various numerical BH solutions with an accuracy that is at least two orders higher than previous ones. More importantly, these BH solutions are the only ones that satisfy the self-consistent conditions and meantime are consistent with all the observational constraints obtained so far. The locations of universal horizons are also identified, together with several other observationally interesting quantities, such as the innermost stable circular orbits (ISCO), the ISCO frequency, and the maximum redshift z_{max} of a photon emitted by a source orbiting the ISCO. All of these quantities are found to be quite close to their relativistic limits.

3.1 Introduction

We have seen the detection of the first GW from the coalescence of two massive BHs by the advanced LIGO marked the beginning of a new era, the GW astronomy [14]. Following this observation, soon more than ten GWs were detected by the LIGO/Virgo scientific collaboration [16, 161, 162]. More recently, about 50 GW candidates have been identified after LIGO/Virgo resumed operations on April 1, 2019, possibly including the coalescence of a neutron star (NS)/BH binary. However, the details of these detections have not yet been released [101]. The outbreak of interest on GWs and BHs has further gained momentum after the detection of the shadow of the M87 BH [163–168].

One of the remarkable observational results is the discovery that the mass of an individual BH in these binary systems can be much larger than what was previously expected, both theoretically and observationally [103–105], leading to the proposal and refinement of various formation scenarios [106, 107]. A consequence of

this discovery is that the early inspiral phase may also be detectable by space-based observatories, such as as the Laser Interferometer Space Antenna (LISA) [169], TianQin [170, 171], Taiji [172, 173], and the Deci-Hertz Interferometer Gravitational wave Observatory (DECIGO) [174], for several years prior to their coalescence [108, 109]. Such space-based detectors may be able to see many such systems, which will result in a variety of profound scientific consequences. In particular, multiple observations with different detectors at different frequencies of signals from the same source can provide excellent opportunities to study the evolution of the binary in detail. Since different detectors observe at disjoint frequency bands, together they cover different evolutionary stages of the same binary system. Each stage of the evolution carries information about different physical aspects of the source.

As a result, multi-band GW detections will provide an unprecedented opportunity to test different theories of gravity in the strong field regime [123–128]. Massive systems will be observed by ground-based detectors with high signal-to-noise ratios, after being tracked for years by space-based detectors in their inspiral phase. The two portions of signals can be combined to make precise tests for different theories of gravity. In particular, joint observations of binary black holes (BBHs) with a total mass larger than about 60 solar masses by LIGO/Virgo and space-based detectors can potentially improve current bounds on dipole emission from BBHs by more than six orders of magnitude [123], which will impose severe constraints on various theories of gravity [129].

In recent works, some authors, including myself, generalized the post-Newtonian (PN) formalism to certain modified theories of gravity and applied it to the quasi-circular inspiral of compact binaries. In particular, we calculated in detail the waveforms, GW polarizations, response functions and energy losses due to gravitational radiation in Brans-Dicke (BD) theory [64], and screened modified gravity (SMG) [96–98] to the leading PN order, with which we then considered projected constraints from the third-generation detectors. Such studies have been further generalized to triple systems in æ-theory [62, 63]. When applying such formulas to the first relativistic triple system discovered in 2014 [132], we studied the radiation power, and found that quadrupole emission has almost the same amplitude as that in GR, but the dipole emission can be as large as the quadrupole emission. This can provide a promising window to place severe constraints on æ-theory with multi-band GW observations [123, 126]. More details could be found in previous chapters and the corresponding references.

More recently, we revisited the problem of a binary system of non-spinning bodies in a quasi-circular inspiral within the framework of æ-theory [32,41,42,57,58,67], and provided the explicit expressions for the time-domain and frequency-domain waveforms, GW polarizations, and response functions for both ground- and space-based detectors in the PN approximation [95]. In particular, we found that, when going beyond the leading order in the PN approximation, the non-Einsteinian polarization modes contain terms that depend on both the first and second harmonics of the orbital phase. With this in mind, we calculated analytically the corresponding parameterized post-Einsteinian parameters, generalizing the existing framework to

allow for different propagation speeds among scalar, vector and tensor modes, without assuming the magnitude of its coupling parameters, and meanwhile allowing the binary system to have relative motions with respect to the aether field. Such results will particularly allow for the easy construction of Einstein-aether templates that could be used in Bayesian tests of GR in the future. This is just the work shown in Chapter Two.

In this chapter, we shall continue to work on GWs and BHs in the framework of æ-theory, but move to the ringdown phase, which consists of the relaxation of the highly perturbed, newly formed merger remnant to its equilibrium state through the shedding of any perturbations in GWs as well as in matter waves. Such a remnant will typically be a Kerr BH, provided that the binary system is massive enough and GR provides the correct description. This phase can be well described as a sum of damped exponentials with unique frequencies and damping times - the quasi-normal modes (QNMs) [66].

The information contained in QNMs provide the keys in revealing whether BHs are ubiquitous in our universe, and more important whether GR is the correct theory to describe the event even in the strong field regime. In fact, in GR according to the no-hair theorem [175–182], an isolated and stationary BH is completely characterized by only three quantities, mass, spin angular momentum and electric charge. Astrophysically, we expect BHs to be neutral, so it must be described by the Kerr solution [9]. Then, the quasi-normal frequencies and damping times will depend only on the mass and angular momentum of the final BH. Therefore, to extract the physics from the ringdown phase, at least two QNMs are needed. This will require the signal-to-noise ratio (SNR) to be of the order 100 [183]. Although such high SNRs

are not achievable right now, it was shown that [184] they may be achievable once the advanced LIGO and Virgo reach their design sensitivities. In any case, it is certain that they will be detected by the ground-based third-generation detectors, such as Cosmic Explorer [185, 186] or the Einstein Telescope [187], as well as the space-based detectors, including LISA [169], TianQin [170], Taiji [172], and DECIGO [174], as just mentioned above.

In the framework of æ-theory, BHs with rotations have not been found yet, while spherically symmetric BHs have been extensively studied in the past couple of years both analytically [33, 75–85] and numerically [86–92]. It was shown that they can also be formed from gravitational collapse [93]. Unfortunately, in these studies, the parameter space has all been ruled out by current observations [60]. Therefore, as a first step to the study of the ringdown phase of a coalescing massive binary system, in this chapter we shall focus ourselves mainly on spherically symmetric static BHs in the parameter space that satisfies the self-consistent conditions and the current observations [60]. As shown explicitly in [94], spherically symmetric BHs in the new physically viable phase space can be still formed from the gravitational collapse of realistic matter.

It should be noted that the definition of BHs in æ-theory is different from that given in GR. As has been mentioned, in æ-theory there are three gravitational modes, the scalar, vector and tensor, which will be referred to as the spin-0, spin-1 and spin-2 gravitons, respectively. Each of them moves in principle with a different speed, given, respectively, by Eq. (1.7). What's more, in order to avoid the existence of the vacuum gravi-Čerenkov radiation by matter such as cosmic rays [38], we must

require

$$c_S,\ c_V, c_T \geq c, \tag{3.1}$$

where c denotes the speed of light. Therefore, as far as the gravitational sector is concerned, the horizon of a BH should be defined by the largest speed of the three different species of gravitons. However, in the spherically symmetric spacetimes, the spin-1 and spin-2 gravitons are not excited, and only the spin-0 graviton is relevant. Thus, the BH horizons in spherically symmetric spacetimes are defined by the metric [27],

$$g^{(S)}_{\mu\nu} \equiv g_{\mu\nu} - \left(c_S^2 - 1\right) u_\mu u_\nu, \tag{3.2}$$

where S in the indices represents a certain mode. Recall that u_μ denotes the four-velocity of the aether field, which is always timelike and unity, $u_\mu u^\mu = -1$.

Because of the presence of the æ-field in the whole spacetime, it uniquely determines a preferred direction at each point of the spacetime. As a result, the Lorentz symmetry is locally violated in æ-theory [188, 189] [1]. It must be emphasized that the breaking of Lorentz symmetry can have significant effects on the low-energy physics through the interactions between gravity and matter, no matter how high the scale of symmetry breaking is [198], unless supersymmetry is invoked [199]. In this

[1] It should be noted that the invariance under the Lorentz symmetry group is a cornerstone of modern physics and strongly supported by experiments and observations [190]. Nevertheless, there are various reasons to construct gravitational theories with broken Lorentz invariance (LI). For example, if space and/or time at the Planck scale are/is discrete, as currently understood [191, 192], Lorentz symmetry is absent at short distance/time scales and must be an emergent low energy symmetry. A concrete example of gravitational theories with broken LI is the Hořava theory of quantum gravity [193, 194], in which the LI is broken via the anisotropic scaling between time and space in the ultraviolet (UV), $t \to b^{-z}t$, $x^i \to b^{-1}x^i$, $(i = 1, 2, ..., d)$, where z denotes the dynamical critical exponent, and d the spatial dimensions. Power-counting renormalizability [195, 196] requires $z \geq d$ at short distances, while LI demands $z = 1$. Of course, the usages of b, d and z in this footnote won't be extended to other parts of this dissertation. For more details about Hořava gravity, see, for example, the review article [197], and references therein.

chapter, we shall not be concerned with this question. First, we consider æ-theory as a low-energy effective theory, and second the constraints on the breaking of the Lorentz symmetry in the gravitational sector is much weaker than that in the matter sector [188,189]. So, to avoid this problem, in this chapter we simply assume that the matter sector still satisfies the Lorentz symmetry. Then, all the particles from the matter sector will travel with speeds less or equal to the speed of light. Therefore, for these particles, the Killing (or metric) horizons still serve as the boundaries. Once inside them, they will be trapped inside the metric horizons (MHs) forever, and never be able to escape to spatial infinities.

With the above in mind, in this chapter we shall carry out a systematical study of spherically symmetric spacetimes in æ-theory, clarify several subtle points, and then present numerically new BH solutions that satisfy all the current observational constraints [60]. In particular, we shall show that, among the five non-trivial field equations (three evolution equations and two constraints), only three of them are independent. As a result, the system is well defined, since in the current case there are only three unknown functions: two describe the spacetime, denoted by $F(r)$ and $B(r)$ in Eq. (3.35), and one describes the aether field, denoted by $A(r)$ in Eq. (3.36).

An important result, born out of the above observations, is that the three independent equations can be divided into two groups, which decouple one from the other, that is, the equations for the two functions $A(r)$ and $F(r)$ [cf. Eqs. (3.39) and (3.40)] are independent of the function $B(r)$. Therefore, to solve these three field equations, one can first solve Eqs. (3.39) and (3.40) for $A(r)$ and $F(r)$. Once they are found, one can obtain $B(r)$ from the third equation. It is even more remarkable, if the third equation is chosen to be the constraint $C^v = 0$, given by Eq. (3.44), from which

one finds that $B(r)$ is then directly given by the algebraic equation (3.45) without the need of any further integration. Considering the fact that the field equations are in general highly involved mathematically, as it can be seen from Eqs. (3.39)-(3.44) and Eqs. (E.1)-(E.4), this is important, as it shall significantly simplify the computational labor, when we try to solve these field equations.

Another important step of solving the field equations is Foster's discovery of the symmetry of the action, the so-called field redefinitions [200]: the action remains invariant under the replacements,

$$(g_{\mu\nu}, u^\mu, c_i) \to (\hat{g}_{\mu\nu}, \hat{u}^\mu, \hat{c}_i)\,, \tag{3.3}$$

where $\hat{g}_{\mu\nu}$, $\hat{u}^\mu$ and $\hat{c}_i$ are given by Eqs. (3.11) and (3.12) through the introduction of a free parameter σ. Taking the advantage of the arbitrariness of σ, we can choose it as $\sigma = c_S^2$, where c_S^2 is given by Eq. (1.7). Then, the spin-0 and metric horizons for the metric $\hat{g}_{\mu\nu}$ coincide [86, 88, 90]. Thus, instead of solving the field equations for $(g_{\mu\nu}, u^\mu)$, we first solve the ones for $(\hat{g}_{\mu\nu}, \hat{u}^\mu)$, as in the latter the corresponding initial value problem can be easily imposed at horizons. Once $(\hat{g}_{\mu\nu}, \hat{u}^\mu)$ is found, using the inverse transformations, we can easily obtain $(g_{\mu\nu}, u^\mu)$, as well be seen later.

With the above observations, we are able to solve numerically the field equations with very high accuracy, as to be shown below [cf. Table 3.1]. In fact, the accuracy is significantly improved and in general at least two orders higher than that of the previous works.

In theories with breaking Lorentz symmetry, another important quantity is the universal horizon (UH) [89, 90], which is the causal boundary even for particles with infinitely large speeds. The thermodynamics of UHs and relevant physics have

been extensively studied (see, for example, Section III of the review article [197], and references therein). In particular, it was shown that such horizons can be formed from gravitational collapse of a massless scalar field [94]. In this chapter, we shall also identify the locations of the UHs of our numerical new BH solutions.

The rest of this chapter is organized as follows: Sec.3.2 provides a brief review to æ-theory (more details have been shown in Chapter One), in which the introduction of the field redefinitions and the definition of the spin-0 horizons (S0Hs) are given.

In Sec.3.3, we systematically study spherically symmetric static spacetimes, and show explicitly that among the five non-trivial field equations, only three of them are independent, so the corresponding problem is well defined: three independent equations for three unknown functions. Then, from these three independent equations we are able to obtain a three-parameter family of exact solutions for the special case $c_{13} = c_{14} = 0$, which depends in general on the coupling constant c_2. However, requiring that the solutions be asymptotically flat makes the solutions independent of c_2, and the metric reduces precisely to the Schwarzschild BH solution with a non-trivially coupling aether field [cf. Eq. (3.68)], which is timelike over the whole spacetime, including the region inside the BH. To further simplify the problem, in this section we also explore the advantage of the field redefinitions [200]. In particular, we show step by step how to choose the initial values of the differential equations Eqs. (3.97) and (3.98) on S0Hs, and how to reduce the phase space from four dimensions, spanned by $(\tilde{F}_H,\ \tilde{F}'_H,\ \tilde{A}_H,\ \tilde{A}'_H)$, to one dimension, spanned only by $\tilde{A}_H$. So, finally the problem reduces to finding the values of $\tilde{A}_H$ that lead to asymptotically flat solutions of the form (3.113) [86, 90].

In Sec.3.4, we spell out in detail the steps to carry out our numerical analysis. In particular, as to be shown explicitly, Eq. (3.99) is not independent from other three differential equations. Taking this advantage, we treat it as a conservative quantity and use it to monitor our numerical errors [cf. Eq. (3.123)]. To check our numerical code further, we reproduce the BH solutions obtained in [86,90], but with an accuracy two orders higher than those obtained in [90] [cf. Table 3.1]. Unfortunately, all these BH solutions have been ruled out by the current observations [60]. So, in this section, I fruther consider cases that satisfy all the observational constraints and obtain various new static BH solutions.

Then, in Sec.3.5, I present the physical metric and æ-field for these viable new BH solutions, by using the inverse transformations from the effective fields to the physical ones. In this section, I also show explicitly that the physical fields, $g_{\mu\nu}$ and u^μ, are also asymptotically flat, provided that the effective fields $\tilde{g}_{\mu\nu}$ and $\tilde{u}^\mu$ are, which are related to $\hat{g}_{\mu\nu}$ and $\hat{u}^\mu$ via the coordinate transformations given by Eq. (3.76). Then, I calculate explicitly the locations of the metric, spin-0 and universal horizons, as well as the locations of the innermost stable circular orbits (ISCO), the Lorentz gamma factor, the gravitational radius, the orbital frequency of the ISCO, the maximum redshift of a photon emitted by a source orbiting the ISCO (measured at the infinity), the radii of the circular photon orbit, and the impact parameter of the circular photon orbit. All of them are given in Tables 3.4-3.5. In Table 3.6 I also show the differences of these quantities obtained in æ-theory and GR. From these results, we will find that the differences are very small, and it is very hard to distinguish GR and æ-theory through these quantities, as far as the cases considered in this thesis are concerned.

Finally, in Sec.3.6 I summarize our main results and present some concluding remarks. There is also an appendix (App. E), in which the coefficients of the field equations for both $(g_{\mu\nu}, u^\mu)$ and $(\tilde{g}_{\mu\nu}, \tilde{u}^\mu)$ are given.

3.2 Æ-theory

The fundamental variables of the gravitational sector are shown in Eq. (1.1) [23]. Again, we are using the signature $(-,+,+,+)$ [41,93]. Note that here we assume that matter fields couple not only to $g_{\mu\nu}$ but also to the aether field u^μ. Then, the variations of the total action [cf. Eq. (1.2)] with respect to the three variables $g_{\mu\nu}$, u^μ and λ yield the the field equations in (2.5) and (2.6).

It is easy to show that the Minkowski spacetime is a solution of æ-theory, in which the aether is aligned along the time direction, $\bar{u}_\mu = \delta^0_\mu$. Then, the linear perturbations around the Minkowski background show that the theory in general possess three types of excitations, scalar (spin-0), vector (spin-1) and tensor (spin-2) modes [37], with their squared speeds given by Eq. (1.7).

In addition, among the ten parameterized post-Newtonian (PPN) parameters [6, 25], in æ-theory the only two parameters that deviate from GR are α_1 and α_2 [cf. Eq. (1.8)], which measure the preferred frame effects. In the weak-field regime, using lunar laser ranging and solar alignment with the ecliptic, Solar System observations constrain these parameters to very small values [25],

$$|\alpha_1| \leq 10^{-4}, \quad |\alpha_2| \leq 10^{-7}. \tag{3.4}$$

Recently, the combination of the GW event GW170817 [201], observed by the LIGO/Virgo collaboration, and the event of the gamma-ray burst GRB 170817A [202] provides a remarkably stringent constraint on the speed of the spin-2 mode, $-3 \times$

$10^{-15} < c_T - 1 < 7 \times 10^{-16}$, which, together with Eq. (1.7), implies that

$$|c_{13}| < 10^{-15}. \tag{3.5}$$

Requiring that the theory: (a) is self-consistent, such as free of ghosts and instability; and (b) satisfies all the observational constraints obtained so far, it was found that the parameter space of the theory is considerably restricted [60]. In particular, c_{14} and c_2 are restricted to

$$0 \lesssim c_{14} \lesssim 2.5 \times 10^{-5}, \tag{3.6}$$

$$0 \lesssim c_{14} \lesssim c_2 \lesssim 0.095. \tag{3.7}$$

The constraints on other parameters depend on the values of c_{14}. The phase space could be divided into three intervals: (i) $0 \lesssim c_{14} \leq 2\times10^{-7}$; (ii) $2\times10^{-7} < c_{14} \lesssim 2 \times 10^{-6}$; and (iii) $2 \times 10^{-6} \lesssim c_{14} \lesssim 2.5 \times 10^{-5}$ according to c_{14}. In the intermediate regime (ii), the following constraints must be satisfied,

$$-10^{-7} \leq \frac{c_{14}\left(c_{14} + 2c_2c_{14} - c_2\right)}{c_2\left(2 - c_{14}\right)} \leq 10^{-7}. \tag{3.8}$$

Note that in writing Eq. (3.8), I had set $c_{13} = 0$, for which the errors are of the order $\mathcal{O}\left(c_{13}\right) \simeq 10^{-15}$, which can be safely neglected for the current and forthcoming experiments. The results in this intermediate interval of c_{14} were shown explicitly by Fig. 1.1. Note that in this figure, the physically valid region is restricted only to the half plane $c_{14} \geq 0$, as shown by Eq. (3.6). More details about the constraints could be found in Eqs. (1.9) and (1.10) as well as in [60].

Since the theory possesses three different modes, and all of them are moving with different speeds, in general these different modes define different horizons [27].

These horizons are the null surfaces of the effective metrics,

$$g^{(A)}_{\alpha\beta} \equiv g_{\alpha\beta} - \left(c_A^2 - 1\right) u_\alpha u_\beta, \tag{3.9}$$

where $A = S, V, T$. If a BH is defined to be a region that traps all possible causal influences, it must be bounded by a horizon corresponding to the fastest speed. Assuming that the matter sector always satisfies the Lorentz symmetry, we can see that in the matter sector the fastest speed will be the speed of light. Then, overall, the fastest speed must be one of the three gravitational modes.

However, in the spherically symmetric case, the spin-1 and spin-2 modes are not excited, so only the spin-0 gravitons are relevant. Therefore, in the present chapter the relevant horizons for the gravitational sector are the S0Hs [2]. In order to avoid the existence of the vacuum gravi-Čerenkov radiation by matter such as cosmic rays [38], we assume that $c_S \geq 1$, so that S0Hs are always inside or at most coincide with the metric horizons, the null surfaces defined by the metric $g_{\alpha\beta}$. The equality happens only when $c_S = 1$.

3.2.1 Field Redefinitions

Due to the specific symmetry of the theory, Foster found that the action $S_{æ}\left(g_{\alpha\beta}, u^\alpha, c_i\right)$ given by Eqs. (1.3)-(1.5) does not change under the following field redefinitions [200],

$$\left(g_{\alpha\beta}, u^\alpha, c_i\right) \to \left(\hat{g}_{\alpha\beta}, \hat{u}^\alpha, \hat{c}_i\right), \tag{3.10}$$

[2] If we consider Hořava gravity [193] as the UV complete theory of the hypersurface-orthogonal æ-theory (the khronometric theory) [203–206], even in the gravitational sector, the relevant boundaries will be the UHs, once such a UV complete theory is taken into account [197].

where

$$\hat{g}_{\alpha\beta} = g_{\alpha\beta} - (\sigma - 1)u_\alpha u_\beta, \quad \hat{u}^\alpha = \frac{1}{\sqrt{\sigma}} u^\alpha,$$
$$\hat{g}^{\alpha\beta} = g^{\alpha\beta} - (\sigma^{-1} - 1)u^\alpha u^\beta, \quad \hat{u}_\alpha = \sqrt{\sigma} u_\alpha, \tag{3.11}$$

and

$$\begin{aligned}
\hat{c}_1 &= \frac{\sigma}{2}\left[\left(1 + \sigma^{-2}\right) c_1 + \left(1 - \sigma^{-2}\right) c_3 - \left(1 - \sigma^{-1}\right)^2\right], \\
\hat{c}_2 &= \sigma\left(c_2 + 1 - \sigma^{-1}\right), \\
\hat{c}_3 &= \frac{\sigma}{2}\left[\left(1 - \sigma^{-2}\right) c_1 + \left(1 + \sigma^{-2}\right) c_3 - \left(1 - \sigma^{-2}\right)\right], \\
\hat{c}_4 &= c_4 - \frac{\sigma}{2}\left[\left(1 - \frac{1}{\sigma}\right)^2 c_1 + \left(1 - \frac{1}{\sigma^2}\right) c_3 - \left(1 - \frac{1}{\sigma}\right)^2\right],
\end{aligned} \tag{3.12}$$

with σ being a positive otherwise arbitrary constant. Then, the following useful relations between c_i and $\hat{c}_i$ hold,

$$\hat{c}_2 = \sigma(c_2 + 1) - 1, \quad \hat{c}_{14} = c_{14}, \quad \hat{c}_{13} = \sigma(c_{13} - 1) + 1,$$
$$\hat{c}_{123} = \sigma c_{123}, \quad \hat{c}_- = \sigma^{-1}(c_- + \sigma - 1). \tag{3.13}$$

Note that $\hat{g}^{\alpha\beta}\hat{g}_{\beta\gamma} = \delta^\alpha_\gamma$ and $\hat{u}_\alpha \equiv \hat{g}_{\alpha\beta}\hat{u}^\beta$. Then, from Eq. (3.11), we find that

$$\hat{g}_{\alpha\beta}\hat{u}^\alpha\hat{u}^\beta = -1, \quad \hat{g} = \sigma g, \tag{3.14}$$

where $\hat{g}$ is the determinant of $\hat{g}_{\alpha\beta}$. Thus, replacing $G_{æ}$ and $\mathcal{L}_\lambda$ by $\hat{G}_{æ}$ and $\hat{\mathcal{L}}_\lambda$ in Eq. (1.3), where

$$\hat{G}_{æ} \equiv \sqrt{\sigma} G_{æ}, \quad \hat{\mathcal{L}}_\lambda \equiv \lambda\left(\hat{g}_{\alpha\beta}\hat{u}^\alpha\hat{u}^\beta + 1\right), \tag{3.15}$$

we find that

$$S_{æ}\left(g_{\alpha\beta}, u^\alpha, c_i, G_{æ}, \lambda\right) = \hat{S}_{æ}\left(\hat{g}_{\alpha\beta}, \hat{u}^\alpha, \hat{c}_i, \hat{G}_{æ}, \lambda\right). \tag{3.16}$$

As a result, when the matter field is absent, that is, $\mathcal{L}_m = 0$, the Einstein-aether vacuum field equations take the same forms for the fields $(\hat{g}_{\alpha\beta}, \hat{u}^\alpha, \hat{c}_i, \lambda)$,

$$\hat{R}^{\mu\nu} - \frac{1}{2}\hat{g}^{\mu\nu}\hat{R} = \hat{S}^{\mu\nu}, \tag{3.17}$$

$$\hat{\text{Æ}}_\mu = 0, \tag{3.18}$$

$$\hat{g}_{\alpha\beta}\hat{u}^\alpha\hat{u}^\beta = -1, \tag{3.19}$$

where $\hat{R}^{\mu\nu}$ and $\hat{R}$ are the Ricci tensor and scalar made of $\hat{g}_{\alpha\beta}$. $\hat{S}^{\mu\nu}$ and $\hat{\text{Æ}}_\mu$ are given by Eq. (2.7) simply by replacing $(g_{\mu\nu}, u^\mu, c_i)$ by $(\hat{g}_{\mu\nu}, \hat{u}^\mu, \hat{c}_i)$.

Therefore, *for any given vacuum solution of the Einstein-aether field equations* $(g_{\mu\nu}, u^\mu, c_i, \lambda)$, *using the above field redefinitions, we can obtain a class of the vacuum solutions of the Einstein-aether field equations, given by* $(\hat{g}_{\mu\nu}, \hat{u}^\mu, \hat{c}_i, \lambda)$ [3]. Certainly, such obtained solutions may not always satisfy the physical and observational constraints found so far [60].

In this chapter, we shall take advantage of such field redefinitions to simplify the corresponding mathematical problems by assuming that the fields described by $(g_{\mu\nu}, u^\mu, c_i, \lambda)$ are the physical ones, while the ones described by $(\hat{g}_{\mu\nu}, \hat{u}^\mu, \hat{c}_i, \lambda)$ as the "effective" ones, although both of the two metrics are the vacuum solutions of the Einstein-aether field equations, and can be physical, provided that the constraints recently given in [60] are satisfied.

The gravitational sector described by $(\hat{g}_{\mu\nu}, \hat{u}^\mu, \hat{c}_i, \lambda)$ has also three different propagation modes, with their speeds $\hat{c}_A$ given by Eq. (1.7) with the replacement c_i by $\hat{c}_i$. Each of these modes defines a horizon, which is now a null surface of the

[3] It should be noted that this holds in general only for the vacuum case. In particular, when matter present, the aether field will be directly coupled with matter through the metric redefinitions.

metric,

$$\hat{g}^{(A)}_{\alpha\beta} \equiv \hat{g}_{\alpha\beta} - \left(\hat{c}^2_A - 1\right) \hat{u}_\alpha \hat{u}_\beta, \tag{3.20}$$

where $A = S, V, T$. It is interesting to note that

$$\hat{c}^2_A = \frac{c^2_A}{\sigma}. \tag{3.21}$$

Thus, choosing $\sigma = c^2_S$, we have $\hat{c}_S = 1$, and from Eq. (3.20) we find that

$$\hat{g}^{(S)}_{\alpha\beta} = \hat{g}_{\alpha\beta}, \ \left(\sigma = c^2_S\right), \tag{3.22}$$

that is, the S0H of the metric $\hat{g}_{\alpha\beta}$ coincides with its MH. Moreover, from Eqs. (3.9) and (3.11) we also find that

$$g^{(S)}_{\alpha\beta} = \hat{g}_{\alpha\beta}, \ \left(\sigma = c^2_S\right). \tag{3.23}$$

Therefore, *with the choice $\sigma = c^2_S$, the MH of $\hat{g}_{\alpha\beta}$ is also the S0H of the metric $g_{\alpha\beta}$.*

3.2.2 Hypersurface-Orthogonal Aether Fields

When the aether field u_μ is hypersurface-orthogonal (HO), the Einstein-aether field equations depend only on three combinations of the four coupling constants c_i's. To see this clearly, let us first notice that, if the aether is HO, the twist ω^μ vanishes [27], where ω^μ is defined as $\omega^\mu \equiv \epsilon^{\mu\nu\alpha\beta} u_\nu D_\alpha u_\beta$. Since

$$\omega_\mu \omega^\mu \ = \ \left(D_\mu u_\nu\right)\left(D^\nu u^\mu\right) - \left(D_\mu u_\nu\right)\left(D^\mu u^\nu\right) - \left(u^\mu D_\mu u_\alpha\right)\left(u^\nu D_\nu u^\alpha\right), \tag{3.24}$$

we can see that the addition of the term

$$\Delta\mathcal{L}_{æ} \equiv c_0 \omega_\mu \omega^\mu, \tag{3.25}$$

to $\mathcal{L}_{æ}$ will not change the action, where c_0 is an arbitrary real constant. However, this is equivalent to replacing c_i by $\bar{c}_i$ in $\mathcal{L}_{æ}$, where

$$\bar{c}_1 \equiv c_1 + c_0, \quad \bar{c}_2 \equiv c_2, \quad \bar{c}_3 \equiv c_3 - c_0, \quad \bar{c}_4 \equiv c_4 - c_0. \tag{3.26}$$

Thus, by properly choosing c_0, we can always eliminate one of the three parameters, $c_1,\ c_3$ and c_4, or one of their combinations. Therefore, in this case only three combinations of c_i's appear in the field equations. Since

$$\bar{c}_{13} = c_{13}, \quad \bar{c}_{14} = c_{14}, \quad \bar{c}_2 = c_2, \tag{3.27}$$

without loss of the generality, we can always choose these three combinations as $c_{13},\ c_{14}$ and c_2.

To understand the above further, and also see the physical meaning of these combinations, following Jacobson [206], we first decompose $D_\beta u_\alpha$ into the form,

$$D_\beta u_\alpha = \frac{1}{3}\theta h_{\alpha\beta} + \sigma_{\alpha\beta} + \omega_{\alpha\beta} - a_\alpha u_\beta, \tag{3.28}$$

where θ [which is different from the one in (2.78)] denotes the expansion of the aether field, $h_{\alpha\beta}$ [which is different from the one in (2.12)] the spatial projection operator, $\sigma_{\alpha\beta}$ the shear, which is the symmetric trace-free part of the spatial projection of $D_\beta u_\alpha$, while $\omega_{\alpha\beta}$ denotes the antisymmetric part of the spatial projection of $D_\beta u_\alpha$, defined, respectively, by

$$\begin{aligned} &h_{\alpha\beta} \equiv g_{\alpha\beta} + u_\alpha u_\beta, \quad \theta \equiv D_\lambda u^\lambda, \\ &\sigma_{\alpha\beta} \equiv D_{(\beta}u_{\alpha)} + a_{(\alpha}u_{\beta)} - \frac{1}{3}\theta h_{\alpha\beta}, \quad \omega_{\alpha\beta} \equiv D_{[\beta}u_{\alpha]} + a_{[\alpha}u_{\beta]}, \end{aligned} \tag{3.29}$$

with $(A,B) \equiv (AB+BA)/2$ and $[A,B] \equiv (AB-BA)/2$ for the subscripts [35]. Recall that a_μ is the acceleration of the aether field, given by Eq. (2.8).

In terms of these quantities, Jacobson found

$$\int d^4x\sqrt{-g}\mathcal{L}_{\text{æ}} \ = \ \int d^4x\sqrt{-g}\left[R - \frac{1}{3}c_\theta\theta^2 + c_a a^2 - c_\sigma\sigma^2 - c_\omega\omega^2\right], \tag{3.30}$$

where

$$c_\theta \equiv c_{13} + 3c_2, \quad c_\sigma \equiv c_{13}, \quad c_\omega \equiv c_1 - c_3, \quad c_a \equiv c_{14}, \tag{3.31}$$

and

$$\sigma^2 = \ -\frac{1}{3}\theta^2 + (D_\mu u_\nu)(D^\mu u^\nu) + a^2. \tag{3.32}$$

Note that in the above action, there are no crossing terms of $\{\theta, \sigma_{\alpha\beta}, \omega_{\alpha\beta}, a_\alpha\}$. This is because the four terms on the right-hand side of Eq. (3.28) are orthogonal to each other, and when forming quadratic combinations of these quantities, only their "squares" contribute [206].

From Eq. (3.31) we can see clearly that c_{14} is related to the acceleration of the aether field, c_{13} to its shear, while its expansion is related to both c_2 and c_{13}. More interesting, the coefficient of the twist is proportional to c_-. When u_μ is hypersurface-orthogonal, we have $\omega^2 = 0$, so the last term in the above action vanishes identically, and only the three free parameters c_θ, c_σ and c_a remain.

It is also interesting to note that the twist vanishes if and only if the four-velocity of the aether satisfies the conditions [207],

$$u_{[\mu} D_\nu u_{\alpha]} = 0. \tag{3.33}$$

When the aether is HO, it can be shown that Eq. (3.33) is satisfied. In addition, in the spherically symmetric case, Eq. (3.33) holds identically.

Moreover, it can be also shown [207] that Eq. (3.33) is the necessary and sufficient condition to write the four-velocity u_μ in terms the gradient of a timelike scalar field ϕ [which has a different meaning comparing to the one in (2.13)],

$$u_\mu = \frac{\phi_{,\mu}}{\sqrt{-\phi_{,\alpha}\phi^{,\alpha}}}. \tag{3.34}$$

Substituting it into the action (3.30), one obtains the action of the infrared limit of the healthy extension [203, 204] of the Hořava theory [193], which is often referred to as *the khronometric theory* [4], where ϕ is called *the khronon field*.

It should be noted that the khronometric theory and the HO æ-theory are equivalent only in the action level. In particular, in addition to the scalar mode, the khronometric theory has also an instantaneous mode [89,208], a mode that propagates with an infinitely large speed. This is mainly due to the fact that the field equations of the khronometric theory are the four-order differential equations of ϕ. It is the presence of those high-order terms that lead to the existence of the instantaneous mode [5]. On the other hand, in æ-theory, including the case with the HO symmetry, the field equations are of the second order for both the metric $g_{\mu\nu}$ and the aether field u_μ. As a result, this instantaneous mode is absent. For more details, we refer readers to [197] and references therein.

3.3 Spherically Symmetric Vacuum Spacetimes

3.3.1 Field Equations for $g_{\mu\nu}$ and u^μ

As shown in the last section, to be consistent with observations, we must assume $c_S \geq 1$. As a result, S0Hs must be inside MHs. Since now S0Hs define the boundaries of spherically symmetric BHs, in order to cover spacetimes both inside and outside the MHs, one way is to adopt the Eddington-Finkelstein (EF) coordinates,

$$ds^2 \equiv g_{\mu\nu}dx^\mu dx^\nu = -F(r)dv^2 + 2B(r)dvdr + r^2 d\Omega^2, \tag{3.35}$$

[4] In [205, 206], it was also referred to as T-theory.

[5] In the Degenerate Higher-Order Scalar-Tensor (DHOST) theories, this mode is also referred to as the "shadowy" mode [209].

where $d\Omega^2 \equiv d\theta^2 + \sin^2\theta d\phi^2$ and $x^\mu = (v, r, \theta, \phi)$ [recall that in last chapter x^μ always refers to (t, x, y, z)], while the aether field takes the general form,

$$u^\alpha \partial_\alpha = A(r)\partial_v - \frac{1 - F(r)A^2(r)}{2B(r)A(r)}\partial_r, \tag{3.36}$$

which is respect to the spherical symmetry, and satisfies the constraint $u_\alpha u^\alpha = -1$. Obviously, the θ and ϕ apperaing here are just the polar and azimuthal angles [26, 29, 142]. Therefore, in the current case, we have three unknown functions, $F(r)$, $A(r)$ and $B(r)$.

The vacuum field equations $E^{\mu\nu} \equiv G^{\mu\nu} - S^{\mu\nu} = 0$ and $\text{Æ}^\mu = 0$ contain no more than 2nd-order derivatives, which guarantees the stability of our dynamic system [210]. They can be divided into two groups [86, 90]: one represents the evolution equations, given by

$$E^{vv} = E^{\theta\theta} = \text{Æ}^v = 0, \tag{3.37}$$

and the other represents the constraint equation, given by

$$C^v = 0, \tag{3.38}$$

where $C^\alpha \equiv E^{r\alpha} + u^r \text{Æ}^\alpha = 0$, and $G^{\mu\nu}$ $[\equiv R^{\mu\nu} - Rg^{\mu\nu}/2]$ denotes the Einstein tensor. Note that in Eq. (35) of [90] two constraint equations $C^v = C^r = 0$ were considered. However, C^r and C^v are not independent. Instead, they are related to each other by the relation $C^r = (F/B)C^v$. Thus, $C^v = 0$ implies $C^r = 0$, so there is only one independent constraint. On the other hand, the three evolution equations can be cast

in the forms [6],

$$
\begin{aligned}
F'' &= \mathcal{F}\left(A, A', F, F', r, c_i\right) \\
&= \frac{1}{2r^2A^4\mathcal{D}}\Big(f_0 + f_1F + f_2F^2 + f_3F^3 + f_4F^4\Big), \qquad (3.39)\\
A'' &= \mathcal{A}\left(A, A', F, F', r, c_i\right) \\
&= \frac{1}{2r^2A^2\mathcal{D}}\Big(a_0 + a_1F + a_2F^2 + a_3F^3\Big), \qquad (3.40)\\
\frac{B'}{B} &= \mathcal{B}\left(A, A', F, F', r, c_i\right) \\
&= \frac{1}{2rA^2\mathcal{D}}\Big(b_0 + b_1F + b_2F^2\Big), \qquad (3.41)
\end{aligned}
$$

where a prime stands for the derivative with respect to r, and

$$\mathcal{D} \equiv d_-\left(J^2+1\right) + 2d_+J, \qquad (3.42)$$

with $J \equiv FA^2$ and

$$d_\pm \equiv \ (c_S^2 \pm 1)c_{14}(1-c_{13})(2+c_{13}+3c_2). \qquad (3.43)$$

The coefficients $f_n,\ a_n$ and b_n are independent of $F(r)$ and $B(r)$ but depend on $F'(r)$, $A(r)$ and $A'(r)$, and are given explicitly by Eqs. (E.1), (E.2) and (E.3) in Appendix E. The constraint equation (3.38) now can be cast in the form,

$$n_0 + n_1F + n_2F^2 = 0, \qquad (3.44)$$

where n_n's are given explicitly by Eq. (E.4) in Appendix E.

Thus, we have three dynamical equations and one constraint for the three unknown functions, F, A and B. As a result, the system seems over determined. However, a closer examination shows that not all of them are independent. For

[6] It should be noted that in [90] the second-order differential equation for F [cf. Eq. (36) given there] also depends on B. But, since from the constraint $C^v = 0$, given by Eq. (3.44), one can express B in terms of A, F and their derivatives, as shown explicitly by Eq. (3.45), so there are no essential differences here, and it should only reflect the facts that different combinations of the field equations are used.

example, Eq. (3.41) can be obtained by manipulating and assembling Eqs. (3.39), (3.40), and (3.44). In fact, from Eq. (3.44), we find that the function B can be written in the form

$$\begin{aligned} B(r) &= \pm\frac{1}{2\sqrt{2}A^2}\Bigg\{2A^2\Big[4J(1+2c_2+c_{13})-(2c_2+c_{13})\big(J+1\big)^2\Big] \\ &\quad +4rA\Big[2AJ'-4JA'+c_2\big(J-1\big)\big(JA'-A'-AJ'\big)\Big] \\ &\quad +r^2\Big[c_{14}\big(JA'+A'-AJ'\big)^2-(c_2+c_{13})\big(JA'-A'-AJ'\big)^2\Big]\Bigg\}^{1/2}. \end{aligned} \tag{3.45}$$

Recall that $J = FA^2$. Note that there are two branches of solutions for $B(r)$ with opposite signs, since Eq. (3.44) is a quadratic equation of B. However, only the "+" sign will give us $B = 1$ at the spatial infinity, while the "-" sign will yield $B(r \to \infty) = -1$. Therefore, in the rest of this chapter, we shall choose the "+" sign in Eq. (3.45). Then, first taking the derivative of Eq. (3.45) with respective to r, and then combining the obtained result with Eqs. (3.39) and (3.40), one can obtain Eq. (3.41) [7].

To solve these equations, in this dissertation we shall adopt the following strategy: choosing Eqs. (3.39), (3.40) and (3.45) as the three independent equations for the three unknown functions, F, A, and B. The advantage of this choice is that Eqs. (3.39) and (3.40) are independent of the function B. Therefore, we can first solve these two equations to find F and A, and then obtain the function B finally and directly from Eq. (3.45). In this approach, we only need to solve two ODEs, which will significantly save the computation labor, although we do use Eq. (3.41) to monitor our numerical errors.

[7] From this proof it can be seen that obtaining Eq. (3.41) from Eq. (3.45) the operation of taking the first-order derivatives was involved. Therefore, in principle these two equations are equivalent modulated an integration constant.

To solve Eqs. (3.39) and (3.40), we can consider them as the "initial" value problem at a given "moment", say, $r = r_0$ [86, 90]. Since they are second-order differential equations, the initial data will consist of the four initial values,

$$\Big\{A(r_0), A'(r_0), F(r_0), F'(r_0)\Big\}. \tag{3.46}$$

In principle, r_0 can be chosen as any given (finite) "moment". However, in the following we shall show that the most convenient choice will be the locations of the S0Hs. It should be noted that a S0H does not always exist for any given initial data. However, since in this chapter we are mainly interested in the case in which a S0H exists, so whenever we choose $r_0 = r_{S0H}$, it always means that we only consider the case in which such a S0H is present.

To determine the location of the S0H for a given spherical solution of the metric (3.35), let us first consider the out-pointing normal vector, N_μ [of course, it is different from the one in, e.g., (2.42)], of a hypersurface $r =$ Constant, say, r_0, which is given by $N_\mu \equiv \partial(r - r_0)/\partial x^\mu = \delta^r_\mu$. Then, the metric and spin-0 horizons of $g_{\mu\nu}$ are given, respectively, by

$$g_{\alpha\beta}N^\alpha N^\beta = 0, \tag{3.47}$$

$$g^{(S)}_{\alpha\beta}N^\alpha N^\beta = 0, \tag{3.48}$$

where $N^\mu \equiv g^{\mu\nu}N_\nu$, and $g^{(S)}_{\alpha\beta}$ is defined by Eq. (3.2). For the metric and aether given in the form of Eqs. (3.35) and (3.36), they become

$$F(r_{MH}) = 0, \tag{3.49}$$

$$\left(c_S^2 - 1\right)\left(J(r_{S0H})^2 + 1\right) + 2\left(c_S^2 + 1\right)J(r_{S0H}) = 0, \tag{3.50}$$

where $r = r_{MH}$ and $r = r_{S0H}$ are the locations of the metric and spin-0 horizons, respectively. Note that Eqs. (3.49) and (3.50) may have multiple roots, say, r^i_{MH} and r^j_{S0H}. In these cases, the location of the metric (spin-0) horizon is always taken to be the largest root of r^i_{MH} (r^j_{S0H}).

Depending on the value of c_S, the solutions of Eq. (3.48) are given, respectively, by

$$J(r^{\pm}_{S0H}) = \frac{1 \mp c_S}{1 \pm c_S} \equiv J^{\pm}, \quad c_S \neq 1, \tag{3.51}$$

and

$$J(r_{S0H}) = 0, \quad c_S = 1. \tag{3.52}$$

It is interesting to note that on S0Hs, we have

$$\mathcal{D}(r_{S0H}) = 0, \tag{3.53}$$

as it can be seen from Eqs. (3.42), (3.43) and (3.50).

As mentioned above, for some choices of c_i, Eq. (3.48) does not always admit a solution, hence a S0H does not exist in this case. A particular choice was considered in [86], in which we have $c_1 = 0.051$, $c_2 = 0.116$, $c_3 = -c_1$ and $c_4 = 0$ (note that these choices have been ruled out by observations). For this choice, we find that $c_S \simeq 1.37404$, $J^+ \simeq -0.157556$ and $J^- \simeq -6.34696$. As shown in Fig. 3.1, the function $J(r)$ is always greater than $J^{\pm}$, so no S0H is formed, as first noticed in [86]. Up to the numerical errors, Fig. 3.1 is the same as that given in [86], which provides another way to check our general expressions of the field equations given above.

In addition, we also find that the two exact solutions obtained in [77] satisfy these equations identically, as it is expected.

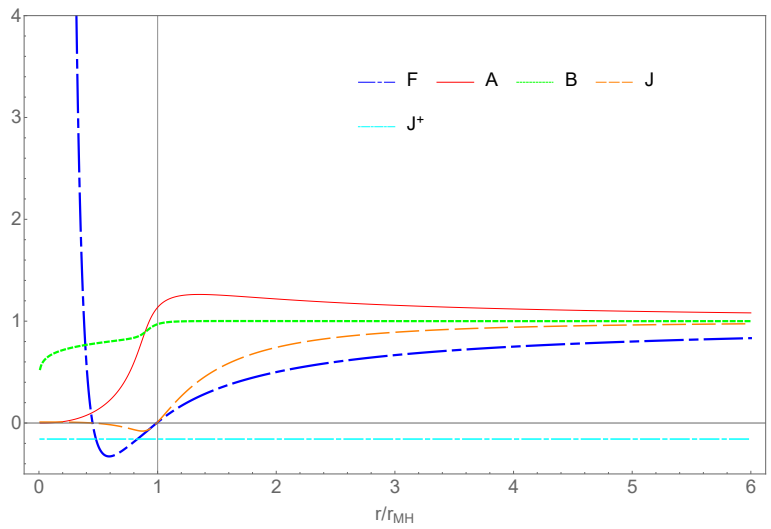

Figure 3.1: The solution for $c_1 = 0.051$, $c_2 = 0.116$, $c_3 = -c_1$ and $c_4 = 0$, first considered numerically in [86]. There are outer and inner MHs, at which F vanishes. However, J does not cross the constant line of J^+, so that a S0H is absent. This graph is the same as the one given in [86] (up to the numerical errors).

3.3.2 Exact Solutions with $c_{14} = c_{13} = 0$

From Eqs. (3.5) - (3.8) we can see that the choice $c_{14} = c_{13} = 0$ satisfies these constraints, provided that c_2 satisfies the condition [8],

$$0 \lesssim c_2 \lesssim 0.095. \tag{3.54}$$

Then, we find that Eqs. (3.39)-(3.40) now reduce to

$$F'' = -\frac{2}{r}F' + \frac{c_2\hat{\mathcal{F}}(r)}{4r^2A^4}, \tag{3.55}$$

$$A'' = \frac{2}{r^2(A+A^3F)}\left[r^2(A')^2 - rAA' - A^2 - rA^3A'(F+rF') + A^4F\right] - \frac{c_2\hat{\mathcal{F}}(r)}{4r^2(A+A^3F)}, \tag{3.56}$$

where

$$\hat{\mathcal{F}}(r) \equiv \left[rA' - 2A + rA^2A'F + A^3\left(2F + rF'\right)\right]^2. \tag{3.57}$$

[8] When $c_{14} = c_{13} = 0$, the speeds of the spin-0 and spin-1 modes can be infinitely large, as it can be seen from Eq. (1.7). Some unexpected problems may occur in such a case. Then, cautions must be taken, including the calculations of the PPN parameters [39].

Combining Eqs. (3.55) and (3.56), we find the following equation,

$$W'' + W'^2 + \frac{2}{r}W' - \frac{2}{r^2} = 0, \tag{3.58}$$

where

$$W \equiv \ln\left(\frac{1 - FA^2}{A}\right). \tag{3.59}$$

Eq. (3.58) has the general solution,

$$W = \ln w_2 + \ln\left(\frac{1 + w_1 r^3}{r^2}\right), \tag{3.60}$$

where w_1 and w_2 are two integration constants. Then, the combination of Eqs. (3.59) and (3.60) yield

$$F(r) = \frac{1}{A^2} - \frac{w_2}{A}\left(\frac{1}{r^2} + w_1 r\right). \tag{3.61}$$

Substituting Eq. (3.61) into Eq. (3.55), we find

$$F'' = -\frac{2}{r}F' + F_0, \tag{3.62}$$

where $F_0 \equiv 9c_2 w_1^2 w_2^2/4$. Integrating Eq. (3.62), we find

$$F(r) = F_2\left(1 - \frac{2m}{r}\right) + \frac{F_0}{6}r^2, \tag{3.63}$$

where m and F_2 are temporarily used as two other integration constants. On the other hand, from Eq. (3.61), we find that

$$A(r) = -\frac{w_2}{2F}\left[\left(\frac{1}{r^2} + w_1 r\right) \pm \sqrt{\frac{4F}{w_2^2} + \left(\frac{1}{r^2} + w_1 r\right)^2}\right]. \tag{3.64}$$

Substituting the above expressions for A and F into the constraint (3.45), we find that

$$B = \sqrt{F_2}. \tag{3.65}$$

Note that the above solution is asymptotically flat only when $w_1 = 0$, for which we have

$$F(r) = F_2\left(1 - \frac{2m}{r}\right), \quad B(r) = \sqrt{F_2}, \quad A(r) = -\frac{w_2}{2F}\left(\frac{1}{r^2} \pm \sqrt{\frac{4F}{w_2^2} + \frac{1}{r^4}}\right). \tag{3.66}$$

Using the gauge residual $v' = C_0 v + C_1$ (note that a prime above v does not stand for a derivative) of the metric (3.35), without loss of the generality, we can always set $F_2 = 1$, so the corresponding metric takes the precise form of the Schwarzschild solution,

$$ds^2 = -\left(1 - \frac{2m}{r}\right)dv^2 + 2dvdr + r^2 d\Omega^2, \tag{3.67}$$

while the aether field is given by

$$A(r) = \quad -\frac{w_2 \pm \sqrt{w_2^2 + 4r^3(r-2m)}}{2r(r-2m)}. \tag{3.68}$$

Interestingly, the analytic solutions here are actually consistent with the ones in [211], where the Schwarzschild solution for $\{F, B\}$ was assumed *a priori*. It is remarkable to note that now the aether field has no contribution to the spacetime geometry, although it does feel the gravitational field, as it can be seen from Eq. (3.68).

It should be also noted that Eqs. (3.67) and (3.68) were a particular case of the solutions first found in [77] for the case $c_{14} = 0$ by further setting $c_{13} = 0$. But, ignoring the potentially unphysical features, the general solutions given by Eqs. (3.63) - (3.65) are new, as far as I know.

3.3.3 Field Equations for $\tilde{g}_{\mu\nu}$ and $\tilde{u}^\mu$

Note that, instead of solving the three independent equations directly for A, B and F, we shall first solve the corresponding three equations for $\tilde{A}$, $\tilde{B}$ and $\tilde{F}$, by taking the advantage of the field redefinitions introduced in the last section, and then

obtain the functions A, B and F by the inverse transformations of Eqs. (3.73) and (3.75) to be given below. This will considerably simplify mathematically the problem of solving such complicated equations. A byproduct of this is the improvement to the accuracy of our solutions.

To this goal, let us first note that, with the filed redefinitions (3.11), the line element corresponding to $\hat{g}_{\mu\nu}$ in the EF coordinates (v, r, θ, ϕ), takes the form,

$$\begin{aligned} d\hat{s}^2 &\equiv \hat{g}_{\mu\nu}dx^\mu dx^\nu \\ &= -\left[F + \frac{(\sigma-1)\left(A^2F+1\right)^2}{4A^2}\right]dv^2 + 2\left[B + \frac{1}{2}(\sigma-1)B\left(A^2F+1\right)\right]dvdr \\ &\quad -(\sigma-1)A^2B^2dr^2 + r^2d\Omega^2. \end{aligned} \tag{3.69}$$

To bring the above expression into the standard EF form, we first make the coordinate transformation,

$$\tilde{v} = C_0 v - C(r), \tag{3.70}$$

where C_0 is an arbitrary real constant, and $C(r)$ is a function of r. Then, choosing $C(r)$ so that

$$\frac{dC(r)}{dr} = \frac{2C_0A^2B\left(\sqrt{\sigma}-1\right)}{J\left(\sqrt{\sigma}-1\right)+\left(\sqrt{\sigma}+1\right)}, \tag{3.71}$$

we find that in the coordinates $\tilde{x}^\mu = (\tilde{v}, r, \theta, \phi)$ the line element (3.69) takes the form,

$$d\hat{s}^2 \equiv \hat{g}_{\mu\nu}dx^\mu dx^\nu = \tilde{g}_{\mu\nu}d\tilde{x}^\mu d\tilde{x}^\nu = -\tilde{F}(r)d\tilde{v}^2 + 2\tilde{B}(r)d\tilde{v}dr + r^2d\Omega^2, \tag{3.72}$$

where

$$\tilde{F} = \frac{J^2(\sigma-1) + 2J(\sigma+1) + (\sigma-1)}{4C_0^2A^2}, \qquad \tilde{B} = \frac{\sqrt{\sigma}B}{C_0}. \tag{3.73}$$

On the other hand, in terms of the coordinates $\tilde{x}^\mu$, the aether four-velocity is given by

$$\hat{u}^\alpha \frac{\partial}{\partial x^\alpha} = \tilde{u}^\alpha \frac{\partial}{\partial \tilde{x}^\alpha} = \tilde{A}(r)\partial_{\tilde{v}} - \frac{1 - \tilde{F}(r)\tilde{A}^2(r)}{2\tilde{B}(r)\tilde{A}(r)}\partial_r, \tag{3.74}$$

where

$$\tilde{A} = \frac{2C_0 A}{J\left(\sqrt{\sigma} - 1\right) + \left(\sqrt{\sigma} + 1\right)}, \tag{3.75}$$

which satisfies the constraint $\tilde{u}^\alpha \tilde{u}^\beta \tilde{g}_{\alpha\beta} = -1$, with

$$\tilde{g}_{\mu\nu} \equiv \frac{\partial x^\alpha}{\partial \tilde{x}^\mu}\frac{\partial x^\beta}{\partial \tilde{x}^\nu}\hat{g}_{\alpha\beta}, \quad \tilde{u}_\mu \equiv \frac{\partial x^\alpha}{\partial \tilde{x}^\mu}\hat{u}_\alpha. \tag{3.76}$$

It should be noted that the metric (3.72) still has the gauge residual,

$$\tilde{\tilde{v}} = C_1 \tilde{v} + C_2, \tag{3.77}$$

where C_1 and C_2 are two arbitrary constants, which will keep the line element in the same form, after an apt rescaling,

$$\tilde{\tilde{F}} = \frac{\tilde{F}}{C_1^2}, \quad \tilde{\tilde{B}} = \frac{\tilde{B}}{C_1}. \tag{3.78}$$

Later we shall use this gauge freedom to fix one of the initial conditions. I want to emphasize that the coefficients C_0, C_1 and C_2 we used here are not the covariant C^v in (3.38).

In the rest of this chapter, we always refer $(\tilde{g}_{\mu\nu}, \tilde{u}^\alpha)$ as the field obtained by the field redefinitions. The latter is related to $(\hat{g}_{\mu\nu}, \hat{u}^\alpha)$ via the inverse coordinate transformations of Eq. (3.76). Then, the Einstein-aether field equations for $(\tilde{g}_{\mu\nu}, \tilde{u}^\alpha)$ will take the same forms as those given by Eqs. (3.17) - (3.19), but now in terms of $(\tilde{g}_{\mu\nu}, \tilde{u}^\alpha, \tilde{c}_i)$ in the coordinates $\tilde{x}^\mu$, where $\tilde{c}_i \equiv \hat{c}_i$.

On the other hand, since the metric (3.72) for $\tilde{g}_{\mu\nu}$ takes the same form as the metric (3.35) for $g_{\mu\nu}$, and so does the aether field (3.74) for $\tilde{u}^\mu$ as the one (3.36) for

u^μ, it is not difficult to see that the field equations for $\tilde{F}(r),\ \tilde{A}(r)$ and $\tilde{B}(r)$ will be given precisely by Eqs. (3.39) - (3.44), if we simply make the following replacement,

$$(F, A, B, c_i) \to \left(\tilde{F}, \tilde{A}, \tilde{B}, \tilde{c}_i\right). \tag{3.79}$$

As a result, we have

$$\begin{aligned}
\tilde{F}'' &= \tilde{\mathcal{F}}\left(\tilde{A}, \tilde{A}', \tilde{F}, \tilde{F}', r, \tilde{c}_i\right) \\
&= \frac{1}{2r^2\tilde{A}^4\tilde{\mathcal{D}}}\Big[\tilde{f}_0 + \tilde{f}_1\tilde{F} + \tilde{f}_2\tilde{F}^2 + \tilde{f}_3\tilde{F}^3 + \tilde{f}_4\tilde{F}^4\Big], \qquad (3.80) \\
\tilde{A}'' &= \tilde{\mathcal{A}}\left(\tilde{A}, \tilde{A}', \tilde{F}, \tilde{F}', r, \tilde{c}_i\right) \\
&= \frac{1}{2r^2\tilde{A}^2\tilde{\mathcal{D}}}\Big[\tilde{a}_0 + \tilde{a}_1\tilde{F} + \tilde{a}_2\tilde{F}^2 + \tilde{a}_3\tilde{F}^3\Big], \qquad (3.81) \\
\frac{\tilde{B}'}{\tilde{B}} &= \tilde{\mathcal{B}}\left(\tilde{A}, \tilde{A}', \tilde{F}, \tilde{F}', r, \tilde{c}_i\right) \\
&= \frac{1}{2r\tilde{A}^2\tilde{\mathcal{D}}}\Big[\tilde{b}_0 + \tilde{b}_1\tilde{F} + \tilde{b}_2\tilde{F}^2\Big], \qquad (3.82)
\end{aligned}$$

and

$$\tilde{C}^{\tilde{v}} \equiv \tilde{n}_0 + \tilde{n}_1\tilde{F} + \tilde{n}_2\tilde{F}^2 = 0, \tag{3.83}$$

where

$$\begin{aligned}
\tilde{\mathcal{D}}(r) &\equiv \tilde{d}_-\left(\tilde{J}^2(r) + 1\right) + 2\tilde{d}_+\tilde{J}(r), \\
\tilde{J}(r) &\equiv \tilde{F}(r)\tilde{A}^2(r), \\
\tilde{d}_\pm &\equiv (\tilde{c}_S^2 \pm 1)\tilde{c}_{14}(1 - \tilde{c}_{13})(2 + \tilde{c}_{13} + 3\tilde{c}_2). \qquad (3.84)
\end{aligned}$$

The coefficients $\tilde{f}_n,\ \tilde{a}_n,\ \tilde{b}_n$ and $\tilde{n}_n$ are given by $f_n,\ a_n,\ b_n$ and n_n after the replacement (3.79) is executed.

Then, the metric and spin-0 horizons for $\tilde{g}_{\mu\nu}$ are given, respectively, by

$$\tilde{g}_{\alpha\beta}\tilde{N}^\alpha\tilde{N}^\beta = 0, \tag{3.85}$$

$$\tilde{g}^{(S)}_{\alpha\beta}\tilde{N}^\alpha\tilde{N}^\beta = 0, \tag{3.86}$$

where $\tilde{N}_\alpha = (\partial x^\mu/\partial\tilde{x}^\alpha)N_\mu = \delta^r_{\tilde{\alpha}} = \delta^r_\alpha$ and

$$\tilde{g}^{(S)}_{\alpha\beta} \equiv \tilde{g}_{\alpha\beta} - \left(\tilde{c}_S^2 - 1\right)\tilde{u}_\alpha\tilde{u}_\beta. \tag{3.87}$$

In terms of $\tilde{F}$ and $\tilde{A}$, Eqs. (3.85) and (3.86) become

$$\tilde{F}(\tilde{r}_{MH}) = 0, \tag{3.88}$$

$$\left(\tilde{c}_S^2 - 1\right)\left(\tilde{J}(\tilde{r}_{S0H})^2 + 1\right) + 2\left(\tilde{c}_S^2 + 1\right)\tilde{J}(\tilde{r}_{S0H}) = 0, \tag{3.89}$$

where $r = \tilde{r}_{MH}$ and $r = \tilde{r}_{S0H}$ are respectively the locations of the metric and spin-0 horizons for the metric $\tilde{g}_{\mu\nu}$. Similarly, at $r = \tilde{r}_{S0H}$ we have

$$\tilde{\mathcal{D}}(\tilde{r}_{S0H}) = 0. \tag{3.90}$$

Comparing the field equations given in this subsection with the corresponding ones given in the previous subsections, we see that we can get one set from the other simply by the replacement (3.79).

In addition, in terms of $\hat{g}_{\alpha\beta}$ and N_α, Eqs. (3.85) and (3.86) reduce, respectively, to

$$\hat{g}_{\alpha\beta}N^\alpha N^\beta = 0, \tag{3.91}$$

$$\hat{g}^{(S)}_{\alpha\beta}N^\alpha N^\beta = 0. \tag{3.92}$$

Since $\tilde{r} = r$, we find that

$$\tilde{r}_{MH} = \hat{r}_{MH}, \quad \tilde{r}_{S0H} = \hat{r}_{S0H}, \tag{3.93}$$

where $\tilde{r}_{MH}$ and $\tilde{r}_{S0H}$ ($\hat{r}_{MH}, \hat{r}_{S0H}$) are the locations of the metric and spin-0 horizons of the metric $\tilde{g}_{\alpha\beta}$ ($\hat{g}_{\alpha\beta}$). The above analysis shows that *these horizons determined by $\tilde{g}_{\alpha\beta}$ are precisely equal to those determined by $\hat{g}_{\alpha\beta}$.*

3.3.4 $\sigma = c_S^2$

To solve Eqs. (3.80) - (3.83), we take the advantage of the choice $\sigma = c_S^2$, so that the speed of the spin-0 mode of the metric $\hat{g}_{\mu\nu}$ becomes unity, i.e., $\hat{c}_S = 1$. Since $\tilde{c}_i = \hat{c}_i$, we also have $\tilde{c}_S = \hat{c}_S = 1$. Then, from Eq. (1.7) we find that this leads to,

$$\tilde{c}_2 = \frac{2\tilde{c}_{14} - 2\tilde{c}_{13} - \tilde{c}_{13}^2\tilde{c}_{14}}{2 - 4\tilde{c}_{14} + 3\tilde{c}_{13}\tilde{c}_{14}}. \tag{3.94}$$

For such a choice, from Eq. (3.84) we find that $\tilde{d}_- = 0$, and

$$\tilde{\mathcal{D}}(r) = 2\tilde{d}_+\tilde{J}(r) = 2\tilde{d}_+\tilde{A}^2(r)\tilde{F}(r). \tag{3.95}$$

Then, Eq. (3.90) yields $\tilde{F}(\tilde{r}_{S0H}) = 0$, since $\tilde{A} \neq 0$, which also represents the location of the MH, defined by Eq. (3.88). Therefore, for the choice $\sigma = c_S^2$ the MH coincides with the S0H for the effective metric $\tilde{g}_{\mu\nu}$, that is,

$$\tilde{r}_{MH} = \tilde{r}_{S0H}, \ \left(\sigma = c_S^2\right). \tag{3.96}$$

As shown below, this will significantly reduce our computational labor. In particular, if we choose this surface as our initial moment, it will reduce the phase space of initial data from four dimensions to one dimension only.

For $\tilde{c}_S = 1$, Eqs. (3.80)-(3.83) reduce to,

$$\tilde{F}'' = \frac{1}{4\tilde{d}_+ r^2\tilde{A}^6}\left(\frac{\tilde{f}_0}{\tilde{F}} + \tilde{f}_1 + \tilde{f}_2\tilde{F} + \tilde{f}_3\tilde{F}^2. + \tilde{f}_4\tilde{F}^3\right), \tag{3.97}$$

$$\tilde{A}'' = \frac{1}{4\tilde{d}_+ r^2\tilde{A}^4}\left(\frac{\tilde{a}_0}{\tilde{F}} + \tilde{a}_1 + \tilde{a}_2\tilde{F} + \tilde{a}_3\tilde{F}^2\right), \tag{3.98}$$

$$\frac{\tilde{B}'}{\tilde{B}} = \frac{1}{4\tilde{d}_+ r\tilde{A}^4}\left(\frac{\tilde{b}_0}{\tilde{F}} + \tilde{b}_1 + \tilde{b}_2\tilde{F}\right), \tag{3.99}$$

$$\tilde{n}_0 + \tilde{n}_1\tilde{F} + \tilde{n}_2\tilde{F}^2 = 0. \tag{3.100}$$

As shown previously, among these four equations, only three of them are independent, and our strategy in this chapter is to take Eqs. (3.97), (3.98) and (3.100) as

the three independent equations. The advantage of this approach is that Eqs. (3.97), (3.98) are independent of $\tilde{B}(r)$, and Eq. (3.100) is a quadratic polynomial of $\tilde{B}(r)$. So, we can solve Eqs. (3.97), (3.98) as the initial value problem first to find $\tilde{F}(r)$ and $\tilde{A}(r)$, and then insert them into Eq. (3.100) to obtain directly $\tilde{B}(r)$, as explicitly given by Eq. (3.45), after taking the replacement (3.79) and the choice of $\tilde{c}_2$ of Eq. (3.94) into account.

From Eqs. (3.97) and (3.98) we can see that they become singular at $r = \tilde{r}_{S0H}$ [recall $\tilde{F}(\tilde{r}_{S0H}) = 0$], unless $\tilde{f}_0(\tilde{r}_{S0H}) = \tilde{a}_0(\tilde{r}_{S0H}) = 0$. As can be seen from the expressions of $f_0(r)$, $a_0(r)$ given in Appendix E, $\tilde{f}_0(\tilde{r}_{S0H}) = \tilde{a}_0(\tilde{r}_{S0H}) = 0$ imply $\tilde{b}_0(\tilde{r}_{S0H}) = 0$. Therefore, to have the field equations regular across the S0H, we must require $\tilde{b}_0(\tilde{r}_{S0H}) = 0$. It is interesting that this is also the condition for Eq. (3.99) to be non-singular across the S0H. In addition, using the gauge residual (3.77), we shall set $\tilde{B}_H = 1$, so Eq. (3.100) [which can be written in the form of Eq. (3.45), after the replacement (3.79)] will provide a constraint among the initial values of $\tilde{F}'_H$, $\tilde{A}_H$ and $\tilde{A}'_H$, where $\tilde{F}'_H \equiv \tilde{F}'(\tilde{r}_{S0H})$ and so on. In summary, on the S0H we have the following

$$\tilde{F}_H = 0, \tag{3.101}$$

$$\tilde{b}_0\left(\tilde{A}_H, \tilde{A}'_H, \tilde{F}'_H, \tilde{r}_{S0H}\right) = 0, \tag{3.102}$$

$$\tilde{B}_H = 1. \tag{3.103}$$

From the expression for $\tilde{b}_0$ given in Appendix E, we can see that Eq. (3.102) is quadratic in $\tilde{A}'_H$, and solving it on the S0H, in general we obtain two solutions,

$$\tilde{A}'^{\pm}_H = \tilde{A}'^{\pm}_H\left(\tilde{A}_H, \tilde{F}'_H, \tilde{r}_{S0H}\right). \tag{3.104}$$

Then, inserting it, together with Eqs. (3.101) and (3.103), into Eq. (3.44), we get

$$\tilde{n}^{\pm}_0\left(\tilde{A}_H, \tilde{F}'_H, \tilde{r}_{S0H}\right) = 0, \tag{3.105}$$

where the "±" signs correspond to the choices of $\tilde{A}'_H = \tilde{A}'^{\pm}_H$. In general, Eq. (3.105) is a 4th-order polynomial of $\tilde{F}'_H$, so it normally has four roots, denoted as

$$\tilde{F}'^{(\pm,n)}_H = \tilde{F}'^{(\pm,n)}_H \left(\tilde{A}_H, \tilde{r}_{S0H}\right), \tag{3.106}$$

where $n = 1, 2, 3, 4$. For each given $\tilde{F}'^{(\pm,n)}_H$, substituting it into Eq. (3.104) we find a corresponding $\tilde{A}'^{(\pm,n)}_H$, given by

$$\tilde{A}'^{(\pm,n)}_H = \tilde{A}'^{(\pm,n)}_H \left(\tilde{A}_H, \tilde{r}_{S0H}\right). \tag{3.107}$$

Thus, once $\tilde{A}_H$ and $\tilde{r}_{S0H}$ are given, the quantities $\tilde{F}'^{(\pm,n)}_H$ and $\tilde{A}'^{(\pm,n)}_H$ are uniquely determined from Eqs. (3.106) and (3.107). For each set of $(\tilde{A}_H, \tilde{r}_{S0H})$, in general there are eight (viz., 2×4) sets of $\left(\tilde{A}'_H, \tilde{F}'_H\right)$.

If we choose $r = \tilde{r}_{S0H}$ as the initial moment, such obtained $\left(\tilde{A}'_H, \tilde{F}'_H\right)$, together with $\tilde{F}_H = 0$, and a proper choice of $\tilde{A}_H$, can be considered as the initial conditions for the differential equations (3.97) and (3.98).

However, it is unclear which one(s) of these eight sets of initial conditions will lead to asymptotically flat solutions, except that the one with $\tilde{F}'_H < 0$, which can be discarded immediately, as it would lead to $\tilde{F} = 0$ at some radius $r > \tilde{r}_{S0H}$, which is inconsistent with our assumption that $r = \tilde{r}_{S0H}$ is the location of the S0H [90]. So, in general what one needs to do is to try all the possibilities [Although we cannot show why, in practice we found that there is always only one branch of $(\tilde{A}_H, \tilde{r}_{S0H})$ that will work both physically and engineeringly.].

Therefore, *if we choose $r = \tilde{r}_{S0H}$ as the initial moment, the four-dimensional phase space of the initial conditions, $\left(\tilde{F}_H, \tilde{F}'_H, \tilde{A}_H, \tilde{A}'_H\right)$, reduces to one-dimensional, spanned by $\tilde{A}_H$ only, as promised previously.*

In the following, I shall show further that $\tilde{r}_{S0H}$ can be chosen arbitrarily. In fact, introducing the dimensionless quantity, $\xi \equiv \tilde{r}_{S0H}/r$, we find that Eqs. (3.97) - (3.99) and (3.83) can be written in the forms

$$\frac{d^2\tilde{F}(\xi)}{d\xi^2} = \mathcal{G}_1\left(\xi, \tilde{c}_i\right), \tag{3.108}$$

$$\frac{d^2\tilde{A}(\xi)}{d\xi^2} = \mathcal{G}_2\left(\xi, \tilde{c}_i\right), \tag{3.109}$$

$$\frac{1}{\tilde{B}(\xi)}\frac{d\tilde{B}(\xi)}{d\xi} = \mathcal{G}_3\left(\xi, \tilde{c}_i\right), \tag{3.110}$$

$$C^{\tilde{v}}\left(\tilde{A}(\xi), \tilde{A}'(\xi), \tilde{F}(\xi), \tilde{F}'(\xi), \tilde{B}(\xi), \xi, \tilde{c}_i\right) = 0, \tag{3.111}$$

where $\mathcal{G}_i$'s are all independent of $\tilde{r}_{S0H}$, $C^{\tilde{v}} \equiv r_{S0H}^2\tilde{C}^{\tilde{v}}$, and the primes in the last equation now stand for the derivatives respect to ξ. Therefore, Eqs. (3.108)-(3.111), or equivalently, Eqs. (3.80)-(3.83), are scaling-invariant and independent of $\tilde{r}_{S0H}$. Thus, without loss of the generality, we can always set

$$\tilde{r}_{S0H} = 1, \tag{3.112}$$

which does not affect Eqs. (3.108) - (3.111), and also explains the reason why in [86,90] the authors set $\tilde{r}_{S0H} = 1$ directly. At the same time, it should be noted that once $\tilde{r}_{S0H} = 1$ is taken, it implies that the unit of length is fixed. For instance, if we have a BH with $\tilde{r}_{S0H} = 1$ km, then setting $\tilde{r}_{S0H} = 1$ means the unit of length is in km.

Once $\tilde{A}_H$ is chosen, we can integrate Eqs. (3.108) and (3.109) in both directions to find $\tilde{F}(\xi)$ and $\tilde{A}(\xi)$, one is toward the center, $\xi = \tilde{r}_{S0H}/r = \infty$, in which we have $\xi \in [1, \infty)$, and the other is toward infinity, $\xi = \tilde{r}_{S0H}/r = 0$, in which we have $\xi \in (0, 1]$. Then, from Eq. (3.45) we can find $\tilde{B}(\xi)$ uniquely, after the replacement of Eq. (3.79). Again, to have a proper asymptotic behavior of $\tilde{B}(r)$, the "+" sign will be chosen.

At the spatial infinity $\xi = \tilde{r}_{S0H}/r \to 0$, we require that the spacetime be asymptotically flat, that is [86, 90] [9],

$$\begin{aligned}
\tilde{F}(\xi) &= 1 + \tilde{F}_1\xi + \frac{1}{48}\tilde{c}_{14}\tilde{F}_1^3\xi^3 + \cdots, \\
\tilde{A}(\xi) &= 1 - \frac{1}{2}\tilde{F}_1\xi + \frac{1}{2}\tilde{A}_2\xi^2 - \left(\frac{1}{96}\tilde{c}_{14}\tilde{F}_1^3 - \frac{1}{16}\tilde{F}_1^3 + \frac{1}{2}\tilde{F}_1\tilde{A}_2\right)\xi^3 + \cdots, \\
\tilde{B}(\xi) &= 1 + \frac{1}{16}\tilde{c}_{14}\tilde{F}_1^2\xi^2 - \frac{1}{12}\tilde{c}_{14}\tilde{F}_1^3\xi^3 + \cdots,
\end{aligned} \tag{3.113}$$

where $\tilde{F}_1 \equiv \tilde{F}'(\xi = 0)$ and $\tilde{A}_2 \equiv \tilde{A}''(\xi = 0)$.

It should be noted that the Minkowski spacetime is given by

$$\tilde{F} = \tilde{F}_M, \qquad \tilde{A} = \frac{1}{\sqrt{\tilde{F}_M}}, \qquad \tilde{B} = \sqrt{\tilde{F}_M}, \tag{3.114}$$

where $\tilde{F}_M$ is a positive otherwise arbitrary constant. Therefore, in the asymptotic expansions of Eq. (3.113), we had set $\tilde{F}_M = 1$ at the zeroth order of ξ. However, the initial conditions imposed at $r = \tilde{r}_{S0H}$ given above usually leads to $\tilde{F}_M \neq 1$, even for spacetimes that are asymptotically flat (As can be seen later, this is not urgent at all since the vital thing is to normalize the physical $\{F, A, B\}$.). Therefore, we need first to use the gauge residual (3.77) to bring $\tilde{F}(\xi = 0) = \tilde{A}(\xi = 0) = \tilde{B}(\xi = 0) = 1$, before using Eq. (3.113) to calculate the constants $\tilde{A}_2$ and $\tilde{F}_1$.

From the above analysis we can see that *finding spherically symmetric solutions of æ-theory now reduces to finding the initial condition $\tilde{A}_H$ that leads to the asymptotic behavior (3.113), for a given set of c_i's.*

Before proceeding to the next section, we would like to recall that when $\sigma = c_S^2$, we have $g^{(S)}_{\alpha\beta} = \hat{g}_{\alpha\beta}$, as shown by Eq. (3.23). That is, the S0H for the metric $g_{\alpha\beta}$ now coincides with the MH of $\hat{g}_{\alpha\beta}$. With this same very choice, $\sigma = c_S^2$, the MH for $\hat{g}_{\alpha\beta}$

[9] Note that in [86, 90] a factor 1/2 is missing in front of A_2 in the expression of $A(x)$.

also coincides with its S0H. Thus, we have

$$r_{S0H} = \hat{r}_{S0H} = \hat{r}_{MH} = \tilde{r}_{S0H} = \tilde{r}_{MH} \equiv r_H, \ \left(\sigma = c_S^2\right). \tag{3.115}$$

It must be noted that r_H defined in the last step denotes the location of the S0H of $g_{\alpha\beta}$, which is usually different from its MH, defined by

$$g_{\alpha\beta}N^\alpha N^\beta\big|_{r=r_{MH}} = 0, \tag{3.116}$$

since in general we have $c_S \neq 1$, so $g^{(S)}_{\alpha\beta} \equiv g_{\alpha\beta} - (c_S^2 - 1)\, u_\alpha u_\beta \neq g_{\alpha\beta}$. As a result, we have $r_{MH} \neq r_{S0H}$ for $c_S \neq 1$.

However, it is worth emphasizing again that, for the choice $\sigma = c_S^2$ we have $\tilde{c}_S = \hat{c}_S = 1$, so the metric and spin-0 horizons of both $\hat{g}_{\alpha\beta}$ and $\tilde{g}_{\alpha\beta}$ all coincide, and are given by the same r_H, as explicitly shown by Eq. (3.115). More importantly, it is also the location of the S0Hs of the metric $g_{\alpha\beta}$.

3.4 Numerical Setup and Results

3.4.1 General Steps

It is difficult to find analytical solutions to Eqs. (3.108)-(3.111). Thus, in this section we are going to solve them numerically, using the shooting method, with the asymptotic conditions (3.113). In particular, our strategy is the following:

(i) Choose a set of physical c_i's satisfying all the currently known physical constraints (see the previous chapters for more details), and then calculate the corresponding $\tilde{c}_i$'s with $\sigma = c_S^2$.

(ii) Assume that for such chosen c_i's the corresponding solution possesses a S0H located at $r = r_H$ [cf. (3.115)], and then follow the analysis given in the last section to impose the conditions $\tilde{F}_H = 0$ and $\tilde{B}_H = 1$.

(iii) Choose a test value for $\tilde{A}_H$ (again, this is the only test quantity to trigger our iterations for searching the unique solutions), and then solve Eq. (3.102) for $\tilde{A}'_H$ in terms of $\tilde{F}'_H$ and $\tilde{A}_H$, i.e., $\tilde{A}'_H = \tilde{A}'_H(\tilde{F}'_H, \tilde{A}_H)$.

(iv) Substitute $\tilde{A}'_H$ into Eq. (3.105) to obtain a quartic equation for $\tilde{F}'_H$ and then solve it to find $\tilde{F}'_H$.

(v) With the initial conditions $\{\tilde{F}_H, \tilde{A}_H, \tilde{F}'_H, \tilde{A}'_H\}$, integrate Eqs. (3.108) and (3.109) from $\xi = 1$ to $\xi = 0$ (the integration here means the numerical strategies for solving ODEs [212, 213] and it will be done by *Mathematica* with some built-in techniques).

However, since the field equations are singular at $\xi = 1$, we will actually integrate these equations from $\xi = 1 - \epsilon$ to $\xi \simeq 0$, where ϵ is a very small quantity, to avoid engineering troubles. To obtain the values of $\mathcal{F}(\xi)$ at $\xi = 1 - \epsilon$, we first Taylor expand [214, 215] them in the form,

$$\mathcal{F}(1-\epsilon) = \sum_{k=0}^{2} \frac{\mathcal{F}^{(k)}|_{\xi=1}}{k!}(-1)^k \epsilon^k + \mathcal{O}\left(\epsilon^3\right), \tag{3.117}$$

where $\mathcal{F} \equiv \left\{\tilde{A}, \tilde{A}', \tilde{F}, \tilde{F}'\right\}$ and $\mathcal{F}^{(k)} \equiv d^k\mathcal{F}/d\xi^k$ (Of course, although it is not necessary, we can expand to any high orders as we wish, given enough time.). For each $\mathcal{F}$, we shall expand it to the second order of ϵ, so the errors are of the order ϵ^3. Thus, if we choose $\epsilon = 10^{-14}$, the errors in the initial conditions $\mathcal{F}(1-\epsilon)$ are of the order 10^{-42}. For $\mathcal{F} = \tilde{A},\ \tilde{F}$, we already obtained $\mathcal{F}(1)$ and $\mathcal{F}'(1)$ from the initial conditions. In these cases, to get $\tilde{A}''(1)$ and $\tilde{F}''(1)$, we use the field equations (3.108) and (3.109) and L'Hospital's rule [216]. On the other hand, for $\mathcal{F} = \tilde{A}'$, expanding it to the second order of ϵ, we have

$$\tilde{A}'(1-\epsilon) = \tilde{A}'(1) - \tilde{A}''(1)\epsilon + \frac{1}{2}\tilde{A}^{(3)}(1)\epsilon^2 + \mathcal{O}\left(\epsilon^3\right), \tag{3.118}$$

where $\tilde{A}^{(3)}(1) \equiv d^3\tilde{A}(\xi)/d\xi^3\Big|_{\xi=1}$ can be obtained by first taking the derivative of Eq. (3.109) and then taking the limit $\xi \to 1$, as now we have already known $\tilde{A}(1)$, $\tilde{A}'(1)$, $\tilde{A}''(1)$, $\tilde{F}(1)$, $\tilde{F}'(1)$ and $\tilde{F}''(1)$. Similarly, for $\mathcal{F} = \tilde{F}'$, from Eq. (3.108) we can find $\tilde{F}^{(3)}(1)$.

(vi) Repeat (iii)-(v) until a numerical solution matched to Eq. (3.113) is obtained, by logically choosing different values of $\tilde{A}_H$ with a bisectional search (this could be done manually or automatically by *Mathematica*). Clearly, once such a value of $\tilde{A}_H$ is found, it means that we obtain numerically an asymptotically flat solution of the Einstein-aether field equations outside the S0H. Note that, to guarantee that Eq. (3.113) is satisfied, the normalization of $\{\tilde{F}, \tilde{A}, \tilde{B}\}$ needs to be done according to Eq. (3.114), by using the remaining gauge residual of Eq. (3.77).

(vii) To obtain the solution in the internal region $\xi \in (1, \infty)$, we simply integrate Eqs. (3.108) and (3.109) from $\xi = 1$ to $\xi \to \infty$ with the same value of $\tilde{A}_H$ found in the last step. As in the region $\xi \in (0, 1)$, we can't really set the "initial" conditions precisely at $\xi = 1$. Instead, we will integrate them from $\xi = 1 + \epsilon$ to $\xi = \xi_\infty \gg 1$. The initial values at $\xi = 1 + \epsilon$ can be obtained by following what we did in Step (v), that is, Taylor expand $\mathcal{F}(\xi)$ at $\xi = 1 + \epsilon$, and then use the field equations to get all the quantities up to the third order of ϵ.

(viii) Sewing the results obtained from steps (vi) and (vii) together, we finally obtain a solution of $\{\tilde{F}(\xi), \tilde{A}(\xi)\}$ on the whole spacetime $\xi \in (0, \infty)$ [or equivalently $r \in (0, \infty)$].

(ix) Once $\tilde{F}$ and $\tilde{A}$ are known, from Eq. (3.45), we can calculate $\tilde{B}$, so that an asymptotically flat black hole solution for $\{\tilde{A}, \tilde{B}, \tilde{F}\}$ is finally obtained over the whole space $r \in (0, \infty)$.

Before proceeding to the next subsection to consider the physically allowed region of the parameter space of c_i's, let us pause here to reproduce the results presented in Table I of [90], in order to check our numerical code, although all these choices have been ruled out currently by observations [60]. To see this explicitly, let us first note that the parameters chosen in [86, 90] correspond to

$$\hat{c}_2 = -\frac{\hat{c}_1^3}{3\hat{c}_1^2 - 4\hat{c}_1 + 2}, \quad \hat{c}_3 = 0 = \hat{c}_4 = 0, \tag{3.119}$$

so that now only $\hat{c}_1$ is a free parameter. With this choice of $\hat{c}_i$'s, the corresponding c_i's can be obtained from Eqs. (3.13) with $\sigma = c_S^2$, which are given by,

$$c_{14} = \hat{c}_1, \quad c_2 = \frac{-2c_{13} + 2\hat{c}_1 + 2c_{13}\hat{c}_1 - 2\hat{c}_1^2 - c_{13}\hat{c}_1^2}{2 - 4\hat{c}_1 + 3\hat{c}_1^2}, \tag{3.120}$$

where c_{13} is arbitrary. This implies that Eqs. (3.13) are degenerate for the choices of Eqs. (4.45). It can be seen from Eq. (3.120), in all the cases considered in [90], we have $c_{14} > 2.5 \times 10^{-5}$. Hence all the cases considered in [86, 90] do not satisfy the current constraints [60].

With the above in mind, we reproduce all the cases considered in [86, 90], including the ones with $\tilde{c}_1 > 0.8$. Our results are presented in Table 3.1, where

$$\tilde{\gamma}_{ff} \equiv \tilde{u}^\alpha u_\alpha^{\rm obs}, \tag{3.121}$$

$$\tilde{r}_g \equiv -r_H \times \lim_{\xi\to 0} \frac{d\tilde{F}(\xi)}{d\xi} = 2G_{æ}M_{\rm ADM}. \tag{3.122}$$

Here, $u_\alpha^{\rm obs}$ is the tangent (unit) vector to a radial free-fall trajectory that starts at rest at spatial infinity, and $M_{\rm ADM}$ denotes the Komar mass, which is equal to the Arnowitt-Deser-Misner (ADM) mass in the spherically symmetric case for the metric $\tilde{g}_{\alpha\beta}$ [77].

Table 3.1: The cases considered in [86, 90] for various $\hat{c}_1$ with the choice of the parameters $\hat{c}_2$, $\hat{c}_3$ and $\hat{c}_4$ given by Eq. (4.45). Note that for each physical quantity, we have added two more significant digits, due to the improved accuracy of our numerical code.

$\hat{c}_1$	$\tilde{r}_g/r_H$	$\tilde{F}'_H\tilde{A}^2_H$	$\tilde{\gamma}_{ff}$
0.1	0.98948936	2.0961175	1.6028048
0.2	0.97802140	2.0716798	1.5769479
0.3	0.96522924	2.0391972	1.5476848
0.4	0.95054650	1.9965155	1.5140905
0.5	0.93304411	1.9405578	1.4748439
0.6	0.91106847	1.8666845	1.4279611
0.7	0.88131278	1.7673168	1.3702427
0.8	0.83583029	1.6283356	1.2959142
0.9	0.74751927	1.4155736	1.1921231
0.91	0.73301185	1.3870211	1.1790400
0.92	0.71650458	1.3563710	1.1652344
0.93	0.69745439	1.3232418	1.1506047
0.94	0.67507450	1.2871125	1.1350208
0.95	0.64816499	1.2472379	1.1183101
0.96	0.61476429	1.2024805	1.1002331
0.97	0.57133058	1.1509356	1.0804355
0.98	0.51038168	1.0889067	1.0583387
0.99	0.41063001	1.0068873	1.0328120

From Table 3.1 we can see that our results are exactly the same as those given in [90] up to the same accuracy. But, due to the improved accuracy of our numerical code, for each of the physical quantity, we provided two more significant digits.

Additionally, in Fig. 3.2 we plotted the functions $\tilde{F}$, $\tilde{B}$, $\tilde{A}$ and $\tilde{\mathcal{C}}$ for four representative cases listed in Table 3.1 ($\hat{c}_1 = 0.1, 0.3, 0.6, 0.99$). Here, the quantity $\tilde{\mathcal{C}}$ is defined as

$$\tilde{\mathcal{C}} \equiv \left| \frac{d\ln\tilde{B}}{d\xi} - \mathcal{G}_3 \right|, \tag{3.123}$$

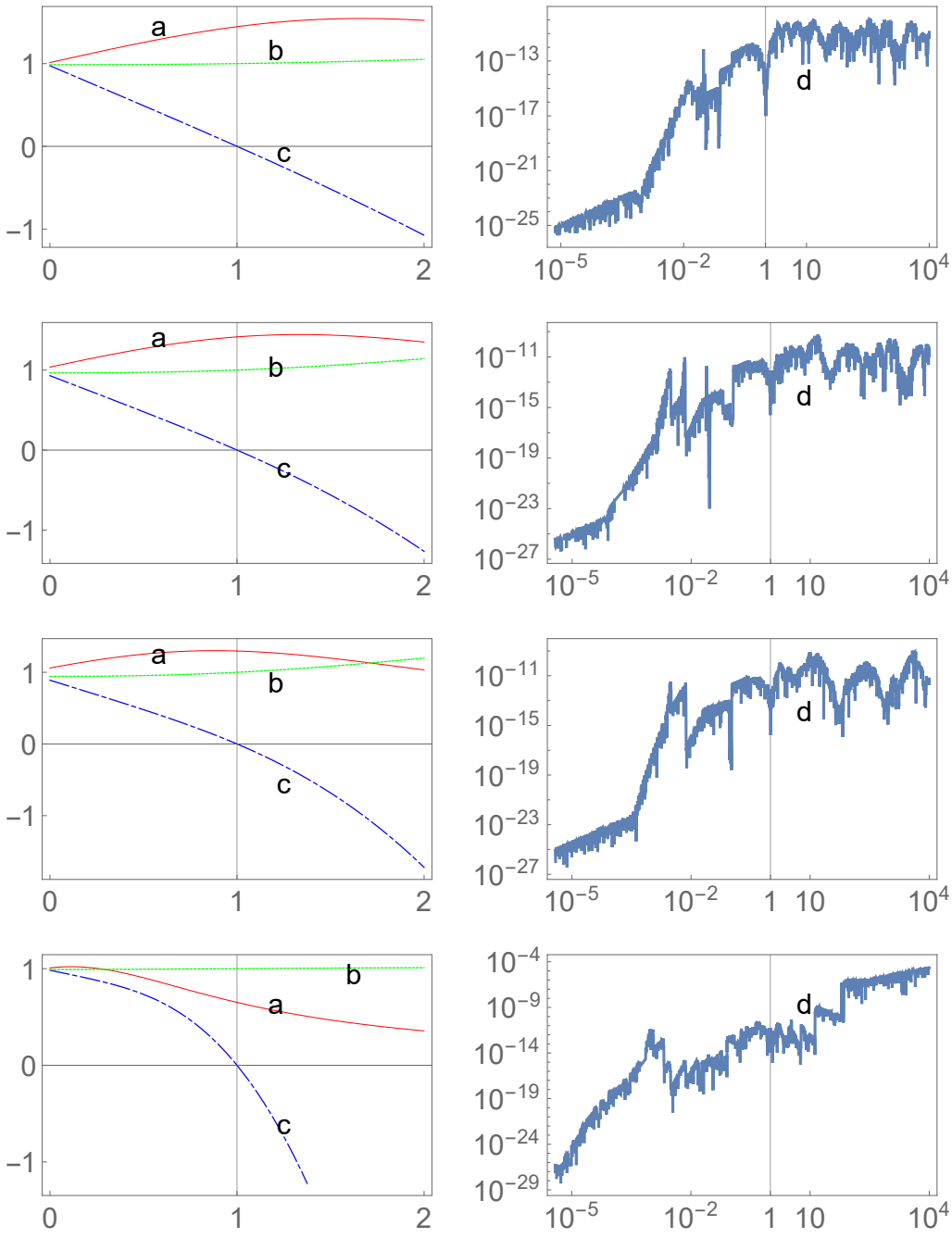

Figure 3.2: In the above graphs, we use a, b, c and d to represent $\tilde{A}$, $\tilde{B}$, $\tilde{F}$ and $\tilde{\mathcal{C}}$. Note that they are functions of ξ. In each row, $\hat{c}_1$ is chosen, respectively, as $\hat{c}_1 = 0.1, 0.3, 0.6, 0.99$, as listed in Table 3.1. The horizontal axis is r_H/r.

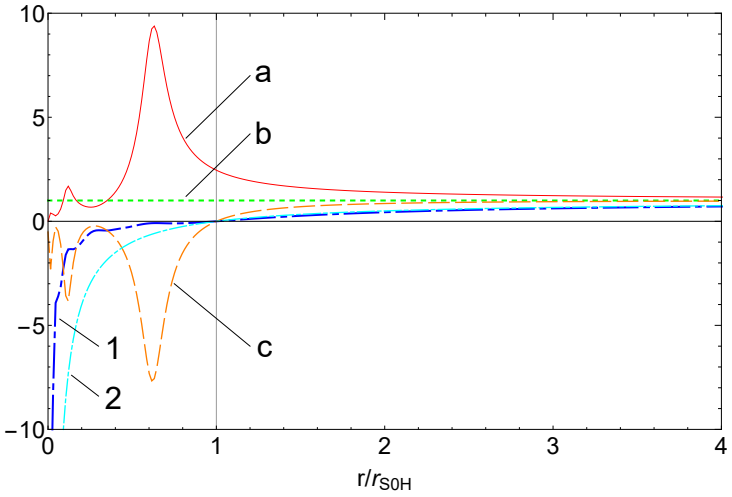

Figure 3.3: The solution for $c_{14} = 2 \times 10^{-7}$, $c_2 = 9 \times 10^{-7}$, and $c_3 = -c_1$. Here, $\tilde{A}$, $\tilde{B}$, $\tilde{J}$, $\tilde{F}$ and $\tilde{F}^{GR}$ are represented by the red line (labeled by a), green line (labeled by b), orange line (labeled by c), blue line (labeled by 1) and cyan line (labeled by 2) respectively.

which vanishes identically for the solutions of the field equations, as it can be seen from Eq. (3.110). In the rest of this chapter, we shall use it to check the accuracy of our numerical code.

From Fig. 3.2, we note that the properties of $\{\tilde{F}, \tilde{A}, \tilde{B}\}$ depend on the choice of $\hat{c}_1$. The quantity $\tilde{\mathcal{C}}$ is approximately zero within the whole integration range, which means that our numerical solutions are quite reliable.

3.4.2 Physically Viable Solutions with S0Hs

With the above verification of our numerical code, we turn to the physically viable solutions of the Einstein-aether field equations, in which a S0H always exists. Since c_{13} is very small, without loss of the generality, in this subsection we only consider the cases with $c_{13} = 0$.

As the first example, let us consider the case $c_{14} = 2 \times 10^{-7}$, $c_2 = 9 \times 10^{-7}$, and $c_3 = -c_1$, which satisfies the constraints (1.9). Fig. 3.3 shows the functions

$\tilde{F}, \tilde{A}, \tilde{B}$, in which we also plot $\tilde{J} \equiv \tilde{F}\tilde{A}^2$ and the GR limit of $\tilde{F}$, denoted by $\tilde{F}^{GR}$ with $\tilde{F}^{GR} \equiv 1 - r_H/r$.

In plotting Fig. 3.3, we chose $\epsilon = 10^{-14}$. With the shooting method, $\tilde{A}_H$ is determined to be $\tilde{A}_H \simeq 2.4558992$ [10]. In our calculations, we stop repeating the bisection search for $\tilde{A}_H$, when the value $\tilde{A}_H$ giving an asymptotically flat solution is determined to within 10^{-23}. Technically, this accuracy could be further improved. However, for our current purposes, it has already been sufficient.

As I have already mentioned, theoretically Eq. (3.110) will be automatically satisfied once Eqs. (3.108), (3.109) and (3.111) hold. However, due to numerical errors, in practice, it can never be zero numerically. Thus, to monitor our numerical errors, we always plot out the quantity $\tilde{\mathcal{C}}$ defined by Eq. (3.123), from which we can see clearly the numerical errors in our calculations. So, in the right-hand panels of Fig. 3.4, we plot out the curves of $\tilde{\mathcal{C}}$, denoted by d, in each case.

Clearly, outside the S0H, $\tilde{\mathcal{C}} \lesssim 10^{-17}$, while inside the S0H we have $\tilde{\mathcal{C}} \lesssim 10^{-10}$. Thus, the solutions inside the horizon are not as accurate as the ones given outside of the horizon. However, since in this chapter we are mainly concerned with the spacetime outside of the S0H, we shall not consider further improvements of our numerical code inside the horizon. The other quantities, such as c_S^2 and $\tilde{r}_g$, are all given by the first row of Table 3.2.

Following the same steps, we also consider other cases, and some of them are presented in Tables 3.2-3.3. In particular, in Table 3.2, we fix the ratio of c_2/c_{14} to be

[10] During the numerical calculations, we find that the asymptotic behavior (3.113) of the metric coefficients at $\xi \equiv r_H/r \simeq 0$ sensitively depends on the value of $\tilde{A}_H$. To make our results reliable, among all the steps in our codes, the precision is chosen to be not less than 37 (Note that "accuracy"$\neq$ "precision").

Table 3.2: c_S^2, $\tilde{A}_H$ and $\tilde{r}_g/r_H$ calculated from different $\{c_2, c_{14}\}$ with $c_{13} = 0$ and a fixed ratio of c_2/c_{14}.

c_2	c_{14}	c_S^2	$\tilde{A}_H$	$\tilde{r}_g/r_H$
9×10^{-7}	2×10^{-7}	4.4999935	2.4558992	1.1450729
9×10^{-8}	2×10^{-8}	4.4999994	2.4559003	1.1450730
9×10^{-9}	2×10^{-9}	4.4999999	2.4559004	1.1450730

Table 3.3: c_S^2, $\tilde{A}_H$ and $\tilde{r}_g/r_H$ calculated from different $\{c_2, c_{14}\}$ with $c_{13} = 0$ and changing c_2/c_{14}.

c_2	c_{14}	c_S^2	$\tilde{A}_H$	$\tilde{r}_g/r_H$
2.01×10^{-5}	2×10^{-5}	1.0049596	1.4562430	1.0005850
7×10^{-7}	5×10^{-7}	1.3999982	1.6196457	1.0381205
9×10^{-7}	2×10^{-8}	44.999939	6.4676346	1.2629671
9×10^{-5}	2×10^{-7}	449.93921	19.053220	1.3091657

9/2. In addition, the values of $\{c_2, c_{14}\}$ are chosen so that they satisfy the constraints of Eq. (1.9). In Table 3.3, the ratio c_2/c_{14} is changing and the values of $\{c_2, c_{14}\}$ are chosen so that they are spreading over the whole viable range of c_{14}, given by Eqs. (3.6)-(3.8).

From these tables we can see that quantities like $\tilde{A}_H$ and $\tilde{r}_g$ are sensitive only to the ratio of c_2/c_{14}, instead of their individual values. This is understandable, as for $c_{13} = 0$ and $c_{14} \lesssim 2.5 \times 10^{-5}$, Eq. (1.7) shows that $c_S \simeq c_S(c_2/c_{14})$. Therefore, the same ratio of c_2/c_{14} implies the same velocity of the spin-0 graviton. Since S0H is defined by the speed of this massless particle, it is quite reasonable to expect that the related quantities are sensitive only to the value of c_S.

The resulting $\tilde{F}$, $\tilde{A}$, $\tilde{B}$ and $\tilde{\mathcal{C}}$ for the cases listed in Tables 3.2 and 3.3 are plotted in Figs. 3.4 and 3.5, respectively.

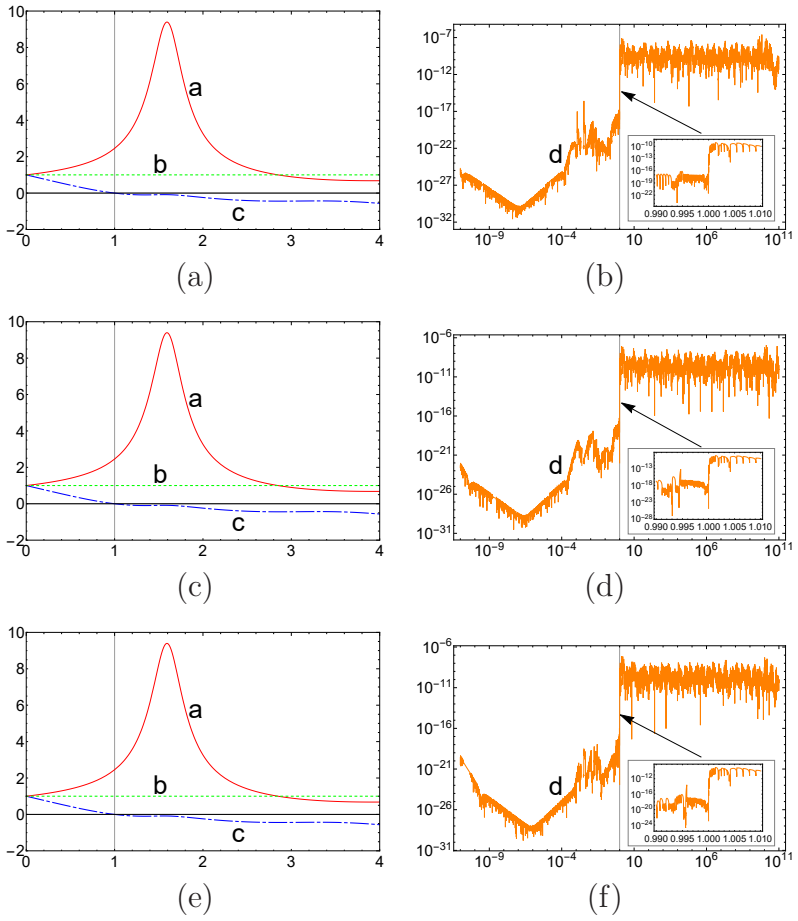

Figure 3.4: $\tilde{A}$, $\tilde{B}$ and $\tilde{F}$ for different combinations of $\{c_2, c_{14}\}$ listed in Table 3.2 and their corresponding $\tilde{\mathcal{C}}$'s. Here the horizontal axis is r_H/r. $\tilde{A}$, $\tilde{B}$, $\tilde{F}$ and $\tilde{\mathcal{C}}$ are represented by the red solid line (labeled by a), green dotted line (labeled by b), blue dash-dotted line (labeled by c) and orange solid line (labeled by d) respectively. To be specific, (a) and (b) are for the case $\{9 \times 10^{-7}, 2 \times 10^{-7}\}$, (c) and (d) are for the case $\{9 \times 10^{-8}, 2 \times 10^{-8}\}$, (e) and (f) are for the case $\{9 \times 10^{-9}, 2 \times 10^{-9}\}$. Note that the small graphs inserted in (b), (d) and (f) show the amplifications of $\tilde{\mathcal{C}}$'s near $r = r_H$.

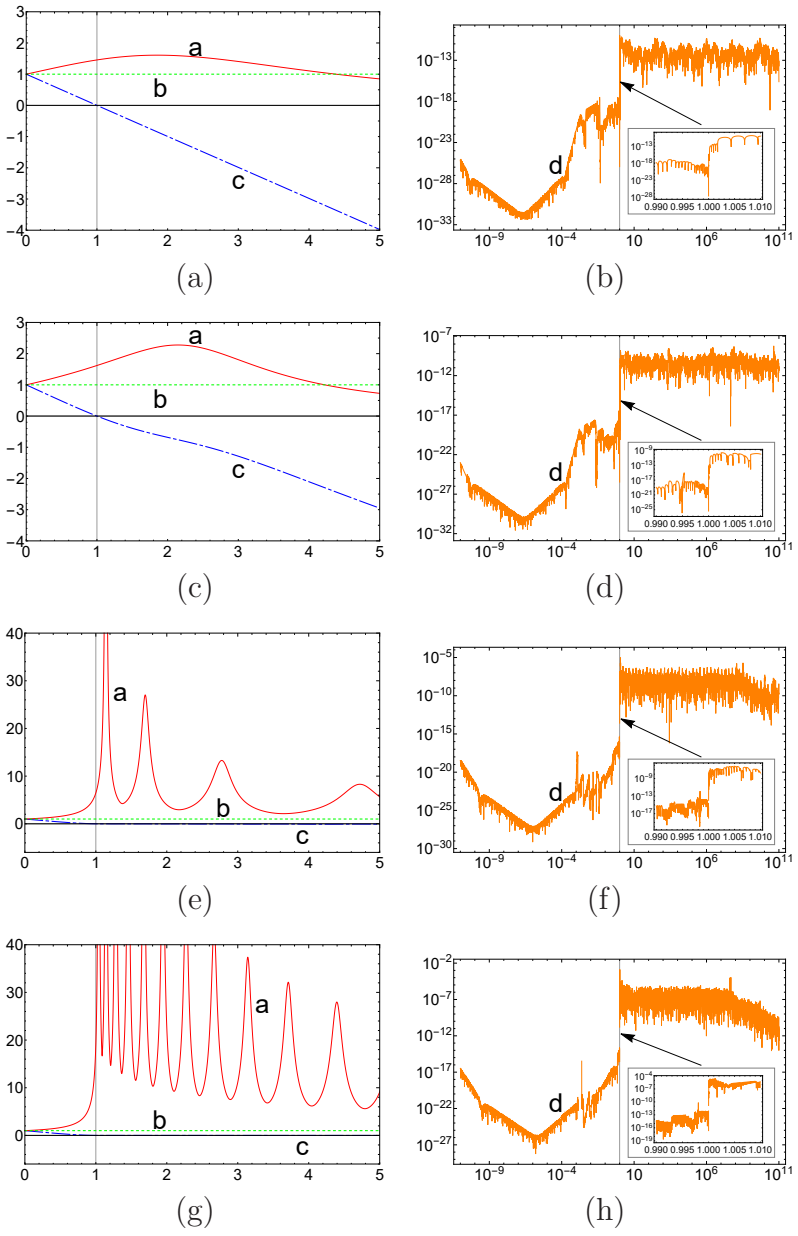

Figure 3.5: $\tilde{A}$, $\tilde{B}$ and $\tilde{F}$ for different combinations of $\{c_2, c_{14}\}$ listed in Table 3.3 and their corresponding $\tilde{\mathcal{C}}$'s. Here the horizontal axis is r_H/r. $\tilde{A}$, $\tilde{B}$, $\tilde{F}$ and $\tilde{\mathcal{C}}$ are represented by the red solid line (labeled by a), green dotted line (labeled by b), blue dash-dotted line (labeled by c) and orange solid line (labeled by d) respectively. To be specific, (a) and (b) are for the case $\{2.01 \times 10^{-5}, 2 \times 10^{-5}\}$, (c) and (d) are for the case $\{7 \times 10^{-7}, 5 \times 10^{-7}\}$, (e) and (f) are for the case $\{9 \times 10^{-7}, 2 \times 10^{-8}\}$, (g) and (h) are for the case $\{9 \times 10^{-5}, 2 \times 10^{-7}\}$. Note that the small graphs inserted in (b), (d), (f) and (h) show the amplifications of $\tilde{\mathcal{C}}$ near $r = r_H$.

3.5 Physical Solutions ($g_{\alpha\beta},\ u^\mu$)

The above steps reveal how we find the solutions of the effective metric $\tilde{g}_{\mu\nu}$ and aether field $\tilde{u}^\mu$. To find the corresponding physical quantities $g_{\mu\nu}$ and u^μ, we shall follow two steps: (a) Reverse Eqs. (3.73) and (3.75) to find a set of the physical quantities $\{F(\xi), A(\xi), B(\xi)\}$ (note that we have $\xi = \tilde{r}_{S0H}/r = r_{S0H}/r$). (b) Apply the rescaling $v \to C_0 v$ to make the set of $\{F(\xi), A(\xi), B(\xi)\}$ take the standard form at spatial infinity $r = \infty$.

To these purposes, let us first note that, near the spatial infinity, Eqs. (3.113), (3.73) and (3.75) lead to

$$\begin{aligned}
F(\xi) &= \frac{C_0^2}{\sigma}\left(1 + F_1\xi + \frac{1}{48}c_{14}F_1^3\xi^3\right) + \mathcal{O}\left(\xi^4\right),\\
B(\xi) &= \frac{C_0}{\sqrt{\sigma}}\left(1 + \frac{1}{16}c_{14}F_1^2\xi^2 - \frac{1}{12}c_{14}F_1^3\xi^3\right) + \mathcal{O}\left(\xi^4\right),\\
A(\xi) &= \frac{\sqrt{\sigma}}{C_0}\left[1 - \frac{1}{2}F_1\xi + \frac{1}{2}A_2\xi^2 - \left(\frac{1}{2}A_2F_1 - \frac{1}{16}F_1^3 + \frac{1}{96}c_{14}F_1^3\right)\xi^3\right] + \mathcal{O}\left(\xi^4\right),
\end{aligned} \tag{3.124}$$

where

$$F_1 = \tilde{F}_1, \quad c_{14} = \tilde{c}_{14}, \quad A_2 = \sqrt{\sigma}\tilde{A}_2 - \frac{3}{4}(\sqrt{\sigma} - 1)\tilde{F}_1^2. \tag{3.125}$$

The above expressions show clearly that *the spacetimes described by* $(g_{\mu\nu}, u^\mu)$ *are asymptotically flat, provided that the effective fields* $(\tilde{g}_{\mu\nu}, \tilde{u}^\mu)$ *are.* In particular, setting $C_0 = \sqrt{\sigma}$, a condition that will be assumed in the rest of this chapter, the functions $F,\ A$ and B will take their standard asymptotically-flat forms.

It is remarkable to note that the asymptotic behavior of the functions $F,\ A$ and B depends only on c_{14} up to the third-order of ξ, but c_2 will show up starting from the four-order, ξ^4. Besides, one may notice that we won't have $F(r \to \infty) = 1$

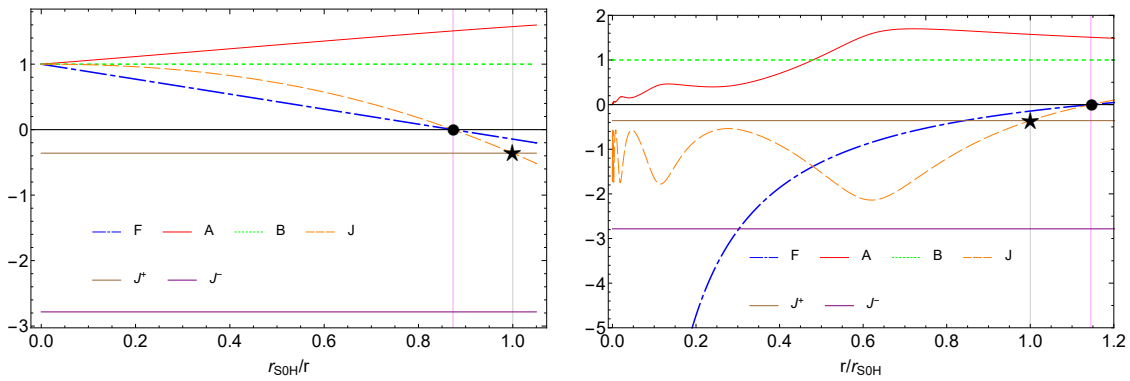

Figure 3.6: The evolutions of the physical quantities F, A, B and J for the case $c_{13} = 0$, $c_2 = 9 \times 10^{-7}$ and $c_{14} = 2 \times 10^{-7}$. Here, A, B, J and F are represented by the red solid line, green dotted line, orange dashed line, and blue dash-dotted line, respectively. The positions of $r = r_{MH} \cap F$ and $r = r_{S0H} \cap J$ are marked by a small full solid circle and a pentagram, respectively. Note that we have $r_{MH} > r_{S0H}$. The values J^+ and J^- are given respectively by the brown and purple solid lines with $J^+ > J^-$. The left panel shows the main behaviors of the functions outside the S0H in the range $r_{S0H}/r \in (0, 1.105)$, while the right panel shows their main behaviors inside the S0H in the range $r/r_{S0H} \in (0, 1.2)$.

and $\tilde{F}(r \to \infty) = 1$ simultaneously once C_0 is chosen (although our calculations show that they could both be close to 1 at the spatial infinity at the same time). Of course, this doesn't matter since $\tilde{F}$, $\tilde{A}$ and $\tilde{B}$ are just some expedient quantities for deriving physical observables, with later are more crucial for this dissertation.

3.5.1 Metric and Spin-0 Horizons

Again, we take the case of $c_{14} = 2 \times 10^{-7}$, $c_2 = 9 \times 10^{-7}$, and $c_3 = -c_1$ as the first example. The results for the normalized F, A, B and J in this case are plotted in Fig. 3.6. To see the whole picture of these functions on $r \in (0, \infty)$, they are plotted as functions of r/r_H inside the horizon, while outside the horizon they are plotted as functions of $(r/r_H)^{-1}$. This explains why in the left-hand panel of Fig. 3.6, the MH ($r = r_{MH}$) stays in the left-hand side of the S0H, while in the right-hand panel, they just reverse the order. In this figure, I didn't plot the GR limits for B and F since

they are almost overlapped with their counterparts. From the analysis of this case, we find the following:

(a) The values of F and B are almost equal to their GR limits all the time. This is true even when r is approaching the center $r = 0$, at which a spacetime curvature singularity is expected to be located.

(b) Inside the S0H, the oscillations of A and J become visible, which was also noted in [86] [11]. Such oscillations continue, and become more violent as the curvature singularity at the center is approaching.

The functions of $\{F, A, B, J\}$ for the other cases listed in Tables 3.2-3.3 are plotted in Fig. 3.7. In this figure, the plots are ordered according to the magnitude of c_S^2. Besides, some amplified figures are inserted in (a)-(d) near the region around the point of $F = 0$. Similarly, in (e)-(f), some amplified figures are inserted near the region around the point of $J = J^+$. The position of $r = r_{MH}$, at which we have $F(r_{MH}) = 0$, is marked by a full solid circle, while the position of $r = r_{S0H}$, at which we have $J(r_{S0H}) = J^+$ [cf., Eq. (3.51)], is marked by a pentagram, and in all these cases we always have $r_{MH} > r_{S0H}$. The values of J^+ and J^- are given by the brown and purple solid lines, respectively. Note we always have $J^+ > J^-$ for $c_S > 1$. By using these two lines, we can easily observe that there is only one r_{S0H} in each case, i.e., r^+_{S0H} in Eq. (3.51).

From the studies of these representative cases, we find the following: (i) As I have already mentioned, in all these cases the functions B and F are very close to their GR limits. (ii) Changing c_S^2 won't influence the maximum of A much. In

[11] In [86], the author just considered the oscillational behavior of $\tilde{A}$. The physical quantities F, A, and B were not considered.

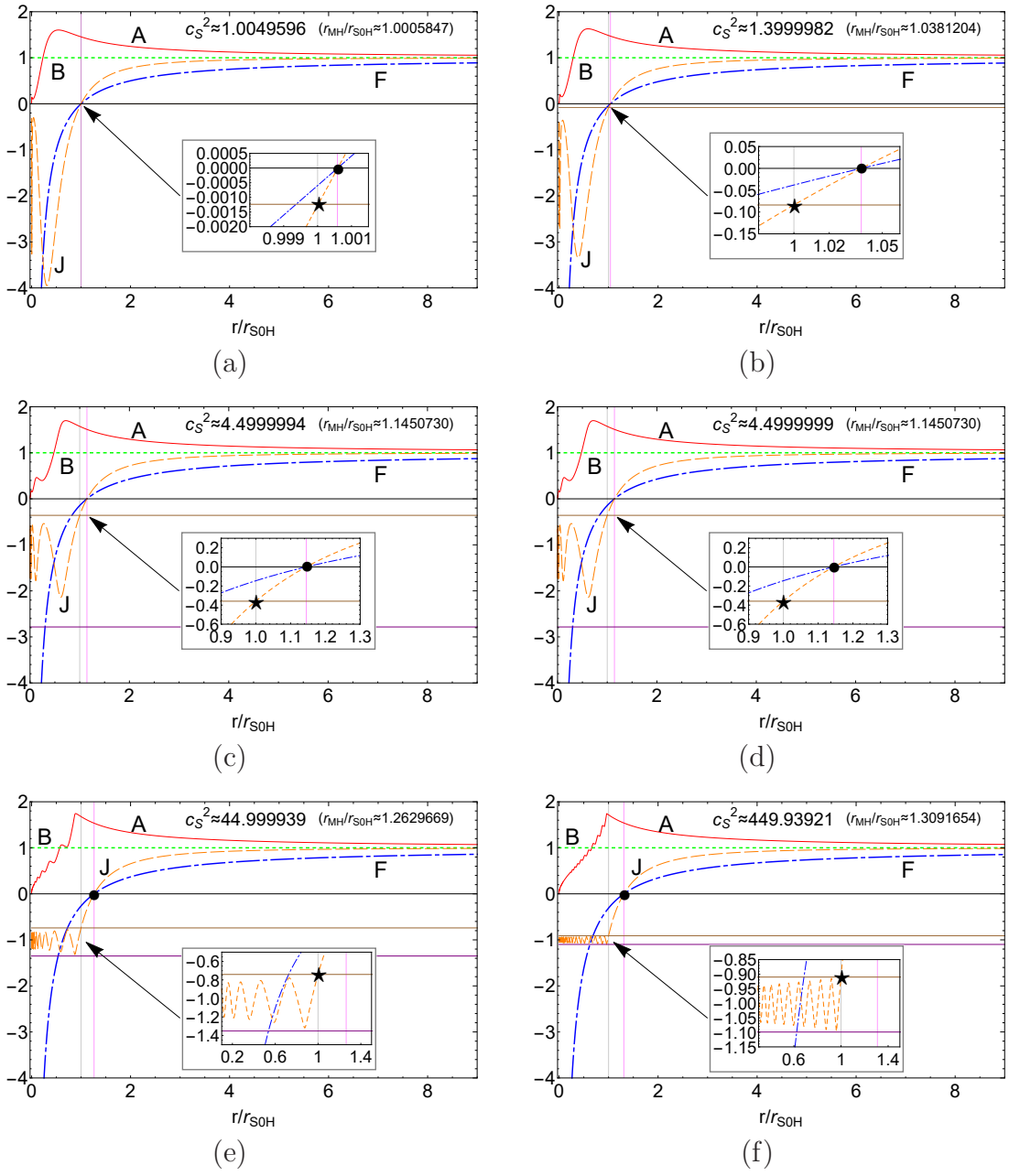

Figure 3.7: Solutions for different combinations of $\{c_2, c_{14}\}$ listed in Tables 3.2-3.3. Here, A, B, J and F are represented by the red solid line, green dotted line, orange dashed line, and blue dash-dotted line, respectively. These figures are ordered according to the magnitude of c_S^2. In each of the figure, the values J^+ and J^- are given respectively by the brown and purple solid lines with $J^+ > J^-$, while the positions of $r = r_{MH} \cap F$ and $r = r_{S0H} \cap J$ are marked by a small full solid circle and a pentagram, respectively. Additionally, the value of r_{MH}/r_{S0H} is also given in each case.

contrast, the maximum of $|J|$ inside the S0H is sensitive to c_S^2. (iii) The oscillation of $A(r)$ gets more violent as c_S^2 is increasing. (iv) The value of $|r_{MH} - r_{S0H}|$ is getting bigger as c_S^2 deviating from 1. (v) In all these cases, we have only one r_{S0H}, i.e., only one intersection between $J(r)$ and $J^{\pm}$, in each case. (vi) Just like what we saw in Tables 3.2-3.3, in the cases with the same c_S (but different values of c_{14} and c_2), the corresponding functions $\{F, A, B, J\}$ are quite similar.

From Tables 3.2-3.3 and Fig. 3.7, we would like also to note that the value of r_{MH} is always close to the corresponding $\tilde{r}_g$. To understand this, let us consider Eq. (3.124), from which we find that

$$F(\xi) \;=\; 1 + F_1\xi + \frac{1}{48}c_{14}F_1^3\xi^3 + \mathcal{O}\left(\xi^4, c_{14}, c_2\right), \tag{3.126}$$

after normalization. Recall $\xi \equiv r_H/r$ and $r_H \equiv r_{S0H}$. Then, from Eqs. (3.122), (3.113), (3.125) and (3.126), we also find that

$$\frac{\tilde{r}_g}{r_{S0H}} = -\tilde{F}_1 = -F_1. \tag{3.127}$$

On the other hand, from Eq. (3.49), we have

$$F(\xi)|_{r=r_{MH}} = 1 + F_1\frac{r_{S0H}}{r_{MH}} + \frac{1}{48}c_{14}F_1^3\left(\frac{r_{S0H}}{r_{MH}}\right)^3 + \mathcal{O}\left(\xi^4, c_{14}, c_2\right) = 0, \tag{3.128}$$

from which we obtain,

$$\begin{aligned}\frac{r_{MH}}{r_{S0H}} &= -F_1 - \frac{1}{48}c_{14}F_1^3\left(\frac{r_{S0H}}{r_{MH}}\right)^2 + \mathcal{O}\left(\frac{r_{S0H}}{r_{MH}}\right)^3 \\ &= \frac{\tilde{r}_g}{r_{S0H}} + \frac{1}{48}c_{14}\left(\frac{\tilde{r}_g}{r_{S0H}}\right)^3\left(\frac{r_{S0H}}{r_{MH}}\right)^2 + \mathcal{O}\left(\xi^3, c_{14}, c_2\right),\end{aligned} \tag{3.129}$$

where Eq. (3.127) was used. For the expansion of F to be finite, we must assume

$$\mathcal{O}\left(\xi^3, c_{14}, c_2\right) \lesssim \mathcal{O}\left[\frac{1}{48}c_{14}\left(\frac{\tilde{r}_g}{r_{S0H}}\right)^3\left(\frac{r_{S0H}}{r_{MH}}\right)^2\right]. \tag{3.130}$$

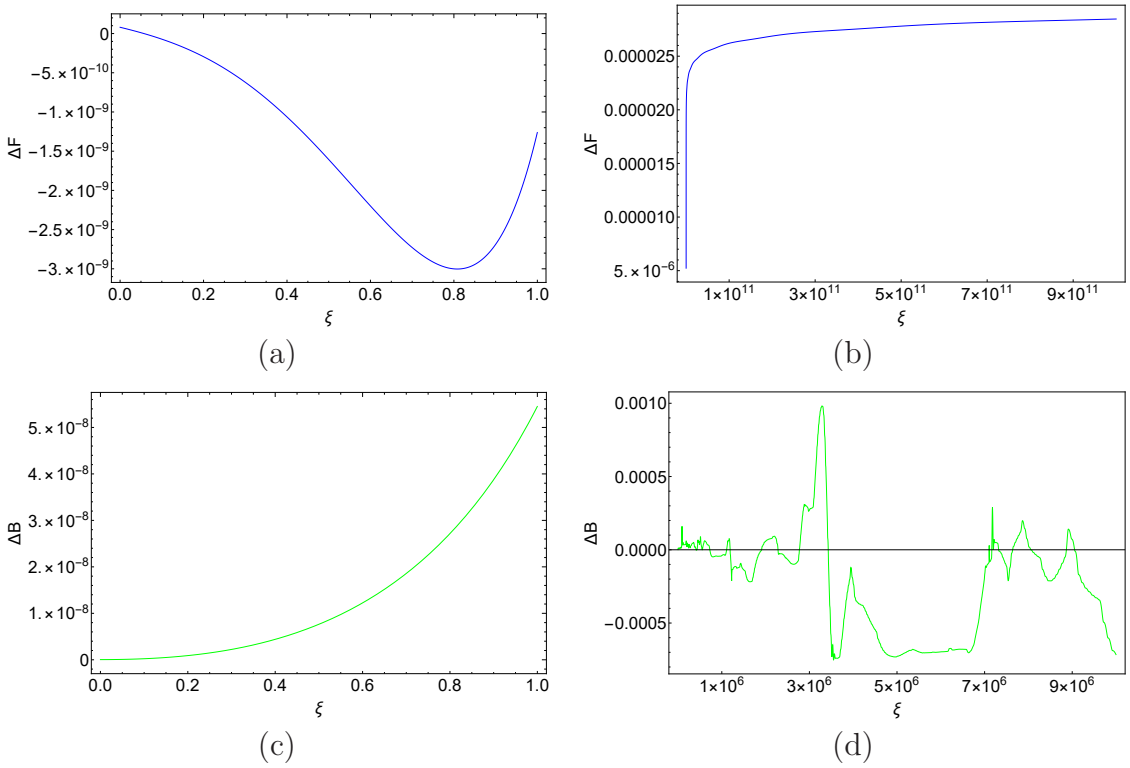

Figure 3.8: ΔF and ΔB for $c_2 = 9 \times 10^{-7}$, $c_{14} = 2 \times 10^{-7}$ and $c_{13} = 0$. The panels (a) and (c) show the region outside the S0H, while the panels (b) and (d) show the region inside the S0H.

At the same time, recall that we have $c_{14} \lesssim 2.5 \times 10^{-5}$ and $r_{S0H} \leqslant r_{MH}$. Besides, we also have $\tilde{r}_g/r_{S0H} \simeq \mathcal{O}(1)$. Thus, from Eq. (3.129) we find

$$\left|\frac{r_{MH}}{r_{S0H}} - \frac{\tilde{r}_g}{r_{S0H}}\right| \lesssim \mathcal{O}(c_{14}). \tag{3.131}$$

This result reveals why the values of r_{MH}/r_{S0H} and $\tilde{r}_g/r_{S0H}$ are very close to each other, although not necessarily the same exactly.

Finally, let us take a closer look at the difference between GR and æ-theory, although in the above we already mentioned that the results from these two theories are quite similar. To see these more clearly, we first note that the GR counterparts

of F and B are given by [35]

$$F^{GR} = 1 - \frac{r_{MH}}{r}, \quad B^{GR} = 1. \tag{3.132}$$

Thus, the relative differences can be defined as

$$\Delta F \equiv \frac{F - F^{GR}}{F^{GR}}, \quad \Delta B \equiv \frac{B - B^{GR}}{B^{GR}}. \tag{3.133}$$

Again, considering the representative case $c_2 = 9 \times 10^{-7}$, $c_{14} = 2 \times 10^{-7}$ and $c_{13} = 0$, we plot out the differences ΔF and ΔB in Fig. 3.8, from which we find that in the range $\xi \in (10^{-12}, 1)$ we have $\mathcal{O}(\Delta F) \lesssim 10^{-9}$. On the other hand, in the range $\xi \in (1, 10^{12})$, we have $\mathcal{O}(\Delta F) \lesssim 10^{-5}$. Similarly, in the range $\xi \in (10^{-12}, 1)$, we have $\mathcal{O}(\Delta B) \lesssim 10^{-8}$. In addition, in the range $\xi \in (1, 10^{7})$ we have $\mathcal{O}(\Delta B) \lesssim 10^{-3}$. Thus, we confirm that F and B are indeed quite close to their GR limits.

3.5.2 Universal Horizons

In theories with the broken LI, the dispersion relation of a massive particle contains generically high-order momentum terms [197],

$$E^2 = m^2 + c_k^2 k^2 \left(1 + \sum_{n=1}^{2(z-1)} a_n \left(\frac{k}{M_*} \right)^n \right), \tag{3.134}$$

from which we can see that both of the group and phase velocities become unbounded as $k \to \infty$, where E and k are the energy and momentum of the particle considered, and c_k and a_n's are expediently borrowed here denoting some coefficients and they depend on the species of the particle, while M_* is the suppression energy scale of the higher-dimensional operators. Note that there must be no confusion between c_k here and the four coupling constants c_i's of the theory. As an immediate result, the causal structure of the spacetimes in such theories is quite different from that given in GR, where the light cone at a given point p plays a fundamental role in determining the

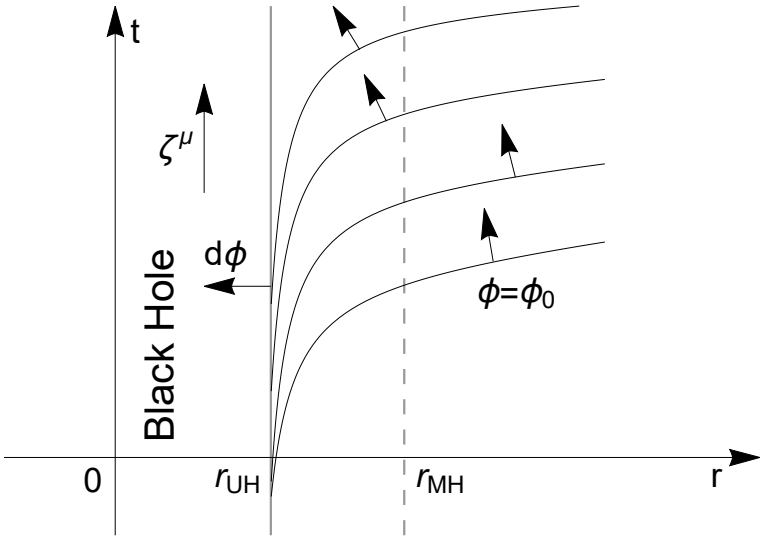

Figure 3.9: Illustration of the bending of the $\phi =$ constant surfaces, and the existence of the UH in a spherically symmetric static spacetime, where ϕ denotes the globally timelike scalar field, and t is the Painlevé-Gullstrand-like coordinates, which covers the whole spacetime [219]. Particles move always along the increasing direction of ϕ. The Killing vector $\zeta^\mu = \delta^\mu_v$ always points upward at each point of the plane. The vertical dashed line is the location of the metric (Killing) horizon, $r = r_{MH}$. The UH, denoted by the vertical solid line, is located at $r = r_{UH}$, which is always inside the MH.

causal relationship of p to other events [217]. In a UV complete theory, the above relationship is expected even in the gravitational sector. One of such examples is the healthy extension [203, 204] of Hořava gravity [193, 197], a possible UV extension of the khronometric theory (the HO æ-theory [205, 206]).

However, once LI is broken, the causal structure will be dramatically changed. For example, in the Newtonian theory, time is absolute and the speeds of signals are not limited. Then, the causal structure of a given point p is uniquely determined by the time difference, $\Delta t \equiv t_p - t_q$, between the two events. In particular, if $\Delta t > 0$, the event q is to the past of p; if $\Delta t < 0$, it is to the future; and if $\Delta t = 0$, the two events are simultaneous. In theories with breaking LI, a similar situation occurs.

To provide a proper description of BHs in such a theory, the concepts of UHs were proposed [89, 90], which represent the absolute causal boundaries. Tachypneic particles even with infinitely large speeds would just move on these boundaries and cannot escape to infinity. The main idea is as follows. In a given spacetime, a globally timelike scalar field (in this subsection, we may call it ϕ without confusions) may exist [218]. In the spherically symmetric case, this globally timelike scalar field can be identified to the HO aether field u_μ via the relation (3.27). Then, similar to the Newtonian theory, this field defines globally an absolute time, and all particles are assumed to move along the increasing direction of the timelike scalar field, so the causality is well defined. In such a spacetime, there may exist a surface at which the HO aether field u_μ is orthogonal to the timelike Killing vector, ζ ($\equiv \partial_v$) [of course, this ζ is different from the one in Eq. (2.27)]. Given that all particles move along the increasing direction of the HO aether field, it is clear that a particle must cross this surface and move inward, once it arrives at it, no matter how large its speed is. This is a one-way membrane, and particles even with infinitely large speeds cannot escape from it, once they are inside it (cf. Fig. 3.9). So, it acts as an absolute horizon to all particles (with any speed), which is often called the UH [89, 90, 197]. At the horizon, as can be seen from Fig. 3.9, we have [211],

$$\zeta \cdot u|_{r=r_{UH}} = -\frac{1}{2A}(1+J)\Big|_{r=r_{UH}} = 0, \tag{3.135}$$

where $J \equiv FA^2$. Therefore, the location of an UH is exactly the crossing point between the curve of $J(r)$ and the horizontal constant line $J = -1$, as one can see from Figs. 3.6 and 3.7. From these figures we can also see that they are always located inside S0Hs, as expected. In addition, the curve $J(r)$ is oscillating rapidly,

Table 3.4: r_{UH-i}'s for different cases listed in Tables 3.2 and 3.3. Note that here we just show first several UHs.

c_S^2	r_{MH}/r_{UH-1}	r_{MH}/r_{UH-2}	r_{MH}/r_{UH-3}	r_{MH}/r_{UH-4}
1.0049596	1.40913534	9.12519836	68.6766490	524.111256
1.3999982	1.39634652	6.27835216	33.1700700	178.825436
4.4999935	1.36429738	2.74101697	6.42094860	15.6447753
4.4999994	1.36429738	2.74101595	6.42094387	15.6447581
4.4999999	1.36429738	2.74101584	6.42094340	15.6447564
44.999939	1.33939835	1.56980254	1.91857535	2.41278107
449.93921	1.33429146	1.39226716	1.46010811	1.53855402

and crosses the horizontal line $J = -1$ back and forth infinite times. Therefore, in each case we have infinite number of r_{UH-i} $(i = 1, 2, ...)$. In this case, the UH is defined as the largest value of r_{UH-i} $(i = 1, 2, ...)$. In Table 3.4, we show the locations of the first several UHs for each case, listed in Tables 3.2 and 3.3. It is interesting to note that the formation of multi-roots of UHs was first noticed in [90], and later observed in gravitational collapse [94].

3.5.3 Other Observational Quantities

Another observationally interesting quantity is the ISCO, which is the root of the equation,

$$2rF'(r)^2 - F\left[3F'(r) + rF''(r)\right] = 0. \tag{3.136}$$

Note that in GR we have $r_{ISCO}/r_H = 3$ [220]. Due to the tiny differences between the Schwarzschild solutions and the ones considered here, as shown in Fig. 3.8, it is expected that r_{ISCO}'s in these cases are also quite close to its GR limit. As a matter of fact, we find that this is indeed the case, and the differences in all the

Table 3.5: The quantities γ_{ff}, r_{ISCO}, ω_{ISCO}, z_{max} and b_{ph} for different cases listed in Tables 3.2 and 3.3 .

c_S^2	γ_{ff}	r_{ISCO}/r_{MH}	$r_g\omega_{ISCO}$	z_{max}	b_{ph}/r_g
1.0049596	1.62614814	3.00000083	0.13608278	1.12132046	2.59807604
1.3999982	1.63971715	3.00000002	0.13608276	1.12132035	2.59807621
4.4999935	1.67376648	3.00000000	0.13608276	1.12132034	2.59807621
4.4999994	1.67376647	3.00000000	0.13608276	1.12132034	2.59807621
4.4999999	1.67376647	3.00000000	0.13608276	1.12132034	2.59807621
44.999939	1.69777578	3.00000000	0.13608276	1.12132034	2.59807621
449.93921	1.70149318	3.00000000	0.13608276	1.12132034	2.59807621

cases considered above appear only after six digits, that is, $\left|r_{ISCO} - r_{ISCO}^{GR}\right| \leq 10^{-6}$, as shown explicitly in Tables 3.5 and 3.6.

In Table 3.5, I also show several other physical quantities. These include the Lorentz gamma factor γ_{ff}, the gravitational radius r_g, the orbital frequency of the ISCO ω_{ISCO}, the maximum redshift z_{max} of a photon emitted by a source orbiting the ISCO (measured at the infinity), and the impact parameter b_{ph} of the circular photon orbit (CPO), which are defined, respectively, by [90],

$$\gamma_{ff} = \left(A + \frac{1}{4A}\right)\Big|_{r=r_{MH}}, \tag{3.137}$$

$$r_g = -r_{S0H}\frac{dF}{d\xi}\Big|_{\xi\to 0}, \tag{3.138}$$

$$\omega_{ISCO} = \sqrt{\frac{dF/dr}{2r}}\Big|_{r=r_{ISCO}}, \tag{3.139}$$

$$z_{max} = \frac{1+\omega_{ISCO} r F^{-1/2}}{\sqrt{F-\omega_{ISCO}^2 r^2}}\Big|_{r=r_{ISCO}} - 1, \tag{3.140}$$

$$b_{ph} = \frac{r}{\sqrt{F}}\Big|_{r=r_{ph}}, \tag{3.141}$$

where the radius r_{ph} of the CPO is defined as

$$\left(2F - r\frac{dF}{dr}\right)\Big|_{r=r_{ph}} = 0. \tag{3.142}$$

As pointed out previously, these quantities are quite close to their relativistic limits, since they depend only on the spacetimes described by F and B. As shown in Fig. 3.8, the differences of these spacetimes between æ-theory and GR are very small. To see this more clearly, let us introduce the quantities,

$$\begin{aligned}
\Delta r_{ISCO} &\equiv \frac{r_{ISCO}}{r_{MH}} - \left(\frac{r_{ISCO}}{r_{MH}}\right)^{GR}, \\
\Delta\omega_{ISCO} &\equiv r_g\omega_{ISCO} - \left(r_g\omega_{ISCO}\right)^{GR}, \\
\Delta z_{max} &\equiv z_{max} - \left(z_{max}\right)^{GR}, \\
\Delta b_{ph} &\equiv \frac{b_{ph}}{r_g} - \left(\frac{b_{ph}}{r_g}\right)^{GR},
\end{aligned} \tag{3.143}$$

where the GR limits of r_{ISCO}/r_{MH}, $r_g\omega_{ISCO}$, z_{max} and b_{ph}/r_g are, respectively, 3, $2\times 6^{-3/2}$, $3/\sqrt{2}-1$ and $3\sqrt{3}/2$. As can be seen from Table 3.6, all of these quantities are fairly close to their GR limits.

Therefore, we conclude that it is quite difficult to distinguish GR and æ-theory through the considerations of the physical quantities r_{ISCO}, ω_{ISCO}, z_{max} or b_{ph}, as far as the cases considered in this thesis are concerned. Thus, it would be very interesting to look for other choices of $\{c_2, c_{13}, c_{14}\}$ (if there exist), which could result in distinguishable values in these observational quantities.

3.6 Summary

In this chapter, we have systematically studied static spherically symmetric spacetimes in the framework of Einstein-aether theory, by paying particular attention to black holes that have regular S0Hs. In æ-theory, a timelike vector - the aether (field), exists over the whole spacetime. As a result, in contrast to GR, now there are three gravitational modes, referred to as, respectively, the spin-0, spin-1 and spin-2 gravitons.

Table 3.6: Δr_{ISCO}, $\Delta\omega_{ISCO}$, Δz_{max} and Δb_{ph} for different cases listed in Tables 3.2 and 3.3 .

c_S^2	Δr_{ISCO}	$\Delta\omega_{ISCO}$	Δz_{max}	Δb_{ph}
1.0049596	8.3×10^{-7}	1.3×10^{-8}	1.2×10^{-7}	-1.7×10^{-7}
1.3999982	1.8×10^{-8}	2.2×10^{-10}	2.0×10^{-9}	-3.2×10^{-9}
4.4999935	4.0×10^{-9}	1.5×10^{-12}	4.9×10^{-11}	-4.2×10^{-10}
4.4999994	4.0×10^{-10}	1.5×10^{-11}	-7.2×10^{-11}	-3.2×10^{-10}
4.4999999	4.0×10^{-11}	2.3×10^{-11}	-1.2×10^{-10}	-4.5×10^{-10}
44.999939	1.5×10^{-10}	9.6×10^{-11}	-5.6×10^{-10}	-1.9×10^{-9}
449.93921	1.1×10^{-9}	1.1×10^{-11}	-4.5×10^{-10}	-1.1×10^{-9}

To avoid the vacuum gravi-Čerenkov radiation, all these modes must propagate with speeds greater than or at least equal to the speed of light [38]. However, in the spherically symmetric spacetimes, only the spin-0 mode is relevant in the gravitational sector [27], and the boundaries of BHs are defined by this mode, which are the null surfaces with respect to the metric $g^{(S)}_{\mu\nu}$ defined in Eq. (3.2), the so-called S0Hs. Since now $c_S \geq c$, where c_S is the speed of the spin-0 mode, the S0Hs are always inside or at most coincide with the metric (Killing) horizons. Then, in order to cover spacetimes both inside and outside the MHs, working in the Eddington-Finkelstein coordinates (3.35) is one of the natural choices.

In the process of gravitational radiations of compact objects, all of these three fundamental modes will be emitted, and the GW forms and energy loss rate should be different from that of GR (see last chapter). In particular, to the leading order, both monopole and dipole emissions will co-exist with the quadrupole emission [32, 42, 58, 62, 63, 67, 68]. Despite of all these, it is remarkable that the theory still remains as a viable theory, and satisfies all the constraints, both theoretical and

observational [60], including the recent detection of the GW, GW170817, observed by the LIGO/Virgo collaboration [201], which imposed the severe constraint on the speed of the spin-2 gravitational mode, $-3 \times 10^{-15} < c_T - 1 < 7 \times 10^{-16}$. Consequently, it is one of few theories that violate Lorentz symmetry and meantime is still consistent with all the observations carried out so far [60, 65].

Spherically symmetric static BHs in æ-theory have been extensively studied both analytically [33, 75–84] and numerically [86–92], and various solutions have been obtained. Unfortunately, all these solutions have been ruled out by current observations [60].

Therefore, as a first step, this chapter has investigated spherically symmetric static BHs in æ-theory that satisfy all the observational constraints found lately in [60] in detail, and presented various numerical new BH solutions. In particular, it has first shown explicitly that among the five non-trivial field equations, only three of them are independent. More importantly, the two second-order ODEs given by Eqs. (3.39) and (3.40) for the two functions $F(r)$ and $A(r)$ are independent of the function $B(r)$, where $F(r)$ and $B(r)$ are the metric coefficients of the Eddington-Finkelstein metric (3.35), and $A(r)$ describes the aether field, as shown by Eq. (3.36). Thus, one can first solve Eqs. (3.39) and (3.40) to find $F(r)$ and $A(r)$, and then from the third independent equation to find $B(r)$. Another remarkable feature is that the function $B(r)$ can be obtained from the constraint (3.44), and is given simply by the algebraic expression of F, A and their derivatives, as shown explicitly by Eq. (3.45). This not only saves the computational labor, but also makes the calculations more accurate, as pointed out explicitly in [90], solving the first-order differential equation (3.41) for

$B(r)$ can "potentially be affected by numerical inaccuracies when evaluated very close to the horizon".

Now solving the (vacuum) field equations of spherically symmetric static spacetimes in æ-theory simply reduces to solving the two second-order differential equations (3.39) and (3.40). This will considerably simplify the mathematical computations, which is very important, especially considering the fact that the field equations involved are extremely intricate, as one can see from Eqs. (3.39)-(3.44) and (E.1) - (E.4). Then, in the case $c_{13} = c_{14} = 0$ we have been able to solve these equations explicitly, and obtained a three-parameter family of exact solutions, which in general depends on the coupling constant c_2. However, requiring that the solutions be asymptotically flat, we have found that the solutions become independent of c_2, and the corresponding metric reduces precisely to the Schwarzschild BH solution with a non-trivially coupling aether field given by Eq. (3.68), which is always timelike even in the region inside the BH.

To simplify the problem further, we have also taken the advantage of the field redefinitions that are allowed by the internal symmetry of æ-theory, first discovered by Foster in [200], and later were used frequently, including the works of [86,88,90]. The advantage of the field redefinitions is that it allows us to choose the free parameter σ involved in the field redefinitions, so that the S0H of the redefined metric $\tilde{g}_{\mu\nu}$ will coincide with its MH. This will reduce the four-dimensional space of the initial conditions, spanned by $\{\tilde{F}_H,\ \tilde{F}'_H,\ \tilde{A}_H,\ \tilde{A}'_H\}$, to one-dimension, spanned only by $\tilde{A}_H$, if the initial conditions are imposed on the S0H. In Sec.3.4.1, we have shown step by step how one can do it. In addition, in this same subsection we have also shown that the field equations are invariant under the rescaling $r \to Cr$ (C denotes an arbitrary

non-zero number). In fact, introducing the dimensionless coordinate $\xi \equiv r_{S0H}/r$, the relevant four field equations take the scaling-invariant forms of Eqs. (3.108) - (3.111), which are all independent of r_{S0H}. Thus, when integrating these equations, without loss of generality, one can assign any value to r_{S0H}.

We would like also to note that in Section 3.3 we worked out the relations in detail among the fields $(g_{\mu\nu}, u^\mu, c_i)$, $(\hat{g}_{\mu\nu}, \hat{u}^\mu, \hat{c}_i)$ and $(\tilde{g}_{\mu\nu}, \tilde{u}^\mu, \tilde{c}_i)$, and clarified several subtle points. In particular, the redefined metric $\hat{g}_{\mu\nu}$ through Eqs. (3.11) and (3.12) does not take the standard form in the Eddington-Finkelstein coordinates, as shown explicitly by Eq. (3.69). Instead, only after a proper coordinate transformation given by Eqs. (3.70) and (3.71), the resulting metric $\tilde{g}_{\mu\nu}$ takes the standard form, as given by Eq. (3.72). Then, the field equations for $(\tilde{g}_{\mu\nu}, \tilde{u}^\mu, \tilde{c}_i)$ take the same forms as the ones for $(g_{\mu\nu}, u^\mu, c_i)$. Therefore, when we solved the field equations in terms of the redefined fields, they are the ones of $(\tilde{g}_{\mu\nu},\ \tilde{u}^\mu)$, not the ones for $(\hat{g}_{\mu\nu},\ \hat{u}^\mu)$.

After clarifying all these subtle points, in Sec.3.4, we have worked out the detail of how to explicitly carry out our numerical analysis. In particular, to monitor the numerical errors of our code, we have introduced the quantity $\tilde{\mathcal{C}}$ through Eq. (3.123), which is essentially Eq. (3.99). Theoretically, it vanishes identically. But, due to numerical errors, it is expected that $\tilde{\mathcal{C}}$ has non-zero values, and the amplitude of it will provide a good indication on the numerical errors that our numerical code could produce.

To show further the accuracy of our numerical code, we have first reproduced the BH solutions obtained in [86, 90], but with an accuracy that are at least two orders higher (cf. Table 3.1). It should be noted that all these BH solutions have been ruled out by the current observations [60]. So, after checking our numerical code,

in Sec.3.4.2, we considered various new BH solutions that satisfy all the observational constraints [60], and presented them in Tables 3.2 and 3.3, as well as in Figs. 3.3-3.5.

Then, in Sec.3.5, we have presented the physical metric $g_{\mu\nu}$ and æ-field u^μ for these viable new BH solutions obtained in the previous section. Before presenting the results, we have first shown that the physical fields, $g_{\mu\nu}$ and u^μ, are also asymptotically flat, provided that the effective fields $\tilde{g}_{\mu\nu}$ and $\tilde{u}^\mu$ are [cf. Eqs. (3.124) and (3.125)]. Then, the physical BH solutions were plotted out in Figs. 3.6 and 3.7. Among several interesting features, we would like to point out the different locations of the metric and spin-0 horizons for the physical metric $g_{\mu\nu}$, denoted by full solid circles and pentagrams, respectively.

Another interesting point is that all these physical BH solutions are quite similar to the Schwarzschild one. In Fig. 3.8 we have shown the differences for the case $c_2 = 9 \times 10^{-7}$, $c_{14} = 2 \times 10^{-7}$ and $c_{13} = 0$, but similar results also hold for the other cases, exhibited in Tables 3.2 and 3.3.

In this section, we have also identified the locations of the UHs of these solutions and several other observationally interesting quantities, which include the ISCO r_{ISCO}, the Lorentz gamma factor γ_{ff}, the gravitational radius r_g, the orbital frequency ω_{ISCO} of the ISCO, the maximum redshift z_{max} of a photon emitted by a source orbiting the ISCO (measured at the infinity), the radii r_{ph} of the CPO, and the impact parameter b_{ph} of the CPO. All of them are given in Table 3.4-3.5. In Table 3.6 we also calculated the differences of these quantities obtained in æ-theory and GR. Looking at these results, we conclude that it's very hard to distinguish GR and æ-theory through these quantities, as far as the cases considered in this paper are concerned. We would also like to note that for each BH solution, there are infinite

number of UHs, $r = r_{UH-i},\ (i \in \mathbb{Z}^+)$, which was also observed in [90]. In Table 3.4 I have listed the first eight of them, and the largest one is usually defined as the UH of the BH. In contrast, there are only one S0H and one MH for each solution. These features are also found in the gravitational collapse of a massless scalar field in æ-theory [94].

An immediate implication of the above results is that the QNMs of these BHs for a test field, scalar, vector or tensor [73], will be quite similar to these given in GR. Our preliminary results on such studies indicate that this is indeed the case at least for particles with finite speeds. However, we expect that there should be significant differences from GR, when we consider the metric perturbations of these BH solutions - the gravitational spectra of perturbations [74], as now the BH boundaries are the locations of the S0Hs, not the locations of the MHs. This should be specially true for the cases with large speeds c_S of the spin-0 modes, as in these cases the S0Hs are significantly different from the MHs, and located deeply inside them. Thus, imposing the non-out-going radiation on the S0Hs will be quite different from imposing the non-out-going radiation on the corresponding MHs. Some of our premature attempts indicate that this conjecture is probably true. However, much more efforts are still needed to obtain some concrete evidences. We wish to report our results along this direction soon in another occasion.

CHAPTER FOUR

Quasi-normal Modes of Black Holes in Einstein-Aether Theory

4.1 Introduction to Quasi-normal Modes

In this chapter, we shall focus on the calculations of quasi-normal mode (QNM) frequencies (or simply referred as QNMs) in Einstein-aether theory (æ-theory). Specially, we will calculate within the circumstance of spherically symmetric static spacetimes. It should be noticed that this task has not been fully accomplished yet and we are still working on that. In this chapter we will only show some current results.

From the classical point of view, QNMs are eigenmodes of dissipative systems. The information contained in QNMs provide the keys in revealing whether black holes (BHs) are ubiquitous in our universe, and more important whether general relativity (GR) is the correct theory to describe the event even in the strong field regime. Readers may find a whole picture of the related concepts in [72]. Basically, the QNM frequency ω contains two parts. Its real part gives the frequency of vibration while its imaginary part provides the damping time. In other words, the ω we are going to calculate is a complex number (although it could be purely imaginary).

QNMs in GR have been studied extensively. Some relative studies have been done for scalar, vector and gravitational perturbations [221]. Besides, the calculation has been extended from Schwarzschild BHs [222] to other more general cases, e.g., Kerr BHs [223,224]. In this procedure, several different techniques of calculations were developed. For instance, the Wentzel-Kramers-Brillouin (WKB) approach [225–228], the continued fraction method [229], etc. [230–232]. Some of these methods are also

effective in different modified theories of gravity [233,234]. Additionally, some special scenarios, e.g., the eikonal limit, are studied [235].

As has been mentioned in previous chapters, the detection of the first gravitational wave (GW) from the coalescence of two massive black holes by advanced LIGO marked the beginning of a new era, the GW astronomy [14]. Following this observation, soon more than ten GWs were detected by the LIGO/Virgo scientific collaboration [16,161,162]. In the future, more ground- and space-based GW detectors will be armed for us [109,148,171], which enable us to probe more weak signals. This triggered the interests on the QNM signals from GWs, especially those from the late-merger and ringdown stages [66].

In fact, in GR according to the no-hair theorem, an isolated and stationary BH is completely characterized by only three quantities, mass, spin angular momentum and electric charge. Astrophysically, we expect BHs to be neutral, so it must be described by the Kerr solution. Then, the quasi-normal frequencies and damping times will depend only on the mass and angular momentum of the final BH. Therefore, to extract the physical information from the ringdown phase, at least two QNMs are needed. This will require the signal-to-noise ratio (SNR) to be of the order 100. Although such high SNRs are not achievable right now, it has been shown that they may be achievable once the advanced LIGO and Virgo reach their design sensitivities. In any case, it is certain that they will be detected by the ground-based third-generation detectors, such as Cosmic Explorer or the Einstein Telescope, as well as the space-based detectors, including LISA, TianQin [71], Taiji, and DECIGO [109].

In GR, the boundary of a test particle is at the metric horizon (MH) of a BH. In other words, a MH is the boundary of a test particle with the speed of light (referred

as c). However, we will have a different story in æ-theory, which breaks the Lorentz invariance (LI). Such a theory allows tachyonic particles to exist. Immediately, some other horizons arise besides the MH, e.g., the spin-0 horizon (S0H), spin-1 horizon (S1H), etc.. These horizons correspond to different types of gravitons with different speeds [in æ-theory, we mean c_S, c_V and c_T, cf. (1.7)]. Some attempts to the QNMs in æ-theory have been done by Konoplya [73, 74]. However, for a certain type of graviton, we need to set the boundary at one of these non-relativistic horizons. A consequence is that some steps introduced in [73] are not valid any more. Therefore, we need to include some additional techniques to generalize the existing techniques in the literature.

Some solutions to the background metric and æ-field (the æ-field is a unit and timelike 4-vector in æ-theory) for specific spherically symmetric static spacetimes have been obtained in [95]. Specially, we got a set of analytic solutions for an *ad hoc* case, namely, $c_{13} = c_{14} = 0$ (see Chapter Three for more details). By using these analytic solutions, the QNMs from our field equations become much more accessible (although there are still many tough barriers). To be more specific, some QNMs could be solved from the field equations by introducing the shooting method and other related techniques. More details are provided in the following article.

The rest of this chapter is organized as follows: In Sec.4.2, we briefly review some important things provided in the previous chapters. Sec.4.3 shows the main steps for achieving the field equations we need. Note that we will focus on the odd-parity gravitational perturbations. Sec.4.4 shows the current attempts for the calculations of QNMs in æ-theory by using the shooting method. Following from the calculations, some comments are given.

4.2 A Quick Review

4.2.1 Particle and Universal Horizons

Since æ-theory possesses three different modes, and all of them are moving in different speeds, in general these different modes define different horizons [27]. These horizons are the null surfaces of the effective metrics,

$$g^{(A)}_{\alpha\beta} \equiv g_{\alpha\beta} - \left(c_A^2 - 1\right) u_\alpha u_\beta, \tag{4.1}$$

where $A = S, V, T$. The null surfaces for $A = S,\ V,\ T$ are called spin-0 horizon (S0H), spin-1 horizon (S1H) and spin-2 horizon (S2H), respectively. These three different horizons will be also referred as particle horizons for the corresponding gravitons, and are given by

$$g^{(A)}_{\alpha\beta} N^\alpha N^\beta \Big|_{r=r_S} = 0, \tag{4.2}$$

where $N_\mu = \delta^r_\mu$, S stands for S0H, S1H, S2H, and r_S refers to the position of the corresponding horizon.

In contrast, the metric horizon is the null surface of metric $g_{\alpha\beta}$, or a particle horizon of $g^{(A)}_{\alpha\beta}$ with $c_A = 1$, given by

$$g_{\alpha\beta} N^\alpha N^\beta \big|_{r=r_{\rm MH}} = 0, \tag{4.3}$$

where $r_{\rm MH}$ is the position of MH.

If a BH is defined to be a region that traps all possible causal influences, it must be bounded by a horizon corresponding to the fastest speed. In theories with the broken LI, the dispersion relation of a massive particle contains generically high-order momentum terms [197],

$$E^2 = m^2 + p_k^2 k^2 \left[1 + \sum_{n=1}^{2(z-1)} q_n \left(\frac{k}{M_*}\right)^n\right], \tag{4.4}$$

from which we can see that both of the group and phase velocities become unbounded as $k \to \infty$, where E and k are the energy and momentum of the particle considered, and p_k and q_n's are coefficients, depending on the species of the particle, while M_* is the suppression energy scale of the higher-dimensional operators. Therefore, in theories with the broken LI, a BH should be defined to be a region that traps all possible causal influences, including particles with arbitrarily large velocities ($c_A \to \infty$). Does such a region exist?

To answer the above question, let us first note that the causal structure of spacetimes in such theories is quite different from that given in GR, where the light cone at a given point p plays a fundamental role in determining the causal relationship of p to other events [217]. In a UV complete theory, the above dispersion relationship is expected even in the gravitational sector. In such theories, the causal structure is dramatically changed. For example, in the Newtonian theory, time is absolute and the speeds of signals are not limited. Then, the causal structure of a given point p is uniquely determined by the time difference, $\Delta t \equiv t_p - t_q$, between the two events (cf. Fig. 4.1). In particular, if $\Delta t > 0$, the event q is to the past of p; if $\Delta t < 0$, it is to the future; and if $\Delta t = 0$, the two events are simultaneous.

In theories with breaking LI, a similar situation occurs. Thus, to build the causal structure of spacetimes in such theories, a globally time-like "coordinate" should be first introduced [89, 90]. In particular, for a given spacetime, we first introduce a globally timelike scalar field ϕ [218]. In the spherically symmetric case, this globally timelike scalar field can be identified as the aether field u_μ via the relation (3.34). Then, similar to the Newtonian theory, this field defines globally an absolute time, and all particles are assumed to move along the increasing direction

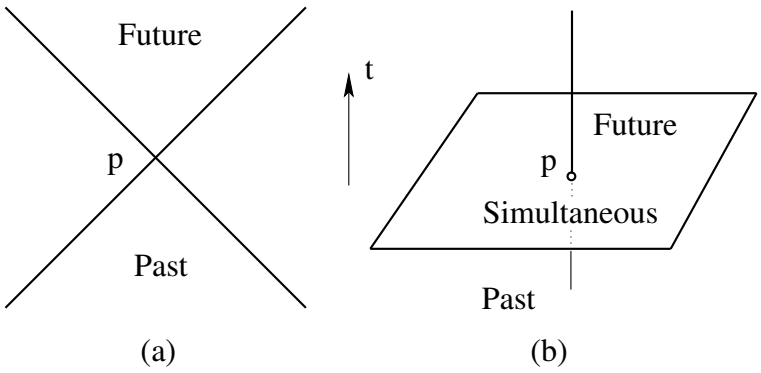

Figure 4.1: Illustration of causal structures of spacetimes in different theories of gravity [217]: (a) The light cone of the event p in special relativity. (b) The causal structure of the event p in Newtonian theory.

of the timelike scalar field, so the causality is well defined (cf. Fig. 3.9). In such a spacetime, there may exist a surface at which the aether field u_μ is orthogonal to the timelike Killing vector, ζ ($\equiv \partial_v$), where v denotes the ingoing Eddington-Finkelstein (EF) coordinate [See Eq. (3.135) and related context for more information.].

4.2.2 A Particular Background Metric

When $c_{13} = c_{14} = 0$, we have shown a particular class of solutions of the Einstein-aether field equations [95],

$$F(r) = 1 - \frac{r_s}{r}, \quad B(r) = 1, \quad A(r) = -\frac{w_2 \pm \sqrt{w_2^2 + 4r^3(r - r_s)}}{2r(r - r_s)}, \tag{4.5}$$

where $r_{MH} = r_s \equiv 2m$ is the Schwarzschild radius. As $r \to \infty$, we find that $\lim_{r\to\infty} A(r) = \mp 1$. Thus, without loss of the generality, we shall choose the "-" sign in the above expression for $A(r)$, so that $\lim_{r\to\infty} A(r) = +1$, which is also consistent with the asymptotic flatness conditions adopted in [95]. Then, to have a UH exist, we must set $w_2 = 3\sqrt{3}r_s^2/8$ [211], for which the UH is located at

$$r_{\rm UH} = \frac{3}{4} r_s. \tag{4.6}$$

Note that in the current case we have $c_S = c_V = \infty$ and $c_T = 1$, as can be seen from Eq. (1.7), which impies that in the current case the S0H and S1H coincide with the UH, while the S2H coincides with the MH.

It is interesting to note that in this particular case, the aether field has no influence on the spacetime geometry, as it is still the Schwarzschild. However, the aether field is non-trivial, and quite different from the one given in the Minkowski spacetime.

4.3 Linear Perturbations and Master Equations

Now, let us consider the perturbations to the background solutions given by Eq. (4.5) with $w_2 = 3\sqrt{3}r_s^2/8$. To distinguish them from the perturbed ones, we denote them by $\bar{g}_{\mu\nu}$ and $\bar{u}^\mu$, respectively, so the total metric and aether field are given by

$$g_{\mu\nu} = \bar{g}_{\mu\nu} + \epsilon h_{\mu\nu}, \quad u^\mu = \bar{u}^\mu + \epsilon w^\mu, \tag{4.7}$$

where ϵ is a book-marker (which is different from the one appearing in Chapter Three), and we expand the perturbations only to its first-order. Later, we can safely set it to one. To write out explicitly the forms of the perturbations, we first note that in the literature they are usually written in the Schwarzschild coordinates, $x^\mu = \{t, r, \theta, \varphi\}$, where t is related to the EF ingoing coordinate v by $v = t + f(r)$ with $df/dr = B/F$, for which the background metric and aether field take the forms of

$$ds^2 = -F(r)dt^2 + \frac{B^2(r)}{F(r)}dr^2 + r^2 d\Omega^2, \tag{4.8}$$

$$\bar{u}^\alpha \partial_\alpha = \frac{FA^2+1}{2AF}\partial_t + \frac{FA^2-1}{2AB}\partial_r. \tag{4.9}$$

Clearly, this metric becomes singular at the MH, $F(r_s) = 0$, so that the coordinates cannot cover the whole region $r \in (0, \infty)$. However, we can first write down the perturbations in these "canonical" coordinates, and once this is done, we transfer them back to the EF coordinates, as in the latter both the background and its linear perturbations are valid in the whole range of $r \in (0, \infty)$. This is crucial, as now the inner boundary is not at the MH, $r = r_s$, but rather at the UH, $r = r_{\rm UH} = 3r_s/4$, which is inside the MH. Therefore, to impose the two boundary conditions at $r = r_{\rm UH},\ \infty$ simutananeously, working out the linear perturbations in the EF coordinates is needed.

With the above in mind, and working with only the the odd-parity part, we find that $h_{\mu\nu}$ and w^μ in spherical coordinate can be cast in the forms [236],

$$h_{\mu\nu} = -\frac{1}{2}\sum_{l=0}^{\infty}\sum_{m=-l}^{l}\frac{r}{B}\begin{pmatrix} 0 & 0 & -2C_{lm}\csc\theta\partial_\varphi & 2C_{lm}\sin\theta\partial_\theta \\ 0 & 0 & 2J_{lm}\csc\theta\partial_\varphi & -2J_{lm}\sin\theta\partial_\theta \\ sym & sym & {\rm G}_1 & sym \\ sym & sym & {\rm G}_3 & {\rm G}_2 \end{pmatrix} Y_{lm}(\theta,\varphi), \tag{4.10}$$

$$w^\mu = \sum_{l=0}^{\infty}\sum_{m=-l}^{l}\frac{1}{r}\begin{pmatrix} 0 \\ 0 \\ -a_{lm}\csc\theta\partial_\varphi \\ a_{lm}\csc\theta\partial_\theta \end{pmatrix} Y_{lm}(\theta,\varphi), \tag{4.11}$$

with the three operators given by

$$\begin{aligned} {\bf G}_1 &\equiv -2rG_{lm}\csc\theta\big(\cot\theta\partial_\varphi - \partial_\theta\partial_\varphi\big), \\ {\bf G}_2 &\equiv 2rG_{lm}\big(\cos\theta\partial_\theta - \sin\theta\partial_\theta\partial_\varphi\big), \\ {\bf G}_3 &\equiv rG_{lm}\big(\csc\theta\partial_\varphi^2 + \cos\theta\partial_\theta - \sin\theta\partial_\theta^2\big), \end{aligned} \tag{4.12}$$

where $Y_{lm}(\theta,\varphi)$ stands for the spherical harmonics, and $C_{lm},\ G_{lm},\ J_{lm}$ and a_{lm} are functions of t and r only. Note that when calculating the field equations we will employ the trick by setting $m=0$ in the above expressions so that $\partial_\varphi Y_{lm}(\theta,\varphi)=0$, as now the background has the spherical symmetry, and the corresponding linear perturbations do not depend on m [236, 237].

4.3.1 Gauge Transformation

For later convenience, we first investigate the infinitesimal gauge transformation (Recall that we only consider the odd-parity part and the $m=0$ case.)

$$x^\alpha \to x'^\alpha = x^\alpha + \epsilon\xi^\alpha, \tag{4.13}$$

where

$$\xi^\alpha = \left\{0,0,0,\frac{\csc\theta\partial_\theta Y_{lm}(\theta,\phi)}{rB}Q(t,r)\right\}. \tag{4.14}$$

Under the transformation of Eq. (4.13), we have (See, e.g., [28].)

$$\begin{aligned}
\Delta w^\mu &\equiv (w^\mu)_{new} - (w^\mu)_{old} = -\mathcal{L}_\xi \bar{u}^\mu,\\
\Delta h_{ab} &\equiv (h_{ab})_{new} - (h_{ab})_{old} = -\mathcal{L}_\xi \bar{g}_{ab},
\end{aligned} \tag{4.15}$$

where $\mathcal{L}$ stands for the Lie derivative [35]. From Eq. (4.15) we find

$$\begin{aligned}
\Delta C_{lm} &\equiv (C_{lm})_{old} - (C_{lm})_{new} = -\dot{Q},\\
\Delta G_{lm} &\equiv (G_{lm})_{old} - (G_{lm})_{new} = \frac{2}{r}Q,\\
\Delta J_{lm} &\equiv (J_{lm})_{old} - (J_{lm})_{new} = Q' - Q\left(\frac{1}{r}+\frac{B'}{B}\right),\\
\Delta a_{lm} &\equiv (a_{lm})_{old} - (a_{lm})_{new} = \frac{W(B+rB')}{rB^2}Q - \frac{W}{B}Q' - \frac{K}{B}\dot{Q},
\end{aligned} \tag{4.16}$$

where $K\equiv\bar{u}^t$, $W\equiv\bar{u}^r$ [this W does not equal to the one in (3.58)], and a prime and a dot stand for the derivatives with respect to r and t, respectively. With the above

gauge transformations, we can construct the gauge-invariant quantities, and due to the presence of the aether field, three such independent quantities can be constructed, in contrast to relativistic case, in which only two such quantities can be constructed. These three gauge invariants can be defined as

$$\begin{aligned}
\mathcal{X}_{lm}(t,r) &\equiv \dot{G}_{lm} + \frac{2}{r}C_{lm}, \\
\mathcal{Y}_{lm}(t,r) &\equiv \dot{J}_{lm} - \left(\frac{1}{r} + \frac{B'}{B}\right) C_{lm} + C'_{lm}, \\
\mathcal{Z}_{lm}(t,r) &\equiv rB'WG_{lm} + B\left(2KC_{lm} - rWG'_{lm}\right) - 2B^2 a_{lm}.
\end{aligned} \tag{4.17}$$

Of course, any combination of these quantities is also gauge-invariant. By properly fixing the gauge, the resultant field equations will be simplified considerably. In the current case, we find that one of the most convenient gauges is to set $(C_{lm})_{new} = 0$.

4.3.2 Linearized Field Equations

When the spacetimes are vacuum, we have $T_{\mu\nu} = 0,\ T_\mu = 0$, and then the field equations (2.5) and (2.6) reduce to

$$E_{\mu\nu} \equiv G_{\mu\nu} - S_{\mu\nu} = 0, \tag{4.18}$$

$$Æ^\mu = 0, \tag{4.19}$$

where $G_{\mu\nu} \equiv R_{\mu\nu} - g_{\mu\nu}R/2$. To the first-order of ϵ and with the gauge $C_{lm} = 0$, we find that there are only four non-trivial equations, which are given by $E_{\phi t} = E_{\phi r} = E_{\phi\theta} = Æ^\phi = 0$, and can be cast in the forms of

$$\begin{aligned}
&\alpha_{101}a_{lm} + \alpha_{102}J_{lm} + \alpha_{103}a'_{lm} + \alpha_{104}J'_{lm} + \alpha_{105}a''_{lm} + \alpha_{106}J''_{lm} + \alpha_{107}\dot{a}_{lm} + \alpha_{108}\dot{J}_{lm} \\
&\quad + \alpha_{109}\dot{a}'_{lm} + \alpha_{110}\dot{J}'_{lm} + \alpha_{111}\ddot{a}_{lm} + \alpha_{112}\ddot{J}_{lm} + \alpha_{113}\dot{G}_{lm} = 0,
\end{aligned} \tag{4.20}$$

$$\begin{aligned}
&\alpha_{201}a_{lm} + \alpha_{202}J_{lm} + \alpha_{203}a'_{lm} + \alpha_{204}J'_{lm} + \alpha_{205}a''_{lm} + \alpha_{206}J''_{lm} + \alpha_{207}\dot{a}_{lm} + \alpha_{208}\dot{J}_{lm} \\
&\quad + \alpha_{209}\dot{a}'_{lm} + \alpha_{210}\dot{J}'_{lm} + \alpha_{211}\ddot{a}_{lm} + \alpha_{212}\ddot{J}_{lm} + \alpha_{213}G'_{lm} = 0,
\end{aligned} \tag{4.21}$$

$$\alpha_{301}J_{lm}+\alpha_{302}J'_{lm}+\alpha_{303}G'_{lm}+\alpha_{304}G''_{lm}+\alpha_{305}\ddot{G}_{lm}=0, \tag{4.22}$$

$$\alpha_{401}a_{lm}+\alpha_{402}J_{lm}+\alpha_{403}a'_{lm}+\alpha_{404}J'_{lm}+\alpha_{405}a''_{lm}+\alpha_{406}J''_{lm}+\alpha_{407}\dot{a}_{lm}+\alpha_{408}\dot{J}_{lm}$$
$$+\alpha_{409}\dot{a}'_{lm}+\alpha_{410}\dot{J}'_{lm}+\alpha_{411}\ddot{a}_{lm}+\alpha_{412}\ddot{J}_{lm}=0. \tag{4.23}$$

It is interesting to note that the coefficients α_{abc} are functions of r, c_1 and l only, and are given explicitly in Appendix F. However, there are only three independent unknowns, $G_{lm},\ J_{lm}$ and a_{lm}. Therefore, one of the above equations must depend on the other three. As to be shown below, this is indeed the case.

4.3.3 Master Equation

Combining Eqs. (4.20), (4.21) and (4.23), we obtain the following master equation,

$$\left(-\frac{\partial^2}{\partial t^2}+\eta_1\frac{\partial^2}{\partial r^2}+\eta_2\frac{\partial}{\partial r}+\eta_3\right)\mathcal{Y}_{lm}(t,r)=\ \ 0, \tag{4.24}$$

where $\mathcal{Y}_{lm}=\dot{J}_{lm}$ for our current gauge choice $C_{lm}=0$, and

$$\begin{aligned}\eta_1(r)&\equiv\frac{(r-r_s)^2}{r^2},\quad \eta_2(r)\equiv\frac{(r-r_s)(4r-3r_s)}{r^3},\\ \eta_3(r)&\equiv-\frac{(r-r_s)[(l+2)(l-1)r-3r_s]}{r^4}.\end{aligned} \tag{4.25}$$

It should be noted that the above equation is quite different from the one obtained in GR [236, 237], due to the presence of the aether field, although the background spacetime is still Schwarzschild. In addition, the above equation is scaling-invariant under $(t,r)\to(t/r_s,r/r_s)$. In fact, this is a general feature of Einstein-aether theory with spherical symmetry, as shown explicitly in [95]. Therefore, without loss of the generality, in the rest of this chapter we shall set $r_s=1$.

As mentioned above, the (t,r)-coordinates cover the black hole spacetime only to the outside region $r>r_s$, and so does Eq. (4.24). To extend it to cover also inside

region $r < r_s$ of the black hole spacetime, we can simply transfer this master equation back to the (v, r)-coordinates. This kind of coordinate transformations could be done either in the final step or at the very beginning. I actually tested both ways and the results are identical (The details are omitted here.). In (v, r, θ, ϕ) coordinate (EF coordinate), we have

$$\left(\frac{4F}{r}\frac{\partial}{\partial v} + 2F\frac{\partial^2}{\partial v \partial r} + \eta_1\frac{\partial^2}{\partial r^2} + \eta_2\frac{\partial}{\partial r} + \eta_3\right)\mathcal{Y}_{lm} = 0, \tag{4.26}$$

where $F = 1 - r_s/r$. Note that in writing the above expression we had also set $B = 1$.

4.3.4 Equations for G_{lm} and a_{lm}

On the other hand, for the gauge choice $C_{lm} = 0$, from Eq. (4.17) one finds that $\mathcal{X}_{lm} = \dot{G}_{lm}$. Then, properly assembling Eqs. (4.20), (4.21) and (4.23), we get

$$\mathcal{X}_{lm} = \frac{2(r-1)}{(l+2)(l-1)r}\left(3 + r\frac{\partial}{\partial r}\right)\mathcal{Y}_{lm}. \tag{4.27}$$

Therefore, once the master equation (4.24) is solved for $\mathcal{Y}_{lm}$, the above expression will directly give $\mathcal{X}_{lm}$, for which we find that

$$G_{lm}(t, r) = \int \mathcal{X}_{lm}(t, r)dt + \hat{G}_{lm}(r), \tag{4.28}$$

where $\hat{G}_{lm}(r)$ is an arbitrary function of r only. However, using a gauge residual led by $Q(t, r)$, we can always set it to zero. Note that, with this choice the gauge residual is completely fixed.

Substituting Eqs. (4.27) and (4.28) into Eq. (4.22), we find it is satisfied automatically. Therefore, we conclude that Eq. (4.22) is not independent, and can be derived from Eqs. (4.20), (4.21) and (4.23). This confirms one of the previous statements.

Finding the equation for a_{lm} is more elaborated. First, from Eq. (4.23) we find

$$\left(\frac{\partial^2}{\partial t^2}+\eta_4\frac{\partial}{\partial t}+\eta_5\frac{\partial^2}{\partial t\partial r}+\eta_6\frac{\partial^2}{\partial r^2}+\eta_7\frac{\partial}{\partial r}+\eta_8\right)a_{lm}=\mathcal{S}(J_{lm},r,l), \quad (4.29)$$

where

$$\begin{aligned}
\eta_4(r) &\equiv +\frac{2r[4r(4r-1)-3]+9}{3\sqrt{3}r^2\sqrt{8r(2r+1)+3}},\\
\eta_5(r) &\equiv -\frac{2\sqrt{3}(4r-3)(r-1)\sqrt{8r(1+2r)+3}}{9r},\\
\eta_6(r) &\equiv +\frac{(4r-3)^2(r-1)^2[8r(2r+1)+3]}{27r^2},\\
\eta_7(r) &\equiv +\frac{2(4r-3)(r-1)^2[4r(4r(4r+1)+3)+9]}{27r^3},\\
\eta_8(r) &\equiv -\frac{2(r-1)^2}{27r^4[8r(2r+1)+3]}\\
&\quad\times\big[8r\left(128\left(l^2+l-4\right)r^4+48\left(l^2+l-4\right)r^3\right.\\
&\quad\left.+256l(l+1)r^5+486r+243\right)+729\big]. \quad (4.30)
\end{aligned}$$

and

$$\begin{aligned}
\mathcal{S}(J_{lm},r,l) &= \frac{3\sqrt{3}}{16r^2}\ddot{J}_{lm}-\frac{(r-1)(4r-3)\sqrt{8r(2r+1)+3}}{8r^3}\dot{J}'_{lm}\\
&\quad+\frac{2r(8r+1)(4r(4r-5)+3)+45}{16r^4\sqrt{8r(2r+1)+3}}\dot{J}_{lm}\\
&\quad+\frac{(3-4r)^2(r-1)^2(8r(2r+1)+3)}{48\sqrt{3}r^4}J''_{lm}\\
&\quad-\frac{(r-1)^2(4r-3)(4r(4r(4r-3)-9)-27)}{24\sqrt{3}r^5}J'_{lm}\\
&\quad-\frac{(r-1)^2}{6\sqrt{3}r^6\left(16r^2+8r+3\right)}\\
&\quad\times\Big[512\left(l^2+l-2\right)r^6+256\left(l^2+l+2\right)r^5+32\left(3l^2+3l+14\right)r^4\\
&\quad+384r^3+432r^2+216r+81\Big]J_{lm}. \quad (4.31)
\end{aligned}$$

In Fig. 4.2, we plot the coefficients η_4 - η_8 so that we could see their ranges.

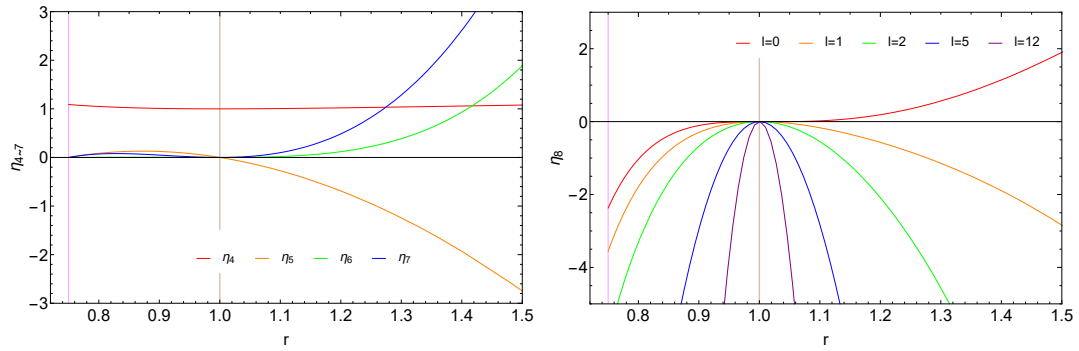

Figure 4.2: Behaviors of the coefficients η_4 - η_8 as functions of r. The upper panel shows the functions of η_4 - η_7. The lower panel shows η_8 for several different l's. In both panels, the positions of $r_{\rm UH}$ and $r_{\rm MH}$ are marked by magenta and brown vertical lines, respectively.

Next, introducing a tortoise-like coordinate

$$\tilde{r}_\star \equiv \int \frac{dr}{\sqrt{\eta_6}} = \frac{3\sqrt{3}}{4\sqrt{2}} \sinh^{-1}\left[\frac{16r+6}{\sqrt{2}|4r-3|}\right] - \sinh^{-1}\left[\frac{20r+7}{4\sqrt{2}|r-1|}\right], \quad (4.32)$$

we find that Eq. (4.29) takes the form

$$\left(\frac{\partial^2}{\partial u^2} + \eta_4 \frac{\partial}{\partial u} + \eta_8\right) a_{lm} = \mathcal{S}(J_{lm}, u, r), \quad (4.33)$$

where $u \equiv t - \tilde{r}_\star$. Clearly, $\mathcal{S}(J_{lm}, u, r)$ represents the source for the aether perturbation a_{lm}, and once the master equation (4.24) is solved, we can obtain a_{lm} from Eq. (4.33).

It is remarkable to note that, in contrast to the master equation (4.24), Eq. (4.33) is not singular across the metric horizon $r = r_s$. Therefore, for any given J_{lm}, we can simply replace t by

$$\begin{aligned} t &= v - \int \frac{B}{F} dr = v - r - \ln(r-1) \\ &\equiv v - r_*, \end{aligned} \quad (4.34)$$

in the expression of u, that is, $u = t - \tilde{r}_\star = v - r_* - \tilde{r}_\star$, and then integrating Eq. (4.33) to find a_{lm}. Clearly, such obtained a_{lm} should be valid over the whole range of $r \in (0, \infty)$. With the above in mind, a general solution to Eq. (4.33) is given by

(See, e.g., [214].)

$$\begin{aligned} a_{lm}(u,r) &= C_1 e^{\kappa_+ u} + C_2 e^{\kappa_- u} \\ &\quad + \frac{e^{\kappa_+ u}}{\kappa_+ - \kappa_-} \int e^{-\kappa_+ u} \mathcal{S}(J_{lm}, u, r) du \\ &\quad - \frac{e^{\kappa_- u}}{\kappa_+ - \kappa_-} \int e^{-\kappa_- u} \mathcal{S}(J_{lm}, u, r) du, \end{aligned} \tag{4.35}$$

where C_1 and C_2 are two arbitrary functions of r (Don't confuse them with the ones in Chapter Three.), and $\kappa_\pm$ are given by

$$\kappa_\pm(r) = \frac{-\eta_4 \pm \sqrt{\eta_4^2 - 4\eta_8}}{2}. \tag{4.36}$$

4.4 QNMs of BHs in Æ-heory

From the last section, we can see that solving the linearized Einstein-aether field equations now reduce to solving the master equation (4.26). For physical boundary conditions, at the UH ($r = r_{\rm UH}$) we require pure in-going waves while at the spatial infinity ($r = \infty$) we require pure out-going waves. Now, with an ODE (4.26) and known boundary conditions, we have a complete system so this problem could in principle be solved. As in GR, Eq. (4.26) has solutions only for some particular choices of ω, which form the spectrum of the QNMs of the corresponding BH. Due to the differences on master equations as well as boundary conditions, it is expected that the corresponding spectrum of the QNMs is different from GR.

Note that the coefficients of the master equation do not depend on v, so the general solution takes the form,

$$\mathcal{Y}_{lm}(v,r) = e^{-i\omega v}(r-1)^{2i\omega}\Psi_{lm}(r), \tag{4.37}$$

from which Eq. (4.26) becomes,

$$\left(\alpha_1 \frac{d^2}{dr^2} + \alpha_2 \frac{d}{dr} + \alpha_3\right) \Psi(r) = 0, \tag{4.38}$$

where

$$\begin{aligned}\alpha_1(r) &\equiv \frac{(r-1)^2}{r^2},\\ \alpha_2(r,\omega) &\equiv \frac{(r-1)[4r-2i(r-2)r\omega-3]}{r^3},\\ \alpha_3(r,\omega,l) &\equiv \frac{(r-1)}{r^4}\{3+r[2-l(l+1)+4r\omega(\omega-i)+6i\omega]\}. \end{aligned} \tag{4.39}$$

Note that when writing down Eq. (4.38), for the sake of simplicity, we had omitted the subscript lm (Here, l stands for the orbital angular momentum quantum number while m is the magnetic quantum number [238]. Note that here is also a principal quantum number, viz., n.) for Ψ without causing any confusion.

In this section, we are going to solve Eq. (4.38) to find out the spectrum of ω. It is worth mentioning here that we have many different candidate methods to choose, just like in GR and some other modified theories. However, here we will try to mimic Chandrasekhar's method [222] only since all the other methods we know just failed. This also implies how cranky our problem is (That is mainly due to the existence of the singularity at $r = 1$. We have different ways to tackle it to a certain degree, but we can never absolutely get rid of it.).

4.4.1 "Initial" Value Problem and Boundary Conditions

For later usage, I want to generate some boundary conditions (which should be consistent the physical ones mentioned previously) at r =3/4, 1 and ∞.

First of all, by introducing

$$\psi(r) \equiv \ r^2 e^{-ir\omega}(r-1)^{i\omega}\Psi, \tag{4.40}$$

we find that Eq. (4.38) can be cast in the form,

$$\left(\omega^2 + \frac{d^2}{dr_*^2} - V_g\right)\psi = 0, \tag{4.41}$$

where

$$V_g(r,l) \equiv \frac{(r-1)[l(l+1)r-3]}{r^4}, \tag{4.42}$$

and r_* is the tortoise coordinate defined in Eq. (4.34). Note that V_g is the same as the one in GR [230]. Clearly, as $r \to +\infty$ Eq. (4.41) has the general solutions,

$$\psi|_{r\to\infty} = \hat{\psi}_+ e^{i\omega r_*} + \hat{\psi}_- e^{-i\omega r_*}, \tag{4.43}$$

where $\hat{\psi}_\pm$ are two integration constants. But considering the physical requirements, we must set $\hat{\psi}_- = 0$. Thus, when r is very large but finite, we expect $\psi(r)$ to take the form,

$$\psi = e^{i\omega r_*} \sum_{n=0}^{\infty} \frac{a_n}{r^n}, \tag{4.44}$$

where a_n are constants. Inserting it together with Eq. (4.40) into Eq. (4.37), we find that

$$\mathcal{Y}(t,r) = e^{-i\omega(t-r)} \left[\frac{(r-1)^{i\omega}}{r^2} \sum_{n=0}^{\infty} \frac{a_n}{r^n} \right], \tag{4.45}$$

which indeed represents a pure out-going wave. On the other hand, substituting it into Eq. (4.41), we find that a_n's satisfy the following recursion relation,

$$\begin{aligned} 0 &= -2in\omega a_n + \left[(n-1)(n+2i\omega) - l^2 - l\right] a_{n-1} \\ &\quad + \left(l^2 + l - 2n^2 + 5n + 1\right) a_{n-2} + (n-4)n a_{n-3}, \end{aligned} \tag{4.46}$$

from which we can write all a_n's ($n \geq 1$) in terms of a_0. Without loss of the generality, we can always set $a_0 = 1$, as to be shown below.

In principle, once the boundary conditions are given, we can solve Eq. (4.38) to find out the spectrum of ω for any given l. However, noticing that Eq. (4.38) is singular at the MH ($r = r_s$), we have to solve Eq. (4.38) on $r \in [r_{UH}, r_-] \cup [r_+, \infty)$, with $r_\mp \equiv r_s \mp \epsilon$ and $\epsilon \ll r_s$ (In reality, we can not get a solution that covers $r \to \infty$.

Instead, we will select a sufficiently large r_{max} to represent the spatial infinity.). To fulfill this, we need the solution of Eq. (4.38) in the neighborhood of $r = 1$. Let us utilize the Frobenius method [150]. That is, suppose

$$\Psi = \sum_{n=0}^{\infty} d_n \left(r-1\right)^{n+s}, \tag{4.47}$$

where d_n's are constants and the factor s is to be determined. Naturally, we will in general obtain two branches of s when solving d_n's [239]. The solution of Ψ in this area should be the linear combination of these two branches and their ratio is unknown (We may call this ratio ℵ [240]). However, just like what we have done in Eq. (4.43), one of these branches will be abandoned due to physical requirements. To be specific, we can find $s = 0$ and therefore ℵ will be absorbed into d_0. The rest of work for solving the coefficients in Eq. (4.47) will be quite similar to that for Eq. (4.44). I will omit the details here.

Following the similar procedures and ideas like above, a solution of Ψ around the $r = 3/4$ could also be found in a polynomial form. Of course, the in-going wave requirement must be considered. Besides, mathematically, there will again be two branches. We denote their ratio as α. We will come back to this α later.

Anyway, in principle, we should be able to obtain some polynomials as the solutions of Ψ in the neighborhood of r=1, 3/4 and ∞. By using them, we could generate the boundary conditions we need for later usages. Besides, given enough time, they could be expanded to any high orders so that the desired accuracy could be met.

4.4.2 Chandrasekhar's Method

To to solve Eq. (4.38), following [222] we introduce the mode function $\Phi(r)$ by

$$\Psi(r) = \ \mathrm{Exp}\left(i\int^{r}\Phi(r)dr\right), \tag{4.48}$$

or equivalently

$$\Phi(r) = \ -i\frac{d\ln\Psi}{dr}. \tag{4.49}$$

Then, Eq. (4.38) reduces to

$$i\Phi' - \Phi^2 + \beta_1\Phi + \beta_2 = 0, \tag{4.50}$$

where

$$\begin{aligned}\beta_1(r,\omega) &\equiv \frac{2r[(r-2)\omega+2i]-3i}{(r-1)r},\\ \beta_2(r,\omega,l) &\equiv \frac{3+r[2-l(l+1)+4r\omega(\omega-i)+6i\omega]}{(r-1)r^2}.\end{aligned} \tag{4.51}$$

It is remarkable to note that such introduced $\Phi(r)$ does not depend on the amplitudes of $\Psi(r)$ at any of the points $r = (r_{\pm},\ r_{\mathrm{UH}},\ r_{\mathrm{max}})$. Using Φ actually implicitly explains why we could set $a_0 = 1$ in Eq. (4.44) (Similar things will occur in the other two polynomial solutions mentioned above.).

For our convenience, we further introduce a new variable x by $x \equiv 2r/(r+3/4)$ in the Eq. (4.50). Note that $r \in [3/4, 1)\cup(1,\infty)$ corresponds to $x \in [1, 8/7)\cup(8/7, 2)$. Therefore, Eq. (4.50) becomes

$$\frac{2i}{3}(2-x)^2\frac{d\Phi}{dx} - \Phi^2 + \gamma_1\Phi + \gamma_2 = 0, \tag{4.52}$$

where

$$\gamma_1(x,\omega) \equiv \frac{2x(11x-16)\omega - 32i(x-2)(x-1)}{x(7x-8)},$$

$$\gamma_2(x,\omega,l) \equiv \frac{16(2-x)}{3x^2(7x-8)} \times\Big\{x^2\left[l^2+l+3\omega(\omega-3i)+2\right]-2x\left(l^2+l-6i\omega+6\right)+16\Big\}. \tag{4.53}$$

In this way, we obtain a complex ODE of the first order, which will be much easier to solve than Eq. (4.38). To solve Eq. (4.52) we use the shooting method. Here are some designed steps according to our experience. Specifically, for any given l, we integrate Eq. (4.52) as follows:

(a) With a good guess, we first choose a (complex) value of ω, and then from Eqs. (4.47) with $s=0$ we create the "initial values" $\Psi_\pm(\omega)\equiv\Psi(r=r_\pm,\omega)$, where $r_\pm=r_s\pm\epsilon$, and ϵ is a small quantity. Then, we calculate $\Phi_\pm(\omega)\equiv\Phi(x=x_\pm,\omega)$ using Eq. (4.49), with $x_\pm=2r_\pm/(r_\pm+3/4)$.

(b) With the initial value $\Phi_-(\omega)$, integrate Eq. (4.52) from x_- to $x_{UH}=r_{UH}/(r_{UH}+3/4)$ to obtain $\Phi_{\rm UH}\equiv\Phi(x_{\rm UH})$.

(c) Compare this value of $\Phi_{\rm UH}$ with the one given by the polynomial solution of Ψ around $r=3/4$ (Of course, we need to choose an α.) and (4.49), to be denoted by $\Phi_{\rm min}$, and if $\delta\Phi_{\rm min}\leq\epsilon_{\rm min}$, we say that such chosen ω satisfies the in-going wave boundary condition, where $\epsilon_{\rm min}$ is a given small value, and $\delta\Phi_{\rm min}\equiv|\Phi_{\rm UH}-\Phi_{\rm min}|$. Otherwise, we need to choose a different value of ω and repeat steps (b) to (c), until the condition $\delta\Phi_{\rm min}\leq\epsilon_{\rm min}$ is fulfilled (In *Mathematica* these iterations are executed automatically.).

(d) With such determined ω we find the "initial value" $\Phi_+(\omega)$ by Eqs. (4.47) and (4.49), with which we integrate Eq. (4.52) from x_+ to $x=x_{\rm max}$ (for a properly chosen $x_{\rm max}$), and obtain a value $\Phi_\infty\equiv\Phi(x_{\rm max})$.

(e) Compare such obtained Φ_∞ with the one obtained from Eqs. (4.44), (4.46) and (4.49), which will be denoted as $\Phi_{\rm max}$. If $\delta\Phi_{\rm max} \equiv |\Phi_\infty - \Phi_{\rm max}| \leq \epsilon_{\rm max}$, we say that such obtained ω satisfies both boundary conditions, and it is exactly this value of ω that we are looking for, where $\epsilon_{\rm max}$ is another small quantity. In this chapter, we shall choose $\epsilon_{\rm min} = \epsilon_{\rm max} = 10^{-21}$. Otherwise, we say that this value of ω does not satisfy the boundary conditions, and should be excluded from the spectrum of the corresponding QNMs.

It needs to be mentioned that, in reality, we observed that the results are quite sensitive to the selections of initial test ω's. This does not only mean different initial ω's will lead to different resulting ω's, but also mean a terrible initial ω may destroy the iterations so that no physically viable resulting ω could be found. Fortunately, we are able to find at least two suitable initial test ω's so far.

4.4.3 Numerical Results

Before carrying out the analysis outlined above, we pause here for a while and first reproduce the results obtained in GR. In GR we will obtain a complex ODE just like Eq. (4.50) with the variable r_*. The integration now starts at $r_* = r_0 \pm \epsilon$ and ends at $r_* = r_0$, where ϵ and r_0 are two real numbers (This ϵ does not need to be a tiny quantity.). We will choose them properly in practice (Note that there are many suitable choices for these two.). By checking the values of $\Phi_{GR}(r_* = r_0)$ [Φ_{GR} is defined in the same manner as in Eq. (4.50)] gained from the two branches of integrations, we are able to determine ω's for each l (More details could be found in [222].).

Table 4.1: Some results of ω in GR by using the method given by Chandrasekhar [222]. Note that we are not able to distinguish its n for each ω purely by [222]. Thus, the results from the 6-th order WKB method are also provided here for matching (we can't confirm if the ω's in the same row share the same n).

l	6-th order WKB	Chandrasekha	Our results
$l=2$	$0.74724-0.17778i$ $(n=0)$	$0.74734-0.17792i$	$0.74733-0.17789i$
	$0.69259-0.54696i$ $(n=1)$	$0.69687-0.54938i$	$0.69789-0.55170i$
$l=3$	$1.19889-0.18540i$ $(n=0)$	$1.19889-0.18541i$	$1.19889-0.18541i$
	$1.16528-0.56258i$ $(n=1)$	$1.16402-0.56231i$	$1.16540-0.56263i$
	$1.10319-0.95809i$ $(n=2)$	$0.85257-0.74546i$	$1.13340-0.94717i$
$l=4$	$1.61836-0.18833i$ $(n=0)$	$1.61835-0.18832i$	$1.61836-0.18833i$
	$1.59326-0.56867i$ $(n=1)$	$1.59313-0.56877i$	$1.59327-0.56866i$
	$1.54539-0.95980i$ $(n=2)$	$1.12019-0.84658i$	$1.54808-0.95194i$

The main results we got are shown in Table 4.1. In there we provided both the results from [222] and our results by repeating Chandrasekhar's work. What's more, since we cannot distinguish its corresponding n number for each ω by using Chandrasekhar's method (This is one of the shortages of this method.), those results from the 6-th order WKB method [227] are also exhibited. Please be aware that those results from the 6-th order WKB method are believed to be more accurate since the numerical errors within such a method are more tractable, we conclude that our results are more credible for most of the cases comparing to Chandrasekhar's by using Table 4.1. Besides, we observe that our results are closer to their WKB counterparts for a larger l and smaller n.

On the other hand, note that the non-trivial field equation (4.22) has not been used in deriving the master equation (4.52). Therefore, we could use it as an independent indicator or a surveillance for our numerical integration of the master

equation. Inserting Eqs. (4.17), (4.27), (4.37) and (4.49) into Eq. (4.22), we find that

$$\mathcal{C}(x) \equiv \rho_1 \frac{d^2\Phi}{dx^2} + \rho_2 \Phi \frac{d\Phi}{dx} + \rho_3 \frac{d\Phi}{dx} + \rho_4 \Phi + \rho_5 \Phi^2 + \rho_6 \Phi^3 + \rho_7, \tag{4.54}$$

where

$$\begin{aligned}
\rho_1(x) &\equiv -4(8-7x)^2(x-2)^4 x^3 \omega, \\
\rho_2(x) &\equiv -18i(8-7x)^2(x-2)^2 x^3 \omega, \\
\rho_3(x) &\equiv -2(x-2)^2 x^2 (7x-8)\omega \\
&\quad \times \big[28x^3 + x^2(-236-99i\omega) + 8x(61+18i\omega) - 256\big], \\
\rho_4(x) &\equiv -6x\omega \big[x^4\left(-56l^2 - 56l - 531\omega^2 + 1556i\omega + 304\right) \\
&\qquad + 8x^3\left(36l^2 + 36l + 198\omega^2 - 843i\omega - 136\right) \\
&\qquad - 96x^2\left(5l^2 + 5l + 12\omega^2 - 97i\omega - 2\right) \\
&\qquad + 256x\left(l^2 + l - 16i\omega + 10\right) - 2048\big], \\
\rho_5(x) &\equiv -3x^2(7x-8)\omega\left[x^2(99\omega - 148i) - 8x(18\omega - 53i) - 256i\right], \\
\rho_6(x) &\equiv 9(8-7x)^2 x^3 \omega, \\
\rho_7(x) &\equiv -16(x-2)\omega \\
&\quad \times \Big\{ x^4\left[3l^2(11\omega - 4i) + 3l(11\omega - 4i) + 99\omega^3 - 417i\omega^2 - 126\omega + 88i\right] \\
&\qquad - 2x^3\left[3l^2(19\omega - 8i) + 3l(19\omega - 8i) + 72\omega^3 - 582i\omega^2 - 66\omega + 304i\right] \\
&\qquad + 48x^2\left[l^2(2\omega - i) + l(2\omega - i) - 16i\omega^2 + 13\omega + 34i\right] \\
&\qquad - 256x(3\omega + 8i) + 1024i \Big\}.
\end{aligned} \tag{4.55}$$

We will use $\mathcal{C}$ to monitor our numerical errors. Clearly, $\mathcal{C}$ is defined in the same manner as the $\tilde{\mathcal{C}}$ in Eq. (3.123).

Table 4.2: Some results of ω in æ-theory for the $l = 2$ case with different α's.

α	ω	α	ω
-40	$0.73210 - 0.60667i$	40	$0.23060 - 0.90273i$
-38	$0.73480 - 0.59948i$	38	$0.23791 - 0.89574i$
-36	$0.73770 - 0.59195i$	36	$0.24559 - 0.88850i$
-34	$0.74084 - 0.58404i$	34	$0.25370 - 0.88098i$
-32	$0.74427 - 0.57569i$	32	$0.26229 - 0.87318i$
-30	$0.74802 - 0.56686i$	30	$0.27143 - 0.86507i$
-28	$0.75215 - 0.55747i$	28	$0.28122 - 0.85665i$
-26	$0.75675 - 0.54743i$	26	$0.29175 - 0.84789i$
-24	$0.76190 - 0.53662i$	24	$0.30317 - 0.83880i$
-22	$0.76774 - 0.52490i$	22	$0.31564 - 0.82937i$
-20	$0.77441 - 0.51207i$	20	$0.32937 - 0.81964i$
-18	$0.78215 - 0.49785i$	18	$0.34462 - 0.80968i$
-16	$0.79125 - 0.48186i$	16	$0.36173 - 0.79961i$
-14	$0.80213 - 0.46355i$	14	$0.38111 - 0.78972i$
-12	$0.81540 - 0.44207i$	12	$0.40325 - 0.78047i$
-10	$0.65847 - 0.89756i$	10	$0.42859 - 0.77270i$
-8	$0.64858 - 0.87874i$	8	$0.45730 - 0.76775i$
-6	$0.63629 - 0.85913i$	6	$0.48878 - 0.76732i$
-4	$0.62103 - 0.83906i$	4	$0.52119 - 0.77284i$
-2	$0.60219 - 0.81914i$	2	$0.55199 - 0.78433i$
-0.05	$0.57986 - 0.80083i$	0.05	$0.57860 - 0.79995i$

Now, we are ready to turn to the QNMs of BHs in Einstein-aether theory. Let us consider the $l = 2$ case. We choose $\epsilon = 0.00001$ and $r_{\max} = 3x_{\max}/(8-4x_{\max}) = 50$. In addition, Eqs. (4.44) and (4.47) are expanded to the orders of $(1/r)^{39}$ and $(r-1)^{39}$, respectively. This guarantees the accuracy of $\Psi(r = r_{\pm})$ and $\Psi(r = r_{\max})$. With the help of Mathematica and by using the shooting method, we could find different solutions of ω for different values of α.

As an example, we show the solutions of ω by choosing the initial test ω as $0.69259 - 0.54696i$ in Table 4.2. Note that the maximum of $|\mathcal{C}|$ on $x \in [x_{\rm UH}, x_{\max}]$ for each solved ω are not equal. Nonetheless, we always have $|\mathcal{C}| \lesssim 10^{-7}$, which

guarantees the accuracy of our calculations. Also note that the results here are quite different from GR values.

4.5 Summary

As we have seen in Chapter Three, it is very hard to distinguish æ-theory from GR by using those commonly used physical observables. This fact initiated our interests on the study of QNMs. In fact, QNMs in different modified theories have been attracting a lot of attentions in recent years. We can find many different works in this area. More importantly, some discrepancies from GR are observed. On the other hand, as mentioned above, the proposed advanced GW detectors such as LISA, Taiji, TianQin, etc. will dramatically improve our detectability to QNM signals within twenty years. Therefore, it is expected that we will be able to confirm a non-relativistic theory or put more severer constraints on some of the modified theories with QNM detection in the near future. Because of this, it is quite necessary to calculate QNMs carefully in æ-theory.

Nonetheless, the calcualtion for QNMs in æ-theory is quite sophisticated. Currently, we can only deal with a simple case. Additionally, many techniques in the literature just failed. In this chapter, the calculation to QNMs is carried out as the following. By considering a set of special analytic solutions of $\{F, A, B\}$ [cf. Eq. (4.5)] and the odd-parity gravitational perturbations [cf. Eqs. (4.10) and (4.11)], we are able to obtain a master equation (4.38). After that, by mimicking Chandrasekhar's shooting method, a series of ω's are found.

Our current results in Table 4.2 imply the possibility of finding QNMs that deviate a lot from the GR results. If this is the case, that will be a remarkable

discovery since it could help us get a deeper understanding to æ-theory. What's more, supposing the future observations keep supporting the GR results, that may help us further confine æ-theory to another level. Of course, more investigations about this problem are still needed and we are still working on that.

CHAPTER FIVE

Conclusion and Outlook

5.1 Conclusion

In this dissertation we have reviewed some aspects about Einstein-æther theory. As a low-energy effective theory [188], æ-theory breaks the Lorentz invariance by introducing an ubiquitous time-like unit vector, the aether field u^μ [cf. Eq. (1.1)]. As a result, three different species of gravitons, spin-0, spin-1 and spin-2, appear in this theory [62] [They could travel faster than the speed of light. See Eq. (1.7).]. Since the LI is one of the pillars of modern physics, this feature immediately provoked our interests. Exploiting this direction may help us uncover the dawn of quantum gravity [25] and may bring us new physics beyond Einstein's framework, which is quite exciting to conceive. Another crucial fact about æ-theory is that it passed all the current tests with flying colors by properly adjusting the c_i's [cf. Eq. (1.5)]. Considering the fact that many modified theories have been ruled out by gravitational wave observations or other experiments, the survival of Einstein-aether theory sheds important light on the role that the Lorentz invariance can play in the construction of theories of gravity and the consistency of such theories with observations. It may stimulate more understandings to the extension of GR in the future.

On the other hand, in this dissertation we focus a lot on GWs. Obviously, the detection of GWs [101] marks a brand new era of astrophysics as well as cosmology both to the experimental level and for the theoretical researches. Actually, in recent years, a lot of work have been devoted to the study of gravitational waves both

experimentally and theoretically. People have shown a great passion in this area. We currently have detectors like the Laser Interferometer Gravitational-Wave Observatory (LIGO), Virgo, International Pulsar Timing Array (IPTA), Gravitational wave high-energy Electromagnetic Counterpart All-sky Monitor (GECAM), etc. distributing in different places of the world. In the future, more of them, e.g., the Cosmic Explorer, DECi-hertz Interferometer Gravitational wave Observatory (DECIGO), Kamioka Gravitational Wave Detector (KAGRA) [148], Laser Interferometer Space Antenna (LISA), Taiji [156] and TianQin [71] will be constructed [109]. These detectors will focus on different frequency bands of GW signals and will provide us a more complete spectrum. One may witness a golden period of the gravitational wave physics in next two decades or so.

Thus, within the circumstance of æ-theory, here I introduce some specific works. Beginning from Foster [32, 39, 41], the linear perturbations of æ-theory was studied extensively in the past years. An important contribution is from Yagi *et al.*, who derived the metric and the equations of motion to the 1PN order for a N-body system [42]. In [42], the sensitivities were also calculated numerically. Nevertheless, the results are out of date as mentioned above. Later, these results were applied to binary [58] and triple [56] systems by different authors.

Therefore, we first studied the triple systems in æ-theory. In [62] we calculated the gravitational waveforms, polarizations, response functions and energy losses in details. The configurations we used there are from the [61]. Besides, the latest constraints on c_i's [60] are also taken into account. In there we found several interesting things. For instance, the GW form, the response function and its Fourier transform of a triple system depend not only on their configuration of orbits but also

on their orientation with respect to the detector and binding energies of the three compact bodies. After that, we moved to a realistic hierarchy triple system, namely, PSR J0337+1715 [132]. Due to the small eccentricities of this system, we were able to study it with quasi-circular approximations in [63]. Similar calculations were carried out like in [62]. In particular, we found that the dipole emission can be as big as the quadrupole emission in Einstein-aether theory. This may provide us a a promising window to place severe constraints on the æ-theory with triple systems in the future.

After that, we went back to the study of binary systems (BBHs, BNs, etc.) with slowly changing orbits. In [68] we first studied the gravitational waveforms and GW polarizations emitted by a binary system in the inspiral phase [cf. Eqs. (2.55) - (2.60)]. During this procedure, we corrected some typos and mistakes in the literature [58]. At the same time, we also provided the explicit expressions for the time-domain and frequency-domain response functions for both ground- (e.g., LIGO, Virgo, KAGRA) and space-based (e.g., LISA, TianQin, Taiji, DECIGO) detectors [cf. Eqs. (2.83), (2.92), etc.]. Again, the latest constraints on c_i's were taken into account. What's more, the influence from sensitivities were also considered. A vital discovery is that we extended the existing ppE framework to allow for different propagation speeds among scalar (spin-0), vector (spin-1) and tensor (spin-2) modes, without assuming the magnitude of the coupling parameters c_i's, and meanwhile allowing the binary system to have relative motions with respect to the aether field. At the same time, the ppE parameters were also derived in there [cf. Eqs. (2.102), (2.111) and (2.112)]. Such results will particularly allow for the easy construction of Einstein-aether templates that could be used in Bayesian tests of GR in the future. Besides, when applying our results to J0337, we observed some discrepancies between GR and

æ-theory. For example, the coalescence times are quite different in these two theories (cf. Fig. 2.1). This suggests another potential method to distinguish them. On the other hand, note that some flaws are found in [68]. Fortunately, the framework and the major conclusions of that paper are not influenced.

The above works are mainly focusing on the inspiral and early merger [65] stages of coalescence. More recently, we paid attention to the merger and ring-down [66] stages. As a first step to dig into this area, we studied the spherically symmetric static natural black holes in [95]. Under the æ-theory, this topic has been visited by several authors [75, 86, 87, 90] before us. Nonetheless, many of their results are out of time due to the latest constraints on coupling constants [60]. What's more, we also analyzed several subtle points of this problem and increased the precision of our *Mathematica* code so that the accuracy of the results were much more guaranteed. Thus, more credible results were found. In this dissertation, we have first reviewed the technique called metric (or field) redefinition [cf. Eq. (3.10) and the context around it]. Secondly, I demonstrated clearly how to reduce the number of ODEs from these original field equations. Specially, I showed that the function $B(r)$ could be given by an algebraic equation [cf. (3.45)]. This is a crucial step for improving our accuracy. After that, I made it clearly on how to retrieve physical $\{F, A, B\}$ [cf. (3.35) and (3.36)] from the redefined $\{\tilde{F}, \tilde{A}, \tilde{B}\}$ [cf. Eqs. (3.73) and (3.75)]. Finally, many useful physical quantities were calculated and exhibited with the choices of physical viable c_i's [60], including the metric (cf. Fig. 3.7), universal horizons (cf. Table 3.4), γ_{ff}, r_{ISCO}, ω_{ISCO}, z_{max}, b_{ph} (cf. Table 3.5), etc.. According to these results, we obtain several concluding remarks. For instance, we find that the background spacetimes for spherically symmetric static natural black holes in æ-theory mainly depend on the

value of c_2/c_{14} in lieu of the individual values of c_2 and c_{14}. I also investigated the differences of these physical quantities (r_{ISCO}, ω_{ISCO}, z_{max}, etc.) obtained in æ-theory and GR. Looking at these results, we conclude that it's very hard to distinguish GR and æ-theory through these quantities, as far as the cases considered in this paper are concerned. Anyway, the results in [95] will enable us to continue our studies of ringdown stage in the æ-theory.

Based on the work of [95], we continued our study in the area of QNMs. As can be seen from Chapter Four, we have reviewed many works from the pioneers and have already got some results. Specially, in there I focus on the odd-parity gravitational perturbations with the analytic background metric and aether field [cf. Eq. (4.5)], with which we have $c_{13} = c_{14} = 0$ and $c_S \to \infty$. Note that the scalar and electromagnetic perturbations are not considered in there since the results in these cases are almost equal to the GR results, even for $c_S^2 \approx 450$ (See Chapter Three for more details about this case.). Although QNMs from scalar and electromagnetic perturbations are easy to be obtained even for some general backgrounds, it is not worth exhibiting the results since they seem to be useless for observations. Using Eq. (4.5) enables us to find the master equation (4.24) (which is different from the one in GR). After that, we are able to obtain those ω's in Table 4.2 by solving Eq. (4.24) with Chandrasekhar's method [222]. We notice that the results in æ-theory deviate a lot from that of GR. This may help us put more severe constraints on æ-theory once QNMs are observed. Actually, there are still some puzzles to solve. Fortunately, we have gained a lot of experience. We are expecting to come back with more good news in deriving QNMs in the near future.

5.2 Outlook

Although Einstein-æther theory has been studied extensively in past years there is still lots of work need to be done to enhance our understandings to this theory and to extend the applications of it. Additionally, there are many branches in the research of æ-theory. We could also choose to exploit more directions in the future.

5.2.1 Ringdown Phase and Quasi-normal Modes

As mentioned earlier, one of the main goals for next step is to get a deeper study to the quasi-normal modes in æ-theory. The information contained in QNMs provide the keys in revealing whether BHs are ubiquitous in our universe, and more important whether GR is the correct theory to describe the event even in the strong field regime.

QNMs in GR have been studied extensively. Some relative studies have been done for scalar, vector [241] and gravitational perturbations [221]. In this procedure, several different techniques of calculations were developed. For instance, the Wentzel-Kramers-Brillouin (WKB) approach [225–228, 242], the continued fraction method [229], etc.. We have investigated many of them when working on Chapter Four.

As has been pointed out, different GW detectors are located all over the world. According to the current proposals, more ground- and space-based GW detectors will be armed for us in the future [109, 148, 171], which enables us to probe more weak signals. Besides, the $n = 0$ mode (the fundamental mode) is more likely to be observed since this mode has longer damping time [71, 243, 244]. The detectabiity of different

detectors are analyzed by different authors. For instance, [245] provides a preliminary analysis to the resolution of certain detectors as well as certain modes. [246] calculates the signal-to-noise (SNR) ratio of certain ground-based detectors with a technique called "stacking". Using certain models, [184] compares the detectability of ground- and space-based detectors. [247] talks about the influence of other overtones ($n \geq 1$ modes). This triggered the interests on the QNM signals from GWs, especially those from the late-merger and ringdown stages [66].

From the experiment point of view, it is certain that the desired QNMs signals will be detected by the ground-based third-generation detectors, such as Cosmic Explorer [248] or the Einstein Telescope [249], as well as the space-based detectors, including LISA, TianQin [71], Taiji [156], and DECIGO [109] and so on.

Some attempts to the QNMs in æ-theory have been done by Konoplya [73,74]. However, for a certain type of tachyonic test particle, we need to set the boundary at one of these non-relativistic horizons. A consequence is that some steps introduced in [73] are not valid any more. Therefore, we need to include some additional techniques to generalize the existing techniques in the literature. Actually, we have already put a lot of efforts on this topic, as could be seen in Chapter Four. The odd-parity perturbations [236,250,251] were studied in there. As expected, there are a lot of barricades. For instance, we need to deal with the singularity at $r = r_{MH}$, which is quite a delicate and annoying problem mathematically [252]. We have already made some progress (See Chapter Four for more details.) but more investigations are still needed.

Since we have gained a lot of experience with QNMs and the relative techniques, our next step to solve for QNMs in æ-theory will be more clear than ever

before. Actually, we have several different plans to do. For instance, we can improve our polynomial solutions, strengthen our *Mathematica* code, etc.. Hopefully, we will get more valuable results after all the plans have been carried out. If we are lucky enough, that will bring us a deeper understanding to the puzzles of æ-theory. What's more, we are also considering the extension of our current work to more general cases of c_i's. Of course, we anticipate that this work will be more difficult.

5.2.2 Other Projects

Besides the study of QNMs, of course there are many other possible projects in æ-theory.

For instance, another direction could be the calculations of sensitivities for compact bodies. Sensitivities in Einstein-aether theory have already been calculated in [42]. Nonetheless, with the latest constraints on the free parameters of the theory [60], the phase space in which those results are valid has been completely ruled out. As can be seen from [68], the values of sensitivities will become significant with the improvement of detectors' resolutions. Thus, it is important to calculate them in the viable region of the phase space found recently.

An analytical expression of sensitivity in the weak-field approximations was found [68]. However, it does not apply to neutron stars or black holes when considering the strong-field effects. Qualitatively, we know that for neutron stars the sensitivities are about an order of magnitude larger and they depend on the equation of state. For black holes, they are expected to be very small, as in the case of khronometric gravity [131]. Of course, a detailed analysis is still absent in both cases.

Apart from that, since the gravitational waveforms have been calculated to a very high post-Newtonian order in GR, we may try to do the similar calculations within Einstein-aether theory. On the other hand, we may keep monitoring the data from the gravitational wave observations and try to provide more severe constraints to Einstein-aether theory, just like what has been done in [60] with the increasing resolution of our detectors.

In addition, it is also our plan to study rotating black holes in Einstein-aether theory. With our experience on spherically symmetric black holes [95], we have great confidence that we are able to do it, although the problem is definitely very challenging.

Once we carry out the studies of the problems mentioned above in Einstein-aether theory, I could also extend such studies to other modified theories of gravity, including general parity-violating gravity, the Einstein-Gauss-Bonnet gravity non-minimally coupled with a real or a complex scalar field, and Dynamical Chern–Simons gravity and so on.

APPENDICES

APPENDIX A

The Stationary Phase Approximation

SPA is a useful method for dealing with the Fourier transform (FT) of the response functions. The details of this method can be found in [70, 96, 134]. Here we will provide a brief introduction to this technique.

For real $g_0(t)$, $\psi_0(t)$, a_0, b_0 and y_0 (These notations are temporarily used in this appendix), we have the following approximation to $g_0(t)$'s Fourier integral [253, 254],

$$\begin{aligned}\lim_{y_0\to\infty} I_0(y_0) &\equiv \lim_{y_0\to\infty}\int_{a_0}^{b_0} g_0(t)e^{iy_0\psi_0(t)}dt \\ &\approx \lim_{y_0\to\infty} g_0(t_a)e^{iy_0\psi_0(t_a)\pm\frac{i\pi}{2l}}\left[\frac{l!}{y_0|\psi_0^{(l)}(t_a)|}\right]^{1/l}\frac{\Gamma(1/l)}{l}, \qquad (A.1)\end{aligned}$$

where $\psi_0^{(l)}(t)$ denotes the l-th derivative to ψ_0 with respect to t. $\Gamma(x)$ denotes the Gamma function [255]. t_a refers to the stationary point that is determined by the conditions

$$\begin{aligned}&\psi_0^{(1)}(t_a) = \psi_0^{(2)}(t_a) = ... = \psi_0^{(l-1)}(t_a) = 0, \\ &\psi_0^{(l)}(t_a) \neq 0, \qquad (A.2)\end{aligned}$$

and we will choose "+" for (A.1) when $\psi_0^{(l)}(t_a) > 0$, and "-" for (A.1) when $\psi_0^{(l)}(t_a) < 0$. Besides, the validity of this approximation requires

$$\left|\int_{a_0}^{b_0} g_0(t)dt\right| < \infty, \qquad (A.3)$$

and $\psi_0(t)$ is not a constant on any interval $U_0 \in [a_0, b_0]$. As an example, we will use SPA to calculate the FT for the response function,

$$H_n(t) = q_n\omega_s^{2/3}(t_r)\cos(2\Phi(t_r)), \qquad (A.4)$$

where $t_r = t - R/v_s$ is the retarded time with v_s denoting the speed of the wave.

To make sure that the approximation (A.1) is valid for the calculation of the FT of (A.4), we need to assume that $d[\ln(q_n\omega_s^{2/3})]/dt \ll d\Phi/dt$ and $d^2\Phi/dt^2 \ll (d\Phi/dt)^2$. Then, using (2.80) and Euler's formula, we find

$$\tilde{H}_n(f) \;=\; \frac{1}{2}q_n e^{i2\pi fR/v_s}\int \omega_s^{2/3}\left[e^{i(-2\Phi+2\pi ft)} + e^{i(2\Phi+2\pi ft)}\right]dt. \tag{A.5}$$

Since $d(2\Phi + 2\pi ft)/dt = 0$, we find $\dot{\Phi}(t_a) = -\pi f$, which leads to a non-physical frequency f and thus can be discarded. Conversely, from the first term in (A.5), we find $\dot{\Phi}(t_a) = \pi f$ by $d(-2\Phi + 2\pi ft)/dt|_{t_a} = 0$. Thus, we obtain $\omega_s(t_a) = \dot{\Phi}(t_a) = \pi f$ and $l = 2$ for (A.1). Now we write $\tilde{H}_n(f)$ as

$$\tilde{H}_n(f) \;=\; \frac{1}{2}q_n e^{i2\pi fR/v_s} I_n(f), \tag{A.6}$$

where

$$I_n(f) \;\equiv\; \int \omega_s^{2/3}\left[e^{i(-2\Phi+2\pi ft)}\right]dt. \tag{A.7}$$

Note that there is no summation in (A.6) with respect to n. At the same time, from (2.67) we find that $d^2(-2\Phi + 2\pi ft)/dt^2|_{t_a} = -2\ddot{\Phi}(t_a) = -2\dot{\omega}(t_a) \sim -\omega^{11/3}(t_a) < 0$, which helps us to determine the sign in (A.1). With all of these in hand, we can apply the approximation (A.1) to (A.7), and find that

$$I_n(f) \;\simeq\; \frac{1}{2}\omega_s^{2/3}(t_a)\sqrt{\frac{\pi}{\dot{\omega}_s(t_a)}} \times 2e^{if\psi_n - \frac{i\pi}{4}}, \tag{A.8}$$

where

$$\psi_n(t) \;\equiv\; -\frac{2\Phi(t)}{f} + 2\pi t. \tag{A.9}$$

Note that in the above expression there is an additional factor of 2, which originates from the analysis of [134]. Substituting (A.8) into (A.6), we find

$$\tilde{H}_n(f) \;=\; \frac{\sqrt{\pi}}{2}q_n\left[\omega_s^{2/3}(t_a)\dot{\omega}_s^{-1/2}(t_a)\right]e^{i\Psi_n}, \tag{A.10}$$

where

$$\Psi_n \equiv -2\Phi(t_a) + 2\pi f t_a + 2\pi f \frac{R}{v_s} - \frac{\pi}{4}. \tag{A.11}$$

Next, using the relation

$$[-2\Phi(t) + 2\pi f t]|_{t_c}^{t_a} = \int_{t_c}^{t_a} \frac{d[-2\Phi(t) + 2\pi f t]}{dt} dt, \tag{A.12}$$

and the fact that $\omega_s(t_c) \to \infty$, we can carry out the integral on the right-hand side of (A.12) approximately, and finally obtain

$$\Psi_n = \frac{9}{20}\kappa_1^{-1}(\mathcal{G}\pi m f)^{-5/3}\left[1 - \frac{4}{7}(\mathcal{G}\pi m f)^{-2/3}\epsilon_x\right] + 2\pi f\left(t_c + \frac{R}{v_s}\right) - 2\Phi(t_c) - \frac{\pi}{4}, \tag{A.13}$$

where the asymptotical form of the $\dot{\omega}_s$ and $\ddot{\omega}_s$ had been used.

Similarly, using the relation

$$[\omega_s^{2/3}(t)\dot{\omega}_s^{-1/2}(t)]|_{t_c}^{t_a} = \int_{t_c}^{t_a} \frac{d[\omega_s^{2/3}(t)\dot{\omega}_s^{-1/2}(t)]}{dt} dt, \tag{A.14}$$

and $\omega_s(t_c) \to \infty$, we can also carry out the integral on the right-hand side of (A.14). Finally, we find

$$\tilde{H}_n(f) = \frac{\sqrt{\pi}}{2}(\mathcal{G}m)^{1/3} q_n \kappa_1^{-1/2} (\mathcal{G}\pi m f)^{-7/6}\left[1 - \frac{1}{2}(\mathcal{G}\pi m f)^{-2/3}\epsilon_x\right] e^{i\Psi_n}, \tag{A.15}$$

where Ψ_n is given by (A.13). The calculations for (2.81) can be obtained by following the same steps[1].

[1] Of course, there is a difference between the demonstration here and the calculations in Sec.2.5. That is, in there, the phase (A.13) is fixed for the 1st and 2nd harmonic terms. At the same time, the term that related to v_s is absorbed into the amplitude part. Logically, this seems to be a big change. Nevertheless, mathematically, this modification is actually quite trivial.

APPENDIX B

The Expressions of $q_{N(l)}$

In (2.81) we introduced $q_{N(l)}$, which are given explicitly by

$$
\begin{aligned}
&q_{+(1)} \equiv d_+ \cos(2\varphi) F_+, \quad q_{+(2)} \equiv d_+ \sin(2\varphi) F_+, \\
&q_{+(3)} = q_{+(4)} = 0, \\
&q_{\times(1)} \equiv d_\times \sin(2\varphi) F_\times, \quad q_{\times(2)} \equiv -d_\times \cos(2\varphi) F_\times, \\
&q_{\times(3)} = q_{\times(4)} = 0, \\
&q_{b(1)} \equiv d_{b1} \cos(2\varphi) F_b, \quad q_{b(2)} \equiv d_{b1} \sin(2\varphi) F_b, \\
&q_{b(3)} \equiv (d_{b2} + d_{b4}) \sin\varphi F_b, \quad q_{b(4)} \equiv -(d_{b2} + d_{b4}) \cos\varphi F_b, \\
&q_{L(1)} \equiv d_{L1} \cos(2\varphi) F_L, \quad q_{L(2)} \equiv d_{L1} \sin(2\varphi) F_L, \\
&q_{L(3)} \equiv (d_{L2} + d_{L4}) \sin\varphi F_L, \quad q_{L(4)} \equiv -(d_{L2} + d_{L4}) \cos\varphi F_L, \\
&q_{X(1)} \equiv d_{X1} \cos(2\varphi) F_X, \quad q_{X(2)} \equiv d_{X1} \sin(2\varphi) F_X, \\
&q_{X(3)} \equiv (d_{X2} + d_{X4}) \sin\varphi F_X, \quad q_{X(4)} \equiv -(d_{X2} + d_{X4}) \cos\varphi F_X, \\
&q_{Y(1)} \equiv d_{Y1} \sin(2\varphi) F_Y, \quad q_{Y(2)} \equiv -d_{Y1} \cos(2\varphi) F_Y, \\
&q_{Y(3)} \equiv [(d_{Y2} + d_{Y4}) \cos\varphi + d_{Y5} \sin\varphi] F_Y, \\
&q_{Y(4)} \equiv [(d_{Y2} + d_{Y4}) \sin\varphi - d_{Y5} \cos\varphi] F_Y,
\end{aligned}
\tag{B.1}
$$

where

$$
d_+ \equiv -\frac{2G_{æ}}{R} \mathcal{G}^{2/3} \mathcal{M}^{5/3} (1 + \cos^2\vartheta), \quad d_\times \equiv \frac{4G_{æ}}{R} \mathcal{G}^{2/3} \mathcal{M}^{5/3} \cos\vartheta, \tag{B.2}
$$

$$
d_{b1} \equiv \frac{2G_{æ}}{R} \frac{c_{14}}{2 - c_{14}} \frac{-3c_{14}(Z-1)c_S^2 + 2\mathcal{S}}{c_{14} c_S^2}
$$

$$
\begin{aligned}
&\times \mathcal{G}^{2/3}\mathcal{M}^{5/3}\sin^2\vartheta,\\
d_{b2} &\equiv \frac{2G_{æ}}{R}\frac{c_{14}}{2-c_{14}}\frac{2\Delta s}{c_{14}c_S}\eta^{1/5}\mathcal{G}^{1/3}\mathcal{M}^{4/3}\sin\vartheta,\\
d_{b4} &\equiv -\frac{2G_{æ}}{R}\frac{c_{14}}{2-c_{14}}\frac{4\Delta s}{c_{14}c_S^2}\eta^{1/5}\mathcal{G}^{1/3}\mathcal{M}^{4/3}\sin\vartheta N^iV^i,\\
d_{L1} &\equiv a_{bL}d_{b1},\\
d_{L2} &\equiv a_{bL}d_{b2},\\
d_{L4} &\equiv a_{bL}d_{b4},
\end{aligned}
\tag{B.3}
$$

$$
\begin{aligned}
d_{X1} &\equiv -\frac{\beta_1 G_{æ}}{R}\frac{1}{2c_1-c_{13}c_-}\frac{1}{c_V}\left(\mathcal{S}-\frac{c_{13}}{1-c_{13}}\right)\mathcal{G}^{2/3}\mathcal{M}^{5/3}\sin(2\vartheta),\\
d_{X2} &\equiv 2\frac{\beta_1 G_{æ}}{R}\frac{1}{2c_1-c_{13}c_-}\Delta s\eta^{1/5}\mathcal{G}^{1/3}\mathcal{M}^{4/3}\cos\vartheta,\\
d_{X4} &\equiv \frac{\beta_1 G_{æ}}{R}\frac{1}{2c_1-c_{13}c_-}\frac{2\Delta s}{c_V}\eta^{1/5}\mathcal{G}^{1/3}\mathcal{M}^{4/3}(\sin\vartheta e_X^i+\cos\vartheta N^i)V^i,\\
d_{Y1} &\equiv \frac{\beta_1 G_{æ}}{R}\frac{1}{2c_1-c_{13}c_-}\frac{2}{c_V}\left(\mathcal{S}-\frac{c_{13}}{1-c_{13}}\right)\mathcal{G}^{2/3}\mathcal{M}^{5/3}\sin\vartheta,\\
d_{Y2} &\equiv 2\frac{\beta_1 G_{æ}}{R}\frac{1}{2c_1-c_{13}c_-}\Delta s\eta^{1/5}\mathcal{G}^{1/3}\mathcal{M}^{4/3},\\
d_{Y4} &\equiv \frac{\beta_1 G_{æ}}{R}\frac{1}{2c_1-c_{13}c_-}\frac{2\Delta s}{c_V}\eta^{1/5}\mathcal{G}^{1/3}\mathcal{M}^{4/3}N^iV^i,\\
d_{Y5} &\equiv \frac{\beta_1 G_{æ}}{R}\frac{1}{2c_1-c_{13}c_-}\frac{2\Delta s}{c_V}\eta^{1/5}\mathcal{G}^{1/3}\mathcal{M}^{4/3}\sin\vartheta e_Y^iV^i,
\end{aligned}
\tag{B.4}
$$

and

$$
a_{bL} \equiv 1+2\beta_2. \tag{B.5}
$$

Note that the all d_X's and d_Y's are proportional to β_1, and therefore proportional to c_{13}.

APPENDIX C

The Expressions of $q'_{N(l)}$

In (2.87) we introduced $q'_{N(l)}$'s, which are given by

$$
\begin{aligned}
&q'_{+(1)} \equiv d_+ \cos(2\varphi) F'_+(t), \quad q'_{+(2)} \equiv d_+ \sin(2\varphi) F'_+(t), \\
&q'_{+(3)} = q'_{+(4)} = 0, \\
&q'_{\times(1)} \equiv d_\times \sin(2\varphi) F'_\times(t), \quad q'_{\times(2)} \equiv -d_\times \cos(2\varphi) F'_\times(t), \\
&q'_{\times(3)} = q'_{\times(4)} = 0, \\
&q'_{b(1)} \equiv d_{b1} \cos(2\varphi) F'_b(t), \quad q'_{b(2)} \equiv d_{b1} \sin(2\varphi) F'_b(t), \\
&q'_{b(3)} \equiv (d_{b2} + d_{b4}) \sin\varphi F'_b(t), \quad q'_{b(4)} \equiv -(d_{b2} + d_{b4}) \cos\varphi F'_b(t), \\
&q'_{L(1)} \equiv d_{L1} \cos(2\varphi) F'_L(t), \quad q'_{L(2)} \equiv d_{L1} \sin(2\varphi) F'_L(t), \\
&q'_{L(3)} \equiv (d_{L2} + d_{L4}) \sin\varphi F'_L(t), \quad q'_{L(4)} \equiv -(d_{L2} + d_{L4}) \cos\varphi F'_L(t), \\
&q'_{X(1)} \equiv d_{X1} \cos(2\varphi) F'_X(t), \quad q'_{X(2)} \equiv d_{X1} \sin(2\varphi) F'_X(t), \\
&q'_{X(3)} \equiv (d_{X2} + d_{X4}) \sin\varphi F'_X(t), \quad q'_{X(4)} \equiv -(d_{X2} + d_{X4}) \cos\varphi F'_X(t), \\
&q'_{Y(1)} \equiv d_{Y1} \sin(2\varphi) F'_Y(t), \quad q'_{Y(2)} \equiv -d_{Y1} \cos(2\varphi) F'_Y(t), \\
&q'_{Y(3)} \equiv [(d_{Y2} + d_{Y4}) \cos\varphi + d_{Y5} \sin\varphi] F'_Y(t), \\
&q'_{Y(4)} \equiv [(d_{Y2} + d_{Y4}) \sin\varphi - d_{Y5} \cos\varphi] F'_Y(t),
\end{aligned}
\tag{C.1}
$$

where d_N or d_{Nl} are given by (B.2-B.4) and,

$$
\begin{aligned}
F'_+(t) &\equiv \frac{1}{2}[1 + \cos^2\theta(t)] \sin[2\phi(t)] \cos[2\psi(t)] + \cos[\theta(t)] \cos[2\phi(t)] \sin[2\psi(t)], \\
F'_\times(t) &\equiv \frac{1}{2}[1 + \cos^2\theta(t)] \sin[2\phi(t)] \sin[2\psi(t)] - \cos[\theta(t)] \cos[2\phi(t)] \cos[2\psi(t)], \\
F'_b(t) &\equiv -\frac{1}{2} \sin^2[\theta(t)] \sin[2\phi(t)],
\end{aligned}
$$

$$
\begin{aligned}
F'_L(t) &\equiv \frac{1}{2}\sin^2[\theta(t)]\sin[2\phi(t)],\\
F'_X(t) &\equiv -\sin[\theta(t)]\{\cos[\theta(t)]\sin[2\phi(t)]\cos[\psi(t)]+\cos[2\phi(t)]\sin[\psi(t)\},\\
F'_Y(t) &\equiv \sin[\theta(t)]\{-\cos[\theta(t)]\sin[2\phi(t)]\sin[\psi(t)]+\cos[2\phi(t)]\cos[\psi(t)]\}.
\end{aligned}
\tag{C.2}
$$

The angles $\theta(t)$, $\phi(t)$ and $\psi(t)$ are given by

$$
\begin{aligned}
\theta(t) &= \cos^{-1}\left\{\frac{1}{2}\Big[\cos\bar{\theta}-\sqrt{3}\cos(\bar{\phi}-\bar{\Phi})\sin\bar{\theta}\Big]\right\},\\
\phi(t) &= -\tan^{-1}\left\{\frac{1}{2}\csc\bar{\theta}\csc(\bar{\phi}-\bar{\Phi})\Big[\sqrt{3}\cos\bar{\theta}+\cos(\bar{\phi}-\bar{\Phi})\sin\bar{\theta}\Big]\right\}+\Lambda,\\
\psi(t) &= -\tan^{-1}\Bigg\{\Big[\sqrt{3}\cos\bar{\phi}(\cos\bar{\psi}\sin\bar{\Phi}-\cos\theta\sin\bar{\psi}\cos\bar{\Phi})\\
&\qquad -\sin\bar{\psi}(\sin\bar{\theta}+\sqrt{3}\cos\bar{\theta}\sin\bar{\phi}\sin\bar{\Phi})-\sqrt{3}\sin\bar{\phi}\cos\bar{\psi}\cos\bar{\Phi}\Big]\\
&\qquad \times\Big[\sqrt{3}(\cos\bar{\theta}\cos\bar{\phi}\cos\bar{\psi}-\sin\bar{\phi}\sin\bar{\psi})\cos\bar{\Phi}\\
&\qquad +\cos\bar{\psi}(\sin\bar{\theta}+\sqrt{3}\cos\bar{\theta}\sin\bar{\phi}\sin\bar{\Phi})+\sqrt{3}\cos\bar{\phi}\sin\bar{\psi}\sin\bar{\Phi}\Big]^{-1}\Bigg\},
\end{aligned}
\tag{C.3}
$$

where [158]

$$
\Lambda = \Lambda_0+\frac{2\pi t}{T_0},
\tag{C.4}
$$

which is the phase for the rotation of the three satellites around the COM of LISA with Λ_0 being a constant, and $\bar{\Phi}$ is provided in (2.89). Just like in (2.89), T_0 here is equal to the sidereal period of the Earth. Here $\bar{\theta}$, $\bar{\phi}$ and $\bar{\psi}$ are the three angles related to the center of the binary with respect to the sun (note that their definitions are different from the general Euler angles [256]), defined explicitly in [158] and Sec.11.5 of [22], and can be treated as constants. Note that once the detector is specified, e.g. LISA, φ and ϑ in $q'_{N(l)}$ will be determined by $\{\bar{\theta},\bar{\phi},\bar{\psi}\}$, i.e. $\{\bar{\theta},\bar{\phi},\bar{\psi},\vartheta,\varphi\}$ are not independent.

APPENDIX D

The Expressions of g_N

In (2.102) we use the factors g_N ($g_N \in \{g_+, g_\times, g_{b1,2,4}, g_{L1,2,4}, g_{X1,2,3,4}, g_{Y1,2,3,4}\}$), which are given as follows:

$$g_+ \equiv -2, \qquad g_\times \equiv 4, \tag{D.1}$$

$$\begin{aligned}
g_{b1} &\equiv \frac{2c_{14}}{2-c_{14}}\frac{-3c_{14}(Z-1)c_S^2+2\mathcal{S}}{c_{14}c_S^2},\\
g_{b2} &\equiv \frac{2c_{14}}{2-c_{14}}\frac{2\Delta s}{c_{14}c_S}\eta^{1/5},\\
g_{b4} &\equiv -\frac{2c_{14}}{2-c_{14}}\frac{4\Delta s}{c_{14}c_S^2}\eta^{1/5}N^iV^i,\\
g_{L1} &\equiv a_{bL}g_{b1},\\
g_{L2} &\equiv a_{bL}g_{b2},\\
g_{L4} &\equiv a_{bL}g_{b4},
\end{aligned} \tag{D.2}$$

$$\begin{aligned}
g_{X1} &\equiv -\frac{\beta_1}{2c_1-c_{13}c_-}\frac{1}{c_V}\left(\mathcal{S}-\frac{c_{13}}{1-c_{13}}\right),\\
g_{X2} &\equiv \frac{2\beta_1}{2c_1-c_{13}c_-}\Delta s\eta^{1/5},\\
g_{X3} &\equiv \frac{\beta_1}{2c_1-c_{13}c_-}\frac{2\Delta s}{c_V}\eta^{1/5}e_X^iV^i,\\
g_{X4} &\equiv \frac{\beta_1}{2c_1-c_{13}c_-}\frac{2\Delta s}{c_V}\eta^{1/5}N^iV^i,\\
g_{Y1} &\equiv \frac{\beta_1}{2c_1-c_{13}c_-}\frac{2}{c_V}\left(\mathcal{S}-\frac{c_{13}}{1-c_{13}}\right),\\
g_{Y2} &\equiv \frac{2\beta_1}{2c_1-c_{13}c_-}\Delta s\eta^{1/5},\\
g_{Y3} &\equiv \frac{\beta_1}{2c_1-c_{13}c_-}\frac{2\Delta s}{c_V}\eta^{1/5}e_Y^iV^i,
\end{aligned}$$

$$g_{Y4} \equiv \frac{\beta_1}{2c_1 - c_{13}c_-}\frac{2\Delta s}{c_V}\eta^{1/5}N^iV^i. \tag{D.3}$$

Here is a comment. Obviously, the definitions in Eq.(D.1) ans ome other parts are quite redundant. This is actually a histrionic problem. For the sake of convenience when editing Sec.2.6.1, the Appendix B was composed at the very beginning. Nearly all the other notations in Appendices C and D were built by following the same logic of Appendix B to keep a consistency with our notation system. Thus, the economic purpose was sacrificed before I realized that. Clearly, remove Eq.(D.1) will introduce a kind of asymmetry to our notation system, although it will save some space. In the future, I may try to reconsider the whole section and reduce some redundant definitions. However, for now, let's just keep this notation system.

APPENDIX E

The Coefficients of f_n, a_n, b_n and n_n

In this appendix, we shall provide the explicit expressions of the coefficients of f_n, a_n, b_n and n_n, encountered in the Einstein-aether field equations in the spherically symmetric spacetimes, for which the metric is written in the Eddington-Finkelstein coordinates (3.35), with the aether field taking the form of Eq.(3.36). In particular, the coefficients of f_n, a_n and b_n appearing in Eqs.(3.39) - (3.41) are given by,

$$
\begin{aligned}
f_0 \;=\;& -4\left(c_2+c_{13}\right)\left(c_2+c_{13}-\left(c_2+1\right)c_{14}\right) rA(r)A'(r)\\
&-\left(c_{14}c_2^2-c_2^2+c_{13}^2+\left(c_2+1\right)c_{14}^2-\left(c_2+2\right)c_{13}c_{14}\right) r^2A'(r)^2\\
&-4\big(\left(c_{14}+1\right)c_{13}^2+2\left(c_2+1\right)c_{13}+\left(c_2-2\right)c_{14}c_{13}+c_2\left(c_2+2\right)\\
&\quad-2\left(c_2^2+3c_2+1\right)c_{14}\big) rA(r)^4F'(r)\\
&+2\big(c_2^2+\left(2-3c_2\right)c_{14}c_2-9c_{13}c_{14}c_2+\left(c_2+1\right)c_{14}^2\\
&\quad-c_{13}^2\left(4c_{14}+1\right)\big) r^2A(r)^3A'(r)F'(r)\\
&-\big(5c_{14}c_2^2-c_2^2+\left(c_2+1\right)c_{14}^2+\left(7c_2-2\right)c_{13}c_{14}\\
&\quad+c_{13}^2\left(4c_{14}+1\right)\big) r^2A(r)^6F'(r)^2\\
&-2\left(c_2+c_{13}\right)c_{14}\left(-c_2+c_{13}+c_{14}-4\right) r^3A(r)^5A'(r)F'(r)^2\\
&+\left(c_2+c_{13}\right)c_{14}\left(c_2-c_{13}+c_{14}\right) r^3A(r)^8F'(r)^3\\
&-\left(c_2+c_{13}\right)A(r)^2\big(-c_{14}\left(c_2-c_{13}+c_{14}\right) r^3A'(r)^2F'(r)+4c_2\left(c_{14}-1\right)\\
&\quad+2c_{13}c_{14}\big),\\
f_1 \;=\;& -8\left(c_2+c_{13}\right)\left(c_{14}c_2+c_2+c_{13}+c_{14}\right) rA(r)^3A'(r)
\end{aligned}
$$

$$
\begin{aligned}
&+4\left(c_2^2-3c_{13}c_{14}c_2+2c_{14}c_2+\left(c_2+1\right)c_{14}^2-c_{13}^2\left(c_{14}+1\right)\right)r^2A(r)^2A'(r)^2\\
&-4\big(\left(1-2c_{14}\right)c_{13}^2+\left(-c_{14}c_2+2c_2+c_{14}+4\right)c_{13}+c_2\left(c_2+4\right)\\
&\quad+\left(5c_2^2+9c_2+4\right)c_{14}\big)rA(r)^6F'(r)\\
&+2\big(c_{14}c_2^2+3c_2^2-3\left(c_2+1\right)c_{14}^2+\left(11c_2+6\right)c_{13}c_{14}\\
&\quad+c_{13}^2\left(4c_{14}-3\right)\big)r^2A(r)^5A'(r)F'(r)\\
&+2\big(c_2^2+\left(3c_2+2\right)c_{14}c_2+3c_{13}c_{14}c_2+\left(c_2+1\right)c_{14}^2\\
&\quad+c_{13}^2\left(2c_{14}-1\right)\big)r^2A(r)^8F'(r)^2\\
&+2\left(c_2+c_{13}\right)c_{14}\left(c_2-c_{13}+c_{14}\right)r^3A(r)^7A'(r)F'(r)^2\\
&-2\left(c_2+c_{13}\right)c_{14}A(r)^4\big(\left(-c_2+c_{13}+c_{14}-4\right)r^3A'(r)^2F'(r)\\
&\quad-4\left(2c_2+c_{13}+1\right)\big),\\
f_2 \;=\;& 2\big(c_{14}c_2^2+3c_2^2-3\left(c_2+1\right)c_{14}^2+\left(11c_2+6\right)c_{13}c_{14}\\
&\quad+c_{13}^2\left(4c_{14}-3\right)\big)r^2A(r)^4A'(r)^2\\
&+4\big(-\left(c_{14}-1\right)c_{13}^2+2\left(c_2-1\right)c_{13}+\left(c_2+4\right)c_{14}c_{13}+\left(c_2-2\right)c_2\\
&\quad+\left(4c_2^2+8c_2+2\right)c_{14}\big)rA(r)^8F'(r)\\
&+6\left(\left(c_{14}+1\right)c_2^2+c_{14}\left(-c_{13}+c_{14}+2\right)c_2-c_{13}^2+c_{14}^2\right)r^2A(r)^7A'(r)F'(r)\\
&+\left(-\left(c_{14}-1\right)c_2^2+\left(c_{13}-c_{14}\right)c_{14}c_2-\left(c_{13}-c_{14}\right)^2\right)r^2A(r)^{10}F'(r)^2\\
&+\left(-c_2-c_{13}\right)A(r)^6\\
&\quad\times\left(-c_{14}\left(c_2-c_{13}+c_{14}\right)r^3A'(r)^2F'(r)+8c_2+4\left(6c_2+3c_{13}+4\right)c_{14}\right),\\
f_3 \;=\;& 8\left(c_2+c_{13}\right)\left(c_{14}c_2+c_2+c_{13}+c_{14}\right)rA(r)^7A'(r)\\
&+8\left(2c_2^2+3c_{13}c_2+c_2+c_{13}^2+c_{13}\right)c_{14}A(r)^8\\
&+4\left(c_2^2-3c_{13}c_{14}c_2+2c_{14}c_2+\left(c_2+1\right)c_{14}^2-c_{13}^2\left(c_{14}+1\right)\right)r^2A(r)^6A'(r)^2
\end{aligned}
$$

$$
\begin{aligned}
&+4\left(c_2+c_{13}\right)\left(c_2+c_{13}-\left(c_2+1\right)c_{14}\right)rA(r)^{10}F'(r)\\
&+2\left(c_2-c_{13}+c_{14}\right)\left(c_2+c_{13}-\left(c_2+1\right)c_{14}\right)r^2A(r)^9A'(r)F'(r),\\
f_4 \;=\;& 4\left(c_2+c_{13}\right)\left(c_2+c_{13}-\left(c_2+1\right)c_{14}\right)rA(r)^9A'(r)\\
&-2\left(c_2+c_{13}\right)\left(2c_2\left(c_{14}-1\right)+c_{13}c_{14}\right)A(r)^{10}\\
&+\left(-c_{14}c_2^2+c_2^2-c_{13}^2-\left(c_2+1\right)c_{14}^2+\left(c_2+2\right)c_{13}c_{14}\right)r^2A(r)^8A'(r)^2, \qquad \text{(E.1)}\\
a_0 \;=\;& 4\Big(-\left(c_{14}-1\right)c_{13}^2+\left(-c_{14}c_2+2c_2+2c_{14}-2\right)c_{13}+\left(c_2-2\right)c_2\\
&\quad+2\left(c_2^2+3c_2+1\right)c_{14}\Big)rA(r)^2A'(r)\\
&+\Big(c_{13}^2+\left(5c_2c_{14}+8\right)c_{13}-\left(c_2+1\right)c_{14}^2-\left(c_2-8\right)c_2\\
&\quad-\left(5c_2^2+18c_2+8\right)c_{14}\Big)r^2A(r)A'(r)^2\\
&+\left(c_2+c_{13}\right)c_{14}\left(c_2-c_{13}+c_{14}\right)r^3A'(r)^3\\
&+4\left(c_2+c_{13}\right)\left(c_{14}c_2+c_2+c_{13}+c_{14}\right)rA(r)^5F'(r)\\
&-2\Big(\left(2c_{14}-1\right)c_{13}^2+\left(\left(3c_2-2\right)c_{14}+4\right)c_{13}-\left(c_2+1\right)c_{14}^2+c_2\left(c_2+4\right)\\
&\quad+\left(3c_2^2+4c_2+4\right)c_{14}\Big)r^2A(r)^4A'(r)F'(r)\\
&+\left(-c_2^2-\left(c_2+2\right)c_{14}c_2+c_{13}c_{14}c_2+c_{13}^2-\left(c_2+1\right)c_{14}^2\right)r^2A(r)^7F'(r)^2\\
&+\left(c_2+c_{13}\right)c_{14}\left(c_2-c_{13}+c_{14}\right)r^3A(r)^6A'(r)F'(r)^2\\
&-2\left(c_2+c_{13}\right)A(r)^3\Big(c_{14}\left(-c_2+c_{13}+c_{14}-4\right)r^3A'(r)^2F'(r)\\
&\quad+2c_2+2c_2c_{14}+c_{13}c_{14}+4\Big),\\
a_1 \;=\;& 4\Big(\left(2c_{14}+1\right)c_{13}^2+\left(3c_{14}c_2+2c_2+c_{14}-4\right)c_{13}+\left(c_2-4\right)c_2\\
&\quad-\left(3c_2^2+7c_2+4\right)c_{14}\Big)rA(r)^4A'(r)\\
&+\Big(-\left(8c_{14}-3\right)c_{13}^2-\left(\left(23c_2+14\right)c_{14}-8\right)c_{13}+3\left(c_2+1\right)c_{14}^2\\
&\quad-c_2\left(3c_2-8\right)-\left(c_2^2-8c_2-8\right)c_{14}\Big)r^2A(r)^3A'(r)^2
\end{aligned}
$$

$$
\begin{aligned}
&-2\left(c_2+c_{13}\right)c_{14}\left(-c_2+c_{13}+c_{14}-4\right)r^3A(r)^2A'(r)^3\\
&-8\left(c_2+1\right)\left(c_2+c_{13}\right)c_{14}rA(r)^7F'(r)\\
&+4\big(\left(c_{14}+1\right)c_{13}^2+2\left(c_2c_{14}-1\right)c_{13}-\left(c_2+1\right)c_{14}^2-c_2\left(c_2+2\right)\\
&\quad+\left(c_2^2+2c_2+2\right)c_{14}\big)r^2A(r)^6A'(r)F'(r)\\
&+\left(c_{14}c_2^2-c_2^2+c_{13}^2+\left(c_2+1\right)c_{14}^2-\left(c_2+2\right)c_{13}c_{14}\right)r^2A(r)^9F'(r)^2\\
&-2\left(c_2+c_{13}\right)A(r)^5\\
&\quad\times\left(-c_{14}\left(c_2-c_{13}+c_{14}\right)r^3A'(r)^2F'(r)-2c_2-\left(6c_2+3c_{13}+4\right)c_{14}\right),
\end{aligned}
$$

$$
\begin{aligned}
a_2 \;=\;& -2\left(c_2+c_{13}\right)\left(\left(6c_2+3c_{13}+4\right)c_{14}-2\left(c_2+2\right)\right)A(r)^7\\
&-4\big(\left(c_{14}+1\right)c_{13}^2+\left(c_2\left(3c_{14}+2\right)+2\right)c_{13}+c_2\left(c_2+2\right)\\
&\quad-2\left(2c_2+1\right)c_{14}\big)rA(r)^6A'(r)\\
&+\big(-3c_2^2+\left(5c_2-6\right)c_{14}c_2+19c_{13}c_{14}c_2-3\left(c_2+1\right)c_{14}^2\\
&\quad+c_{13}^2\left(8c_{14}+3\right)\big)r^2A(r)^5A'(r)^2\\
&+\left(c_2+c_{13}\right)c_{14}\left(c_2-c_{13}+c_{14}\right)r^3A(r)^4A'(r)^3\\
&-4\left(c_2+c_{13}\right)\left(c_2+c_{13}-\left(c_2+1\right)c_{14}\right)rA(r)^9F'(r)\\
&-2\left(c_2-c_{13}+c_{14}\right)\left(c_2+c_{13}-\left(c_2+1\right)c_{14}\right)r^2A(r)^8A'(r)F'(r),\\
a_3 \;=\;& 2\left(c_2+c_{13}\right)\left(2c_2\left(c_{14}-1\right)+c_{13}c_{14}\right)A(r)^9\\
&-4\left(c_2+c_{13}\right)\left(c_2+c_{13}-\left(c_2+1\right)c_{14}\right)rA(r)^8A'(r)\\
&+\left(c_{14}c_2^2-c_2^2+c_{13}^2+\left(c_2+1\right)c_{14}^2-\left(c_2+2\right)c_{13}c_{14}\right)r^2A(r)^7A'(r)^2, \qquad \text{(E.2)}
\end{aligned}
$$

and

$$
\begin{aligned}
b_0 \;=\;& 4\left(c_2+1\right)\left(c_2+c_{13}\right)c_{14}A(r)^2-4\left(c_2+c_{13}\right)^2c_{14}rA(r)A'(r)\\
&+\left(c_2+c_{13}\right)c_{14}\left(c_2-c_{13}+c_{14}\right)r^2A'(r)^2-4\left(c_2+c_{13}\right)^2c_{14}rA(r)^4F'(r)
\end{aligned}
$$

$$
\begin{aligned}
& -2\left(c_2+c_{13}\right)c_{14}\left(-c_2+c_{13}+c_{14}-4\right)r^2A(r)^3A'(r)F'(r) \\
& +\left(c_2+c_{13}\right)c_{14}\left(c_2-c_{13}+c_{14}\right)r^2A(r)^6F'(r)^2, \\
b_1 \;=\; & -2\left(c_2+c_{13}\right)c_{14}\left(-c_2+c_{13}+c_{14}-4\right)r^2A(r)^2A'(r)^2- \\
& 8\left(c_2+1\right)\left(c_2+c_{13}\right)c_{14}A(r)^4 \\
& +2\left(c_2+c_{13}\right)c_{14}\left(c_2-c_{13}+c_{14}\right)r^2A(r)^5A'(r)F'(r) \\
& +4\left(c_2+c_{13}\right)^2c_{14}rA(r)^6F'(r), \\
b_2 \;=\; & 4\left(c_2+c_{13}\right)^2c_{14}rA(r)^5A'(r)+4\left(c_2+1\right)\left(c_2+c_{13}\right)c_{14}A(r)^6 \\
& +\left(c_2+c_{13}\right)c_{14}\left(c_2-c_{13}+c_{14}\right)r^2A(r)^4A'(r)^2. \qquad \text{(E.3)}
\end{aligned}
$$

On the other hand, the coefficients n_n's appearing in Eq.(3.44) are given by

$$
\begin{aligned}
n_0 \;=\; & \frac{c_2A'(r)}{2rA(r)^3B(r)^3}-\frac{c_2}{2r^2A(r)^2B(r)^3}-\frac{c_{13}}{4r^2A(r)^2B(r)^3}-\frac{1}{r^2B(r)} \\
& -\frac{\left(c_2+c_{13}+c_{14}\right)A'(r)F'(r)}{4A(r)B(r)^3}-\frac{\left(c_2+c_{13}-c_{14}\right)A'(r)^2}{8A(r)^4B(r)^3} \\
& +\frac{\left(c_2+2\right)F'(r)}{2rB(r)^3}-\frac{\left(c_2+c_{13}-c_{14}\right)A(r)^2F'(r)^2}{8B(r)^3}, \\
n_1 \;=\; & \frac{\left(-c_2-c_{13}-c_{14}\right)A'(r)^2}{4A(r)^2B(r)^3}-\frac{c_2A(r)^2F'(r)}{2rB(r)^3}+\frac{2c_2+c_{13}+2}{2r^2B(r)^3} \\
& +\frac{\left(-c_2-c_{13}+c_{14}\right)A(r)A'(r)F'(r)}{4B(r)^3}, \\
n_2 \;=\; & -\frac{c_2A(r)A'(r)}{2rB(r)^3}+\frac{\left(-c_2-c_{13}+c_{14}\right)A'(r)^2}{8B(r)^3}+\frac{\left(-2c_2-c_{13}\right)A(r)^2}{4r^2B(r)^3}. \qquad \text{(E.4)}
\end{aligned}
$$

When $c_S=1$, i.e. $c_2=\left(-2c_{13}+2c_{14}-c_{13}^2c_{14}\right)/\left(2-4c_{14}+3c_{13}c_{14}\right)$, the coefficients f_0, a_0, b_0 and n_0 reduce to

$$
\begin{aligned}
f_0 \;=\; & \left[rA(r)^2F'(r)+\frac{c_{14}c_{13}+2c_{13}-2c_{14}}{2\left(c_{13}-1\right)c_{14}}\right]b_0, \\
a_0 \;=\; & \frac{2\left(c_{13}-1\right)c_{14}rA'(r)+\left(c_{13}-2\right)\left(c_{14}-2\right)A(r)}{c_{13}\left(c_{14}\left(2rA(r)^2F'(r)+1\right)+2\right)-2c_{14}\left(rA(r)^2F'(r)+1\right)}f_0, \\
b_0 \;=\; & \frac{1}{\left(\left(3c_{13}-4\right)c_{14}+2\right)^2} \\
& \times\Big\{2\left(1-c_{13}\right)^2c_{14}^2\left(4c_{14}c_{13}^2+\left(-3c_{14}^2-4c_{14}+4\right)c_{13}+4\left(c_{14}-1\right)c_{14}\right)r^2A'^2
\end{aligned}
$$

$$
\begin{aligned}
&-4\left(c_{13}-1\right)^{2} c_{14}^{2} r A(r) A^{\prime}(r) \\
&\quad \times\left[\left(4 c_{14} c_{13}^{2}+\left(3 c_{14}^{2}-16 c_{14}+4\right) c_{13}-4\left(c_{14}^{2}-4 c_{14}+2\right)\right) r A(r)^{2} F^{\prime}(r)\right. \\
&\qquad \left.+4\left(c_{13}-1\right)^{2} c_{14}\right] \\
&-2\left(c_{13}-1\right)^{2} c_{14}^{2} A(r)^{2} \\
&\quad \times\left[\left(4 c_{14} c_{13}^{2}+\left(-3 c_{14}^{2}-4 c_{14}+4\right) c_{13}+4\left(c_{14}-1\right) c_{14}\right) r^{2} A(r)^{4} F^{\prime}(r)^{2}\right. \\
&\qquad \left.++8\left(c_{13}-1\right)^{2} c_{14} r A(r)^{2} F^{\prime}(r)+4\left(c_{13}-1\right)\left(\left(c_{13}-2\right) c_{14}+2\right)\right]\Big\},
\end{aligned}
\tag{E.5}
$$

and

$$
\begin{aligned}
n_{0} \;=\; & \frac{c_{14}\left(-2 c_{13}^{2}+\left(3 c_{14}+4\right) c_{13}-4 c_{14}\right) A(r)^{2} F^{\prime}(r)^{2}}{8\left(\left(3 c_{13}-4\right) c_{14}+2\right) B(r)^{3}} \\
& +F^{\prime}(r)\left[c_{14}\left(-2 c_{13}^{2}-3 c_{14} c_{13}+4 c_{13}+4 c_{14}-4\right) r A^{\prime}(r)\right. \\
& \qquad \left.-2\left(c_{14} c_{13}^{2}+\left(2-6 c_{14}\right) c_{13}+6 c_{14}-4\right) A(r)\right] \\
& \qquad \times\left[4\left(\left(3 c_{13}-4\right) c_{14}+2\right) r A(r) B(r)^{3}\right]^{-1} \\
& +\left[8\left(\left(3 c_{13}-4\right) c_{14}+2\right) r^{2} A(r)^{4} B(r)^{3}\right]^{-1} \\
& \qquad \times\left[c_{14}\left(-2 c_{13}^{2}+\left(3 c_{14}+4\right) c_{13}-4 c_{14}\right) r^{2} A^{\prime}(r)^{2}\right. \\
& \qquad\qquad -4\left(c_{14} c_{13}^{2}+2 c_{13}-2 c_{14}\right) r A(r) A^{\prime}(r) \\
& \qquad\qquad -8\left(\left(3 c_{13}-4\right) c_{14}+2\right) A(r)^{4} B(r)^{2} \\
& \qquad\qquad \left.+\left(-2 c_{14} c_{13}^{2}+\left(8 c_{14}+4\right) c_{13}-8 c_{14}\right) A(r)^{2}\right].
\end{aligned}
\tag{E.6}
$$

It should be noted that, due to the complexities of the expressions given in Eqs.(E.1) - (E.6), we extract these coefficients directly from our *Mathematica* code to avoid typos. In addition, they are further tested by the exact solutions presented in [75, 77], as well as by the numerical solutions presented in [86, 90]. In the latter,

we find that there are no differences between our numerical solutions and the ones presented in [86, 90], within the errors allowed by the numerical codes.

APPENDIX F

The Coefficients of α_{101}-α_{412}

$$
\begin{aligned}
\alpha_{101} &\equiv 32c_1(3-4r)^2(r-1)^2r^2\big(8r\big(128\left(l^2+l-4\right)r^4+48\left(l^2+l-4\right)r^3 \\
&\quad +256l(l+1)r^5+486r+243\big)+729\big), \\
\alpha_{102} &\equiv -24\sqrt{3}c_1\left(4r^2-7r+3\right)^2 \\
&\quad \times\big(512\left(l^2+l-2\right)r^6+256\left(l^2+l+2\right)r^5+32\left(3l^2+3l+14\right)r^4 \\
&\quad\quad +384r^3+432r^2+216r+81\big), \\
\alpha_{103} &\equiv -32c_1(r-1)^2r^3(4r-3)^3 \\
&\quad \times\left(1024r^5+768r^4+512r^3+288r^2+108r+27\right), \\
\alpha_{104} &\equiv -6\sqrt{3}c_1(r-1)^2r(4r-3)^3 \\
&\quad \times\left(1024r^5-256r^4-768r^3-864r^2-324r-81\right), \\
\alpha_{105} &\equiv -16c_1(3-4r)^4r^4\left(-16r^3+8r^2+5r+3\right)^2, \\
\alpha_{106} &\equiv 3\sqrt{3}c_1(3-4r)^4r^2\left(-16r^3+8r^2+5r+3\right)^2, \\
\alpha_{107} &\equiv -48c_1r^4\sqrt{768(r-1)r^3+81}\left(128r^4-128r^3+54r-27\right), \\
\alpha_{108} &\equiv 3r^2\sqrt{256(r-1)r^3+27} \\
&\quad \times\left(9c_1\left(1024r^5-1920r^4+896r^3+162r-135\right)-32768(r-1)^3r^6\right), \\
\alpha_{109} &\equiv 96c_1(3-4r)^2r^5\left(16r^3-8r^2-5r-3\right)\sqrt{768(r-1)r^3+81}, \\
\alpha_{110} &\equiv -2(r-1)r^3\sqrt{256(r-1)r^3+27} \\
&\quad \times\left(27c_1\left(256r^4-256r^3+27\right)+16384(r-1)^2r^6\right),
\end{aligned}
$$

$$
\begin{aligned}
\alpha_{111} &\equiv -432c_1r^6\left(256r^4-256r^3+27\right),\\
\alpha_{112} &\equiv 81\sqrt{3}c_1r^4\left(256r^4-256r^3+27\right),\\
\alpha_{113} &\equiv 16384\left(l^2+l-2\right)(r-1)^2r^9\sqrt{256(r-1)r^3+27}. \qquad \text{(F.1)}\\
\alpha_{201} &\equiv -96c_1(r-1)^2r^2\sqrt{768(r-1)r^3+81},\\
&\quad\times\big(1024\left(l^2+l-4\right)r^5+384\left(l^2+l-4\right)r^4+2048l(l+1)r^6\\
&\qquad+3888r^2+1944r+729\big),\\
\alpha_{202} &\equiv 8(r-1)^2\sqrt{256(r-1)r^3+27}\\
&\quad\times\big(27c_1\left(512\left(l^2+l-2\right)r^6+256\left(l^2+l+2\right)r^5+32\left(3l^2+3l+14\right)r^4\right.\\
&\qquad\left.+384r^3+432r^2+216r+81\right)\\
&\qquad+4096\left(l^2+l-2\right)\left(16r^3-8r^2-5r-3\right)r^7\big),\\
\alpha_{203} &\equiv 96c_1(r-1)^2r^3\sqrt{768(r-1)r^3+81}\\
&\quad\times\left(4096r^6-256r^4-384r^3-432r^2-216r-81\right),\\
\alpha_{204} &\equiv 54c_1(r-1)^2r\sqrt{256(r-1)r^3+27}\\
&\quad\times\left(4096r^6-4096r^5-2304r^4-1152r^3+1296r^2+648r+243\right),\\
\alpha_{205} &\equiv 48c_1r^4\sqrt{768(r-1)r^3+81}\left(64r^4-80r^3+4r^2+3r+9\right)^2,\\
\alpha_{206} &\equiv -27c_1r^2\sqrt{256(r-1)r^3+27}\left(64r^4-80r^3+4r^2+3r+9\right)^2,\\
\alpha_{207} &\equiv 432c_1r^4\left(2048r^6-1024r^5-640r^4+480r^3-54r-81\right),\\
\alpha_{208} &\equiv -81\sqrt{3}c_1r^2\\
&\quad\times\big(16384r^7-22528r^6+2048r^5+1408r^4+5280r^3-864r^2\\
&\qquad-594r-405\big),\\
\alpha_{209} &\equiv -864c_1(r-1)r^5\left(-64r^3+16r^2+12r+9\right)^2,
\end{aligned}
$$

$$
\begin{aligned}
\alpha_{210} &\equiv 162\sqrt{3}c_1(r-1)r^3\left(-64r^3+16r^2+12r+9\right)^2, \\
\alpha_{211} &\equiv 1296c_1r^6\left(16r^2+8r+3\right)\sqrt{768(r-1)r^3+81}, \\
\alpha_{212} &\equiv r^4\left(16r^2+8r+3\right)\sqrt{256(r-1)r^3+27}\left(32768(r-1)^2r^6-729c_1\right), \\
\alpha_{213} &\equiv -16384\left(l^2+l-2\right)(r-1)^3r^8\left(16r^2+8r+3\right)\sqrt{256(r-1)r^3+27}. \qquad \text{(F.2)}
\end{aligned}
$$

$$
\begin{aligned}
\alpha_{301} &\equiv 2-2r, \\
\alpha_{302} &\equiv -2(r-1)^2, \\
\alpha_{303} &\equiv 2r^2-3r+1, \\
\alpha_{304} &\equiv (r-1)^2r, \\
\alpha_{305} &\equiv -r^3. \qquad \text{(F.3)}
\end{aligned}
$$

$$
\begin{aligned}
\alpha_{401} &\equiv -32(r-1)^2r^2\sqrt{256(r-1)r^3+27} \\
&\quad \times\big(1024\left(l^2+l-4\right)r^5+384\left(l^2+l-4\right)r^4+2048l(l+1)r^6 \\
&\qquad +3888r^2+1944r+729\big), \\
\alpha_{402} &\equiv 24(r-1)^2\sqrt{768(r-1)r^3+81} \\
&\quad \times\big(512\left(l^2+l-2\right)r^6+256\left(l^2+l+2\right)r^5+32\left(3l^2+3l+14\right)r^4 \\
&\qquad +384r^3+432r^2+216r+81\big), \\
\alpha_{403} &\equiv 32(r-1)^2r^3\sqrt{256(r-1)r^3+27} \\
&\quad \times\left(4096r^6-256r^4-384r^3-432r^2-216r-81\right),
\end{aligned}
$$

$$
\begin{aligned}
\alpha_{404} &\equiv 6(r-1)^2 r\sqrt{768(r-1)r^3+81} \\
&\quad \times \left(4096r^6-4096r^5-2304r^4-1152r^3+1296r^2+648r+243\right), \\
\alpha_{405} &\equiv 16r^4\sqrt{256(r-1)r^3+27}\left(64r^4-80r^3+4r^2+3r+9\right)^2, \\
\alpha_{406} &\equiv -3r^2\sqrt{768(r-1)r^3+81}\left(64r^4-80r^3+4r^2+3r+9\right)^2, \\
\alpha_{407} &\equiv 48\sqrt{3}r^4\left(2048r^6-1024r^5-640r^4+480r^3-54r-81\right), \\
\alpha_{408} &\equiv -27r^2\big(16384r^7-22528r^6+2048r^5+1408r^4+5280r^3 \\
&\quad -864r^2-594r-405\big), \\
\alpha_{409} &\equiv -96\sqrt{3}(r-1)r^5\left(-64r^3+16r^2+12r+9\right)^2, \\
\alpha_{410} &\equiv 54(r-1)r^3\left(-64r^3+16r^2+12r+9\right)^2, \\
\alpha_{411} &\equiv 432r^6\left(16r^2+8r+3\right)\sqrt{256(r-1)r^3+27}, \\
\alpha_{412} &\equiv -81r^4\left(16r^2+8r+3\right)\sqrt{768(r-1)r^3+81}. \qquad \text{(F.4)}
\end{aligned}
$$

BIBLIOGRAPHY

[1] S. W. Hawking, The Universe in a Nutshell (Butler and Tanner Ltd., Somerset, UK, 2001).

[2] An Liu (author), J. S. Major (translator), S. A. Queen (translator), *et al.*, The Essential Huainanzi (Columbia University Press, New York, 2012).

[3] S. W. Hawking and W. Israel, Three hundred years of gravitation (Cambridge University Press, Cambridge, 1987).

[4] A. Einstein, Die Feldgleichungen der Gravitation, Sitzungsberichte der Preussischen Akademie der Wissenschaften zu Berlin: 844847 (1915).

[5] F. Őzel and P. Freire, Masses, Radii, and the Equation of State of Neutron Stars, Annu. Rev. Astron. Astrophys., 54:401-40 (2016).

[6] C. M. Will, Theory and Experiment in Gravitational Physics (2nd ed.) (Cambridge University Press, Cambridge, 2018).

[7] A. Ashtekar, B. K. Berger and J. Isenberg, GENERAL RELATIVITY AND GRAVITATION: A Centennial Perspective (Cambridge University Press, UK, 2015).

[8] K. Schwarzschild, Über das Gravitationsfeld eines Massenpunktes nach der Einsteinschen Theorie, Meeting Reports of the Royal Prussian Academy of Sciences, Pp. 189-196 (Berlin, 1916).

[9] R. P. Kerr, Gravitational Field of a Spinning Mass as an Example of Algebraically Special Metrics, Phys. Rev. Lett. **11**, 237 (1963).

[10] H. Reissner, Über die Eigengravitation des elekirischen Feldes nach der Einsteinschen Theorie, Ann. Phys. **50** (1916).

[11] H. Weyl, Zur Gravitationstheorie, Ann. Phys. **54** (1917).

[12] S. E. Gralla, A. Lupsasca and D. P. Marrone, The shape of the black hole photon ring: A precise test of strong-field general relativity, Phys. Rev. D**102**, 124004 (2020).

[13] E. Schucking, *et al.,* The Collected Papers of Albert Einstein, Volume 6, The Berlin Years (Princeton University Press, Princeton, New Jersey, 1997).

[14] B. P. Abbott, *et al.,* [LIGO/Virgo Scientific Collaborations], Observation of Gravitational Waves from a Binary Black Hole Merger, Phys. Rev. Lett. **116**, 061102 (2016).

[15] B.P. Abbott, *et al.*, [LIGO Scientific and Virgo Collaborations], Binary Black Hole Mergers in the First Advanced LIGO Observing Run, Phys. Rev. X**6**, 041015 (2016).

[16] B. P. Abbott, *et al.,* [LIGO/Virgo Collaborations], GWTC-1: A Gravitational-Wave Transient Catalog of Compact Binary Mergers Observed by LIGO and Virgo during the First and Second Observing Runs, Phys. Rev. X **9**, 3, 031040 (2019).

[17] B. P. Abbott, *et al.*, [LIGO Scientific and Virgo Collaborations], GW151226: Observation of Gravitational Waves from a 22-Solar-Mass Binary Black Hole Coalescence, Phys. Rev. Lett. **116**, 241103 (2016).

[18] B. P. Abbott, *et al.*, [LIGO Scientific and Virgo Collaborations], GW170104: Observation of a 50-Solar-Mass Binary Black Hole Coalescence at Redshift 0.2, Phys. Rev. Lett. **118**, 221101 (2017).

[19] B. P. Abbott, *et al.*, [LIGO Scientific and Virgo Collaborations], GW170608: Observation of a 19 Solar-mass Binary Black Hole Coalescence, Astrophys. J. **851**, L35 (2017).

[20] B. P. Abbott, *et al.*, [LIGO Scientific and Virgo Collaborations], GW170814: A Three-Detector Observation of Gravitational Waves from a Binary Black Hole Coalescence, Phys. Rev. Lett. **119**, 141101 (2017).

[21] B. P. Abbott, *et al.,*[LIGO/Virgo Collaborations], Gravitational Waves and Gamma-Rays from a Binary Neutron Star Merger: GW170817 and GRB 170817A, Astrophys. J. Lett., 848:L13 (27pp) (2017).

[22] E. Poisson and C. Will, Gravity, Newtonian, Post-Newtonian, Relativistic (Cambridge University Press, Cambridge, 2014).

[23] T. Jacobson and D. Mattingly, Gravity with a dynamical preferred frame, Phys. Rev. D**64**, 024028 (2001).

[24] C. W. Misner, K. S. Thorne and J. A. Wheeler, Gravitation (W. H. Freeman and Company, San Francisco, 1973).

[25] C. M. Will, The Confrontation between General Relativity and entent, Living Reviews in Relativity **9**, 3 (2006).

[26] J. r. Taylor, Classical mechanics (University Science Books, USA, 2005).

[27] T. Jacobson, Einstein-æther gravity: a status report, arv:0801.1547v2 (2008).

[28] Sean Carroll, Spacetime and Geometry-An Introduction to General Relativity (Pearson Education Inc., Glenview, IL, 60025, USA, 2004).

[29] G. B. Arfken, H. J. Weber and F. E. Harris Mathematical Methods for Physicists (7th ed) (Elsevier Inc, UK, 2013).

[30] E. Poisson, A Relativist's Toolkit - The Mathematics of Black-Hole Mechanics (Cambridge University Press, Cambridge, 2004).

[31] M. Abramowitz and A. Stegun, Handbook of Mathematical Functions - with Formulas, Graphs, and Mathematical Tables (Dover Publications, Inc., New York, 1972).

[32] B. Z. Foster, Strong field effects on binary systems in Einstein-aether theory, Phys. Rev. D**76**, 084033 (2007).

[33] K. Lin, F.-H. Ho and W.-L. Qian, Charged Einstein-æther black holes in n-dimensional spacetime, Int. J. Mod. Phys. D**28**, 1950049 (2019).

[34] D. Eardley, Observable effects of a scalar gravitational field in a binary pulsar, Astrophys. J. **196**, L59 (1975).

[35] R. d' Inverno, Introducing Einstein's Relativity (Oxford University Press, New York, 2000).

[36] S. M. Carroll and E. A. Lim, Lorentz-violating vector fields slow the universe down, Phys. Rev. D**70**, 123525 (2004).

[37] T. Jacobson and D. Mattingly, Einstein-aether waves, Phys. Rev. D**70**, 024003 (2004).

[38] J. W. Elliott, G. D. Moore and H. Stoica, Constraining the New Aether: gravitational Cherenkov radiation, JHEP **0508**, 066 (2005)

[39] B. Z. Foster and T. Jacobson, Post-Newtonian parameters and constraints on Einstein-aether theory, Phys. Rev. D**73**, 064015 (2006).

[40] L. Shao and N. Wex, New tests of local Lorentz invariance of gravity with small-eccentricity binary pulsars, Classical Quantum Gravity **29**, 215018 (2012).

[41] B. Z. Foster, Radiation Damping in æ-theory, Phys. Rev. D**73**, 104012 (2006).

[42] K. Yagi, D. Blas, E. Barausse, and N. Yunes, Constraints on Einstein-Æther theory and Hořava gravity from binary pulsar observations, Phys. Rev. **D**89, 084067 (2014).

[43] X.-M. Li and S.-J. Liao, More than six hundred new families of Newtonian periodic planar collisionless three-body orbits Science China, **60**, 129511 (2017).

[44] L. Euler, De motu rectilineo trium corporum se mutuo attrahentium, Novo Comm. Acad. Sci. Imp. Petrop. **11**, 144 (1767).

[45] L. Lagrange, ESSAI SUR PROBLÈME DES TROIS CORPS, Oeuvres, **6**, 229 (1772).

[46] Z.E. Musielak and B. Quarles, The three-body problem, Rep. Prog. Phys. **77**, 065901 (2014).

[47] T. Imai, T. Chiba, and H. Asada, Choreographic Solution to the General-Relativistic Three-Body Problem, Phys. Rev. Lett. **98**, 201102 (2007).

[48] C. O. Lousto and H. Nakano, Three-body equations of motion in successive post-Newtonian approximations, Class. Quantum Grav. **25**, 195019 (2008).

[49] V.A. Brumberg, Special Solutions in a Simplified Restricted Three-Body Problem with Gravitational Radiation Taken into Account, Celest. Mech. Dyn. Astron. **85**, 269 (2003).

[50] S. Naoz, The Eccentric Kozai-Lidov Effect and Its Applications, Annu. Rev. Astron. Astrophys. **54**, 441 (2016).

[51] E. Battista, G. Esposito and S. Dell'Agnello, On the foundations of general relativistic celestial mechanics, Inter. J. Mod. Phys. A**32**, 26, 1730022 (2017).

[52] L. Randall and Z.-Z. Xianyu, An Analytical Portrait of Binary Mergers in Hierarchical Triple Systems, Astrophys. J. **864**, 134 (2018).

[53] V. Dmitrasinovic, M. Šuvakov, and A. Hudomal, Gravitational Waves from Periodic Three-Body Systems, Phys. Rev. Lett. **113**, 101102 (2014).

[54] T.-Y. Zhou, W.-G. Cao, and Y. Xie, Collinear solution to the three-body problem under a scalar-tensor gravity, Phys. Rev. D**93**, 064065 (2016).

[55] W.-G. Cao, T.-Y. Zhou, and Y. Xie, Uniqueness of First Order Post-Newtonian Collinear Solutions for Three-Body Problem under a Scalar-Tensor Theory, Phys. Commun. Theor. Phys. **68**, 455 (2017).

[56] C. Will, Testing general relativity with compact-body orbits: a modified Einstein-Infeld-Hoffmann framework, Class. Quantum Grav. **35**, 085001 (2018).

[57] Y.-G. Gong, S.-Q. Hou, D.-C. Liang, E. Papantonopoulos, Gravitational waves in Einstein-æther and generalized TeVeS theory after GW170817, Phys. Rev. D**97**, 084040 (2018).

[58] D. Hansen, N. Yunes, and K. Yagi, Projected constraints on Lorentz-violating gravity with gravitational waves, Phys. Rev. D**91**, 082003 (2015).

[59] A. Saffer and N. Yunes, Angular momentum loss for a binary system in Einstein-Æther theory, Phys. Rev. D**98**, 124015 (2018).

[60] J. Oost, S. Mukohyama and A. Wang, Constraints on æ-theory after GW170817, Phys. Rev. D**97**, 124023 (2018).

[61] `http://three-body.ipb.ac.rs`.

[62] K. Lin, X. Zhao, C. Zhang, T. Liu, B. Wang, S.-J. Zhang, X. Zhang, W. Zhao, T. Zhu, A. Wang, Gravitational waveforms, polarizations, response functions, and energy losses of triple systems in Einstein-aether theory, Phys. Rev. D**99**, 023010 (2019).

[63] X. Zhao, C. Zhang, K. Lin, T. Liu, R. Niu, B. Wang, S.-J. Zhang, X. Zhang, W. Zhao, T. Zhu, A. Wang, Gravitational waveforms and radiation powers of the triple system PSR J0337+1715 in modified theories of gravity, Phys. Rev. D**100**, 083012 (2019).

[64] X. Zhang, J.-M. Yu, T. Liu, W. Zhao, and A. Wang, Testing Brans-Dicke gravity using the Einstein telescope, Phys. Rev. D**95**, 124008 (2017).

[65] E. Berti, K. Yagi, and N. Yunes, Extreme gravity tests with gravitational waves from compact binary coalescences: (I) inspiral-merger, Gen. Relativ. Grav. **50**, 46 (2018).

[66] E. Berti, K. Yagi, H. Yang, N. Yunes, Extreme gravity tests with gravitational waves from compact binary coalescences: (II) ringdown, Gen. Relativ. Grav. **50**, 49 (2018).

[67] K. Yagi, D. Blas, N. Yunes and E. Barausse, Strong Binary Pulsar Constraints on Lorentz Violation in Gravity, Phys. Rev. Lett. **112**, 16, 161101 (2014).

[68] C. Zhang, X. Zhao, A. Wang, B. Wang, K. Yagi, N. Yunes, W. Zhao and T. Zhu, Gravitational waves from the quasicircular inspiral of compact binaries in Einstein-aether theory, Phys. Rev. D**101**, 044002 (2020).

[69] N. Yunes and F. Pretorius, Fundamental theoretical bias in gravitational wave astrophysics and the parametrized post-Einsteinian framework, Phys. Rev. D**80**, 122003 (2009).

[70] K. Chatziioannou, N. Yunes and N. Cornish, Model-Independent Test of General Relativity: An Extended post-Einsteinian Framework with Complete Polarization Content, Phys. Rev. D**86**, 022004 (2012).

[71] C.-F. Shi, *et al.*, Science with the TianQin observatory: Preliminary results on testing the no-hair theorem with ringdown signals, Phys. Rev. D**100**, 044036 (2019).

[72] E. Berti, V. Cardoso and A. O. Starinets, Quasinormal modes of black holes and black branes, Class. Quantum. Grav. **26**, 163001 (2009).

[73] R. A. Konoplya, A. Zhidenko, Perturbations and quasi-normal modes of black holes in Einstein-Aether theory, Phys. Lett. B**644**, 186 (2007).

[74] R.A. Konoplya, A. Zhidenko, Gravitational spectrum of black holes in the Einstein-Aether theory, Phys. Lett. B**648**, 236 (2007).

[75] C. Eling and T. Jacobson, Spherical Solutions in Einstein-Aether Theory: Static Aether and Stars, Class. Quantum. Grav. **23**, 5625 (2006).

[76] J. Oost, Observational Constraints, Exact Plane Wave Solutions, and Exact Spherical Solutions in æ-theory, `http://inspirehep.net/record/1778817/files/2104_10724.pdf`.

[77] P. Berglund, J. Bhattacharyya and D. Mattingly, Mechanics of universal horizons, Phys. Rev. D**85**, 124019 (2012).

[78] C. Ding, A. Wang and X. Wang, Charged Einstein-aether black holes and Smarr formula, Phys. Rev. D**92**, 084055 (2015).

[79] C. Ding, C. Liu, A. Wang and J. Jing, Three-dimensional charged Einstein-aether black holes and the Smarr formula, Phys. Rev. D**94**, 124034 (2016).

[80] C. Ding, A. Wang, Thermodynamical study on universal horizons in higher D-dimensional spacetime and aether waves, Phys. Rev. D**99**, 124011 (2019).

[81] C. Gao and Y. Shen, Static spherically symmetric solution of the Einstein-aether theory, Phys. Rev. D**88**, 103508 (2013).

[82] R. Chan, M. F. A. da Silva and V. H. Satheeshkumar, The General Spherically Symmetric Static Solutions in the æ-theory, arXiv:2003.00227v1 [gr-qc] (2020).

[83] A. Coley and G. Leon, Static spherically symmetric Einstein-aether models I: perfect fluids with a linear equation of state and scalar fields with an exponential self-interacting potential, Gen. Relativity Gravitation, 51, 115 (2019).

[84] G. Leon, A. Coley and A. Paliathanasis, Static spherically symmetric Einstein-æther models II: Integrability and the modified Tolman-Oppenheimer-Volkoff approach, Annals Phys.**412**, 168002 (2020).

[85] M. Azreg-Aïnou, Z.-H. Chen, B.-J. Deng, M. Jamil, T. Zhu, Q. Wu, Y.-K. Lim, Orbital mechanics and quasiperiodic oscillation resonances of black holes in Einstein-æther theory, Phys. Rev. D**102**, 044028 (2020).

[86] C. Eling and T. Jacobson, Black holes in Einstein-aether theory, Class. Quantum. Grav. **23**, 5643 (2006).

[87] C. Eling, T. Jacobson and M.C. Miller, Neutron stars in Einstein-aether theory, Phys. Rev. D**76**, 042003 (2007).

[88] T. Tamaki and U. Miyamoto, Generic features of Einstein-Aether black holes, Phys. Rev. D**77**, 024026 (2008).

[89] D. Blas and S. Sibiryakov, Hořava gravity versus thermodynamics: The black hole case, Phys. Rev. D**84**, 124043 (2011).

[90] E. Barausse, T. Jacobson and T.P. Sotiriou, Black holes in Einstein-aether and Hořava-Lifshitz gravity, Phys. Rev. D**83**, 124043 (2011).

[91] E. Barausse, T.P. Sotiriou, and I. Vega, Slowly rotating black holes in Einstein-æther theory, Phys. Rev. D**93**, 044044 (2016).

[92] T. Zhu, Q. Wu, M. Jamil and K. Jusufi, Shadows and deflection angle of charged and slowly rotating black holes in Einstein-Æther theory, Phys. Rev. D**100**, 044055 (2019).

[93] D. Garfinkle, C. Eling, and T. Jacobson, Numerical simulations of gravitational collapse in Einstein-aether theory, Phys. Rev. D**76**, 024003 (2007).

[94] M. Bhattacharjee, S. Mukohyama, M.-B. Wan, and A. Wang, Gravitational collapse and formation of universal horizons in Einstein-æther theory, Phys. Rev. D**98**, 064010 (2018).

[95] C. Zhang, X. Zhao, K. Lin, S.-J. Zhang, W. Zhao and A.-Z. Wang, Spherically symmetric static black holes in Einstein-aether theory, Phys. Rev. D**102**, 064043 (2020).

[96] T. Liu, X. Zhang, W. Zhao, K. Lin, C. Zhang, S.-J. Zhang, X. Zhao, T. Zhu, and A. Wang, Waveforms of compact binary inspiral gravitational radiation in screened modified gravity, Phys. Rev. D**98**, 083023 (2018).

[97] X. Zhang, W. Zhao, T. Liu, K. Lin, C. Zhang, X. Zhao, S.-J. Zhang, T. Zhu, and A. Wang, Angular momentum loss for eccentric compact binary in screened modifed gravity, JCAP **01**, 019 (2019).

[98] X. Zhang, W. Zhao, T. Liu, K. Lin, C. Zhang, X. Zhao, S.-J. Zhang, T. Zhu, and A. Wang, Constraints of general screened modified gravities from comprehensive analysis of binary pulsars, Astrophys. J. **874**, (2019) 121.

[99] K. Lin, S.-J. Zhang, C. Zhang, X. Zhao, B. Wang and A. Wang, No static regular black holes in Einstein-complex-scalar-Gauss-Bonnet gravity, Phys. Rev. D**102**, 024034 (2020).

[100] Ø. Grøn and A. Næss, Einstein's Theory: a Rigorous Introduction to General Relativity for the Mathematically Untrained (Ad Infinitum AS, Oslo, Norway, 2002).

[101] `https://www.ligo.caltech.edu/`.

[102] B.P. Abbott, *et al.,* [KAGRA, LIGO/Virgo Collaborations], Prospects for observing and localizing gravitational-wave transients with Advanced LIGO, Advanced Virgo and KAGRA, Living Rev. Relativ. **21** (2018) 3.

[103] C. L. Fryer, *et al.,* COMPACT REMNANT MASS FUNCTION: DEPENDENCE ON THE EXPLOSION MECHANISM AND METALLICITY, Astrophys. J. **749**, 91 (2012).

[104] F. Ozel, *et al.,* THE BLACK HOLE MASS DISTRIBUTION IN THE GALAXY, Astrophys. J. **725**, 1918 (2010).

[105] W. M. Farr, *et al.,* THE MASS DISTRIBUTION OF STELLAR-MASS BLACK HOLES, Astrophys. J. **741**, 103 (2011).

[106] B.P. Abbott, *et al.,* [LIGO/Virgo Collaborations], ASTROPHYSICAL IMPLICATIONS OF THE BINARY BLACK HOLE MERGER GW150914, Astrophys. J. Lett. **818**, L22 (2016).

[107] T.-Z. Wang, *et al.,* An Alternative Channel for High-mass Binary Black Holes—Dark Matter Accretion onto Black Holes, Astrophys. J. **863**, 17 (2018).

[108] A. Sesana, Prospects for Multi-band Gravitational-Wave Astronomy after GW150914, Phys. Rev. Lett. **116**, 231102 (2016).

[109] C. J. Moore, R. H. Cole and C. P. L. Berry, Gravitational-wave sensitivity curves, Class. Quantum. Grav. **32**, 015014 (2015).

[110] K. Breivik, *et al.,* DISTINGUISHING BETWEEN FORMATION CHANNELS FOR BINARY BLACK HOLES WITH LISA, Astrophys. J. Lett. **830**, L18 (2016).

[111] A. Nishizawa, *et al.,* Constraining stellar binary black hole formation scenarios with eLISA eccentricity measurements, MNRAS **465**, 4375 (2016).

[112] D. Gerosa and E. Berti, Are merging black holes born from stellar collapse or previous mergers?, Phys. Rev. D**95**, 124046 (2017).

[113] D. Gerosa, E. Berti, *et al.,* Spin orientations of merging black holes formed from the evolution of stellar binaries, Phys. Rev. D**98**, 084036 (2018).

[114] B. Farr, D. E. Holz and W. M. Farr, Using Spin to Understand the Formation of LIGO and Virgo's Black Holes, Astrophys. J. Lett. **854**, L9 (2018).

[115] M. Zevin, C. Pankow, *et al.,* Constraining Formation Models of Binary Black Holes with Gravitational-wave Observations, Astrophys. J. **846**, 82 (2017).

[116] D. E. Holz, Measuring cosmic distances with standard sirens, Phy. Today **71**, 12, 34 (2018).

[117] K. Kyutoku and N. Seto, Gravitational-wave cosmography with LISA and the Hubble tension, Phys. Rev. D**95**, 083525 (2017).

[118] A.G. Riess, *et al.,* A 2.4% DETERMINATION OF THE LOCAL VALUE OF THE HUBBLE CONSTANT*, Astrophys. J. **826**, 56 (2016).

[119] Plank Collaboration, Planck intermediate results, XLVI. Reduction of large-scale systematic effects in HFI polarization maps and estimation of the reionization optical depth, Astron. Astrophys. **596**, A107 (2016).

[120] Scott Dodelson and Fabian Schmidt, Modern Cosmology (2nd ed.) (Elsevier Inc., London, 2021).

[121] A. Nishizawa, Measurement of Hubble constant with stellar-mass binary black holes, Phys. Rev. D**96**, 101303(R) (2017).

[122] Hsin-Yu Chen and D. E. Holz, Finding the One: Identifying the Host Galaxies of Gravitational-Wave Sources, arXiv: astro-ph.HE/1612.01471v1 (2015).

[123] E. Barausse, N. Yunes, and K. Chamberlain, Theory-Agnostic Constraints on Black-Hole Dipole Radiation with Multiband Gravitational-Wave Astrophysics, Phys. Rev. Lett. **116**, 241104 (2016).

[124] Z. Carson and K. Yagi, Multi-band gravitational wave tests of general relativity, Class. Quantum Grav. **37**, 02LT01 (2020)

[125] Z. Carson, B. C. Seymour and K. Yagi, Future prospects for probing scalar–tensor theories with gravitational waves from mixed binaries, Class. Quantum Grav. **37**, 065008 (2020)

[126] Z. Carson and K. Yagi, Parameterized and Consistency Tests of Gravity with Gravitational-Waves: Current and Future, Proceddings, 17(1), 5 (2019).

[127] G. Gnocchi, A. Maselli, T. Abdelsalhin, N. Giacobbo and M. Mapelli, Bounding alternative theories of gravity with multiband GW observations, Phys. Rev. D**100**, 064024 (2019).

[128] Z. Carson and K. Yagi, Parametrized and inspiral-merger-ringdown consistency tests of gravity with multiband gravitational wave observations, Phys. Rev. D**101**, 044047 (2020).

[129] E. Berti, et al., Testing general relativity with present and future astrophysical observations, Class. Quantum Grav. **32**, 243001 (2015).

[130] L. Blanchet, Gravitational Radiation from Post-Newtonian Sources and Inspiralling Compact Binaries, Living Rev. in Relativ. **17**, 2 (2014).

[131] A. Mangiagli, A. Klein, A. Sesana, E. Barausse, and M. Colpi, Post-Newtonian phase accuracy requirements for stellar black hole binaries with LISA, Phys. Rev. D**99**, 064056 (2019).

[132] S. Ransom, *et al.*, A millisecond pulsar in a stellar triple system, Nature **505** (2014) 520.

[133] A. Archibald, *et al.*, Universality of free fall from the orbital motion of a pulsar in a stellar triple system, Nature **559**, 73 (2018).

[134] N. Yunes, K. G. Arun, E. Berti, and C. M. Will, Post-circular expansion of eccentric binary inspirals: Fourier-domain waveforms in the stationary phase approximation, Phys. Rev. D**80**, 084001 (2009).

[135] O. Sarbach, E. Barausse and J. A. Preciado-López, Well-posed Cauchy formulation for Einstein-æther theory, Class. Quant. Grav. **36**, 16, 165007 (2019).

[136] H. C. Ohanian and R. Ruffini, Gravitation and Spacetime (Cambridge University Press, New York, USA, 2013).

[137] M. Maggiore, Gravitational Waves Volume 1: Theory and Experiments (Oxford University Press, New York, 2016).

[138] B. R. Martin, Nuclear and Particle Physics: An Introduction (2nd ed.) (John Wiley & Son Ltd., UK, 2011).

[139] D. J. Griffiths, Introduction to electrodynamics (4th ed.) (Pearson Education, Inc., IL., 2013).

[140] A. Saffer, N. Yunes and K. Yagi, The Gravitational Wave Stress-Energy (pseudo)-Tensor in Modified Gravity, Class. Quant. Grav. **35** 055011 (2018).

[141] M. Kramer, *et al.*, Tests of General Relativity from Timing the Double Pulsar, Science, **314**, 97 (2006).

[142] S. T. Thornton and J. B. Marion, Classical Dynamics of Particles and Systems (5th ed.) (Cengage Learning, India, 2012).

[143] L. D. Landau and E. M. Lifshitz, Mechanics: Volume 1 (3rd ed.) (Elsevier Butterworth-Heinemann, Oxford, 2005).

[144] J. D. Jackson, Classical Electrodynamics (3rd ed.) (John Wiley and Sons, Inc., USA, 1999).

[145] A. Zangwill, Modern Electrodynamics (Cambridge University Press., UK, 2013).

[146] J. Schwinger, L. L. DeRaad Jr., k. A. Milton and W.-Y. Tsai, Classical Electrodynamics, (CRC Press, FL., USA, 2018).

[147] L. Shao, Testing the strong equivalence principle with the triple pulsar PSR J0337+1715, Phys. Rev. D**93**, 084023 (2016).

[148] Y. Aso, Y. Michimura, *et al.*, Interferometer design of the KAGRA gravitational wave detector, Phys. Rev. D**88**, 043007 (2013).

[149] T. Akutsu, *et al.*, First cryogenic test operation of underground km-scale gravitational-wave observatory KAGRA, Class. Quant. Grav. **36** 165008 (2019).

[150] Eugene Butkov, Mathematical Physics (Addison-Wesley Publishing Company, Canada, 1972).

[151] T. Robson, N.J. Cornish, N. Tamanini and S. Toonen, Detecting hierarchical stellar systems with LISA, Phys. Rev. D**98**, 064012 (2018).

[152] K. Kremer, *et al.*, Post-Newtonian dynamics in dense star clusters: Binary black holes in the LISA band, Phys. Rev. D**99**, 063003 (2019).

[153] X. Hu, *et al.*, Fundamentals of the orbit and response for TianQin, Class. Quantum Grav. **35**, 095008 (2018).

[154] Z. Guo, R. Cai and Y. Zhang, Taiji Program: Gravitational-Wave Sources, International Journal of Modern Physics A**35**, 17, 2050075 (2020).

[155] N. Seto, S. Kawamura and T. Nakamura, Possibility of Direct Measurement of the Acceleration of the Universe Using 0.1 Hz Band Laser Interferometer Gravitational Wave Antenna in Space, Phys. Rev. Lett. **87**, 221103 (2001).

[156] G. Orlando, M. Pieroni and A. Ricciardone, Measuring Parity Violation in the Stochastic Gravitational Wave Background with the LISA-Taiji network, arXiv: 2011.07059v1 (2020).

[157] Y. Gong, *et al.*, Frequency response of space-based interferometric gravitational-wave detectors, Phys. Rev. D**99**, 104027 (2019).

[158] C. Cutler, Angular resolution of the LISA gravitational wave detector, Phys. Rev. D**57**, 7089 (1998).

[159] B. W. Carrroll and D. A. Ostlie, An Introduction to Modern Astrophysics (2nd ed.) (Pearson Education, Inc., Addison Wesley, 1301 Sansom St., San Francisco, CA, 2007).

[160] S. Tahura and K. Yagi, Parameterized Post-Einsteinian Gravitational Waveforms in Various Modified Theories of Gravity, Phys. Rev. D **98**, no. 8, 084042 (2018).

[161] B.P. Abbott, *et al.,* [LIGO/Virgo Collaborations], Open data from the first and second observing runs of Advanced LIGO and Advanced Virgo, arXiv:1912.11716 [gr-qc].

[162] B. P. Abbott, *et al.,* [LIGO/Virgo Collaborations], GW190425: Observation of a Compact Binary Coalescence with Total Mass $\sim 3.4 M_{\odot}$, Astrophys. J. Lett., **892**:L3, 1 (2020).

[163] K. Akiyama, *et al.*, [The Event Horizon Telescope Collaboration], First M87 Event Horizon Telescope Results. I. The Shadow of the Supermassive Black Hole, Astrophys. J. L. **875**, L1 (2019).

[164] K. Akiyama, *et al.*, [The Event Horizon Telescope Collaboration], First M87 Event Horizon Telescope Results. II. Array and Instrumentation, Astrophys. J. L. **875**, L2 (2019).

[165] K. Akiyama, *et al.*, [The Event Horizon Telescope Collaboration], First M87 Event Horizon Telescope Results. III. Data Processing and Calibration, Astrophys. J. L. **875**, L3 (2019).

[166] K. Akiyama, *et al.*, [The Event Horizon Telescope Collaboration], First M87 Event Horizon Telescope Results. IV. Imaging the Central Supermassive Black Hole, Astrophys. J. L. **875**, L4 (2019).

[167] K. Akiyama, *et al.*, [The Event Horizon Telescope Collaboration], First M87 Event Horizon Telescope Results. V. Physical Origin of the Asymmetric Ring, Astrophys. J. L. **875**, L5 (2019).

[168] K. Akiyama, *et al.*, [The Event Horizon Telescope Collaboration], First M87 Event Horizon Telescope Results. VI. The Shadow and Mass of the Central Black Hole, Astrophys. J. L. **875**, L6 (2019).

[169] P. Amaro-Seoane, *et al.*, Laser Interferometer Space Antenna, arXiv:1702.00786v3 (2017).

[170] J. Luo, *et al.*, TianQin: a space-borne gravitational wave detector, Class. Quantum Grav. **33**, 035010 (2016).

[171] S. Liu, Y. Hu, *et al.*, Science with the TianQin observatory: Preliminary results on stellar-mass binary black holes, Phys. Rev. D**101**, 103027 (2020).

[172] Z.-R. Luo, Z.-K. Guo, G. Jin, Y.-L. Wu, and W.-R. Hua, A brief analysis to Taiji: Science and technology, Results in Phys. **16**, 102918 (2020).

[173] W.-H. Ruan, Z.-K. Guo, R.-G. Cai, Y.-Z. Zhang, Taiji Program: Gravitational-Wave Sources, Int. J. Mod. Phys. A **35**, 2050075 (2020).

[174] S. Sato, *et al.*, The status of DECIGO, J. Phys.: Conf. Series **840**, 012010 (2017).

[175] W. Israel, Event Horizons in Static Vacuum Space-Times, Phys. Rev. **164**, 1776 (1967).

[176] R. Ruffini and J.A. Wheeler, Introducing the black hole, Phys. Today **24**, 1, 30 (1971).

[177] B. Carter, Axisymmetric Black Hole Has Only Two Degrees of Freedom, Phys. Rev. Lett. **26**, 331 (1971).

[178] J.D. Bekenstein, Transcendence of the Law of Baryon-Number Conservation in Black-Hole Physics, Phys. Rev. Lett. **28**, 452 (1972).

[179] C. Teitelboim, Nonmeasurability of the lepton number of a black hole, Lett. Nuovo Cimento **3**, 397 (1972).

[180] D. C. Robinson, Uniqueness of the Kerr Black Hole, Phys. Rev. Lett. **34**, 905 (1975).

[181] J. D. Bekenstein, Novel "no-scalar-hair" theorem for black holes, Phys. Rev. D**51**, R6608(R) (1995).

[182] C. A. R. Herdeiro and E. Radu, Asymptotically flat BHs with scalar hair: A review, Int. J. Mod. Phys. D**24**, 1542014 (2015).

[183] E. Berti, J. Cardoso, V. Cardoso, M. Cavaglia, Matched filtering and parameter estimation of ringdown waveforms, Phys. Rev. D**76**, 104044 (2007).

[184] E. Berti, A. Sesana, E. Barausse, V. Cardoso, K. Belczynski, Spectroscopy of Kerr Black Holes with Earth- and Space-Based Interferometers, Phys. Rev. Lett. **117**, 101102 (2016).

[185] S. Dwyer, D. Sigg, S. W. Ballmer, L. Barsotti, N. Mavalvala, M. Evans, Gravitational wave detector with cosmological reach, Phys. Rev. D**91**, 082001 (2015).

[186] B. P. Abbott, *et al.*, Exploring the sensitivity of next generation gravitational wave detectors, Class. Quantum Grav. **34**, 044001 (2017).

[187] M. Punturo, *et al.*, The Einstein Telescope: a third-generation gravitational wave observatory, Class. Quantum Grav. **27**, 194002 (2010).

[188] D. Mattingly, Modern Tests of Lorentz Invariance, Living Rev. Relativity, **8**, 5 (2005).

[189] S. Liberati, Tests of Lorentz invariance: a 2013 update, Class. Quantum Grav. **30**, 133001 (2013).

[190] A. Kostelecky and N. Russell, Data tables for Lorentz and CPT violation, Rev. Mod. Phys. **83** 11 (2011) [arXiv:0801.0287v13, January 2020 Edition].

[191] S. Carlip, Quantum Gravity in 2+1 Dimensions, Cambridge Monographs on Mathematical Physics (Cambridge University Press, Cambridge, 2003).

[192] C. Kiefer, Quantum Gravity (Oxford Science Publications, Oxford University Press, 2007).

[193] P. Hořava, Membranes at quantum criticality, JHEP **0903** (2009) 020.

[194] Quantum gravity at a Lifshitz point, Phys. Rev. D**79**, 084008 (2009).

[195] C. Itzykson and Z. Zuber, Quantum Field Theory (McGraw-Hill Inc., USA, 1980).

[196] James D. Bjorken and Sidney D. Drell, Relativistic Quantum Mechanics (McGraw-Hill Inc., New York, 1965).

[197] A. Wang, Hořava gravity at a Lifshitz point: A progress report, Inter. J. Mod. Phys. **D**26, 1730014 (2017).

[198] J. Collins, A. Perez, D. Sudarsky, L. Urrutia, and H. Vucetich, Lorentz invariance and quantum gravity: an additional fine-tuning problem?, Phys. Rev. Lett. **93**, 191301 (2004).

[199] S. G. Nibbelink and M. Pospelov, Lorentz Violation in Supersymmetric Field Theories, Phys. Rev. Lett. **94**, 081601 (2005).

[200] B. Z. Foster, Metric redefinitions in Einstein-Æther theory, Phys. Rev. D**72**, 044017 (2005).

[201] B. P. Abbott, *et al.*, [LIGO Scientific and Virgo Collaborations], GW170817: Observation of Gravitational Waves from a Binary Neutron Star Inspiral, Phys. Rev. Lett. **119**, 161101 (2017).

[202] B. P. Abbott *et. al.*, [Virgo, Fermi-GBM, INTEGRAL, LIGO Scientific Collaboration], Gravitational Waves and Gamma-rays from a Binary Neutron Star Merger: GW170817 and GRB 170817A, Astrophys. J. **848**, L13 (2017).

[203] D. Blas, O. Pujolas, and S. Sibiryakov, A healthy extension of Hořava gravity, Phys. Rev. Lett. **104**, 181302 (2010).

[204] D. Blas, O. Pujolas, and S. Sibiryakov, Models of non-relativistic quantum gravity: the good, the bad and the healthy, JHEP **04** (2011) 018.

[205] T. Jacobson, Extended Hořava gravity and Einstein-aether theory, Phys. Rev. D**81**, 101502 (2010); *ibid.*, D**82**, 129901(E) (2010).

[206] T. Jacobson, Undoing the twist: the Hořava limit of Einstein-aether, Phys. Rev. D**89**, 081501 (2014).

[207] R.M. Wald, General Relativity (University of Chicago Press, 2010).

[208] K. Lin, S. Mukohyama, A. Wang, and T. Zhu, No static black hole hairs in gravitational theories of gravity with broken Lorentz invariance, Phys. Rev. D**95**, 124053 (2017).

[209] A. De Felice, D. Langlois, S. Mukohyama, K. Noui, A. Wang, "Shadowy" modes in Higher-Order Scalar-Tensor theories, Phys. Rev. D**98**, 084024 (2018).

[210] M. Ostrogradsky, Mémoire sur les équations differéntielles relatives au problème des isopérimètres, Mem. Ac. St. Petersbourg, 6, 4, 385-517 (1850).

[211] K. Lin, O. Goldoni, M. F. da Silva and A. Wang, New look at black holes: Existence of universal horizons, Phys. Rev. D**91**, 024047 (2015).

[212] D. W. Jordan and P. Smith, Nonlinear Ordinary Differential Equations: An introduction for Scientists and Engineers (4th ed.) (Oxford University Press, New York, 2007).

[213] Morris Tenenbaum and Harry Pollard, Ordinary Differential Equations (Dover Publications, Inc., New York, 1963).

[214] M. R. Spiegel, S. Lipschutz and J. Liu, Mathematical Handbook of Formulas and Tables (4th ed.) (Mc Graw Hill, New York, 2013).

[215] I. S. Gradshteyn and I. M. Ryzhik, Table of Integrals, Series, and Products (7th ed.) (Translated from Russian by Scripta Technica, Inc., USA, 2007).

[216] V. A. Zorich, Mathematical Aanlysis I (2nd ed.) (Springer, Heidelberg, 2015).

[217] J. Greenwald, J. Lenells, J.-X. Lu, V.H. Satheeshkumar, A. Wang, Black holes and global structures of spherical spacetimes in Hořava-Lifshitz theory, Phys. Rev. D**84**, 084040 (2011).

[218] K. Lin, E. Abdalla, R.-G. Cai and A. Wang, Universal horizons and black holes in gravitational theories with broken Lorentz symmetry, Int. J. Mod. Phys. D**23**, 1443004 (2014).

[219] K. Lin, V.H. Satheeshkumar, and A. Wang, Static and rotating universal horizons and black holes in gravitational theories with broken Lorentz invariance, Phys. Rev. D**93**, 124025 (2016).

[220] P. I. Jefremov, O.Y. Tsupko and G.S. Bisnovatyi-Kogan, Innermost stable circular orbits of spinning test particles in Schwarzschild and Kerr space-times, Phys. Rev. D**91**, 124030 (2015).

[221] S. Iyer, Black-hole normal modes: A WKB approach. II. Schwarzschild black holes, Phys. Rev. D**35**, 12 (1987).

[222] S. Chandrasekhar, F. R. S., and S. Detweiler, The quasi-normal modes of the Schwarzschild black hole, Proc. R. Soc. Lond. A. **344**, 411-452 (1975).

[223] S. Detweiler, BLACK HOLES AND GRAVITATIONAL WAVES. III. THE RESONANT FREQUENCIES OF ROTATING HOLES, Astrophys. J. **239**, 292-295 (1980).

[224] E. Seidel and S. Iyer, Black-hole normal modes: A WKB approach. IV. Kerr black holes, Phys. Rev. D**41**, 2 (1990).

[225] B. F. Schutz and C. M. Will, BLACK HOLE NORMAL MODES: A SEMIANALYTIC APPROACH, Astrophys. J. **291**, L33-L36 (1985).

[226] S. Iyer and C. M. Will, Black-hole normal modes: A WKB approach. I. Foundations and application of a higher-order WKB analysis of potential-barrier scattering, Phys. Rev. D**35**, 12 (1987).

[227] R. A. Konoplya, Quasinormal behavior of the D-dimensional Schwarzschild black hole and the higher order WKB approach, Phys. Rev. D**68**, 024018 (2003).

[228] J. Matyjasek and M. Opala, Quasinormal modes of black holes: The improved semianalytic approach, Phys. Rev. D**96**, 024011 (2017).

[229] E. W. Leaver, An analytic representation for the quasi-normal modes of Kerr black holes, Proc. R. Soc. Lond. A. **402**, 285-298 (1985).

[230] R. A. Konoplya and A. Zhidenko, Quasinormal modes of black holes: From astrophysics to string theory, Rev. Mod. Phys. **83**, 793 (2011).

[231] C. Gundlach, R. H. Price and J. Pullin, Late-time behavior of stellar collapse and explosions. I. Linearized perturbations, Phys. Rev. D**49**, 883 (1994).

[232] B. Wang, C.-Y. Lin and C. Molina, Quasinormal behavior of massless scalar field perturbation in Reissner-Nordstro¨m anti-de Sitter spacetimes, Phys. Rev. D**70**, 064025 (2004).

[233] X. Li and S.-P. Zhao, Quasinormal modes of a scalar and an electromagnetic field in Finslerian-Schwarzschild spacetime, Phys. Rev. D**101**, 124012 (2020).

[234] O. J. Tattersall and P. G. Ferreira, Forecasts for low spin black hole spectroscopy in Horndeski gravity, Phys. Rev. D**99**, 104082 (2019).

[235] H. Yang, D. A. Nichols, F. Zhang, *et al.*, Quasinormal-mode spectrum of Kerr black holes and its geometric interpretation, Phys. Rev. D**86**, 104006 (2012).

[236] J. E. Thompson, H. Chen and B. F. Whiting, Gauge invariant perturbations of the Schwarzschild spacetime, Class. Quantum Grav. **34** 174001 (2017).

[237] T. Regge and J. A. Wheeler, Stability of a Schwarzschild Singularity, Phys. Rev. **108**, 4 (1957).

[238] D. H. McIntyre, QUANTUM MECHANICS: A Paradigms Approach (Pearson Addison-Wesley, San Francisco, USA, 2012).

[239] W. W. Bell, Special Functions for Scientists and Engineers (Dover Publications, Inc., New York, 2004).

[240] Frank Mittelbach, *et al.*, The Latex Companion (2nd ed.) (Pearson Education, Inc., MA., 2004).

[241] A. Övgün, *et al.*, Quasinormal modes of a Schwarzschild black hole immersed in an electromagnetic universe, Chinese Phys. C**42**, 105102 (2018).

[242] N. Zettili, Quantum Mechanics: Concepts and Applications (2nd ed.) (CPI Antony Rowe Ltd, Chippenham, Wiltshire, UK, 2009).

[243] I. Kamaretsos, *et al.*, Black-hole hair loss: Learning about binary progenitors from ringdown signals, Phys. Rev. D**85**, 024018 (2012).

[244] M. Maggiore, Gravitational Waves Volume 2: Astrophysics and Cosmology (Oxford University Press, New York, 2018).

[245] S. Gossan, J. Veitch and B. S. Sathyaprakash, Bayesian model selection for testing the no-hair theorem with black hole ringdowns, Phys. Rev. D**85**, 124056 (2012).

[246] H. Yang, K. Yagi, *et al.*, Black Hole Spectroscopy with Coherent Mode Stacking, Phys. Rev. Lett. **118**, 161101 (2017).

[247] M. Giesler, M. Isi, *et al.*, Black Hole Ringdown: The Importance of Overtones, Phys. Rev. X **9**, 041060 (2019).

[248] B. P. Abbott, R. Abbott, T. D. Abbott, M. R. Abernathy, K. Ackley, C. Adams, P. Addesso, R. X. Adhikari, V. B. Adya, C. Affeldt, *et al.*, Exploring the sensitivity of next generation gravitational wave detectors, Class. Quantum Grav. **34**, 044001 (2017).

[249] M. Punturo, M. Abernathy, F. Acernese, B. Allen, N. An-dersson, K. Arun, F. Barone, B. Barr, M. Barsuglia, M. Beker, *et al.*, The Einstein Telescope: A third-generation gravitational wave observatory, Class. Quantum Grav. **27**, 194002 (2010).

[250] V. Cardoso and J. P. S. Lemos, Quasinormal modes of Schwarzschild–anti-de Sitter black holes:Electromagnetic and gravitational perturbations, Phys. Rev. D**64**, 084017 (2001).

[251] S. Chandrasekhar, The Mathematical Theory of Black Holes (Oxford University Press, Inc., New York, 1992).

[252] K. B. Howell, Differential Equations-An Introduction the Fundamentals (2ed.) (CRC Press, Boca Raton, FL, 33487-2742, USA, 2020).

[253] C. M. Bender and S. A. Orszag, Advanced Mathematical Methods for Scientists and Engineers I: Asymptotic Methods and Perturbation Theory (Springer-Verlag, New York, USA, 1999).

[254] W. J. Olver, Asymptotics and Special Functions (A K Peters, Ltd., Wellesley, MA, 1997).

[255] S. S. Bayin, Mathematical Methods in Science and Engineering (John Wiley & Sons, Inc., Hoboken, New Jersey, 2006).

[256] H. Goldstein, C. P. Poole and J. Safko, Classical Mechanics (3rd ed.) (Pearson Education, Inc., Addison Wesley, 1301 Sansom St., San Francisco, CA, 2002).